Antisense-based Therapy for Duchenne Muscular Dystrophy: Targeting Periostin and Myostatin for the Reduction of Fibrosis

By Golnoush Golshirazi

School of Biological Science

Royal Holloway, University of London

A Thesis Presented for the Degree of Doctor of Philosophy

2019

Statement

I hereby declare that this thesis has been composed by myself, that it has not been accepted in any previous application for a degree, that the work of which it is a record has been done by myself, that any personal data have been processed in accordance with the provision of the Data Protection Act 1998, and that all quotation have been distinguished by quotation marks and the sources of information specifically acknowledged.

Golnoush Golshirazi

April 2019

Abstract

Fibrosis causes muscle dysfunction and contributes to the fatal Duchenne muscular dystrophy (DMD) phenotype. By reducing fibrosis and scar formation, antifibrotic therapies aim to improve muscle function and enhance muscle regeneration. In addition, antifibrotic therapy may also serve as an adjunct to gene and cell therapies for DMD. Periostin(POSTN) is a TGF-β regulated gene and its inhibition has shown to reduce fibrosis. Myostatin (MSTN), a member of the Transforming Growth factor β family of signalling molecules, is a key regulator of muscle mass and its inhibition has been shown to increase muscle mass and strength as well as reduce fibrosis. Periostin and myostatin are now promising therapeutic targets for the treatment of Duchenne muscular dystrophy (DMD). The current project is focused on working towards a combination therapy for Duchenne muscular dystrophy through development of antisense oligonucleotides that target POSTN and MSTN and prevent their successful transcription and translation, ultimately leading to a reduction in the amount of functional protein produced by the muscle. Theoretically this should lead to a subsequent amelioration of fibrosis and increase muscle mass in the dystrophic muscle. More specifically, the project looks at inhibition of MSTN by targeting its poly(A) tail and inhibition of POSTN through disruption of the reading frame by exon skipping. These methods were examined *in vitro* in human muscle cell lines as well as mouse muscle and fibroblast cell lines; therapeutic potential of the best oligonucleotide was then investigated *in vivo* using mice.

First novel contribution in this project is MSTN downregulation through targeting of the poly(A) signal and comparison of this method to the previously established exon exclusion method. This investigation showed the targeting of poly(A) signal to be successful but not as effective as exon exclusion.

Another novel contribution by this project was the investigation of POSTN downregulation through exon exclusion in the berberine induced damaged TA muscle of the C57 mouse model. This investigation showed berberine induced damage in mice to be an ineffective model to assess the effects of POSTN downregulation on fibrosis.

Acknowledgments

First and foremost, I would like to express my gratitude to Dr Linda Popplewell who chose to take me on as her first PhD student. It has been an honour and a privilege to work alongside Dr Popplewell and witness her laboratory grow. I would also like to thank Professor George Dickson for meeting me 5 years ago and offering me the opportunity to pursue my goal of research in gene therapy.

To all those in the Popplewell and Dickson lab, and those who have left the lab in my time there, I would like to thank you all for welcoming me in the lab as well as coming to my aid when I needed it.

Finally, I would like to thank my family and friends. My Parents Hassan Mojtaba and Fereshteh, having spent their lives ensuring I have everything I may need. Dad, you taught me to find a purpose in life bigger than myself, and that led me to this PhD. Mum, you taught me to always prioritise kindness and love, and that has made my journey through this PhD a successful one. Thank you both for everything I have and everything I am.

To my siblings Farnoush and Mohammad Ali: you are always there for me with pride and enthusiasm. Thank you for making this journey happier and brighter. You give me reason to gather courage and strength. Together we are always stronger.

To my friends with whom life is hopeful. Maryam Achoukhi, you have been there to put me back on my feet and help me find my way, every time I needed it! Thank you for being so patient with me. Lukasz Ciszewski, you believe in me and see the woman I thrive to be. Without your support (and distraction) I would not have made it through this PhD. Meeting you was a blessing that this project brought into my life, I am eternally grateful for everything! As a wise man once said, 'Friendship above all!'

Last but not least, to all those I have not mentioned here but who have been a part of my life throughout my PhD and supported me one way or another, I would like to extend my thanks!

'If a blessing descends upon you, then make it last by being grateful.'

-**Ali Ibn Abi Talib**

Abbreviations

3'UTR	3' Untranslated region
α-SMA	α-Smooth muscle actin
AON	Antisense oligonucleotide
COL	Collagen
DMD	Duchenne muscular dystrophy
DMEM	Dulbecco's modified Eagle medium
ECM	Extracellular matrix
EDTA	Ethylenediaminetetraacetic acid
ESE	Exonic splicing enhancer
ESS	Exonic splicing suppressor
Fbn	Fibronectin
MSTN	Myostatin
NMD	Nonsense mediated degradation (of mRNAs with out-of-frame exons skipping)
PMO	Phosphorodiamidate morpholino oligomer
POSTN	Periostin
qPCR	Quantitative polymerase chain reaction
RD	Rhabdomyosarcoma
RNA	Ribonucleic acid
RT-PCR	Reverse transcriptase polymerase chain reaction
RT-qPCR	Reverse transcriptase quantitative polymerase chain reaction
TA	Tibialis Anterior
TAE	Tris-acetate-EDTA gel running buffer
TBE	Tris-borate-EDTA gel running buffer
TGF-β	Transforming growth factor-β

Table of Contents

List of Figures

List of Tables

1. Introduction

What is Duchenne Muscular Dystrophy

Duchenne Muscular Dystrophy (DMD) is the most common type of muscular dystrophy with a prevalence of 1 in 3,500 live male births (Kharraz, Guerra, Pessina and Serrano, 2014). DMD is a fatal X-linked and recessive disorder and hence effects mainly boys. The disease is characterised by progressive loss of muscle mass and function and is caused by mutations in the dystrophin gene that results in an out-of-frame transcript (Kharraz, Guerra, Pessina and Serrano, 2014).

All three muscle types, skeletal, cardiac and smooth, are affected severely in DMD, which leads to a shortening of life expectancy. Patients are usually wheelchair-bound by the age of 12 and eventually death occurs as a result of cardiac and/or respiratory failure (O'Brien and Kunkel, 2001).

Becker Muscular Dystrophy

Becker Muscular Dystrophy (BMD) is similar to DMD but less severe with a milder clinical course. BMD is caused by the production of a shortened yet partly functional dystrophin protein. This is due to the fact that the mutation in BMD leads to an in-frame transcript. Muscle wasting and weakness is also central in this type of dystrophy but the weakness is mainly proximal with difficulties in walking beginning after the age of 16. Death in BMD due to the dystrophy is not common but can occur due to cardiac failure in severely affected individuals. BMD clinical signs and severity varies greatly between patients.

Severity of disease ranges between losing the ability to walk in late teens to experiencing some weakness in proximal muscles or even simply cramping upon exercising (Emery and Mutoni, 2003).

1.1 Skeletal Muscle

Healthy skeletal muscle has a capacity for regeneration due to the presence of satellite cells, a source of muscle progenitor cells which can regulate skeletal muscle growth and regeneration (Mauro, 1961; Fukada *et al.*, 2013). In DMD patient however the capacity for functional muscle regeneration and growth is absent (McLoon, 2008; Lu *et al.*, 2014).

Muscle fibres are composed of single multinucleated cells that provide the basis for the locomotion of vertebrates and invertebrates. Muscle fibres can shorten and produce force. Myofibrils are the most basic contractile unit of muscle fibres. Myofibrils consist of approximately 10,000 sarcomeres attached end to end. These contractile units span the length of each muscle fibre and are physically attached to the sarcolemma of the muscle fibre (Martini 2011). The tension exerted by myofibrils on the surrounding extracellular matrix generates force and allows the contraction of muscle fibres (Small, 1995).

1.3.1 Myogenesis

Myogenesis is the process by which the mesodermal layer of embryonic germ cells gives rise to muscle cells (Buckingham, 2006). Myogenesis is a highly conserved process among vertebrates. It involves the commitment of stem cells to Myogenic Precursor Cell (MPC) pools. These precursor cells then differentiate into myoblasts and migrate and fuse to form myofibres (Rochlin *et al.,* 2010).

The myogenic process in post-natal muscle and *in vitro* involves the use of satellite cells as precursors. Satellite cells are located between the basal lamina and the sarcolemma of the multinucleated fibres. These cells are thought to be the foremost contributors to postnatal muscle growth and regeneration (Mauro, 1961; Schultz, 1996). Satellite cells are also the major source of primary myoblast (Partridge, 1997). During adult life, the absolute number of satellite cells stays relatively constant (Schultz, 1996) though there has been evidence of progressive loss of satellite cells more particularly in old age. With cycles of degeneration and regeneration in mind, this indicates that self-renewal is at work to maintain satellite cell pools (Zammit and Beauchamp, 2001).

In adults, muscles have reached their adult size, and satellite cells are normally quiescent. However, various stimuli, such as exercise, muscle stretch, muscle injury and electrical stimulation, induce satellite cells to re-enter the cell cycle and take part in myogenesis (Schultz and McCormik, 1994; Appell, Forsberg *et al*., 1998). Activation of satellite cells induces expression of myogenic genes, myogenic precursor cell, myoblasts, then differentiate and fuse with pre-existing myofibres or with each other to form new or replacement myofibres (Sabourin and Rudnicki, 2000). Myogenesis is a complex process that is tightly controlled throughout the organism lifetime. Many proteins are involved in signalling pathways to coordinate muscle degeneration and regeneration; one of the essential proteins involved is myostatin.

1.3.2 Muscle Mass Regulation

Muscle mass can increase through hypertrophy, an increase in myofibre size, or hyperplasia, an increase in the number of myofibres that, as described above, consists of the fusion of satellite cells. As mentioned already, the consensus is that an increase

in muscle mass in adulthood is mainly due to hypertrophy rather than hyperplasia as the general number of fibres is constant during this period. Having said this, small myotubes and myofibres expressing myogenic markers are found in adult muscle cells following training, indicating the formation of new myofibres (Kadi and Thornell, 1999).

Change in muscle mass is measured in a change in muscle cross sectional area. It is the balance between protein synthesis and protein degradation that determines the muscle cross-sectional area (Gibson, Smith and Rennie, 1988). An increase in protein synthesis leads to an increase in myofibril content which is contained in larger myofibres (Velloso, 2008). In myofibres the ratio of DNA/protein is more or less considered to be constant (Roy *et al.,* 1999) and therefore, in addition to an increase in protein synthesis, hypertrophy requires an increase in myonuclei to maintain a constant myonuclear domain (Velloso, 2008). As myofibres are post-mitotic, their nuclei cannot proliferate and additional nuclei, when required, are provided by satellite cells (Zammit, Partridge and Yablonka-Reuveni, 2006).

Many signalling pathways are involved in the regulation of muscle mass. One of the most important pathways is thought to be the PI3K/AKT pathway. This pathway works to activate protein synthesis and inhibit protein degradation. The PI3K/AKT (phosphatidylinositol 3-kinase/protein kinase B) pathway is activated by exercise and lies downstream of IGF-1 (insulin like growth factor 1) and insulin receptors; both IGF-1 and insulin stimulate protein synthesis in muscle cells (Bolster, Jefferson and Kimball, 2004).

Growth Hormone (GH) is synthesised in the pituitary and leads to the synthesis of IGF-1 in many tissues but mainly the liver and the muscle although exercise also leads to the

synthesis of IGF-1 in muscle. The IGF-1 in circulation is primarily secreted by the liver and is referred to as cIGF-1. cIGF-1 is involved in negatively regulating GH synthesis. The IGF-1 synthesised in muscle cells is referred to as mIGF-1 and is involved in stimulating hypertrophy in an autocrine/paracrine way.

Upon secretion of mIGF-1 from muscle cells, it binds to its receptors on muscle cell surfaces and activates the PI3K/AKT pathway. Among isoforms of AKT it is AKT1 that is important in growth regulation. Upon activation, AKT1 protein degradation is prevented, through inactivation of FOXO (Forkhead box protein) transcription factors, then protein synthesis is increased through activation of mTOR1 (mammalian target of rapamycin). mTOR1 is downstream of AKT1 and which activates translation regulators leading to both ribosomal biogenesis and translation initiation (Figure 1.1) (Glass, 2005; Velloso, 2008).

Furthermore, AKT is also regulated by myostatin, a negative regulator of muscle mass which signals to increase protein degradation. There seems to be cross talk between IGF-1 and myostatin activity. In normal circumstances, the IGF-1 signalling pathway is dominant and blocks the myostatin pathway. Having said that, it has been shown that upon increased expression of Myostatin the IGF-1 pathway is inhibited (Amirouche *et al.*, 2009; Trendelenburg *et al.*, 2009; Elkina *et al.*, 2011). It is thought that in muscle wasting conditions, where we have a decrease in cross-sectional area of muscle, myostatin works to prevent AKT1 from activating mTOR1 and inhibiting FOXO transcription factors that lead to a reduction in protein synthesis and an increase in protein degradation (Elkina *et al.*, 2011).

In DMD the regenerative capacity of skeletal muscle is compromised, as recurrent myofibre damage demands a continuous need for repair; ultimately leading to a depletion of the proginator cell pool and loss of succesful muscle regenration (Lu, poddar 2014).Despite the presence of the dystrophin mutation at birth, DMD does not manifest itself as muscle wekaness untill 3-5 years of age coinciding with the depletion of proginator cells. Below we will discuss the clinical and pathological features of DMD.

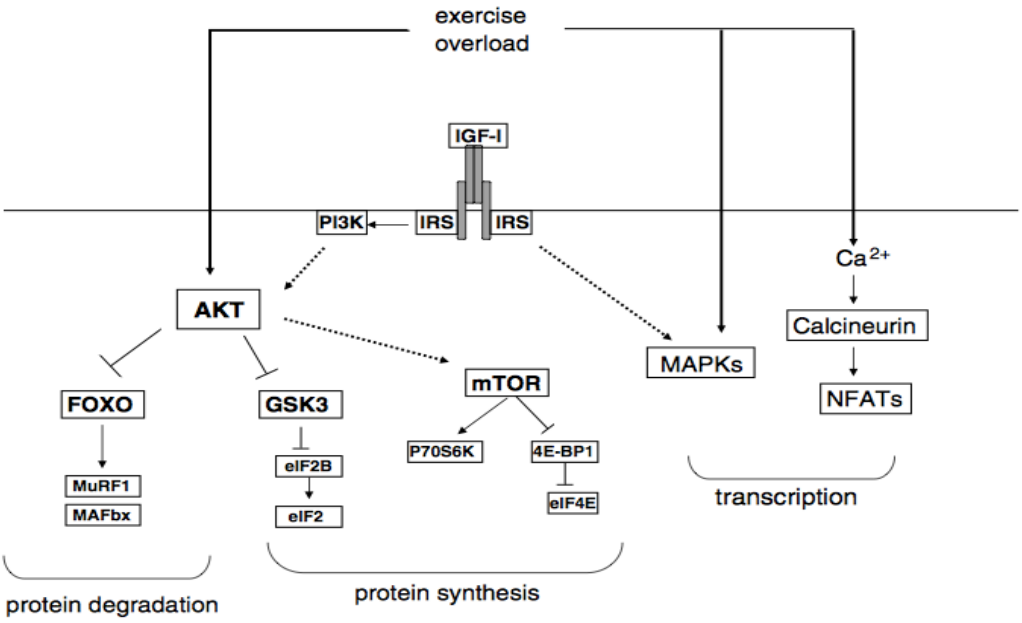

Figure 1.1 IGF-1 regulation of muscle growth through AKT growth axis

IGF1 binding to receptors on muscle cell surfaces initiates AKT signalling, leading to muscle growth. PI3K, activated by IGF1 binding its receptor, phosphorylates AKT. Phosphorylated AKT leads to the inhibition of FOXO-induced protein degradation and also activates the mTOR complexes which leads to protein synthesis. (Adapted from Vellos *et al.,* 2008.)

1.2 Clinical and pathological features of Duchenne muscular dystrophy

Clinically, symptoms in DMD are split into four phases: early phase; late childhood; adolescence and adulthood.

1.2.1 Early Phase

This phase starts at birth and ends at age eight. Boys will usually start walking late and also struggle in performing simple motor tasks and find difficulty in keeping up with friends when playing. One clinical feature of DMD at this phase is increased Serum creatine kinase (CK), at between 20 and 100 times normal levels, which reflects degeneration (Sun, Peng and He, 2008). CK, made in the degenerating muscle, is released into the serum as the muscle degenerates; levels peak in 3-5-year-olds. CK levels then decrease with age and this may be due to decreased activity of the boys as they become less able to move and also due to increased fibrosis as muscle is replaced with fibrotic tissue and hence less muscle is available to produce CK. One characteristic clinical feature seen in DMD boys is the Gower's manoeuvre which is where boys in a sitting position will use their hands to push down on the floor and then climb up their thighs in order to extend their hip and trunk in helping them stand (Figure 1.2). This is due to weakness in the knees and hips preventing young boys from being able to stand up without help from their hands. Another feature seen in young boys with DMD is walking on their toes. This is a reaction to a lack of balance from lumbar lardosis which develops as compensation to gluteal maximum weakness (Figure 1.3) (Emery, 1993). Lumbar lardosis is in turn exaggerated by the toe walking seen in these children.

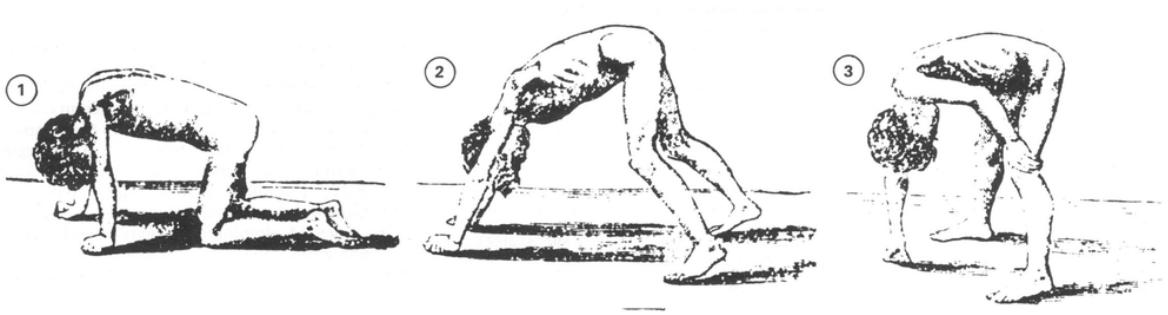

Figure 1.2 Gowers Manoeuvre

Characteristic feature seen in early phase of DMD patients where the child uses his hand to press on the floor and then climb up his thigh to stand up (figure from Emery 1993)

1.2.2 Late childhood phase

This stage usually refers to features seen between the age of 6-13. At this phase, an increase in contractures is seen in the lower extremities along with decreased muscle strength. There is an increase in the frequency of falling over, and it is in this phase that the ability to walk is severely affected and even lost. The decrease in muscle strength leads to a more exaggerated lumbar lardosis.

1.2.3 Adolescence phase

This phase occurs between 8-15 years of age. Patients get fully dependent on wheelchairs as there is a significant loss of skeletal muscle strength and a rapid increase in joint contractures. Severe kyphoscolisosis, a curvature of the thoraco-lumbar spine, can develop in this phase due to a lack of necessary support in the wheelchair (Figure 1.3). If the kyphoscolisosis progresses beyond 20-30 degrees, it will continue to progress, and this progression is associated with a decline in cardiac and pulmonary function.

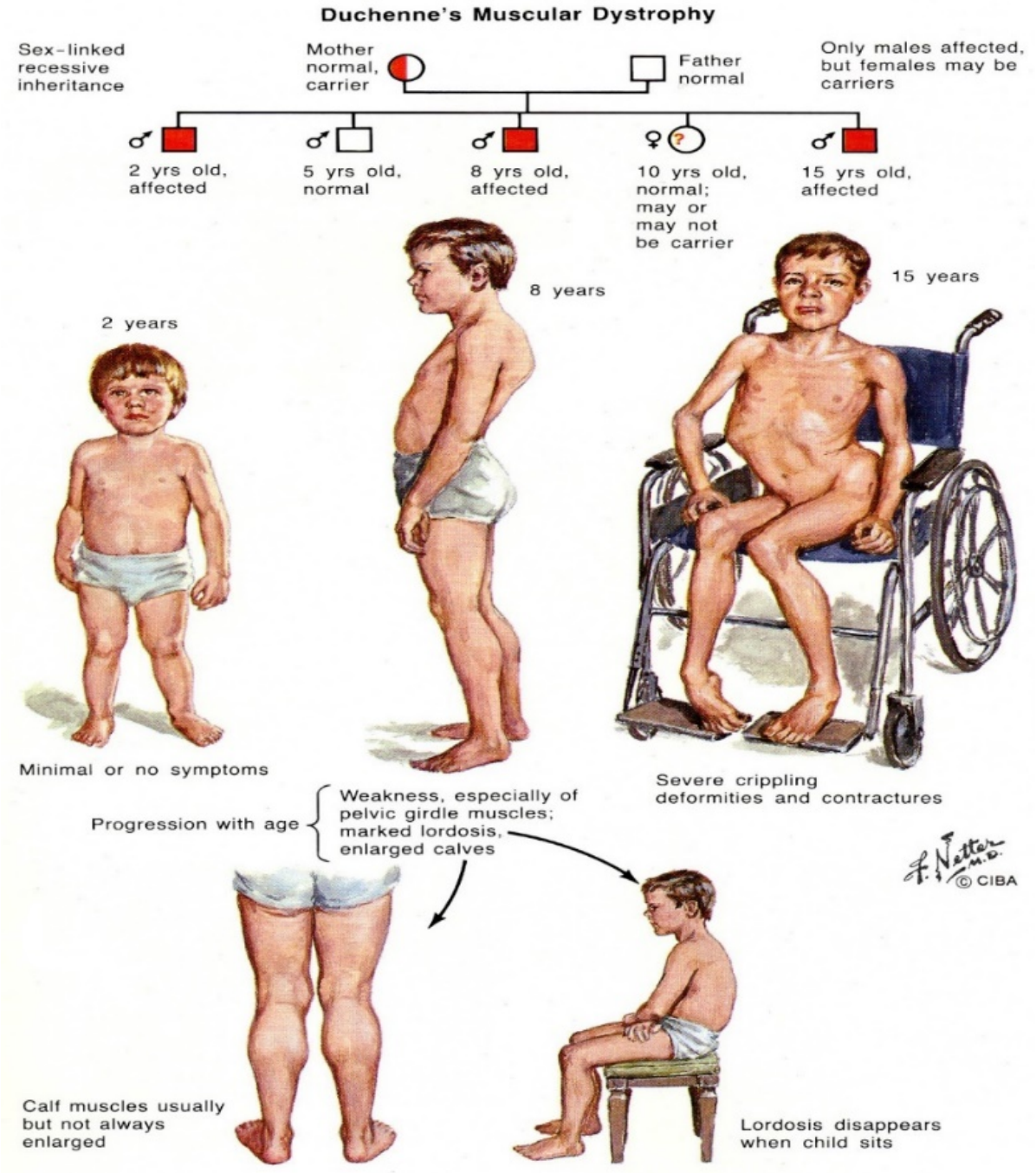

Figure 1.3 Genetic inheritance of DMD Progression of orthopaedic clinical features in DMD boys

Lumbar lordosis develops in the early phase between the age of 3-8 and gets exaggerated with age. When wheelchair bound in adolescence phase extreme kyphoscoliosis commonly occurs (Adapted from Greene *et al.,* 2006).

1.2.3 Adulthood

It is in the adulthood phase when symptoms become life-threatening in DMD patients. In this phase, deterioration of the myocardium, due to cardiac muscle necrosis and fibrosis, becomes a threat to heart failure. Around 90% of patients show cardiac manifestations of DMD and only a decade ago many boys would die before the age of 20 from respiratory failure (McDonald *et al.*, 1995). In the last decade, improved care and improved access to appropriate equipment and ventilation have increased this life span by up to 10 years (Eagle *et al.*, 2016).

1.3 Dystrophin

1.3.1 Dystrophin gene

Dystrophin has the longest gene in the human genome with a length of 2.4 Mbp consisting of 79 exons and 8 tissue-specific promoters (Giacca, 2010). It was first discovered in 1987 and localised to band Xp 21 on the human X chromosome (Hoffman, Brown and Kunkel, 1987). The gene takes 16 hours to be fully transcribed and once spliced makes a 14kb mRNA, 11kb of which codes for the 427 kDa dystrophin protein made of 3685 amino acids. The dystrophin gene is mainly expressed in skeletal muscle, heart and cortical neurons.

1.3.2 Dystrophin protein

The dystrophin protein (427 kDa) is a very long filamentous protein located on the cytosolic side of the plasma membrane of striated muscle fibres (Sarcolemma). The protein is in particular concentrated around neuromuscular junctions (Giacca, 2010) and

is made of 4 structural domains: the N terminal region (actin binding domain, ABD), a central rod domain made of a series of repeats each composed of 3 α-helix bundles, a cysteine-rich domain (CR) and the C terminal domain (CT) (Figure 1.4A). The N terminal region binds to actin filaments; the CR domain is essential for binding and localises to the sarcolemma through the dystrophin-associated glycoprotein complex (DGC) (Figure 1.4B). The DGC connects the internal cytoskeleton to the extracellular matrix hence stabilising the sarcolemma while muscle fibres stretch or shorten (Giacca, 2010). Other than a structural role, dystrophin and DGC also contribute to intracellular processes such as maintaining the intracellular calcium levels (Niebroj-dobosz *et al.*, 2001).

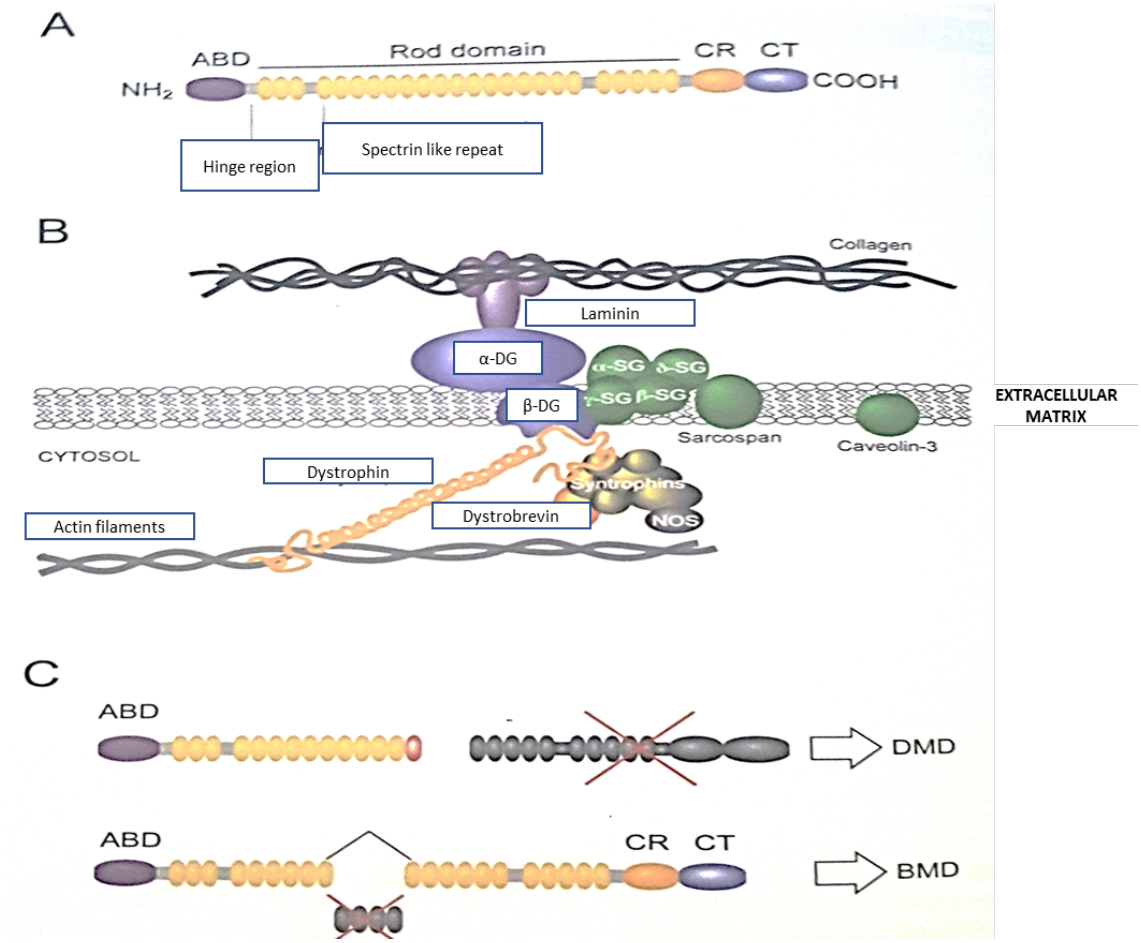

Figure 1.4 Dystrophin and the dystrophin glycoprotein complex

A) Dystrophin protein is made of 4 structural domains: the N terminal region (actin binding domain, ABD), a central rod domain made of a series of repeats each composed of 3 α-helix bundles, a cysteine rich domain (CR) and the C terminal domain (CT).

B) The N terminal region binds to actin filaments, the CR domain is essential to bind and localises to the sarcolemma through the dystrophin associated glycoprotein complex (DGC)

C) In patients with DMD the dystrophin protein is significantly reduced in quantity or the CT domain is missing. In BMD patients the ABD domain and CT domain are intact but there are deletions present in the central rod domain. (Figure adapted from Giacca, 2010).

1.3.3 Dystrophin in DMD

Dystrophin has been shown to be absent or greatly diminished in the muscle of patients with Duchenne muscular dystrophy (McArdle, Edwards and Jackson, 2016). The absence of dystrophin leads to the lack of a link between contractile actin and the cell membrane. This has been shown to correlate directly with a clear reduction in the DGC proteins. This, in turn, disrupts the link between the subsarcolemmal cytoskeleton and the extracellular matrix. The lack of membrane integrity leads to a 'leaky membrane' and so unregulated transit of extracellular calcium into the cytoplasm of muscle cells; this considerable rise in calcium levels lead to activation of calcium-dependent proteases such as calpains and activation of inflammatory and necrotic signalling pathways (Spencer, Croall and Tidball, 1995). Dystrophin-deficient muscle is therefore constantly undergoing inflammation, death and fibrosis (Matsumura, Campbell and Nonaka, 1993). As mentioned in previous sections the presence of satellite cells means the muscle fibres can regenerate, but the new muscle is also dystrophin-deficient and so with every cycle of death and regeneration the extent of fibrosis within the muscle increases (Figure 1.5) (Wehling, Spencer and Tidball, 2001).

Several mutations have been identified in the dystrophin gene. Two third of patients have deletions in two vital areas of the gene, the first 20 exons and exon 45-53. The remaining third of patients have point mutations introducing stop codons, frame shifts, modification of splicing signals and some are present in the promoter region of the gene. In patients with DMD, the dystrophin protein is significantly reduced in quantity, or the CT domain is missing. In BMD patients, the ABD domain and CT domain are intact, but there are deletions present in the central rod domain (Figure 1.4C). The mutations in the

central rod domain allows the production of a shorter yet functional protein, translated from an in-frame transcript as oppose to an out of frame transcript seen in DMD, and explains the milder phenotype observed in BMD patients compared to DMD patients.

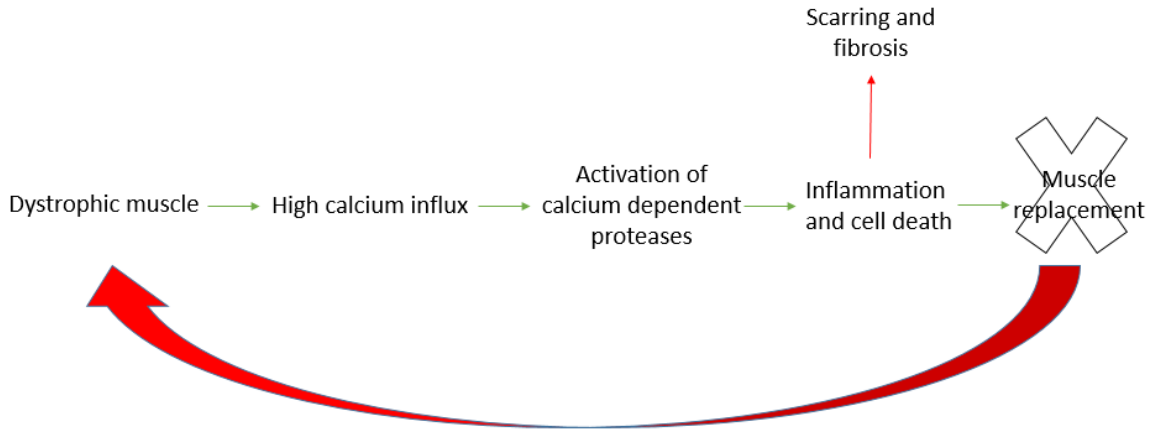

Figure 1.5 Cycle of damage in dystrophin deficient muscle

Lack of dystrophin leads to membrane instability which in turn allows calcium influx and activation of calcium dependent proteases and inflammatory and necrotic pathways. Cell death is followed by muscle replacement using present satellite cells leading to depletion of satellite pools. New muscle fibres are also dystrophin-deficient and so undergo the same cycle of calcium influx and cell death. Chronic inflammation and necrosis leads to fibrosis and replacement of muscle fibres with fatty fibrous tissue.

1.4 Utrophin

In 1989, utrophin, a 400kDa dystrophin-related protein, was discovered on chromosome 6 (Love *et al.*, 1989). Utrophin has been found to be expressed in all tissues and is expressed in DMD patients at elevated levels (Feener, Koenig and Kunkel, 1989; Koenig *et al.*, 1989). Utrophin was found to be enriched at neuromuscular junctions where it binds components of the DPAC including dystroglycans and syntrophins allowing the connection of the intracellular cytoskeleton to the extracellular matrix. Primary sequence and protein structure similarities between utrophin and dystrophin led to an interest in up-regulation of utrophin for therapeutic purposes in DMD patients.

1.5 Animal models for DMD

Following the identification and characterisation of dystrophin and its mutations in DMD patients, animal models were identified to resemble DMD in that they lack dystrophin and that skeletal muscle fibres undergo the cycle of damage involving fibrosis, necrosis and replacement (Partridge, 1991). The most beneficial models in the field are mouse, dog, cat and most recently, rat.

1.5.1 Golden Retriever (GRMD dog)

The *GRDM* golden retriever carries a mutation in the dystrophin gene leading to the exclusion of exon 7 of the protein. The *GRMD* dog shows the most similarity to DMD out of all the models. The neonatal dog shows a severe phenotype with muscle weakness followed by progressive loss of muscle tissue and the development of fibrosis. Investigation of disease pathology in the *GRMD* dog showed the presence of early fibre necrosis and regeneration resulting in severe myopathy (Valentine *et al.*, 1990).

1.5.2 Mouse (mdx mouse)

The *mdx* mouse is one of the most frequently used animal models in DMD research. This is due to similar pathological features between the *mdx* mouse and DMD patients as well as advantages such as short breeding time and low cost.

The *mdx* mouse was first reported by Bulfield *et al.* (1984) as a spontaneous mutation in a C57BL10Sc/Sn(C57) colony of mice. This has made C57 a very good control when using *mdx* mice as a model. The genetic defect in these mice is a point mutation in exon 23 of the dystrophin gene giving rise to a premature stop codon (Sicinski *et al.*, 1989).

In the *mdx* mouse the muscle membrane is damaged due to lack of dystrophin. This leads to an influx of calcium by the cells and so over-contraction of muscle fibres and activation of intracellular proteases (Porte, Morin and Koenig, 1999). Between 3 weeks to 18 months, muscle fibres show cycles of degeneration and regeneration as well as necrosis (Pastoret and Sebille, 1995). *mdx* mice also show replacement of muscle with connective tissue and fat due to necrosis and the inadequacy to regenerate healthy muscle fibres; unlike human patients, these mice show fibrosis at very late stages of the disease (Zeman *et al.*, 2000) . The fibrosis evident in the *mdx* mouse is first present in the diaphragm (Stedman *et al.*, 1991) and in the limbs towards the end of the second year of the mouse's life (Pastoret and Sebille, 1995).

The *mdx* mouse also shows similar cardiac parameters to that observed in DMD patients (Bridges, 1986; Chu *et al.*, 2002). Cardiac muscle in these mice shows myocardial lesions accompanied by necrosis, macrophage infiltration and inflammation. Cardiomyocytes in *mdx* mice of 8-10 weeks have a reduced threshold for development of sarcolemmal injury under mechanical stress. At 12-14 weeks the pathophysiology of the *mdx*

myocardium is evident from altered contractile function (Sapp, Bobet and Howlett, 1996; Danialou *et al.*, 2001).

1.5.3 Feline (FXMD cat)

The feline X-linked muscular dystrophy is a dystrophin-deficient model characterised by muscular hypertrophy. This model is not often used in DMD research as it never exhibited loss of muscle mass and muscle maintains its contractile strength. In addition, although there is some fibrosis present in the dystrophic cat, no fatty infiltration is observed, unlike the *mdx* and *GRMD* models (Porte, Morin and Koenig, 1999).

1.5.4 Rat (dmdmdx rat)

In 2014, two lines of Duchenne muscular dystrophy rats were generated using TALENs targeting exon 23 of the rat dystrophin gene (Larcher, Lafoux, Tesson, Remy *et al.*, 2014) .At 3 months of age, the limb and diaphragm muscles of the *dmdmdx* rats show considerable necrosis and regeneration, and by 7 months of age, severe fibrosis and adipose tissue infiltration are displayed. Cardiac parameters in the Duchenne rat is also comparable to that of DMD patients with signs of dilated cardiomyopathy accompanied by necrotic and fibrotic changes. The rat is, therefore, a relatively new but promising small animal model of DMD.

1.6 Treatment strategies for Duchenne muscular dystrophy

There are a variety of treatment options for DMD patients. Most treatments in use are directed at controlling symptoms though there are numerous research projects as well as clinical trials in the development of genetic drugs that address the cause of Duchenne muscular dystrophy.

1.6.1 Glucocorticoids

One of the most important medications in use for DMD patients are glucocorticoids such as prednisone (Merlini *et al.*, 2003) and its derivative deflazacort (Campbell and Jacob, 2003). Glucocorticoids have been shown to increase muscle function and strength significantly but have some severe side effects associated with them such as weight gain and lenticular cataracts (Griggs *et al.*, 1993) as well as psychological side effects such as difficulty concentrating, sleeping and controlling emotions.

There are several modes of action proposed for the mechanism of action of glucocorticoids. The first mode of action is thought to be due to glucocorticoid anti-inflammatory actions; prednisone, for example, has shown to decrease the total T cell number as well as cytotoxic cells (Kissel *et al.*, 1991). It is thought that the decrease in concentration of inflammatory cells causes an immunosuppressive effect and so slows down the rate of muscle degeneration (Wehling-Henricks, Lee and Tidball, 2004). Another mode of action could be a decrease in the calcium influx and size of calcium pools in the dystrophic muscle fibres which was shown by Matzinger *et al.* (1995) using prednisone. Prednisone has also been shown to enhance the myogenesis of satellite cells and increase dystrophin-related protein expression in *mdx* skeletal muscle cell

cultures (Passaquin *et al.*, 1993). mRNA levels of structural, signalling and immune response genes are changed after steroid treatment which also helps explain how steroid-induced gene expression may improve strength (Mutoni *et al.,* 2002).

1.6.2 Gene therapy

Duchenne muscular dystrophy is an attractive candidate for gene therapy since it is caused by a single gene mutation. Many advances have been made in developing a primary therapy for DMD, but they still remain unsuccessful (Konieczny, Swiderski and Chamberlain, 2013) with current trials showing extremely promising results such as that reported by Serepta therapeutics on the SRP-4045 resulting in significant dystrophin expression in DMD boys. Gene therapy in DMD faces many challenges such as the mode of delivery to affected muscles, overcoming immune challenges to technique and introduced genetic material, as well as deciding upon what technique is best. It is also important to mention that other than the amount of dystrophin delivered the efficiency of therapy is also very dependent on the pathological features of the disease and so the stage of the disease. In patients were the disease has progressed to the point where most muscle fibres are replaced with fatty deposition access to dystrophic muscle limited and efficiency of gene or cell therapy to restore dystrophin is compromised (Kharraz *et al.*, 2014).

As mentioned previously, the dystrophin gene is the biggest gene in the human genome and so delivering such a big gene is one of the greatest challenges in gene therapy for DMD. A lot of effort has gone into developing shorter yet functional dystrophin constructs, similar to those seen in BMD patients, which can be used in instead of dystrophin in DMD patients (Konieczny, Swiderski and Chamberlain, 2013). Following

the generation of transgenic mice that carried dystrophin constructs lacking various domains, it was shown that the majority of the rod domain and the C-terminal domain are not essential for dystrophin function (Wang, Li and Xiao, 2000; Sakamoto *et al.*, 2002; Gregorevic *et al.*, 2006). Following this discovery mini-dystrophin and micro-dystrophin constructs (Figure 1.6) are now being tested using both viral and non-viral

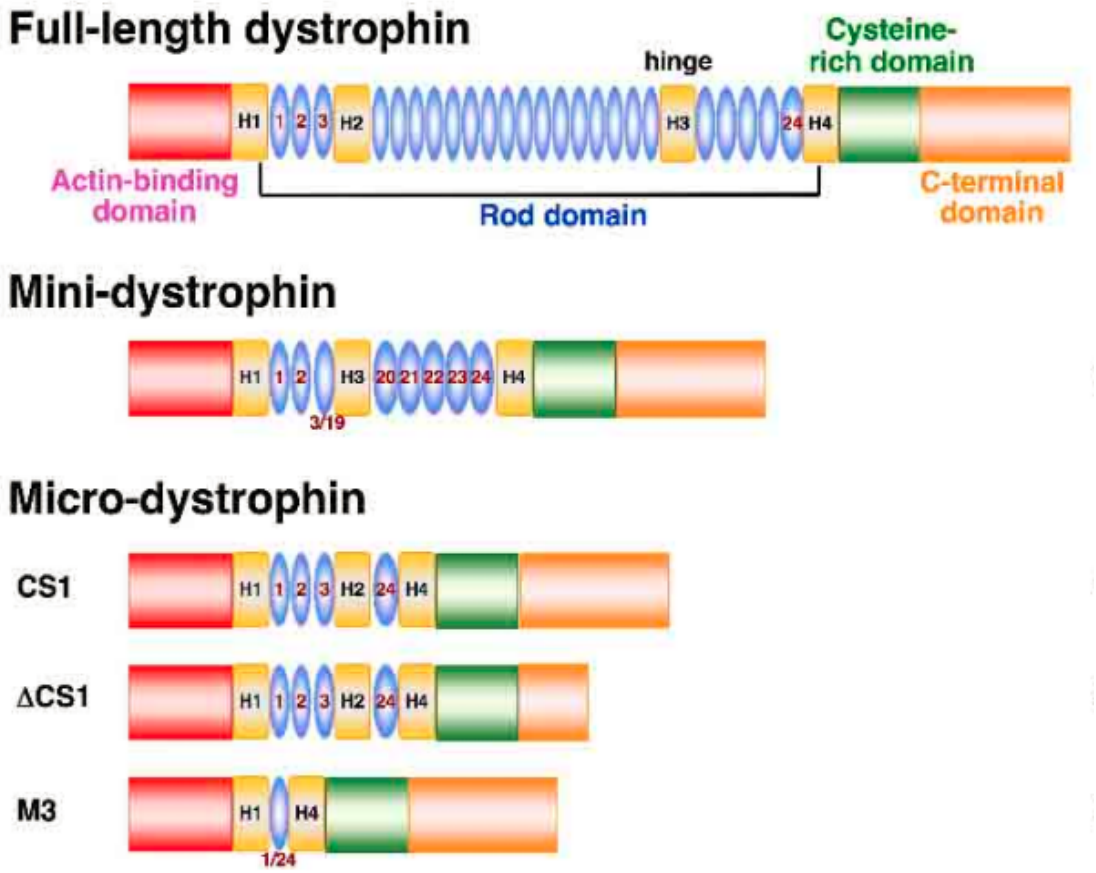

Figure 1.6 Mini and micro-dystrophin

This figure shows one mini-dystrophin and 3 micro-dystrophins found to compensate for the lack dystrophin in DMD animal models. The spectrin-like repeat of these proteins is indicated and compared to wild type protein (Figure taken and modified from DMDHelp.org).

1.6.2.1 Viral vector-based gene addition therapy

1.6.2.1.1 Lentivirus

Murine retroviral vectors were the first vectors to be tested in gene addition therapy for DMD (Konieczny, Swiderski and Chamberlain, 2013). These vectors were capable of successfully transducing proliferating myoblasts. *Mdx* mice were injected with this vector containing a mini-dystrophin construct, and only a small portion of fibres at the injection site expressed the construct (Dunckley *et al.*, 1993). Due to this poor outcome with murine retroviral vectors, new retroviral vectors were generated based on human or feline lentiviruses (Konieczny, Swiderski and Chamberlain, 2013). The lentivirus has a capacity of approximately 8kb and efficiently transduces non-cycling cells including muscle fibres (Naldini *et al.*, 1996; Kafri *et al.*, 1997). Lentiviral delivery of a GFP-dystrophin fusion was shown to be successful in both skeletal muscle and resident satellite cells when injected into neonatal *mdx* mice (Kimura *et al.*, 2009). With all of this said, lentiviral vectors have a high chance of inducing an immune response when used in high doses, which would be required for transduction in humans. Another problem with the use of lentiviral vectors is their ability to integrate into the host genome, and this gives rise to the risk of insertional mutagenesis (Konieczny, Swiderski and Chamberlain, 2013).

1.6.2.1.2 Adenovirus

Adenoviruses are medium-sized, non-enveloped viruses that carry a double-stranded DNA genome. The wild type adenovirus has a capacity of approximately 35kb (Konieczny, Swiderski and Chamberlain, 2013). Adenoviruses can successfully transduce

both dividing and non-dividing cells, and this makes them attractive for the treatment of muscle fibres (Dai *et al.*, 1995). Furthermore, adenoviral infection with the most common serotype has shown minimum pathogenicity in human populations and is therefore considered safer than lentiviral vectors.

First- and second-generation adenoviral vectors were constructed and modified to have a capacity of 8kb. A first-generation adenoviral vector was the first vector to successfully deliver a miniaturised human dystrophin cDNA into *mdx* mice (Ragot *et al.*, 1993). Following this, first- and second-generation adenoviral vectors showed leaky expression of remaining viral proteins *in vivo*, leading to a host immune response (Konieczny, Swiderski and Chamberlain, 2013).

To improve the adenoviral vector delivery technique viruses were 'gutted', where the vector backbone was eliminated of all viral coding sequences, allowing the vector to carry the whole dystrophin gene (Haecker *et al*., 1996). These vectors have reduced the immune response, improved transgene expression and a larger transgene carrying capacity (Schiedner *et al.*, 1998). Despite the improvements in these vectors, neutralising antibodies were found to be produced against them straight after first administration, preventing repetitive administration, which makes them of no use in the case of humans where repetitive administration is required for persistence and long-term transduction (Morral *et al.*, 1999). Therefore, improvements are required to make the use of adenoviral vectors safe in gene therapy.

1.6.2.1.3 Adeno-associated virus (AAV)

Another common vector used in gene therapy are the adeno-associated vectors. Many AAV vectors efficiently transduce skeletal muscle fibres, and the resulting gene

expression can be persistent for years in healthy muscle (Gilbert *et al.*, 2003). Several serotypes of AAV even have a natural tropism for skeletal muscle (Schultz and Chamberlain, 2008). Recombinant AAV (rAAV) vectors have all their viral genes deleted. rAAV vectors are good candidates for gene therapy in DMD, but their limited capacity is the limitation. This limitation has led to them being used to deliver micro or mini dystrophin genes shown to be successful in neonatal and adult *mdx* mice(Gregorevic *et al.*, 2004). Other approaches such as trans-splicing also make use of the rAAV. Here the gene is split into two one with a splice donor and one with splice acceptor site. They are delivered using different vectors co-transfected in cells (Lai *et al.*, 2005; Liu *et al.*, 2005). This method potentially enables rAAV-mediated delivery of full-length dystrophin, though this would require three vectors.

Several clinical studies have been initiated to test the safety and tolerability of AAV micro-dystrophin which have shown very promising results in preclinical data (Chamberlain, 2017)

1.7.2.2 Non-viral gene therapies

1.7.2.2.1 Unencapsulated plasmids

In the early nineties, it was reported that gene expression could be achieved by injection of naked plasmid DNA (Wolff *et al.*, 1990). The simplicity, low cost and safety of this method outweighed the low initial efficacy of gene transfer it showed, and so it became very attractive for further investigations and optimisations. *Mdx* mice were injected with plasmids (both locally and systemically) and have shown expression of dystrophin persisting 6 months as well as an increase in peripheral nuclei indicating increased

muscle regeneration (Liang *et al.*, 2004). A clinical trial was carried out with a group of 9 Duchenne and Becker patients ({Romero, Norma B and Braun et al., 2004). Plasmids of full-length dystrophin were injected into the radial muscle of patients. Using low dose injections 6 patients showed moderate dystrophin expression. Further to this, no adverse effects were observed from the treatment.

Although it was shown that dystrophin positive fibres were stable in *mdx* mice following intra-arterial delivery the number of plasmid DNA molecules decreases over time(Molnar *et al.*, 2004; Sandri *et al.*, 2004). In order to prevent this limitation of plasmid DNA decreasing over time it was suggested that co-administration of the plasmid with phage integrase could mediate the integration of plasmids into the mammalian genome(Bertoni *et al.*, 2006). The study carried out by Hence, Bertoni *et al.* showed sustained higher levels of dystrophin expression. However the risk of insertional mutagenesis limits the application of this approach (Maherali, 2007).

1.7.2.2.2 Antisense oligonucleotide-induced modulation of splicing

Pre-mRNA Splicing

The main focus of this thesis will be using small antisense oligonucleotide (AON) reagents to modulate gene expression either through masking of key regulatory elements such as the polyA signal or through modulating splicing of pre-mRNA to disrupt the translational reading frame. The mechanisms of pre-mRNA splicing will initially be discussed

The mammalian genome is made up of short exons (50-300 nucleotides) with longer intronic sequences in between (Black, 2003). Exons are defined by 5' splice sites, which

act as splice donor sites, the branchpoint followed by a pyrimidine-rich region and the 3' splice site, which acts as a splice acceptor site

In a mature mRNA, introns are spliced out, and exons are joined together. This process occurs in pre-mRNA and is catalysed by the spliceosome complex made up of small nuclear RNAs (snRNA) and 50-100 non snRNP (small nuclear ribonucleoproteins) factors. The snRNAs work by binding to the pre-mRNA sequence and identify the 5' splice site, branch point and 3' splice site. There are no strong splice consensus sequences identified (Cartegni *et al*., 2002).

Initially, an early complex is formed on the pre-mRNA; it is made up of the U1 snRNP binding to the s5' splice site, the U2 snRNP auxiliary factor ($U2AF^{65}$) binding to the pyrimidine-rich region, and $U2AF^{35}$ to the 3' splice site (Mollet *et al.,* 2006). $U2AF^{65}$ then recruits U2 snRNP to the branch point, leading to U1 being displaced by a U4-U5-U6 snRNP complex forming the B complex. U4 is then displaced forming the catalytically active spliceosome C complex with U6 snRNP interacting with U2 snRNP. This is followed by two transesterification reactions which join the two exons together and release the intervening intron in a branched lariat structure (Black, 2003). The intron is very shortly after splicing dissociated from the snRNPs and degraded; snRNPs, on the other hand, are recycled and used in a new round of splicing. The spliced pre-mRNA then undergoes 3' end processing where a polyA tail is added to the 3'end (for more detail see section 1.3). The mature mRNA is then exported out of the nucleus into the cytoplasm to undergo translation (Proudfoot, et al, 2002).

As mentioned, splice donor and acceptor sites are very weakly defined (Zhang, 1998). Additional sequences in the exons are used in order to distinguish correct splice sites

from pseudo splice sites, which are very similar to splice sites but are never used, (Faustino and Cooper, 2003). These additional sequences are termed exonic splicing enhancers (ESE) and exonic splicing silencers (ESS).

ESEs are located 80-120 bases away from exon splice acceptor sites. ESEs bind SR (serine/arginine-rich) proteins to enable exon recognition (Wu *et al.,* 2005). At weakly defined exons, SR proteins bind to ESE sequences and recruit snRNPs, aiding the initiation of splicing but not directly participating in the splicing mechanism (Wong *et al.,* 2005; Cortegni *et al*., 2002).

ESS sequences interact with negative regulatory proteins such as heterogeneous nuclear ribonucleoprotein (hnRNP) (Cartegni *et al*., 2002).

Pre-mRNA can also be alternatively splices leading to several different isoforms of the gene. In these cases, the pre-mRNA contains certain exons that are always required to be included in the transcript to maintain the reading frame, as well as alternatively spliced exons which can be spliced and not disrupt the reading frame (Black, 2003).

15% of point mutations that lead to human disease cause splicing defects, and though the mutations can be some distance away from the splice site they often alter ESE sequences, disrupting splicing (Krawczak *et al*., 1992).

Antisense oligonucleotide reagents

Antisense oligonucleotides (AON) are synthetic, short nucleic acids that are made complementary to target sequences and hence bind RNA or DNA through Watson Crick base pairing. (Danckwardt, Hentze and Kulozik, 2008; van Roon-Mom and Aartsma-Rus, 2012). The use of AONs to target the pre-mRNA is one of the most widely studied gene therapy approaches used, particularly in the correction of aberrant splicing or the

restoration of the functional reading frame (Figure 1.8). In addition to this AONs can also be used to knockdown or reduce the expression of a gene by skipping an out of frame exon (Veltrop and Aartsma-Rus, 2014) or skipping a fundamental regulatory sequence.

Regular RNA and DNA oligonucleotides are rarely used as alternative AON chemistries. Alternative chemistries (Figure 1.7) have been designed to improve affinity, increase stability in circulation and target cells and augment cell penetration and nuclear accumulation (Siva, Covello and Denti, 2014).

Phosphorothioate (PS) AONs have a sulphate atom in place of the non-bridging oxygen in the phosphate backbone. PS AONs have increased cellular uptake and resistance to nucleases but have decreased the affinity of AON to its target (Siva, Covello and Denti, 2014).

2'OMe and 2'OME have been synthesised by the addition of a methyl or methocyethyl group respectively. This modification renders the RNA-AON hybrid RNase H-resistant and also increases the affinity of the AON to its target (Sproat *et al.*, 1989). Most AON in this study has both the PS and the 2'O modification giving rise to both 2'OMe-PS and 2'O-MOE-PS. These AONs have a good safety profile and are relatively cheap to synthesise. 2'OMe-PS were the first AONs to be used for dystrophin exon-skipping in cultured primary muscle cells from *mdx* dystrophic mice (Dunckley *et al.*, 1998).

Another type of AON is the locked nucleic acid or LNA. The AON is made by the addition of a methylene bridge that connects the 2'O and the 4'Cof the ribose, clamping the nucleotide in the 'endo' formation. These LNAs have a high affinity for target nucleic acid but a low specificity. To increase specificity, a mixture of LNA and DNA backbone

sequence or LNA and 2'OMe backbone are used (Fabani and Gait, 2008; Siva, Covello and Denti, 2014).

Not all antisense oligonucleotide chemistries are negatively charged like the ones already discussed. Peptide nucleic acids (PNAs) and phosphorodiamidate morpholino oligomers (PMOs) are charge neutral AON. Both these AONs are resistant to exo- and endonucleases as well as RNase H-cleavage (Siva, Covello and Denti, 2014). PNAs have a high affinity to RNA and DNA targets and increase sequence specificity (Egholm *et al.*, 1993).

PMOs contain morpholine rings that are connected through phosphorodiamidate groups. PMOs are usually longer that 2'OMe-PS AONs due to their marginally lower affinity (Siva, Covello and Denti, 2014). A study by Schmajuk and colleagues demonstrated that an 18-mer PMO was more effective than a corresponding 18-mer 2'OMe-PS (Schmajuk, Sierakowska and Kole, 1999). Gebski and colleagues demonstrated that a 25-mer PMO targeting the dystrophin gene in the *mdx* mouse achieved higher exon skipping and dystrophin expression compared to the identical 2'OMe-PS version of the AON (Gebski *et al.*, 2003). A 30-mer PMO targeting exon 51 has proven to be successful in intramuscular clinical trials (Kinali *et al.*, 2009a) (Figure 1.8). IV administration of PMO chemistries are currently in clinical trials and showing promising results. Another clinical trial was also conducted using 2'OMePS targeting exon 51 of the dystrophin gene (van Deutekom *et al*., 2007). This trial was successful with patient biopsies after 4 weeks showing restoration of dystrophin in 64-97% of myofibres. The trial was discontinued due to limited efficacy after 5 weeks of treatment. Eteplirsen, a PMO targeting dystrophin exon 51, has received FDA approval (Rus and

Krieg 2016) . There are currently other PMOs targeting exon 52 and 45 in clinical trials (Motohashi et al 2019)

Due to their neutral charge, PMOs are difficult to transfect. Various cell-penetrating peptides have been designed to be conjugated to PMOs, generating pPMOs, and facilitate the delivery into cells *ex vivo* and *in vivo* (Siva, Covello and Denti, 2014).

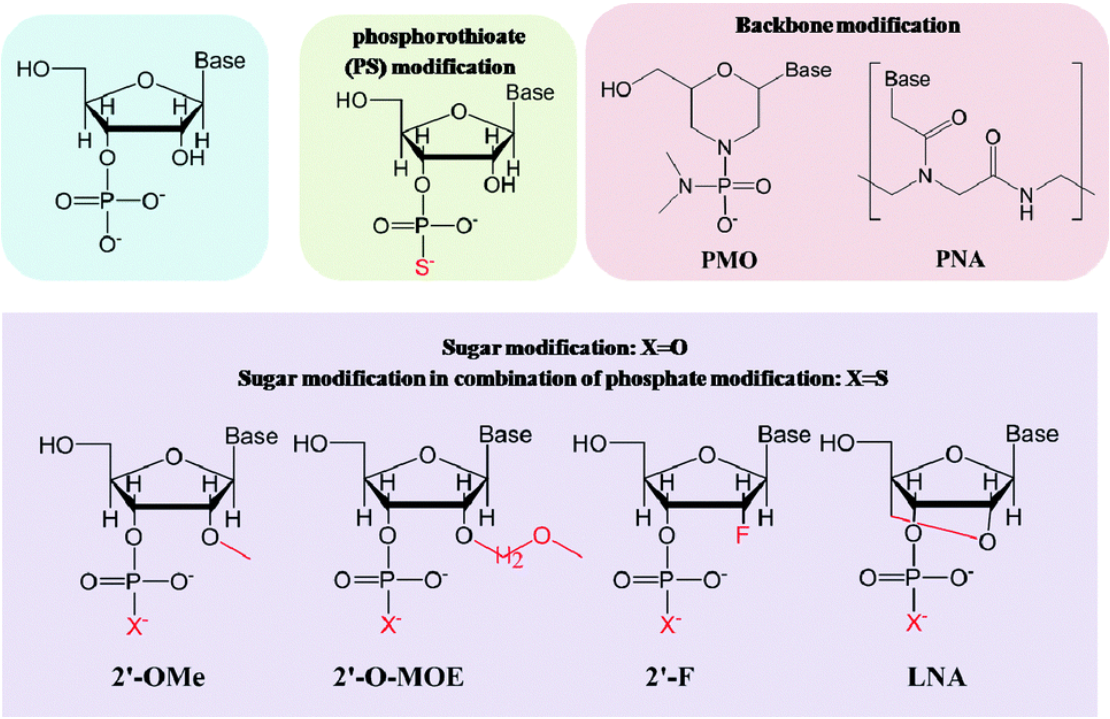

Figure 1.7 Antisense oligonucleotide chemistries

The figure shows the backbone of two adjacent nucleotides in natural DNA and in various types of modified oligonucleotides. For phosphorothioate (in yellow background) and second and third generation chemistries (in purple background) relevant modifications over natural DNA are shown in red (Figure from Li, Tan, Kooger, Zhang *et al.,* 2014).

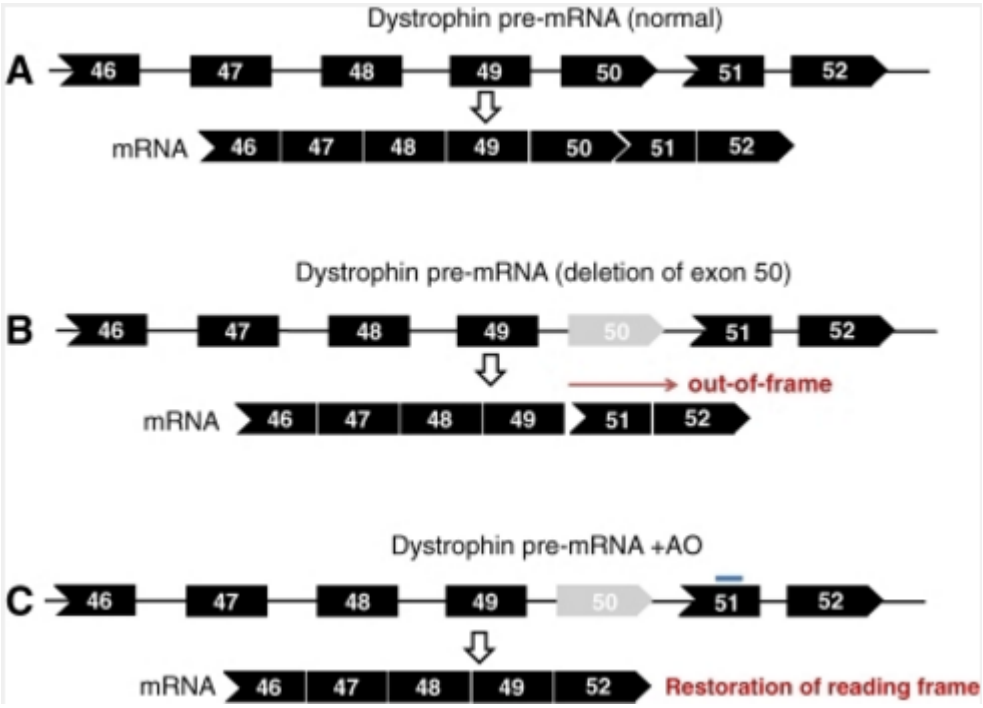

Figure 1.8 Exon 51 skipping therapy in DMD patients

An example of exon skipping to restore the reading frame of dystrophin in patients with a deletion of exon 50. A is a normal dystrophin transcript and mRNA. B shows deletion of exon 50 which disrupts the reading frame, leading to a premature stop codon, unstable mRNA and a truncated unstable protein. C portrays targeted skipping of exon 51 using antisense oligonucleotides (blue line), restoring the reading frame and producing a truncated but functional dystrophin that lacks exon 50 and 51 (Image from Sugita and Takeda, 2010).

1.7 Fibrosis and DMD

Most emphasis in therapeutic research of muscular dystrophy has been placed on correcting the genetic fault causing the disease in the case of DMD the correction of dystrophin expression. Little attention has been given to understanding and modifying the pathological background of the disease. Recently, therapeutic research has shown that the pathogenesis of the well-developed fibrosis and fat replacement affecting the muscle has a big impact on the outcome of treatment for restoring dystrophin expression. It is now well established that many of the pathological features of DMD are not only caused by the lack of dystrophin and/or the failure of satellite cells but are also due to the complex interactions of these cells with the surrounding environment (Kharraz *et al.*, 2014).

It is commonly assumed that the proliferation of connective tissue is a secondary phenomenon and even a compensatory mechanism in DMD patients for the lack of muscle regeneration. In contradiction, many researchers have reported an increase in endomysial tissue volume before any apparent muscle degeneration. It has been suggested that the increase in collagenous connective tissue could be a significant co-determining factor in DMD pathology including an adverse effect on the nutrition of the enclosed muscle cells (Bell and Conen, 1968; Duance *et al.*, 1980). A study was carried out over 10 years on 25 DMD patients examining the correlation of the severity of the pathology and the different pathological features including myofibre atrophy, necrosis and fatty degeneration. The study showed that endomysial fibrosis was the only myopathologic parameter that significantly correlated with poor motor outcome (Desguerre *et al.*, 2009). In DMD, membrane instability of muscles leads to constant

myofibre breakdown which is not compensated for by satellite cell proliferation. Inflammation following muscular necrosis leads to fibrotic remodelling of tissue and fatty cell replacement (Klingler *et al.*, 2012). These changes in the environment can delay existing muscle repair and regeneration and further enhance inflammation leading to disease exacerbation and further fibrosis development.

Fibrosis refers to the unregulated and excessive deposition of extracellular matrix (ECM) components. During normal repair and growth, there is a regulated and controlled deposition of ECM components, but excessive and uncontrolled deposition can lead to the replacement of tissue with fatty cells and loss of tissue function. In the case of DMD, there is an additional problem to loss of muscle function because of fibrosis, which is the loss of muscle fibres which can be targets for therapy and repair. It is therefore now clear that in order to treat DMD we also need to understand, address and treat fibrosis in this disease.

1.7.1 Molecular mechanism of fibrosis in DMD

1.7.1.1 Cation influx

Due to the lack of dystrophin and membrane instability in muscle fibres of DMD patients the cells have decreased resistance to mechanical shear and are prone to the excess influx of electrolytes such as calcium and sodium. The increase of intracellular sodium levels leads to ATP depletion as the Na^+/K^+ pumps must work to their full capacity in an attempt to restore homeostasis. Water molecules follow sodium into cells, and this leads to cellular oedema (Klingler *et al.*, 2012). At rest, the extracellular calcium concentration exceeds the cytoplasmic calcium concentration by a factor of 10,000. This

leads to calcium overload which causes mitochondrial uncoupling and reactive oxygen species (ROS) production (Klingler *et al.*, 2012). All these changes lead to downstream effects such as necrosis, accumulation of acidic metabolites and amplification of inflammatory substances such as cytokines (Klingler *et al.*, 2012) (Figure 1.9).

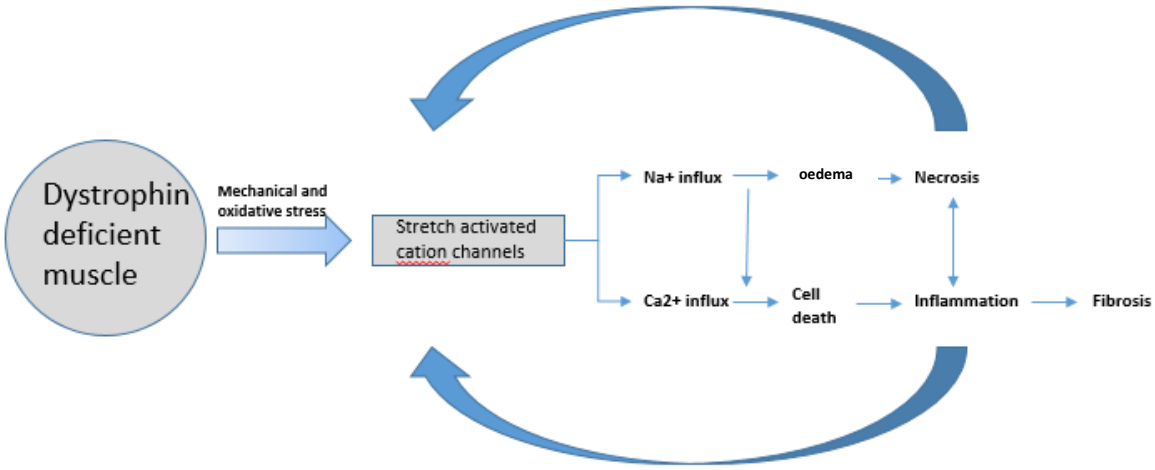

Figure 1.9 From dystrophin deficiency to fibrosis

Muscle fibre membranes lacking dystrophin are more vulnerable to mechanical and oxidative stress. Overuse and overstrain leads to activation of stretched activated cation channels. The high influx of sodium and calcium is not compensated for by pumps and so leads to oedema. The Oedema and calcium overload lead to energy depletion. Calcium a cascade of inflammatory processes. Further stress on the muscle membrane and activation of cation channels occurs. This leads to unsustainable cellular integrity. Myofibre necrosis and inflammation finally lead to tissue remodelling and fibrosis.

1.7.1.2 Acidosis induced tissue damage

Lactic acid produced by the dystrophic muscle breaks down into lactate (La^-) and H^+ at physiological pH. La^- in return increases collagen (a key component of the ECM) promoter activity leading to an increase in procollagen messenger RNA production and collagen synthesis (Trabold *et al.*, 2003). La^+ also causes an increase in vascular growth factor (VEGF) production in macrophages (Trabold *et al.*, 2003; Klingler *et al.*, 2012).

1.7.1.3 Fibrous tissue production

Fibrous tissue consists of extracellular fluid containing fibronectin, glycosaminoglycans and proteoglycans, in addition collagen fibres and elastin is also present in the ECM. Mechanical stimuli as well as chemotaxis is known to initiate the production of fibrous tissue (Klingler *et al.*, 2012). The main cells present in fibrous tissue are fibrocytes and myofibroblasts. Precursor cells differentiate into these cells with different stimuli (Figure 1.10). Fibrocytes and myofibroblasts are present for the short term during tissue repair such as that in wound healing. In DMD, myofibroblasts are persistently activated due to the continuous presence of stimuli as myofibres continue to break down. This results in an altered ECM. The composition of the ECM produced in fibrosis is different from that seen in healthy tissue, and the components mainly originate from myofibroblasts. In the early stages of fibrosis, the ECM has a high content of fibronectin and hyaluronan. This creates a much-hydrated matrix which aids cell migration to the area. This provisional matrix is then replaced with a denser ultrastructure (Kjær *et al.*, 2009; Klingler *et al.*, 2012). There are various growth factors and cytokines involved in the process of fibrosis; some key players are discussed here.

1.7.1.3.1 Transforming growth factor β (TGF-β)

Transforming growth factor β (TGF-β1) is one of the most important profibrogenic factors that not only stimulates ECM component transcription but also leads to fibrocyte and myofibroblast differentiation (Bowen, Jenkins and Fraser, 2013). Latent TGF-β1 is stored in the ECM where it is activated upon tissue damage or by other growth factors (Horiguchi, Ota and Rifkin, 2012). TGF-β1 is expressed in regenerating muscle after injury and in dystrophic muscle of DMD patients and *mdx* mice (Zhou *et al.*, 2006; Ardite *et al.*, 2012; Kharraz *et al.*, 2014). Here TGF-β1 stimulates fibroblasts to produce ECM proteins like collagen and fibronectin as well as proteins required for ECM deposition such as periostin (POSTN). TGF-β1 and other profibrogenic polypeptides can also be produced by infiltrating immune, inflammatory, mesenchymal and tissue-specific cells (Wynn, 2008; Kharraz *et al.*, 2014).

TGF-β1 is known to signal through the canonical TGF-β1 signalling pathway or other alternative pathways (Figure 1.10). It has been shown that the extent of signalling through these different pathways modulates fibrotic effect. In fibroblasts, the canonical signalling pathway works through phosphorylation of Smad2 and 3 which then bind to Smad4 to form a complex targeting the nucleus and activating transcription of profibrotic genes (Wynn, 2007; Samarakoon *et al.*, 2013; Kharraz *et al.*, 2014). TGF-β can also signal through Ras/MEK/ERK, P38 MAPK, c-abl, and NJK pathways (Shi and Massague, 2003). Signalling through these pathways changes gene expression in a promoter selective fashion. For example, signalling through ERK is required for collagen I expression whereas FAK, NJK and TAKI are required for ECM contraction and myofibroblast differentiation (Shi-Wen *et al.*, 2009; Kharraz *et al.*, 2014).

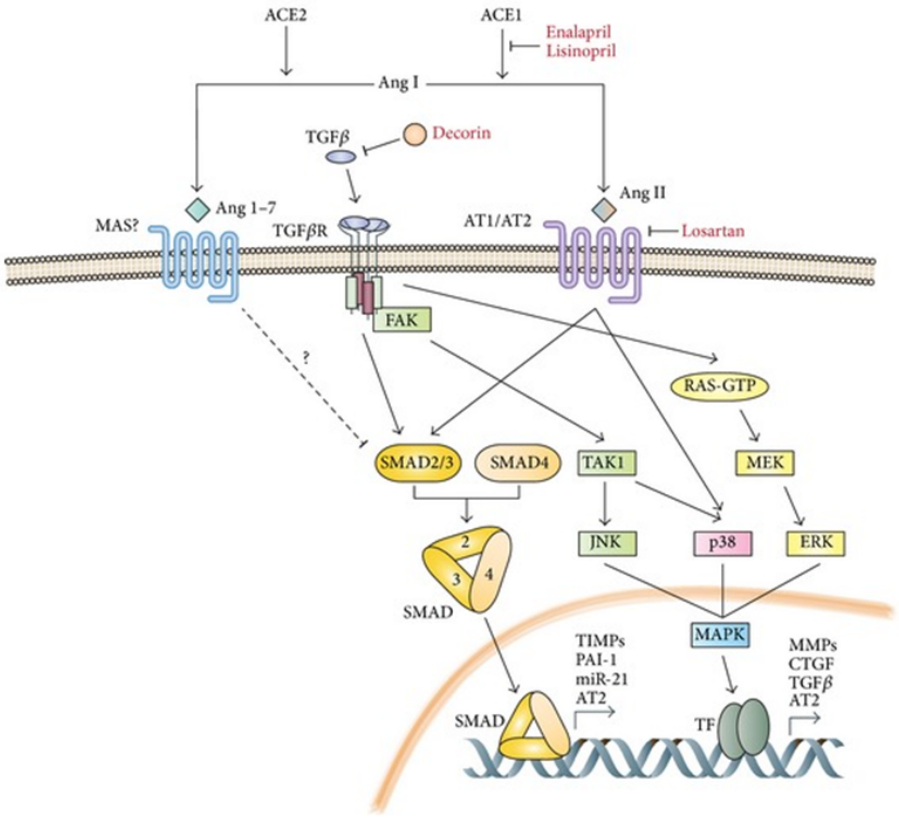

Figure 1.10 TGF-β Signalling

TGF-β is known to signal through the canonical TGF-β signalling pathway or other alternative pathways. The canonical signalling pathway works through phosphorylation of Smad2 and 3 which then bind to Smad4 to form a complex targeting the nucleus and activating transcription of profibrotic genes. TGF-β1 also signals through Ras/MEK/ERK, P38 MAPK, c-abl, and NJK pathways leading to promoter selective gene expression. AngII also signals through AT1 and AT2 leading to Smad activation and increased expression of profibrotic genes. (Image taken and modified from Kharraz et all 2014)

1.7.1.3.2 Connective tissue growth factor (CTGF)

In addition to TGF-β signalling through smad in the fibrotic pathway, the renin-angiotensin pathway also signals through smad as well as P38 to increase TGF- β and connective tissue growth factor (CTGF) which has also been found to have an important role in fibrosis (Figure 1.10).

CTGF is a non-structural regulatory protein present in the ECM. Dystrophic muscle from DMD patients as well as the dystrophic dog and the *mdx* mouse all show elevated levels of CTGF (Sun *et al.*, 2008). CTGF has also been shown to reproduce effects of TGF- β, a good example being its ability to increase collagen type 1, α5 integrin and fibronectin expression in fibroblasts (Morales *et al.*, 2013; Kharraz *et al.*, 2014). It is therefore established that the renin-angiotensin system along with the TGF- β system are key signalling pathways in the process of fibrosis.

1.7.1.3.3 Inflammatory cells and cytokines

One of the first events following damage to tissue is the infiltration of inflammatory cells in the site of injury. In response to muscle injury, the first cells that infiltrate the muscle are principally neutrophils and macrophages (Arnold *et al.*, 2007). Disruption in the organised and coordinated initiation, progression and resolution of inflammation can cause persistent muscle damage, impairment of regeneration and so the development of fibrosis (Kharraz *et al.*, 2014).

1.7.1.3.3.1 Macrophages

Studies carried out on the diaphragm of the *mdx* mouse have shown that macrophages are an important source of TGF- β suggesting they have a role in the development of

fibrotic tissue (Zhou *et al.*, 2006). Further investigation into the role of macrophages in fibrosis revealed that not all macrophages have a profibrotic role. More and more studies show evidence of M2, or alternatively activated, macrophages being profibrotic as appose to the M1, or classically activated, macrophages which have more of a proinflammatory role (Gordon, 2003).

M2 macrophages are activated by Th2 derived cytokines such as IL-13. Further to this IL-13 in conjugation to TGF- β amplify the expression of arginase I, a key enzyme in the initiation of collagen synthesis in fibroblasts, in M2 macrophages (Wynn, 2004). In support of this, it has been demonstrated that M2 macrophages are expressing TGF- β and arginase I are present in the *mdx* diaphragm; and this expression increases with age correlating with an increase in IL-13 (Kharraz et al., 2014, Vidal et al 2008).

Having discussed the important role of M2 macrophages in fibrosis development, it is important to mention that though M1 macrophages are proinflammatory, they could have a role in sustaining chronic inflammation which is an important cause of fibrosis. This has been indicated by looking at fibrinogen and its signalling through Mac-1 which is expressed on M1 macrophages. Fibrinogen stimulates expression of proinflammatory cytokines and chemokines, thereby potentially promoting muscle degeneration (RYU, DAVALOS and AKASSOGLOU, 2009; Kharraz *et al.*, 2014).

1.7.1.3.3.2 Lymphocytes

Lymphocytes, in particular, T helper (Th) and cytotoxic cells (CTL), have also been suggested to have a role in the development of fibrosis in muscular dystrophies. Studies done in the scid/mdx mouse, which lack T and B lymphocytes, showed a decrease in fibrosis in the diaphragm which correlates with a decrease in TGF- β protein in the

dystrophic muscle (Farini *et al.*, 2007). To identify which lymphocyte is responsible for the decrease in fibrosis in the scid/mdx mice further studies were carried out in the mouse mode of immunodeficiency, the nu/nu/mdx mice, which lacks functional T cells but not B cells (Morrison, Lu, Pastoret, Partridge, & Bou-Gharios, 2000). Studies using antibodies against Th and CTL cells showed that both T cells contribute to the development of fibrosis in the *mdx* mice (Wehling, Spencer and Tidball, 2001).

1.7.2 Treatment of fibrosis

While it is generally perceived that gene therapy is used to address the core cause of the disease, ie the missing gene, treatment in order to prevent fibrosis or its progression should be seen as adjunct therapy for muscular dystrophy. There are three main reasons that targeting fibrosis is very important in the future of gene therapy for DMD (Kharraz *et al.*, 2014). The most obvious reason is that the presence of fibrotic tissue and replacement of muscle with fibrous tissue interferes in gene and cell therapies as it reduces the amount of available tissue for therapy. Secondly preventing fibrosis on its own can significantly improve quality of life and lifespan of dystrophic patients (Kharraz *et al.*, 2014). Thirdly Pharmacological treatments targeting fibrosis are being tested, and some show very good results in human and animal models(Abdel-Hamid and Clemens, 2012).

1.7.2.1 Targeting the RAS

Losartan targets the angiotensin 2 type 1 receptor involved in the RAS (Figure 1.11) (discussed above). Losartan is commonly used to lower blood pressure but administration in dy(2J) /dy(2J) mice, with laminin 2α deficient congenital muscular

dystrophy, has been shown to increase muscle strength and ameliorate fibrosis(Elbaz *et al.*, 2012) . Another study on mdx mice has also shown decrease cardiac fibrosis upon losartan administration (Bish *et al.*, 2011).

Another drug targeting the RAS is Lisinopril. Lisinopril is an ACE-inhibitor (Figure 1.11) and has been shown to preserve cardiac and skeletal muscle integrity in *mdx* mice (Rafael Fortney 2011). A clinical trial has been started comparing Lisinopril and Losartan in a double-blind randomised trial on human DMD patients (Allen *et al.*, 2013; Kharraz *et al.*, 2014). So far both drugs have shown to be effective in tackling dilated cardiomyopathy. Interestingly administration of angiotensin1-7n contrast to angiotensin 2, inhibited TGF-β smad signalling and decreased a number of fibroblasts leading to lower fibrosis (Acuña *et al.*, 2014).

1.7.2.2 Targeting the growth factor and cytokines

Antibodies against profibrotic growth factors have been shown to decrease fibrosis. FG-3019 antibody which neutralises CTGF as well as antibodies against TGF-β have been shown to slow down fibrosis and improve phenotype of *mdx* mice (Andreetta *et al.*, 2006).Having said this, these growth factors are pleiotropic and targeting them has many undesired side effects such as increased amount of CD4+T cells infiltrating muscle (Andreetta *et al.*, 2006). Severe immune dysregulation has been shown in TGF-β1 knockout mice, where approximately 2 weeks after birth mice showed severe wasting syndromes and death (Christ *et al.*, 1994).

Imantinib, a tyrosine kinase inhibitor and a cancer drug, has been shown to be beneficial for muscular dystrophy when tested in *mdx* mice (da Silva Bizario *et al.*, 2009). Imantinib

has been shown to target mesenchymal proginators specifically by inhibiting their proliferation and expression of fibrosis markers *in vitro* (Ito *et al.*, 2013). Halofuginone, a synthetic halogenated derivative of febrifugine, is an anti-inflammatory molecule and has been shown to significantly improve muscle histopathology and fibrosis in the dysferlin-deficient mouse (Sundrud *et al.*, 2009). A clinical trial was carried out to assess the safety of halofuginone in DMD patients, but results are not yet available.

Although anti-inflammatory molecules, as well as drugs targeting the fibrotic signalling pathways, have shown encouraging results in animal models very few, have currently progressed into clinical trials in DMD patients.

1.8 Periostin

Periostin (POSTN), originally known as osteoblast-factor 2, was first identified in mouse osteoblastic cell line (Takeshita 1993, thesis). It was later named periostin due to its expression in the periodontal ligament and the periosteum in the adult mice. The human homologue was found using murine cDNA as probes (Takeshita 1993, Hoersch 2010).

1.8.1 Periostin gene and protein

In the human genome, *POSTN* is 36 kilobases, found on chromosome 13 and contains 23 protein-coding exons (Figure 1.11) (Hoersch and Andrade-Navarro, 2010). The POSTN protein is made of an N-terminal region, a cysteine-rich Emilin-Like (EMI) domain, four repeats of FAS1 domain and a C terminal domain (Takeshita *et al.*, 1993; Hoersch and Andrade-Navarro, 2010). Exon 1 codes for 23 amino acids that make up the N terminal signal sequence. This signal sequence lacks a transmembrane domain indicating

POSTNis a secreted protein. Exons two and three code for the EMI domain which is involved in protein-protein interactions (Callebaut *et al.*, 2003). The FAS1 repeats, which are homologous to the insect axon guidance protein fascilin 1, are coded for by exon 3-14. The FAS1 domains are thought to be involved in cell adhesion and protein-protein interactions. Proteins such as bone morphogenic protein-1(BMP1), tenascin C, and integrins are reported to bind to POSTN at the FAS1 domain (Kim, Kim and Lee, 2000; Kii *et al.*, 2010; Maruhashi *et al.*, 2010). Exon 16-23 encode for the C terminal domain which doesn't contain many known motifs. Exon 17-21 are subjected to alternative splicing, and therefore there are various POSTN isoforms ranging in size from 83-93 kDa (Morra and Moch, 2011). A nuclear localisation signal present in the C terminal domain is encoded by exon 22-23 and indicates an intracellular role of POSTN (Litvin, Selim and Montgomery, 2004; Hoersch and Andrade-Navarro, 2010). In addition to this, there is a hairpin binding site in exon 23 which provides a potential site for glycoproteins and proteoglycans.

Secondary structure studies have shown consecutive beta strands present in the C terminal domain of POSTN. These beta strands are thought to play an important part in facilitating the binding of POSTN to collagen and fibronectin (Hoersch and Andrade-Navarro, 2010). The interaction of POSTN with the ECM is therefore affected by the number of beta strands present in the C terminus of the mature protein, and that's dictated by alternative splicing (Hoersch and Andrade-Navarro, 2010).

Nine *POSTN* splice variants have been reported on ENSEMBEL with six splice variants being protein coding. *POSTN* splicing is regulated in multiple tissues, and additional *POSTN* splice variants are expressed in lung and kidney during foetal development

(Morra *et al.*, 2012). *POSTN* alternative splicing and the specific function of each isoform is not very well understood, having said that tissue-specific expression of certain isoforms have been reported with isoform 6 detected in renal tissue but not in lung and isoform 1 expressed in breast, ovary and heart tissue while isoform 3 is expressed in adipose, colon, kidney, lymph and prostate (Viloria and Hill, 2016)(ENSEMBEL accessed March 2016).

Research in bladder cancer has revealed that the bladder cancer tissue had lost the full-length mRNA, isoform 1, but commonly expressed isoform 4. This variant showed to be unable to inhibit cell invasion and metastasis that were observed in isoform 1, and 3 suggesting that switching from isoform 1 to alternative splicing is involved in bladder cancer metastasis (Bai *et al.*, 2010). Bai et al identified eight coexisting isoforms of POSTN in the thyroid, this is the first time eight isoforms have been reported in the same issue (Bai *et al.*, 2010).

Of the nine reported splice variants only four have been fully sequenced, and many further studies are needed to characterise these splice variants and assess their function and differences In interacting with various ECM components.

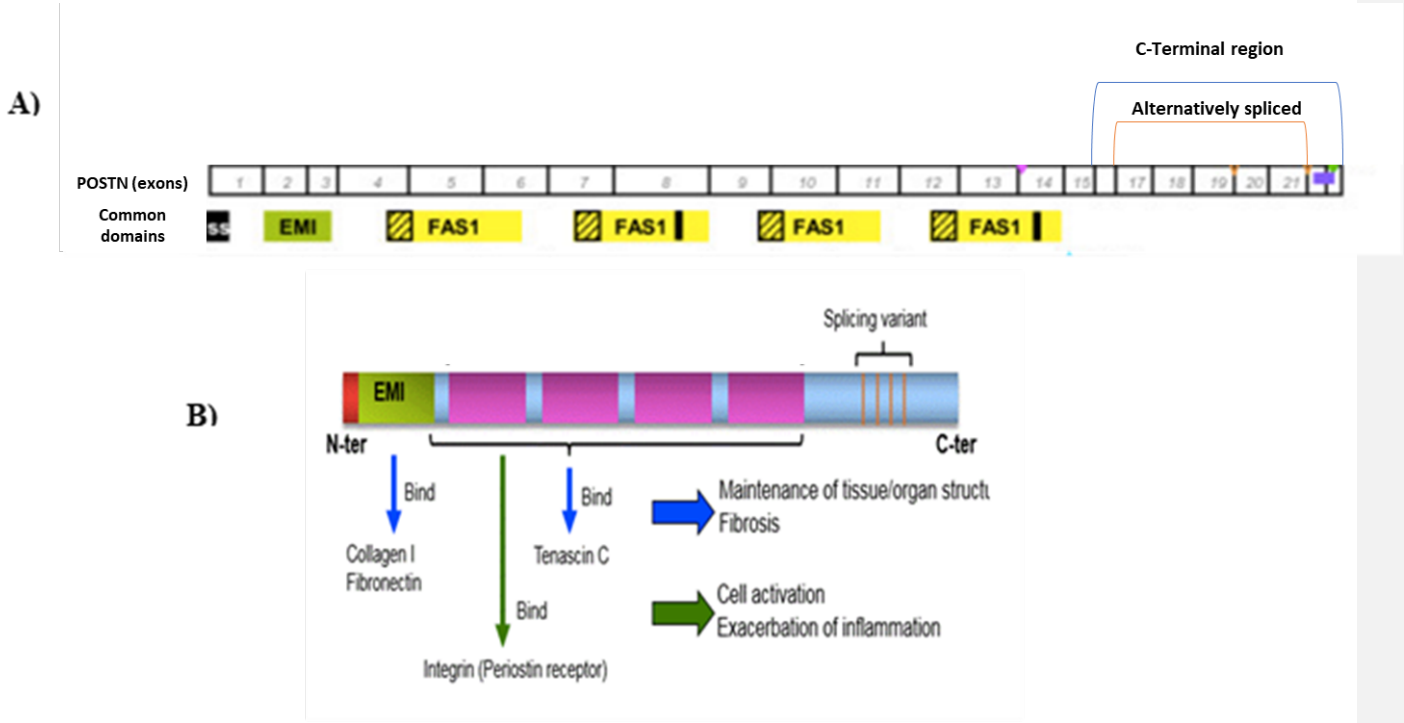

Figure 1.11 *POSTN* gene and periostin protein

A) Showing 23 exons of the *POSTN* gene and portraying which domain of the protein each exon codes for. B) Showing the function of different domains in POSTN. The FAS1 repeats are involved in tenascinC binding as well as interaction with integrins. The EMI domain is responsible for binding of collagen-I and fibronectin. (Figure A modified from www. Shino-test.co and Hoerch and Navarro 2010).

1.8.2 Role of Periostin

POSTN is classified as an extracellular protein. This means that POSTN does not directly serve a structural role in the ECM but is a link between the ECM and cells and helps modify cellular response to external stimuli (Bornstein *et al.*, 1995).

POSTN has been shown to interact with a several structural ECM proteins such as collagen I and V, fibronectin and tenascin-C (Takayama, Arima and Kanaji, 2006; Norris, Damon and Mironov, 2007; Kii *et al.*, 2010) as well as interacting with bone morphogenic protein 1 (BMP-1) which promotes proteolytic activation of lysyl oxidase required for collagen cross-linking (Kii *et al.*, 2010). POSTN has also been shown to serve as a ligand for of integrins such as $\alpha v\beta 3$ and $\alpha v\beta 5$ and promote cell motility and has been shown to promote tumour cell survival through PI3K/Akt in human colon cancer cells and pancreatic ductal adenocarcinoma cells cultured *in vitro* (Bao, Ouyang and Bai, 2004; Baril, Gangeswaran and Mahon, 2007).

As with other matricellular proteins, POSTN is expressed at low levels in most normal adult tissue but is up-regulated during embryonic development and in response to injury. POSTN is expressed at very low levels in the adult heart but is up-regulated in severe heart disease such as dilated cardiomyopathy, myocardial hypertrophy or myocardial infarction (Zhao *et al.*, 2014). Up-regulation of POSTN in myocardium infarction plays an important role in early scar formation and collagen deposition preventing cardiac rupture (Oka, Xu and Kaiser, 2007; Shimazaki, Nakamura and Kii, 2008). POSTN has also been shown to be highly expressed locally during renal disease contributing to fibrotic tissue replacement and loss of healthy tissue architecture in the kidneys (Mael-ainin *et al.*, 2014). Mael Ainin et al. demonstrated that renal inflammation

and fibrosis could be reduced with the inhibition of POSTN using antisense oligonucleotides. A recent proteomic study has also shown that in Duchenne muscular dystrophy POSTN expression is up-regulated more than any other protein (Ozdemir et al 2014). A study by Lorts et al. demonstrates genetic knockdown of POSTN in the *Sgcd-/-* model of muscular dystrophy leads to reduced muscular dystrophy and fibrosis by modulating the TGF-β pathway (Lorts *et al.*, 2012).

POSTN null mice have been generated and as expected with matricellular proteins lack of POSTN results in subtle abnormalities in the mouse which look normal at birth, and there is no embryonic lethality (Rios, Koushik and Wang, 2005; Oka, Xu and Kaiser, 2007). Serious abnormalities become apparent as the mouse gets older and is exposed to injury. Approximately 15% of POSTN-null mice die in the first three weeks due to cardiac defects (Rios, Koushik and Wang, 2005; Snider, Hinton and Moreno-Rodriguez, 2008). POSTN null mice show delayed wound healing due to defective re-epithelialization and decreased myofibroblast population (Nishiyama *et al.*, 2011; Ontsuka *et al.*, 2012). These mice also have increased the rate of cardiac rupture following myocardium infarction, and this is due to impaired collagen fibrillogenesis and myofibroblast differentiation (Oka, Xu and Kaiser, 2007; Shimazaki *et al.*, 2008). Decreased bone formation and mass are also evident in these mice due to defects in collagen fibrillogenesis and osteoclast inactivation in the periosteum (Bonnet *et al.*, 2009; Merle and Garnero, 2012).

Based on the above observations POSTN has a role in the repair process across the body and is also heavily involved in the process of fibrosis and scar formation. The

matricellular nature of POSTN and its role in repair and specifically in fibrosis has made it an attractive candidate for tackling fibrosis.

1.8.3 Mechanistic view of periostin function

A shown in the diagram below (Figure 1.12) following injury macrophages and neutrophils (in the case of inflammation) and other types of cells such as muscle cells (in the case of mechanical stress induced injury) begin expressing TGF-β and/or IL-4 and IL-13 (Takayama, Arima and Kanaji, 2006; Kudo, 2011). The expressed cytokines induce the expression of POSTN, fibronectin and tenascin-C in fibroblasts. Some POSTN is secreted and placed in the ECM where it interacts with integrins such as $\alpha v\beta 3$ on myofibroblasts and induces their cell migration. The myofibroblasts then, in turn, express type I collagen to repair the tissue. Inside the cell, POSTN comes together with tenascin C to form a meshwork with fibronectin to produce a scaffold for the cross-linking of type I collagen. POSTN is also involved in the cross-linking in that it associated with BMP-1 activating lysyl oxidase to enhance cross-linking inside the cells.

Consistent damage or stress on a tissue leads to an over-protective reaction by POSTN leading to pathological fibrillogenesis which gives rise to fibrosis. In the studies mentioned above in the roles of POSTN, it was discussed that many studies have looked at deletion or inhibition of POSTN in disease and seen a considerable reduction in fibrosis and maintenance of normal tissue architecture. This portrays POSTN's role in tight collagen fibre formation.

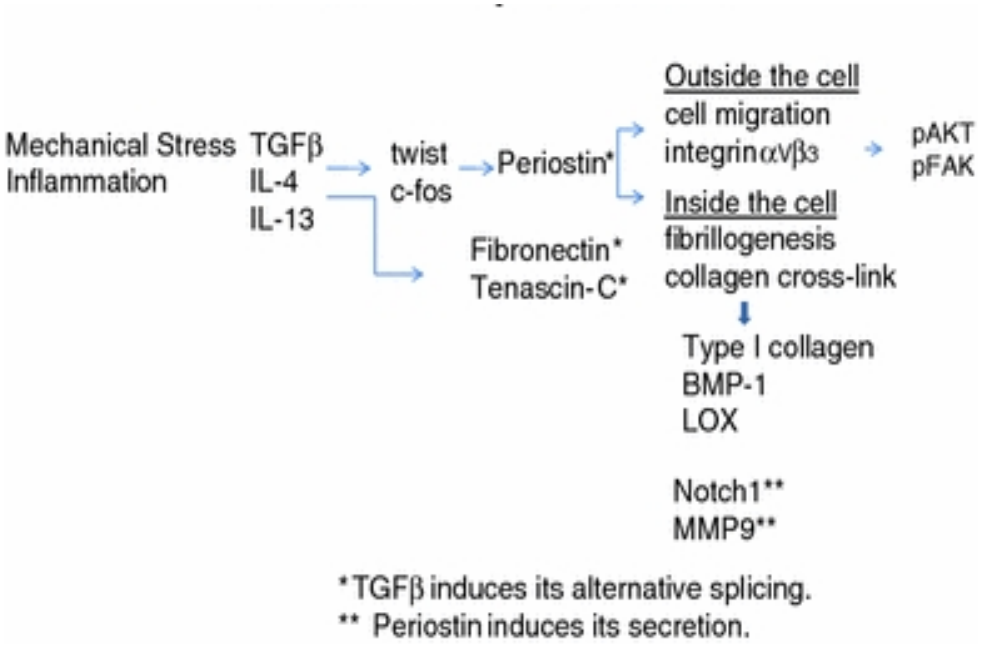

Figure 1.12 Mechanistic view of POSTN function

Mechanical stress and inflammation lead to the expression of chemokines and TGF-β from inflammatory cells or muscle cells under mechanical stress. These chemokines and growth factor induce expression of POSTN and other ECM proteins such as fibronectin and tenascin C. In the event of repair or fibrosis the POSTN forms a meshwork with tenascin C and fibronectin for collagen I to be incorporated and cross-linked (Figure taken and modified from Kudo 2011).

1.9 Myostatin

Myostatin or growth and differentiation factor 8 (GDF-8) was discovered in 1997 in a screen for novel mammalian members of the transforming growth factor(TGF-β) (McPherron, Lawler and Lee, 1997). The expression pattern of myostatin suggested that it could be involved in the regulation of muscle function and development. The involvement of myostatin was confirmed when myostatin-deficient mice were generated and were shown to have a significant increase in muscle mass (McPherron, Lawler and Lee, 1997). It is now clear that myostatin acts as a negative regulator of muscle mass and it acts in part by inhibition and activation of satellite cells in skeletal muscle. Over the last few years, myostatin has emerged as a novel therapeutic target for the treatment of a range of disease that involves muscle degeneration including muscle dystrophies, cachexia, sarcopenia and a variety of chronic disease.

1.9.1 Conservation of myostatin

The myostatin gene is conserved across a broad range of species ranging from zebrafish to humans. The conservation of the myostatin sequence suggests conservation of function. One of the best-known phenotypes associated with Myostatin in nature is seen in the double muscle muscling phenotype in cattle; where mutations in the Myostatin gene have been shown to be responsible (McPherron, Lawler and Lee, 1997). Interestingly the zebrafish has shown to express myostatin in some non-muscle tissue such as the eyes, gill filament, gut, brain, ovaries and testes, as well as muscle tissue. (Rodgers and Garikipati, 2008).

1.9.2 Validation of myostatin as a therapeutic target

Myostatin-deficient mice were generated to investigate the role of myostatin. These mice showed a considerable increase in muscle mass. These models confirmed the hypothesis that myostatin is involved in the regulation of muscle function and development (McPherron, Lawler and Lee, 1997; Tobin and Celeste, 2005). The increase in muscle mass was shown to be due to both hypertrophy and hyperplasia. These heterozygote animals also showed partial muscle phenotype indicating that complete inhibition of Myostatin is not necessary to achieve an increase in muscle mass (Tobin and Celeste, 2005). There is contradicting evidence as to whether myostatin regulates muscles mass through hyperplasia or hypertrophy. It seems like both pathways are used at different points depending on the stage of the development and the method used to antagonise myostatin (Tobin and Celeste, 2005).

Several studies have shown that myostatin action regulates adult muscle mass as well as embryonic development. Use of neutralising antibodies in adult mice, and the generation of myostatin-deficient mice, where the myostatin genes have been deleted postnatally, are examples where adult animals showed an increase in muscle mass (Bogdanovich *et al.*, 2002; Grobet *et al.*, 2003).

There are several examples of naturally occurring myostatin phenotypes. The first are the well-known double muscle phenotype cattle, the Belgian blues and the Piedmontese (Ménissier, 1982; Tobin and Celeste, 2005). The double muscle phenotype segregates with a region of the bovine chromosome 2 that is comparable to the human myostatin gene on chromosome 2 (McPherron and Lee, 1997; Tobin and Celeste, 2005). The first case of myostatin mutation in a human child was reported in 2004 (Hübner *et al.*, 2004).

The child showed extraordinary muscle mass at birth. It was shown that a point mutation caused a mis-spliced myostatin mRNA in this child and this lead to undetectable levels of myostatin protein. At four years of age, this child was reported to be healthy, and exceptionally strong with increased muscle mass.

It is, therefore, evident that myostatin can regulate muscle mass during development and in adult life when muscle size has reached its adult size. This regulation occurs through both hyperplasia and hypertrophy of muscle fibres.

1.9.3 Molecular organisation of the MSTN1 gene

The human *MSTN1* gene maps to chromosome 2q:32:2 (McPherron and Lee, 1997) and in the mouse to chromosome 1 27.8cM (Szabo *et al.*, 1998). The myostatin gene is 7.8kb with a simple molecular arrangement. It contains three exons with 2 intervening introns along with a 5' untranslated region and a 3' untranslated region which contains the core elements required for 3' end processing following transcription. The myostatin gene gives rise to a 3.1kb mRNA. Exon 1-3 in humans are approximate of equal size and give rise to a protein containing 375aa (Gonzalez-Cadavid *et al.*, 1998). It is the third exon that codes for the mature myostatin protein. Comparison of the myostatin protein between human and mouse has revealed 90% identity and this identity increases to a 100% when only the mature proteins are aligned. (McPherron and Lee, 1997). Myostatin is found to be predominantly expressed in skeletal muscle and to a lesser extent in fat tissue (McPherron, Lawler and Lee, 1997).

1.9.4 Processing and signalling of myostatin

Myostatin belongs to the subgroup of Growth and Differentiation Factors and is therefore also called GDF-8. The myostatin gene encodes for a small N-terminus signal sequence followed by a large propeptide and an 18kDa mature region at the C-terminus (McPherron, Lawler and Lee, 1997). The signal sequence is responsible for the processing and secretion of the protein. The propeptide is involved in the biological regulation of myostatin and renders the mature protein inactive. When active the mature myostatin then binds to one of the two activin type II (ActRII) receptors and initiates a signalling cascade (Lee, 2004).

Myostatin can exist in an active or inactive state depending on the post-transcriptional modification (McPherron, Lawler and Lee, 1997; Hill *et al.*, 2002). Following the transcription of myostatin, the propeptide and the mature region form a homodimeric protein as disulphide bonds form in both portions. Peptide bonds are then broken, and the propeptide remains in contact with the mature region via non-covalent forces and renders myostatin inactive. When secreted from muscle cells proteases on muscle cells free the mature protein from the propeptide, and the Myostatin is then activated and free to bind to its Activin type II receptors(Zimmers *et al.*, 2001; Patel and Amthor, 2005) (Figure 1.13).

This binding of myostatin leads to the phosphorylation and activation of Activin type I receptor, which then goes on to phosphorylate the receptor-regulated proteins Smad2 and Smad3 and initiates an intracellular signalling cascade. When activated these Smads form heterodimers with Smad4 and Smad complexes then translocate from the cytoplasm to the nucleus and activate target genes (Shi and Massague, 2003) (Figure

1.13). The systematic effects of myostatin have been documented, and latent myostatin is detected in serum (Zimmers *et al.*, 2001), but there is contradicting evidence on the distribution of active myostatin. One study has shown that active myostatin is detectable in human serum (Gonzalez-Cadavid *et al.*, 1998) whereas another study by, Zimmers and colleagues (Zimmers *et al.*, 2001), was unable to detect it. In both studies, antibodies were used to detect myostatin, and, therefore, one reason for the inconsistencies may be related to the different antibodies used to detect the active myostatin.

The signalling process described above is referred to as the canonical signalling pathway of myostatin. Myostatin also signals via two other pathways: MAPK activation and inhibition of Akt signalling. MAPK activation is mediated via myostatin through two pathways: TAK1/MAPKK or Ras/Raf/MEK1.MAPK activation leads to the inhibition of genes responsible for myogenesis. Myostatin signalling through inhibition of Akt signalling is outlined in the above section called muscle mass regulation but is briefly described here. Myostatin inhibits Akt1 from phosphorylating FOXO and inhibiting protein degradation. Hence FOXO is dephosphorylated and accumulates in the nucleus leading to transcription of E3 ubiquitin ligase responsible for protein degradation (Figure 1.14) (Sandri *et al.*, 2004; Yang *et al.*, 2007; Elkina *et al.*, 2011)

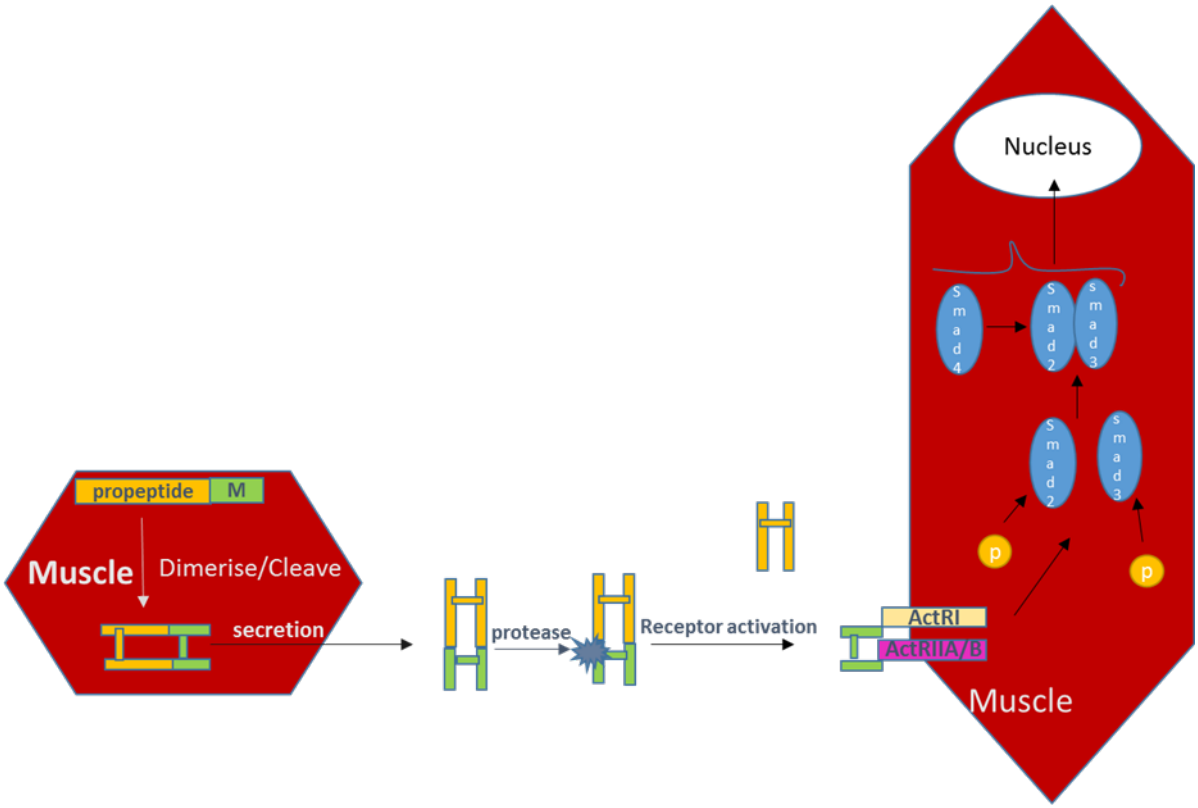

Figure 1.13 Processing of myostatin and myostatin canonical signalling

Myostatin processing and signalling via the activin receptor. Dimerised myostatin and propeptide are cleaved, and the propeptide stays attached to the mature portion with non-covalent links rendering it inactive. Inactive myostatin is secreted by muscle cells. Proteases on muscle cells cleave the propeptide from the mature myostatin. Mature myostatin binds type II activin receptor. Transphosphorylation leads to activation of type I receptor. Type I receptor phosphorylates Smad3 and Smad2, which recruit Smad4 into a Smad complex. The Smad complex is translocated into the nucleus to elicit transcriptional changes of downstream genes that result in muscle wasting.

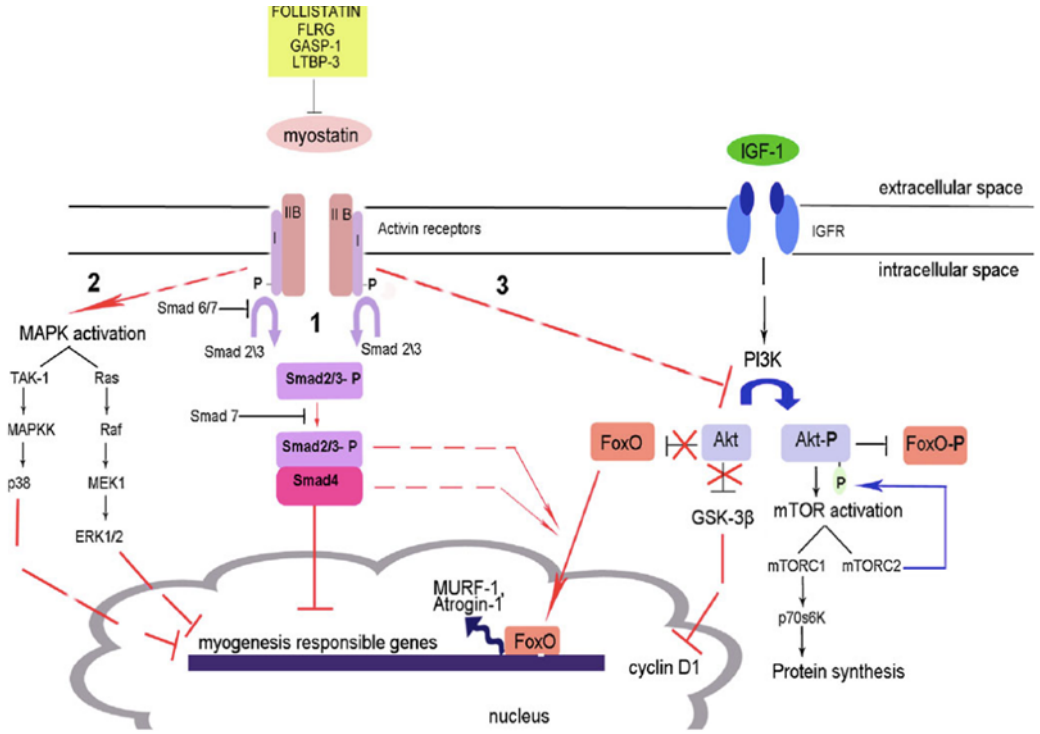

Figure 1.14 Myostatin signalling

Myostatin signals through three known pathways. The canonical pathway labelled 1 is described in figure 1.13. Myostatin also signals through its interplay with the IP3K/AKT signalling pathway. When bound to the activin type II receptor myostatin inhibits AKT phosphorylation and so inhibits muscle growth by decreasing mTOR regulated protein synthesis and increasing FOXO regulated protein degradation. Furthermore, myostatin leads to MAPK (p38 and ERK1/2) activation which lead to the inhibition of myogenesis responsible genes (Figure taken and modified from Yulia, 2011)

1.9.5 Myostatin splice variants

The conservation of the myostatin gene in a broad range of species ranging from sea urchins to humans indicates a common ancestral gene about 900 million years ago (McPherron, Lawler and Lee, 1997). Gene duplication events have given rise to multiple Myostatin genes in bony fish, but only one Myostatin gene was reported in mammals (McPherron and Lee, 1997; Maccatrozzo *et al.*, 2001). The presence of only one myostatin gene does not exclude the possibility of the presence of splice variants of myostatin. The presence of multiple poly(A) signal and alternative splicing of pre-mRNA allows the generation of multiple mRNA transcripts and so the translation of distinct proteins from one gene (Jeanplong *et al.*, 2013). Alternative splicing contributes to the wide variety of proteins present in mammals. Splice variants of myostatin have been identified in crabs, fish, chickens, and ducks (Castelhano-Barbosa *et al.*, 2005; Covi, Kim and Mykles, 2008; Huang *et al.*, 2011). Among mammals, Myostatin splice variants have not been as easy to identify, and only recently two reports have been made of a splice variant, one in the sheep skeletal muscle and the other in mice (Jeanplong *et al.*, 2013). Interestingly Jeanplong and colleagues showed that the alternative splice variant in sheep had a role in negatively regulating myostatin, so this way stimulated myogenesis.

Due to the high conservation of the myostatin gene and its function among species, it seems likely that myostatin splice variants are present in other mammals including humans. It could be that these alternative splice variants are present in specific muscles at particular stages of development, and this could contribute to the challenge of identifying them.

1.9.6 Roles of myostatin

The role of myostatin as a negative regulator of muscle mass was established very early on with the discovery of the molecule and generation of myostatin-deficient mice which showed abnormally high muscle mass (McPherron, Lawler and Lee, 1997). Further confirmation was made with the association of the double-muscled phenotype in cattle with mutations in the myostatin gene and recently, the report of a human child born with gross muscle hypertrophy due to a point mutation in his myostatin gene (McPherron and Lee, 1997; Hübner *et al.*, 2004) .

A year after that, in a study by Gonzalez and colleagues, it was shown that myostatin expression levels correlate inversely with fat-free mass in humans. It was also shown that there seems to be a correlation between the increase in the expression of myostatin and weight loss in men with AIDS wasting syndrome (Gonzalez-Cadavid *et al.*, 1998). In another study by McPherron and colleagues, it was revealed that myostatin null mice showed reduced fat accumulation with increased age, compared to wild-type mice; they concluded that the loss of myostatin improves upon the obese and diabetic phenotype of mouse models (McPherron and Lee, 2002).

1.9.7 Myostatin binding proteins

There is great interest in discovering the identity of myostatin-binding proteins due to their potential in antagonizing myostatin's downregulation of muscle mass. The identified binding proteins consist of Myostatin Propeptide, Follistatin, Follistatin related proteins FLGR (Follistatin Related Gene) , GASP-1 (Growth and Differentiation Factor-Associated Serum Protein-1) and Activin Receptor (Patel and Amthor, 2005). In addition to this, antibodies have been developed based on the findings on the structure

of myostatin. These antibodies bind and inactivate myostatin or bind and inhibit the dissociation of the propeptide from myostatin.

1.9.8 Myostatin inhibition and its clinical application

Muscle wasting is not only the hallmark of muscle disorders such as muscular dystrophies but it's also a hallmark of immobility and chronic disease such as kidney failure, tumour cachexia moreover, it also accompanies patients with AIDS wasting syndrome (Gonzalez-Cadavid *et al.*, 1998; Patel and Amthor, 2005). In addition to this sarcopenia, the decrease in muscle mass with age causes various health problems in addition to immobility. Therefore, being able to increase muscle mass would greatly benefit a large proportion of the world's population.

A wide range of approaches to inhibit myostatin have been evaluated clinically and preclinically. Most of these approaches target myostatin extracellularly, by binding myostatin itself or targeting components of the receptor complex. Some of these approaches consist of antibody administration of myostatin propeptide, Follistatin or soluble ActRIIB receptors. The targeting of the myostatin ActRIIB receptor has been found to be quite non-specific as the receptor has other ligands such as Activin and BMP9 (Smith and Lin, 2013a). Therefore targeting the ActRIIB receptor or use of an ActRIIB as a soluble decoy may not inhibit myostatin action only. Other than extracellular targeting of myostatin there has recently been promising advances in the use of antisense oligonucleotides to disrupt the myostatin reading frame by exon skipping (Han and Mitch, 2011; Kang *et al.*, 2011a; Malerba *et al.*, 2012; Veltrop and Aartsma-Rus, 2014).

1.9.8.1 Preclinical application of myostatin inhibition

Cachexia is a muscle wasting condition associated with a disease such as cancer. Approximately 80% of patients with cancer develop cachexia, and cachexia causes 25% of deaths associated with cancer. Mice with Colon-26 and Lewis Lung carcinoma treated with ActRIIB-Fc antibody, a soluble myostatin receptor, showed an increase in body and muscle weight, grip strength and a decrease in resting time (Zhou *et al.*, 2010; Busquets *et al.*, 2012). In another study, the same animal model was used to look at an antibody to myostatin which was able to revoke completely the reduction in total muscle force induced by tumours (Murphy *et al.*, 2011). These results show that inhibiting myostatin can significant benefits to patients with decreased mobility due to decreased muscle function.

Muscular dystrophies are inherited myogenic disorders that are characterised by progressive muscle degeneration and weakness (Emery, 2002). Myostatin inhibition in animal models of dystrophy has shown a positive effect on muscle mass but inconsistent results on muscle function and histopathology(Amthor and Hoogaars, 2012). Having said that, there have been promising improvements, and research is moving at a fast pace. Methods looked at so far in dystrophic models consist of the use of ActRIIB-Fc soluble receptor and ActRIIB shRNA to target the receptor. Both these approaches show an increase in muscle mass and total force but no change in the specific force (George Carlson *et al.*, 2011; Pistilli *et al.*, 2011). In contrast to these results, in another study, there was an increase in the specific force of the soleus muscle in dystrophic models exposed to a myostatin propeptide over an extended period (Morine *et al.*, 2010). The use of antisense oligonucleotides for exon skipping of myostatin is also under

investigation. It has been shown in a study that the administration of PMOs targeting exon two in dystrophic mice leads to a considerable increase in the soleus muscle of the mice (Kang *et al.*, 2011a). It is thought that skipping of myostatin alongside dystrophin in Duchenne Muscular Dystrophy, could attenuate the severity of the disease as shown in mdx mice models (Wagner, 2002). In a recent study, it was shown that combining two antisense oligonucleotides to inhibit myostatin and restore the dystrophin reading led to significant muscle mass growth and dystrophin expression(Malerba *et al.*, 2012). It is also hoped that by inhibiting myostatin, it would be possible to attenuate muscle fibrosis in dystrophic muscle due to the role myostatin plays in inducing dystrophic muscle fibroblast proliferation (Bo, Zhang and Wagner, 2012).

There has also been evidence that is inhibiting myostatin effects metabolism. Models show a decrease in fat mass and an increase in insulin sensitivity. There is a promise that myostatin inhibition could also be used to target obesity and obesity-related insulin resistance (Argilés *et al.*, 2012).

1.9.8.2 Clinical application of myostatin inhibition

There are currently clinical trials studying the effect of myostatin inhibition in patients with severe cachexia using antibodies. One of the antibodies being used is LY2495655. In healthy volunteers, this antibody was well tolerated and lead to an increase in thigh muscle volume (Smith and Lin, 2013a). In the Phase 1 study in advanced cancer patients without chemotherapy, there was an increase in muscle volume and an increase in handgrip strength. Phase 2 trials involving locally advanced or metastatic pancreatic cancer patients receiving chemotherapy treatment is ongoing, with overall survival as an endpoint (Smith and Lin, 2013a). Another antibody also in phase 2 trials is an ActRIIB

antibody BYM-338. This antibody is being used in patients with stage IV non-small cell lung cancer and stage III/IV adenocarcinoma of the pancreas. The endpoint in this study is the thigh muscle volume at eight weeks assessed by MRI. In healthy volunteers, this antibody has been well tolerated and leads to an increase in thigh muscle volume (Smith and Lin, 2013b).

There have been recent developments in the clinical investigations of myostatin inhibition for the treatment of muscular dystrophies. A phase I/II trial using an anti-myostatin antibody, Myo-029, failed to show effects on muscle strength or function in patients with Becker muscular dystrophy, limb girdle and facioscapulohumeral muscular dystrophy, at a clinically relevant dose and was therefore discontinued (Wagner *et al.*, 2008). ACE-031, an anti-ActRIIB antibody, was shown to be very effective in healthy volunteers, leading to an increase in lean body mass and thigh muscle volume. In phase 2 trials involving DMD boys, it was also very efficient and slowed down the decline in thigh muscle mass and a six-minute walk and increased lean body mass. However, due to the onset of side effects such as nose bleeds and skin telangiectasia in healthy volunteers as well as in the phase 2 study, the trials were discontinued (Attie *et al.*, 2013). PF-06252616 is an anti-myostatin antibody currently in Phase I healthy volunteer trial and has been given an orphan drug designation for the treatment of Duchenne muscular dystrophy (Smith and Lin, 2013a).

1.10 Polyadenylation

All eukaryotic mRNA, except some histone mRNAs, contain poly (A) tails at their 3' end. The pre-mRNA undergoes a two-step reaction to obtain a poly (A) tail: 1) endonucleolytic cleavage and 2) poly (A) tail addition. The presence of specific elements at the 3' end of the pre-mRNA is required for the recruitment of multiprotein complexes which then allows the pre-mRNA to undergo 3'end processing. Most cellular mRNAs contain two core elements: the polyadenylation (poly(A)) signal (canonical signal AUAAA or the less frequent AUUAAA) and the downstream sequence element (DSE) characterised by a high-density G/U or U residues. The polyadenylation signal is located upstream of the cleavage site and is recognized by the multimeric cleavage and polyadenylation specificity factor (CPSE). The binding of this factor to the poly(A) signal determined the cleavage site (10-30nt downstream). The DSE is recognised and bound by a subunit of the cleavage stimulating factor (CstF) which promoted the efficacy of the 3' end processing (Danckwardt, Hentze and Kulozik, 2008). The length of the poly(A) tail (which is similar in different mRNAs) is thought to be determined by the interaction of the nuclear poly(A) binding protein (PABPN1 and PABPN2), CPSF and PAP) (Kuhn and Wahle, 2004; Danckwardt, Hentze and Kulozik, 2008). It is worth mentioning that approximately half of human mRNAs contain more than one poly(A) site (Tian *et al.*, 2005a). Alternative poly(A) site choice is influenced by the intrinsic strength of the sequence elements, the concentration and activity of polyadenylation factors and by tissue or stage-specific regulatory factors (Barabino and Keller, 1999).

Following the assembly of the basal 3' end processing machinery, the endonucleolytic cleavage is catalysed by CPSF 73 (Ryan, Calvo and Manley, 2004). A nuclear poly(A)

polymerase (PAP) then adds approximately 250 adenine nucleotides to the 3' end in a template-independent manner (Danckwardt, Hentze and Kulozik, 2008).

1.10.1 Role of the poly(A) tail

Correct 3' end processing is functionally interconnected with transcription termination, mRNA capping and correct splicing of the pre-mRNA (Colot, Stutz and Rosbash, 1996; Danckwardt, Hentze and Kulozik, 2008). The poly(A) tail is also required for the release and export of the mRNA from the nucleus as well as mRNA abundance and correct translation of the mRNA (Proudfoot, Furger and Dye, 2002a; Danckwardt, Hentze and Kulozik, 2008). Loss or gain of function of the poly(A) tail therefore severely interferes with other gene expression steps.

Mutations of sequence elements in the 3' end of pre-mRNAs are known to be associated with a variety of disease. A good example is Alpha thalassemia and beta thalassemia where mutation of the poly(A) signal is a well-known cause of illness (Maniatis *et al.*, 1976; Danckwardt, Hentze and Kulozik, 2008). It is, however, important to note that mutation in the poly(A) signal does not always cause disease. Sometimes mutations reduce but do not completely inactivate mRNA translation and protein expression. An example of this is seen in individuals who carry an AAUAAC TO AGUAAC mutation of the arylsulfatase a gene poly(A) signal. This mutation reduces but does not halt mRNA and enzyme expression (Barth, Fensom and Harris, 1993).

1.11 Aims, objectives and methods

A diverse range of methods are being investigated for the treatment of Duchenne muscular dystrophy, and there are some promising results. Having said this none of the methods address the fibrotic replacement of muscle tissue simultaneously or prior to dystrophin restoration. The scope of this project is to block myostatin production using alternative methods such as the use of antisense oligonucleotides to interfere with the polyadenylation (poly(A)) of the myostatin mRNA and compare to previously developed exon skipping method, block POSTN production using antisense oligonucleotides to induce exon skipping, go in-vivo, treating C57 mice with antisense targeting POSTN and testing the effect of the designed antisense oligonucleotides on POSTN expression and muscle regeneration. This method, in theory, would lead to a multicombinatorial treatment for DMD, reducing fibrotic tissue allowing better restoration of dystrophin in muscle fibres as there would be more of them and increasing muscle mass, overall improving muscle function and pathology in DMD patients.

The short-term goal of this project was to see a decrease in *MSTN* RNA produced by muscle cells following treatment with antisense oligonucleotides targeting the poly(A) signal and induce exon skipping of POSTN in muscle cells and fibroblasts following treatment with antisense oligonucleotides inducing disruption in open reading frame . Given the *in vitro* nature of the short-term goal of this study, the use of appropriate culture models is an important consideration. Firstly, many studies have used rhabdomyosarcoma, RD muscle cells as a model of healthy human muscle, then DMD patient cells as a disease model of human muscle. These two cell lines are ideal for the *in vitro* experiments in this study as they produce myostatin as well as POSTN, can be

maintained in proliferation for multiple passages and do not differentiate. C2C12 (healthy myoblasts) mouse cells are also an ideal model for *in vitro* muscle studies as they produce abundant myostatin and perisotin, and they provide an additional model to investigate the antagonistic activities of myostatin and perisotin. Mouse myofibroblasts were also used as they are a main source of POSTN expression in fibrotic tissue. The use of mouse cells will allow further validation of the results obtained from the human muscle cells. *In vitro* investigations will be carried out to test two hypotheses:

1. **Blocking the polyadenylation (PolyA) of myostatin pre-mRNA will lead to decreased RNA abundance in the cytoplasm and, therefore, decrease the production of myostatin by muscle cells.**
2. **Blocking out-of-frame exons of perisotin will lead to the production of out-of-frame transcripts which will not give rise to mature POSTN protein and therefore will reduce production of functional POSTN by cells.**

The long-term goal was to take the study *in vivo* and look at the effect of antisense mediated POSTN knockdown in C57 mice injected with $BaCl_2$.

Specific objectives of this project and planned methods:

Objective 1: **Identify polyadenylation (ATTAAA) signal in human and mice and investigate the homology of this region between various species.**

Methods:

- Perform a pairwise sequence alignment of mouse and human at the third exon and analyse for homologous runs containing polyadenylation signals.

- Should a region of homology exist, analyse sequence and design of PMO capable of targeting both species.

Objective 2: Design PMOs targeting the polyA signal

Methods:

- Identify the poly(A) used in the human and mouse Myostatin transcript.
- Following identification look at all possible 30-mer sequences of PMOs, targeting the signals, varying by one base.
- Determine the overall strength of all antisense oligonucleotide sequences to target sequence and their % GC.
- Look at where the PMO would bind on the folded pre-mRNA structure

Objective 3: Determine whether the use of the designed PMOs to polyA signal causes a decrease in the Myostatin mRNA

Methods:

- Set up RD (rhabdomyosarcoma muscle cells) cell lines
- Harvest of mRNA using Qiagen RNAeasy kit.
- Running a 1 step RT-PCR, with primers in exon 1 and exon 3 of Myostatin (table 5), to look for a change in band intensity between treated and non-treated cells. This represents the amount of RNA exported from the nucleus. Use of a house-keeping gene such as 18s to compare expression rate.
- Use of gene tool to semi-quantify the gels from the RT-PCR by densitometry
- Run a q-PCR for accurate quantitative results.

Objective 4: Identify out of frame exons in POSTN in human and mice and assess homology

Methods:

- Look at *POSTN*1 exons and identify those not divisible by 3
- Upload POSTN sequence of human and mouse onto SnapGene and align sequences, assessing homology of identified exons.
- Identify Exons with highest percentage homology which would be ideal to design PMOs to.

Objective 5: Design PMOs to induce exon exclusion and disruption of the open reading frame

Methods:

- Identify exonic splice enhancers in the selected exons
- Design PMOs targeting strong ESE sites and avoiding ESS sites.
- Determine the overall strength of all antisense oligonucleotide sequences to the target sequence and their % GC.
- Assess the position of binding of PMO to pre-mRNA secondary structure

Objective 6: Determine whether the designed PMOs induce exon skipping in patient muscle cells, murine C2C12 muscle cells and murine muscle fibroblasts

Methods:

- Design primers to all selected exons and optimize PCR
- Transfect human patient cells with 10uM PMOs, 20ng TGF-β and Endo-Porter
- Harvest RNA 24 hours after transfection

- Run PCR and look at product on 3% agarose gel
- Semi-quantitatively calculate percentage skipping using gene tools
- Select most successful PMOs and test them in C2C12 cell line
- Assess PMO bioactivity in C2C12 cells using RT-PCR as well as quantitatively using RT-qPCR.
- Assess Fibronectin mRNA expression
- Carry out western blots to assess POSTN and Fibronectin protein expression
- Identify successful PMOs and repeat in murine myofibroblast cell line

Objective 7: Antisense modulation of POSTN per-mRNA splicing in the C57 mouse model.

Methods:

- Injection of mouse TA with $BaCl_2$ and harvesting of TA at various time points
- Injection of mouse TA with $BaCl_2$ followed by PMO and harvest at various time points
- Investigate POSTN and fibronectin expression through RT-qPCR
- Investigate POSTN and fibronectin protein expression via Western blots
- Assess muscle regeneration and expression of POSTN, fibronectin, collagen VI and α-SMA via immunohistochemistry.
- Assess fibrosis using Sirius red staining.

2. Material and Methods

2.1 General laboratory reagents

All general chemical reagents were purchased from Sigma, Invitrogen, BDH or VWR (unless stated otherwise) with chemical purity grade AnalaR (Analytical Reagents for analysis applications). More commonly used chemicals are listed below, whereas the reagents required for only more specialised assays are described in the relevant materials section. All the reagents were dissolved in double distilled H_2O (ddH_2O) unless stated otherwise. The majority of solutions required as sterile for tissue culture were autoclaved at 1210°C for 15 min, except for solutions containing protein, detergents or glucose which were sterilized by passing through a brand new 0.22 µm filter (Falcon) under sterile conditions. All solutions were stored at room temperature unless indicated otherwise.

Reagent :	Manufacturer:
Acetic acid (CH_3COOH)	VWR
Agarose	Invitrogen
Ammonium acetate $AcO(NH_4)_2$	BDH
Bovine Serum Albumin	Sigma
Boric acid	Sigma
$CaCl_2$	Sigma
Citric acid	Sigma
Dimethyl sulphoxide (DMSO)	Sigma
EDTA	Sigma
Ethanol (EtOH)	VWR
Glucose	Sigma
Hydrochloric acid (HCl)	BDH
Methanol	VWR
Magnesium chloride ($MgCl_2$)	Sigma
Magnesium sulphate ($MgSO_4$)	BDH
NaOH	Sigma
Na_2HPO_4	Sigma
NP-40	Fluka Biochemica
Paraformaldehyde (PFA)	Sigma
Potassium chloride (KCl)	Sigma
Phosphate buffered saline (PBS) pH 7.3	Oxoid Ltd
Sodium chloride (NaCl)	Sigma
Sodium dodecylsulphate (SDS)	Sigma
Sodium bicarbonate ($NaHC0_3$)	Sigma
Sucrose	Sigma
Tri-sodium citrate	Sigma
Trizma Base	Sigma
Trizma hydrochloride (HCl)	Sigma

Table 2.1 General reagents

2.2 Tissue culture techniques

2.2.1 Materials

- Dulbecco's Modified Eagle's Medium (DMEM): High glucose (4.5 g/l), GlutMAXTM-I (862 mg/l), Pyruvate (110 mg/l) and phenol red (15 mg/l) (ThermoFisher). Stored at 4°C.
- Skeletal Muscle Cell Growth Medium (SMGM) (PromoCell)
- Foetal bovine serum (FBS), certified heat inactivated (Invitrogen). Stored at -20°C in 50 ml aliquots.
- L-glutamine (Sigma)
- L-methionine (Sigma)
- L-proline (Sigma)
- Penicillin-streptomycin 100 Units/ml (Sigma)
- Trypan blue (Gibco)
- Trypsin-EDTA (10x)- 0.5% trypsin, 0.2% EDTA in PBS (Sigma)

2.2.2 Cell lines

Rhabdomyosarcoma (RD) cells (ATCC CCL-136^{TM}): stored in vapour phase of liquid nitrogen at 1,000,000 cells/vial in growth media plus 10% DMSO.

DMD Patient immortalised myoblast cells (Δ52 Vincent Mouly Institute of Myology) stored in the vapour phase of liquid nitrogen at 1,000,000 cells/vial in growth media plus 10% DMSO. They grown in muscle SMGM media with 20% FCS, 1%P/S, 25ml Gentamycin and 5ml Glutamine.

Mouse Muscle Fibroblast Cells (Mocha MH cell line, ATCC) were purchased from ATCC, stored in the vapour phase of liquid nitrogen at 1,000,000 cells/vial in growth media plus 10% DMSO. They were grown in DMEM with FCS.

2.2.3 Culture of cells

All work for this project was performed under sterile conditions, using new, sterile plastic inside a grade 2 laminar flow hood. Cells were incubated at 37°C with 5% CO_2.

1 x 10^6 cells were seeded in T175 flask using 25 ml of the corresponding growth media. When 80% confluency was observed, the media was aspirated, and cells were washed with 5 ml of sterile 1X PBS. PBS was replaced with 5 ml of 1X Trypsin/EDTA solution and incubated at 37°C for 2-3 minutes to encourage cells to detach from the surface of the flask. 10ml of growth media was then used to neutralise the trypsin, and the cell suspension transferred to a 50ml falcon tube (Corning) and spun at 200 rpm for 5 minutes to RT pellet the cells. The supernatant was aspirated and the pellet of cells resuspended in their growth media to achieve a concentration of 1x10^6 cells/ml. 1 ml of the resuspended cells were then placed in a T175 flask containing 25ml of their corresponding growth media and incubated for 3-4 days until 80% confluency was reached again.

2.2.4 Cell viability and quantifying assessment

Trypan blue stain was used to assess the viability of cells. This staining method is based on the assumption that dead cells have a damaged cell membrane and will take up the dye. Viable cells maintain a clear cytoplasm in the presence of Trypan blue, while dead or damaged cells stain blue. Typically, 10 µl of cell suspension was mixed with 10 µl of

Trypan blue (0.4%) and left for 1 minute before assessing and counting the cells using a haemocytometer under a light microscope. The ratio of live to dead cells was assessed.

2.2.5 TGF-β treatment of cells

TGF-β was dissolved in filtered citric acid pH 3 to produce a stock solution of 1µg/20µl. The stock was diluted to 5 ng/µl using pH 3 citric acid.

Cells were seeded in 6-well plates using their corresponding media as described in section 2.2.3. Each well contained 8.3 x 10^4 cells in 2ml of corresponding media. When 80% confluent, around 48 hours after seeding, the media was aspirated off and replaced with 2 ml of corresponding media. 4µl of TGF- β was pipetted into each well and the plates gently swirled to mix. RNA was harvested and analysed 24 hours after exposure to TGF-β.

2.2.6 PMO transfection of cells

PMOs, supplied by GeneTools, LLC, were dissolved in ddH_2O to produce a stock solution of 1mM and transfections were carried out in a final volume of 1 ml.

Cells were seeded at 8.3 x 10^4 in 6-well plates using 2ml of corresponding media per well. When 80% confluent the media was aspirated off and replaced with the appropriate volume of corresponding media with 10% FCS instead of the usual 20%. For Perisotin investigations, 20ng of TGF-β was added to each well and plates were incubated at 37°C for 1 hour before transfection with PMO. For myostatin investigations, PMO transfection was carried out with no prior treatment.

Each well was then transfected using 3µl of aqueous Endo-Porter and the PMO concentration range used between 0-10µM. PMO was added to each well followed by 3 µl Endo-Porter. The final volume of each well was made up to 1 ml using appropriate media with 10% FCS.

Plates were incubated for 24 hours at 37 °C with 5% CO_2 and then RNA harvested; alternatively, the plates were incubated for 48 hours and protein harvested.

2.3 RNA extraction from cells and muscle tissue

2.3.1 Materials

- QIAshredder kit (Qiagen Ltd.): Stored at room temperature.
- RNeasy Mini Kit (Qiagen Ltd.): Stored at room temperature.
- RNeasy Fibrous Tissue Mini Kit (Qiagen Ltd): stored at room temperature
- RNase-free DNase-I (Qiagen Ltd.): Stored at 4°C. Once reconstituted, stored in 50 µl aliquots at -20°C.
- Absolute ethanol (100%)
- ND-1000 NanoDrop spectrophotometer (Thermo Fisher).
- TissueLysser (Qiagen)
- Stainless steel 5mm beads (Qiagen)

2.3.2 RNA extraction from cells

RNeasy mini kits and QiaShredder columns were used to extract RNA from cells seeded in 6-well plates. 350 µl of RLT lysis buffer was added to each well. The buffer was pipetted over the well surface 3-4 times to ensure complete lysis of cells. The cell lysate

was transferred into Qiashredder column and placed into the 2 ml collection vessel provided. The column in the collection tube was then centrifuged for 2 minutes at full speed. The flow-through could then be stored at -80°C at this point and defrosted at 37°C for 10 minutes before further processing. To process it, 350 µl of 70% ethanol was added to the flow-through and pipetted up and down several times to ensure mixing. 700 µl of the mixture was transferred to an RNeasy mini column placed in a 2ml collection tube. The column inside the tube was then centrifuged for 30 seconds at ≥8,000xg. The flow-through was discarded for this and all of the following steps. 350 µl of buffer RW1 was added to the RNeasy column. The column was then centrifuged for 30 seconds at ≥8,000xg. 10 µl of reconstituted RNase-free DNase and 70 µl of RPE buffer were mixed together and carefully pipetted on to the column. The column was then incubated at room temperature for 15 minutes. After incubation 350 µl of RW1 buffer was pipetted to the column and centrifuged for 30 seconds at ≥8,000xg. 500 µl of RLP buffer (with ethanol added prior to this as indicated on the label of the bottle) was pipetted onto the column. The column was centrifuged for 30 seconds at ≥8,000xg. Another 500 µl of RLP buffer was added to the column and centrifuged for 2 minutes at ≥8,000xg. The column was then transferred into an RNase-free; DNase-free 1.5 ml Eppendorf tube and 30 µl of RNase-free, DNase-free water was added onto the membrane directly, and this time the flow-through was kept. The column was then centrifuged for 1 minute at ≥8,000xg to elute the RNA. The quality and concentration of the harvested RNA were then assessed using an ND-1000 NanoDrop spectrometer. RNA was stored in a -80°C freezer.

2.3.3 RNA extraction protocol from sectioned TA muscle

Eppendorf tubes containing tibialis anterior sections were placed on ice and very quickly 1x5mm steel bead was added to each tube along with 300µl of Buffer RLT. Tubes were placed in the TissueLyser, and the Tissuelyser was operated for 2 minutes at 20Hz allowing even homogenization. The lysate was then pipetted into a new microcentrifuge tube. 590 µl of RNase free water was added to the lysate followed by 10µl of proteinase K solution and mixed by pipetting. The tubes were then incubated at 55°C for 10 minutes. The tubes were then centrifuged for 3 minutes at 10,000 x g. The supernatant was pipetted into a new 1.5ml microcentrifuge tube. A 0.5 volume (usually 450µl) of ethanol was added to the lysate and mixed by pipetting. 700µl of the sample was transferred to an RNeasy Mini spin column placed in a 2ml collection tube, and the columns were then centrifuged for 30 seconds at 8000 x g. The flow-through was discarded. This was repeated for any sample remaining in the 1.5ml microcentrifuge tube. 350µl of buffer RW1 was added to the RNeasy Mini column and centrifuged for 30 seconds at 8000 x g. In order to eliminate DNA, the RNase-free DNase-I kit was used at this point. 10 µl DNase I solution was added to 70µl of Buffer RDD for each sample. The DNase I mix (80 µl) was then directly added onto the RNeasy spin column membrane and left on the benchtop for 15 minutes at room temperature. 350µl of RW1 buffer was then added to each RNeasy Mini column and the columns centrifuged for 30 seconds at 8000 x g. The flow-through was discarded after this and after every centrifuge step after this. 500µl of buffer RPE was added to the columns and centrifuged for 30 seconds at 8000 x g. Another 500µl of buffer RPE was added to the columns and centrifuged for 2 minutes at 8000 x g. The RNeasy Mini spin columns were then placed in new 1.5ml collection tubes. 30µl RNase free water was directly pipetted onto the columns and the

flow-through kept by centrifuging the tubes for 1 minute at 8000 x g. The columns were discarded, and the flow-through containing the RNA was stored at -80°C. The quality and concentration of harvested RNA were assessed using an ND-1000 NanoDrop spectrometer.

2.4 Polymerase chain reaction-based methods

2.4.1 Reverse transcriptase polymerase chain reaction (RT-PCR)

2.4.1.1 Materials for PCR

- cDNA generated using Methods 2.4.2
- GoTaq DNA polymerase kit (Promega). Stored at -20°C.
- Gene specific primers and housekeeping primers designed using PrimerQuest tool at https://eu.idtdna.com/PrimerQuest/Home/Index (IDT).
- Peltier Thermal cycler PCT-200 (MJ Research)

2.4.1.2 PCR standard conditions

In this section, only general procedures for PCR will be outlined. The more detailed details of the primer sequences and PCR program will be outlined in the appropriate section.

Typically, cDNA was previously prepared by RT-PCR. Primers were diluted to 1 µM. All components of the GoTaq kit were thawed on ice except the polymerase which was kept at -20°C until needed. Master stock solution for each reaction was prepared in the order shown in the table below:

RT-PCR reaction set up

Component	Volume
GoTaq polymerase 5u/µl	0.25µl
Forward primers (10 µM each)	0.5 µl
Reverse primers (10 µM each)	0.5 µl
$MgCl2_2$ (25mM)	1.5 µl
GoTaq Buffer (5x)	5 µl
dNTP (5nM)	1 µl
Nuclease-Free water	12.25 µl
Final volume	**21 µl**

21µl of the master mix reaction was added to each PCR tube containing 4µl of cDNA template. At least one negative control was set up that lacked cDNA, which was replaced with nuclease-free water. The PCR tubes were placed in the PCR machine, and the appropriate programmes were run. In the standard PCR protocol, the template was initially denatured at 94°C for 2 minutes followed by 30 to 45 cycles of 1-minute denaturation, 1-minute annealing and 30 seconds extension (or 1 minute per 1000bp) at 92°C, 45-68°C and 72°C respectively. The final extension was carried out at 72°C for 5 min. The final product was stored at 4°C or -20°C. The annealing temperature was predicted separately for each primer pair.

2.4.1.3 Mstn PCR

The expected amplicon size of the *mstn* gene was 938bp. Sequence of the primers used were: forward primer, 5'-CCTCAGTAAACTTCGTCTGGA-3'; reverse primer, 5'-CACAGCGGTCTACTACCATC-3'. The reaction was set up as described in *2.4.1.1* with annealing temperature of 56.4°C and a total of 30 cycles.

This protocol was also used for multiplex PCR where 18S was amplified alongside Mstn as a housekeeping gene to assess expression. In this case, 0.38µl of 10µM 18S sense and antisense primers were added, and the volume of water decreased to 7.89µl to accommodate the addition of primers in the same total volume.

2.4.1.4 Periostin PCR

2.4.1.4.1 Human:

Nested PCR was optimised for exons 3, 7, 10 and 16. In the first round of PCR, 4µl of cDNA product was used and the reaction set up as described in 2.4.1.1 with annealing temperatures of 53°C, 55°C, 54°C and 51°C respectively for each exon, with a total of 20 cycles. In the second round, 0.25-1µl of the first round PCR product was used, and the reaction was set up as described in *2.4.1.1* with the annealing temperatures 50°C, 52°C, 60°C and 53°C respectively for each exon and a total of 30 cycles.

Primers specific to each exon of human Periostin are listed in the tables below:

Primers used to amplify the human Periostin exon 3 in RT-PCR

	Primer	Sequence (5'-3')	Location	Product size
Exon 3 1st round PCR	Forward:	TTGGGCACCAAAAAGAAATACT	Exon2	264bp
	Reverse	CGGTGCAAAGTAAGTGAAGGAT	Exon4	
Exon 3 2nd round PCR	Forward:	TTGGGCACCAAAAAGAAATACT	Exon2	159bp
	Reverse	ATAAACATGGTCAATGGGCAA	Exon4	

Primers used to amplify the human Periostin exon 7 in RT-PCR

	Primer	Sequence (5'-3')	Location	Product size
Exon 7 1st round PCR	Forward:	TATCCGTAGAGGTTTGGAGAGC	Exon6	643bp
	Reverse	ATCAATCAAATGGATCACACCA	Exon8	
Exon 7 2nd round PCR	Forward:	TGGCATGATTATTCCTTCAATG	Exon6	544bp
	Reverse	ATCAATCAAATGGATCACACCA	Exon8	

Primers used to amplify the human Periostin exon 7 in RT-PCR

	Primer	Sequence (5'-3')	Location	Product size
Exon 10 1st round PCR	Forward:	TGGAATCAAAATGGTGAACAAA	Exon9	608bp
	Reverse	TTCCCTTAAAAGCATCATTGGT	Exon11	
Exon 10 2nd round PCR	Forward:	ATGGTGTGATCCATTTGATTGA	Exon9	521bp
	Reverse	AGGTTGTGTCAGGAGCTCTTTC	Exon11	

Primers used to amplify the human Periostin exon 16 in RT-PCR

	Primer	Sequence (5'-3')	Location	Product size
Exon 16 1st round PCR	Forward:	TGACATCATGACAACAAATGGT	Exon15	263bp
	Reverse	GTGTGGGTCCTTCAGTTTTGAT	Exon17	
Exon 16 2nd round PCR	Forward:	CTGTTGGAAATGATCAACTGCT	Exon15	168bp
	Reverse	GAAGACTGCCTTCAATCACTTT	Exon17	

2.4.1.4.2 Mouse

Nested PCR was optimised for exons 3 and 16. In the first round of PCR, 4 µl of cDNA product was used and the reaction set up as described in 2.4.1.1 with annealing temperatures of 60°C and 69°C respectively for each exon with a total of 20 cycles. In the second round, 0.5-1µl of the first round PCR product was used, and the reaction was set up as described in *2.4.1.1* with the annealing temperatures 65° and 64°C respectively for each exon and a total of 30 cycles.

Primers specific to each exon of human Periostin are listed in the tables below:

Primers used to amplify the mouse Periostin exon 3 in RT-PCR

	Primer	Sequence (5'-3')	Location	Product size
Exon 3 1st round PCR	Forward:	CTGGGCACCAAAAAGAAATACT	Exon2	260bp
	Reverse	GCGAAGTACGTCTATGACCCTT	Exon4	
Exon 3 2nd round PCR	Forward:	GTATCAAGGTGCTATCTGCGG	Exon2	169bp
	Reverse	GACATCGGAGTAGTGCTGAGTG	Exon4	

Primers used to amplify the mouse Periostin exon 3 in RT-PCR

	Primer	Sequence (5'-3')	Location	Product size
Exon 16 1st round PCR	Forward:	CGTCGTGGACAAACTCCTCTAT	Exon15	229bp
	Reverse	GTGGATCACTTCTGTCACCGT	Exon17	
Exon 16 2nd round PCR	Forward:	GGAAATGATCAGCTCTTGGAAT	Exon15	131bp
	Reverse	TCAATTTGGATCTTCGTCATTG	Exon17	

2.4.2 cDNA synthesis

2.4.2.1 Materials

- GoScript reverse transcription system kit (Promega): Stored at -20°C.
- Random primers (Invitrogen)
- Oligo(dT) primers (Promega)
- Thermal cycler (VWR)

2.4.2.2.Protocol

The GoScript Kit (Promega) was used for cDNA synthesis. All components of the kit were thawed on ice except for the reverse transcriptase, which was kept at temperatures close to -20°C until needed.

600ng of RNA and 500ng of random primers and oligo(dT) were pipetted into an RNase-free PCR tube. RNase-free water was then used to adjust the total volume of RNA/primer mixture to 10 µl. The PCR tube was then placed in a PCR machine, and a single cycle was run for 5 minutes at 70°C followed by at least 5 minutes at 4°C. The resulting samples were stored on ice until the reverse transcription master mix was ready.

The reverse transcription reaction master mix was prepared on ice in the order listed in the table below.

Composition of the reverse transcription reaction master mix:

Components	**Volume**
GoScript 5x Reaction Buffer	4 µl
$MgCl_2$ (25 mM)	2 µl
dNTP (5 mM)	2 µl
GoScript Reverse Transcriptase	1 µl
Nuclease-free water	6 µl
Final volume	**15 µl**

15 µl of the reverse transcription master mix was then added to the 10µl RNA/primer mix and placed in the PCR heat block. The PCR programme run consisted of: annealing for 5 minutes at 25°C, extension for 1 hour at 42°C and heat denaturation for 15 minutes at 70°C. cDNA samples were then stored at -20°C for long term storage.

2.4.3 Quantitative real-time PCR

2.4.3.1 Materials

- 3LightCycler 488 SYBR Green I Master (Roche). Stored at -20°C.
- cDNA generated in Methods 2.4.2
- LightCycler 480 (Roche) for quantitative PCR
- Housekeeping realtime primers and gene-specific primers (Primetime qPCR primers from IDT)
- DEPC-treated water (Ambion)

2.4.3.2 Standard Protocol

The described protocol has been optimised for use with ROCHE SyBr Green master mix and the Roche LightCycler 480 machine using 380-well plates. All procedures described were carried out in a UV-treated, nucleic acid-free safety cabinet. Sequences of human and mouse primers used for qPCR are detailed in the table below.

List of primers

Target gene	Accession No	Primer	Sequence (5'-3')	Location	Species
Posnt	Hs.PT.58.4452022	Forward Reverse	GTTGCTCTCCAAACCTCTACG CGCTATTCTGACGCCTCAA	Exon4 Exon5	Human
Posnt	Mm.PT.58.9884244	Forward Reverse	CCTTTCATCCCTTCCAATTCTCA CCTGTAAGAACTGGTATCAAGGT	Exon2 Exon3	Mouse
GAPDH	Hs.PT.58.40035104	Forward Reverse	GCGCCCAATACGACCAA CTCTCTGCTCCTCCTGTTC	Exon1 Exon4	Human
GAPDH	Mm.PT.39a.1	Forward Reverse	GTGGAGTCATACTGGAACATGTAG AATGGTGAAGGTCGGTGTG	Exon2 Exon3	Mouse
Fbn1	Mm.PT.58.8135568	Forward Reverse	TTGTTCGTAGACACTGGAGAC GAGCTATCCATTTCACCTTCAGA	Exon26 Exon27	Mouse
Mstn	Hs.PT.58.40523213	Forward Reverse	TCGTGATTCTGTTGAGTGCT TGTAACCTTCCCAGGACCA	Exon2 Exon3	Human

The cDNA generated (section 2.4.2) was diluted in nuclease-free water. Control sample cDNA was used to set up standard dilutions (i.e., 1:50, 1:500, 1:5,000 and 1:50,000) for calculation of primer binding efficiency. The final volume of each dilution was made up to at least 50µl. A 380-well plate was set up by including the four serial dilution standards and one negative control that included nuclease-free water instead of cDNA. Each plate included at least three biological replicates of treated and untreated samples. Each of the biological replicates had 3 technical replicates to control for machine and pipetting errors.

The master mix for each reaction, gene-specific and the housekeeping gene, was set up as outlined in the table below: 6µl of master mix was pipetted into each well followed by 4µl of diluted cDNA making a total volume of 10 µl.

Composition of RT-qPCR reaction

Components	Initial concentration	Volume	Final concentration
SYBR Green	2x	5 µl	1x
Primer concentration	10 µM	0.5 µl	0.5 µM/primer
cDNA	n.a.	4 µl	n.a.
Nuclease-free water	n.a.	0.5 µl	n.a.
Final volume/well	n.a.	10 µl	n.a.

The plate was sealed using the provided covers and spun at high speed briefly to ensure all components are mixed and at the bottom of the wells. The plate was then placed inside the machine, and the programme shown in the table below was initiated:

RT-qPCR cycling parameters

PCR programme	No. of cycles	Temp. (°C)	Time
Preincubation	1	95	10 minutes
Amplification	40	95 60 72	10 seconds 5 seconds 10 seconds

A melting curve programme was added at the end of the programme to assess any off target amplification (Figure 2.1). Each primer set is expected to have a single distinct peak if there are no off-target primer binding or contamination present.

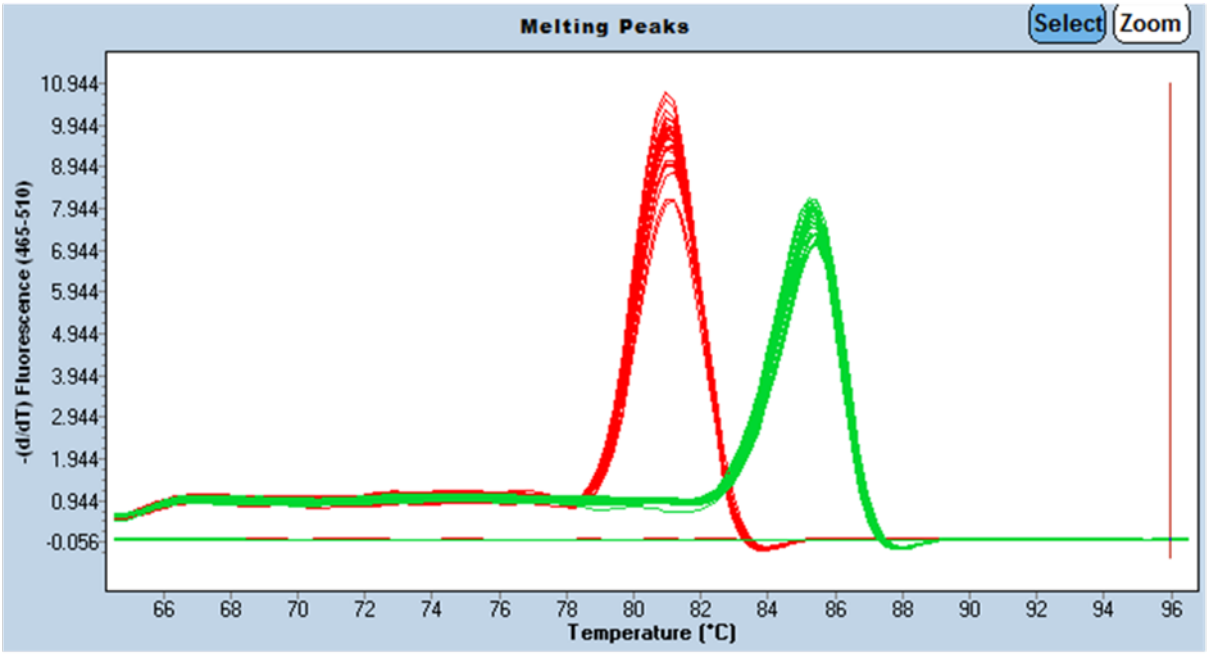

Figure 2.1 Example of a melting curve acquired at the end of a reaction from the Roche LightCyclers480

Two distinct peaks specific for Postn (green) and GAPDH (red) housekeeping gene indicate that the primers are amplifying a single product and no off-target amplification or sample contamination is present.

2.5 Semi-quantitative densiometric analysis of gene expression

2.5.1 Materials

- Agarose. Stored at room temperature.
- 10x TAE buffer: diluted to a 1X solution. containing 40mM Tris, 40mM acetate, and 1mM EDTA, pH 8.3. Stored at room temperature.
- 5x TBE buffer: diluted to a 1X solution. containing 45mM Tris-borate and 1mM EDTA, pH 8.0. Stored at room temperature (http://cshprotocols.cshlp.org/content/2006/1/pdb.rec8458.full).
- SYBR Safe (x10,000) DNA gel stain (Invitrogen). Stored at room temperature.
- DNA Hyperladder IV and V (Bioline UK Ltd.). Stored at 4°C.
- Horizontal electrophoresis system (Bio-Rad).
- E-BOX VX2 gel documentation system (PeqLab).
- Access to GeneTools software (Syngene) for densitometric analysis.
- Polyacrylamide 10% precast TBE gels (Invitrogen). Stored at 4°C.

2.5.2 Protocol

To examine the expression of a skipped target gene relative to the full-length target gene or the expression of the target gene relative to a housekeeping gene, the specific PCR products were separated by agarose gel electrophoresis. For separation of products amplified using periostin specific primers, products were run on a horizontal 3% (w/v) agarose gel, prepared by dissolving 3g of agarose in 100ml of 1x TAE buffer and heated in a microwave to aid dissolving. The mixture was heated until a transparent solution was formed; 10µl of 10,000xSYBR safe was added to the solution and mixed thoroughly by swirling. After allowing to cool to 65°C. The gel was then poured into a casting tray

with the appropriate comb inserted and allowed to solidify at room temperature. The gel was submerged in 1X TAE running buffer. Each sample, containing loading dye, is loaded directly into the well at consistent volumes. 7 µl of the appropriate molecular weight markers were used to measure PCR product sizes and loaded at each side of the gel. The gel was then run at 100 volts for 45 minutes and visualised under UV light using an Ebox VX2 imaging system. The semiquantitative analysis of skipped Postn mRNA expression was done by normalising its expression to the total level of expression (skipped plus full-length). In cases where the skipped transcript was not being quantified, the expression level of Postn and Mstn were analysed by normalising to the level of the housekeeping gene (i.e. 18S). The analysis was performed using GeneTools software. The two formulae below were used to calculate expression levels (pixel count was used).

$$\text{Skipped Postn expression} = \frac{(\text{Skipped POSTN} - \text{background})}{((\text{Full length POSTN} - \text{background}) + (\text{Skipped POSTN-background}))}$$

$$\text{Postn expression} = \frac{(\text{POSTN} - \text{background})}{(18\text{S} - \text{background})}$$

$$\text{Mstn expression} = \frac{(\text{MSTN} - \text{background})}{(18\text{S} - \text{background})}$$

2.6 Protein extraction from cells and tissue

2.6.1 Materials

- RIPA Buffer (TBS PH7.5(25nM Tris/HCl, 140nM NaCl), 1%Triton (v/v) x100, 0.5% (w/v) SDS, 1mM EDTA, 1mM PMSF, 1mM Na3V04, 1mM NaF, 1 tablet of Protease inhibitor cocktail (Roche)).
- 5mm steel bead (Qiagen Ltd)
- TissueLyser (Qiagen Ltd)

2.6.2 Protocol

2.6.2.1 Protein extraction from sectioned TA muscle

Frozen Eppendorf tubes containing sections of TA muscle were placed on ice and very quickly one bead, and 100 µl of RIPA buffer was added to each tube. Tubes were then placed in the TissueLyser which was then operated for 2 minutes at 20Hz. The homogenised TA was then centrifuged at 4°C for 10 minutes at 13,000 rpm, and the supernatant containing total protein was transferred to a new tube and stored at -80°C.

2.6.2.2 Protein extraction from cells

All procedures were carried out on ice to avoid protein degradation.

Media was aspirated from each well. Wells were rinsed with PBS. 50µl of RIPA buffer was pipetted onto the surface of each well. The surface of each well was scraped to ensure lysis of all cells, then the buffer pipetted into Eppendorf tubes and vortexed. The lysate was then kept on ice for 2 minutes. The tubes were then centrifuged at 4°C with

at 13,000 rpm for 10 minutes. The supernatant containing the protein was then pipetted into fresh Eppendorf tubes and the pellet discarded. Protein was stored at -80°C.

2.7 Protein quantification using DC assay

2.7.1 Materials

- DC protein assay kit (BIO-RAD)
- BioTek spectrophotometer
- 96 well microtiter plate

2.7.2 Protocol

All steps in this protocol were carried out on ice.

10 dilutions of BSA protein standard containing 0.2mg/ml to 2mg/ml in RIPA buffer was made. 5µl of each standard and 0.5 µl of each protein sample was pipetted into a dry 96-well plate. Each well was replicated three times in order to have three technical replicates. 25µl of reagent A' (made up of 20 µl of reagent S in 1 ml of reagent A) was then pipetted into each well followed by 200µl of reagent B. The plate was then gently rocked to mix the reagents. The plate was left on ice for 15 minutes before being placed in the spectrophotometer and read at 750 nm; the concentration of protein in each well was calculated based on the standard curve produced using the BSA standard curve.

2.8 Western Blotting

2.8.1 Materials

- NuPAGE Novex Gels: 4-12% Bis-Tris gel and 3-8% Tris-Acetate gel (stored at 4°C)

- NuPAGE MOPS Running Buffer (20x) (stored at room temperature)
- NuPAGE T/A Running Buffer (20x) (Stored at room temperature)
- NuPAGE Transfer buffer (20x) (Stored at room temperature)
- NuPAGE LDS sample buffer (Invitrogen) (Stored at 4°C)
- NuPAGE sample reducing agent (Invitrogen)(Stored at 4°C)
- NuPAGE antioxidant (Invitrogen) (Stored at 4°C)
- Novex Sharp Pre-stained protein standard (Invitrogen) (Stored at -20°C)
- HiMark pre-stained protein standard (Stored at -20°C)
- Chameleon protein standard (LI-COR Bioscience) (Stored at -20°C)
- nitrocellulose membrane
- Phosphate Buffered Saline (PBS)
- Dried skimmed milk (Marvel)
- Odyssey Blocking Buffer (PBS) (LI-COR) (Stored at 4°C)
- Rabbit anti-Periostin (Abcam. ab14041),Stored at -20°C.
- Rabbit anti-Fibronectin (Abcam, ab2413): Stored at -20°C.
- Rabbit α-tubulin antibody
- Mouse Vinculin antibody
- IRDye 800CW Goat anti-rabbit antibody (LI-COR) (Stored at 4°C)
- IRDye 680RD Goat anti-rabbit antibody (LI-COR) (Stored at 4°C)
- IRDye 680RD Goat anti-mouse antibody (LI-COR) (Stored at 4°C)
- High salt buffer: (0.5g SDS, 10.2g NaCl in 500ml of PBST)
- Odyssey CLx Imager (LI-COR Bioscience)

2.8.2 Protocol

Protein samples were diluted to 4µg/µl with 4µl of reducing agent, 10µl of LDS sample buffer and water to make up a final volume of 40µl. The samples were then heated at 70°C for 10 minutes. Appropriate gels were set up using their corresponding running buffers (4-12% Bis-Tris gel with 1xMOPS running buffer for periostin and 3-8% TA gel with 1xTA running buffer). 10µl of each sample was loaded into the premade gels. 7 µl of a protein standard was loaded on either side of the gel. The middle chamber of the tank was filled with running buffer and 500µl of antioxidant. The gel was run for 1 hour at 200V for the Bis-Tris and 1 hour 20 minutes at 200V for the TA gel.

Transfer buffer was prepared by adding 100ml of methanol and 1ml of NuPage antioxidant to 50ml of 20xNuPage transfer buffer and made up to 1 litre using water. 2x filter paper, 4x blotting sponge and nitrocellulose membrane were cut to the same size as the gel and soaked in the transfer buffer prepared. The gel cassette was opened and the gel placed in a Novex blot module in a sandwich in the following order: 2x blotting sponge, filter paper, gel, transfer membrane, filter paper, 2x blotting sponge. The module was placed in the electrophoresis running tank and secured. The module was filled with running buffer leaving 1cm at the top of the module empty. The outside of the module was filled with leftover transfer buffer or water. The lid was placed on the gel tank, and it was run for 2 hours at 30V.

Appropriate blocking buffer was used to block the membranes. For periostin Western blots, Odyssey Blocking Buffer (Li-Cor) was used. For fibronectin, 5% milk in PBS was used. Membranes were placed in appropriate blocking buffers and placed on a shaker for 1 hour.

Primary antibody was prepared in the appropriate blocking buffer with 0.1% (v/v) Tween 20 added. For periostin Western blots primary antibody was prepared with a dilution of 1:4000 of rabbit anti-periostin antibody and 1:2000 dilution of rabbit α-tubulin antibody (independently, as host species are the same). For fibronectin Western blots, primary antibody was prepared with a 1:1000 dilution of rabbit anti-Fibronectin antibody and a 1:10,000 dilution of mouse Vinculin antibody (in the same solution, as host species are different).

Blocked membranes were placed in boxes and covered with their appropriate primary antibody solutions. Boxes were placed on shakers at 4°C overnight.

The membranes were then washed with PBST (0.1% Tween 20 in PBS) 3 times for 3 minutes on a shaker at RT. The periostin blots were also washed with a high salt buffer for 10 seconds prior to PBST wash.

Secondary antibody solutions were made with the appropriate blocking buffers with an additional 0.1% Tween 20 at a dilution of 1:10,000. Membranes were placed in black boxes with lids and covered in secondary antibody solution. The boxes were placed on shakers at room temperature for 1 hour. The membranes were then washed with PBST 3 times for 3 minutes on the shaker. This was followed by 2 washes with PBS for 3 minutes each, on the shaker.

The developed membranes were then imaged using the Odyssey CLx and analysed using the Image Studio software configured to use with Odyssey CLx images. Alternatively, or NIR fluorescence imaging using Odyssey was used to visualise the blot and the Odyssey software, Image Studio, was used to quantify the obtained image. All analysis was

performed blind (without prior knowledge of which sample was being measured) and normalised to tubulin or vinculin expression.

2.9 *In-vivo* study

2.9.1 Materials

- Sterile 0.9% injectable sodium chloride solution (Sigma)
- Isoflurane (Sigma)
- Pain relief cream
- Isopropanol (Sigma)
- Liquid nitrogen
- OCT (Thermo scientific)
- Mice used were: C57BL/10

Animals for all *in vivo* experiments were purchased from Harlan (UK) and maintained in-house. All experiments were carried out under statutory Home Office recommendations, regulatory, ethical and licensing procedures under the Animals (Scientific Procedures) Act 1986. Licence Holder Name: Golnoush Golshirazi

2.9.2 Protocol

The desired antisense oligonucleotide dilution was prepared in sterile injectable saline as was the desired $BaCl_2$. Mice were anesthetised using Isoflurane and injection of 25µl of sterile saline solution, AO in sterile saline or $BaCl_2$ carried out into the tibialis anterior (TA). Pain relief cream was applied to the TA of animals injected with $BaCl_2$. Animals were placed into an isolated chamber until fully conscious and then returned to their normal

cage where they were monitored daily. TAs from mice was excised *post mortem* and weights were recorded. The muscles were embedded in OCT embedding medium and frozen in iso-propanol cooled with liquid nitrogen. Cryosectioning was performed with OTF 5000 cryostat, and 10µm transverse sections of each TA were sectioned up to 10 levels through the muscle length. The tissue cut in the intervening sections between the levels of a block was collected at 10µm in 1.5ml Eppendorf tubes for protein and RNA extraction and stored at -80°C.

2.10 Picro-red Sirius red staining

2.10.1 Materials

- Slides with 10µm thick sections cut as outlined in section 2.9
- Sirius Red
- Saturated aqueous solution of picric acid
- 4% (v/v) formaldehyde solution in PBS
- 100% Absolute Ethanol
- 0.5% (v/v) Acetic acid
- Xylene (BDH)
- DPX mountant (BDH)
- Nikon NiE upright microscope

2.10.2 Protocol

0.3g of Sirius red was dissolved in 100ml of saturated aqueous solution of picric acid to make a 0.3% picro-sirius red solution. This solution was filtered before use.

Slides were air dried and fixed in 4% formaldehyde for 10 minutes. They were then washed twice in tap water for 5 minutes and once in distilled water for 5 minutes. The slides were then placed in 100% ethanol for 5 minutes and air dried for 20 minutes at least, to allow slides to be completely dry. The dry slides were then submerged in 0.3% Sirius red solution for one hour. The slides were then washed quickly in distilled water and fixed in two washes of 0.5% acetic acid, 5 minutes each wash. After fixing, the slides were dehydrated in three washes of 100% ethanol, 5 minutes each wash. The slides were then placed in xylene for 10 minutes and mounted using DPX. The slides were then visualised and photographed using the Nikon NiE upright microscope where Collagen I and III were stained in red and cytoplasm in yellow. Random regions of a section were captured at 10X making sure no overlaps took place. Three images were taken per section. The images were recorded and processed using identical parameters of exposure and saturation between differentially treated and control samples. Analysis was performed using ImageJ. All analysis was performed blind.

2.11 Immunofluorescence staining

2.11.1 Materials

- 4% Formaldehyde solution in PBS
- Phosphate Buffered Saline (PBS)
- Goat Serum
- Triton X-100
- Tween 20
- Rabbit anti-Periostin (Abcam. ab14041): 1/400 dilution. Stored at -20°C.
- Rabbit anti-Fibronectin (Abcam, ab2413): 1/400 dilution. Stored at -20°C.

- Rabbit alpha-SMA (abcam, ab5694): 1/200 dilution. Stored at -20°C.
- Rabbit anti-Collagen VI: 1/400 dilution. Stored at -20°C
- Rat anti-Laminin (Sigma, L9393): 1/800 dilution. Stored at -20°C.
- Goat anti rabbit-Alexa Fluor 488 (ab150077): 1:200 dilution. Stored at 4°C
- Goat anti Rat Alexa Fluor 568 (ab175476): 1:200 dilution. Stored at 4°C
- Dapi (Sigma)(1µg/ml):1/1000 dilution Stored at -20°C.
- Mounting medium (Vector Labs)
- Nikon NiE upright microscope

2.11.2 Protocol

Blocking buffers were made individually for different staining:

- Periostin staining blocking buffer: 1xPBS, 20% Goat Serum, 0.1% Triton X-100
- Alpha-SMA staining blocking buffer: 1xPBS, 5% Goat Serum, 0.1% Triton X-100
- Collagen VI and Fibronectin staining blocking buffer: PBST(0.05% Tween 20), 5% milk

Slides were air dried at room temperature for 15 minutes. The slides were then fixed in 4% PFA for 10 minutes. Slides were washed quickly with PBS then blocked in appropriate blocking buffer for either 1 hour for Alpha-SMA, Collagen and Fibronectin staining or 1 hour 30 minutes for Periostin staining, all at room temperature. Slides were then quickly dipped into a jar filled with 1XPBST (0.05% Tween 20). Antibody dilutions containing the appropriate antibody as well as laminin antibody were made in the specific blocking buffer and added directly onto the slides; slides were incubated either overnight at 4°C

in the case of Periostin and Alpha-SMA staining or 1 hour at room temperature in the case of Collagen VI and Fibronectin.

Slides were washed three times in 1XPBST (0.05% Tween 20) for 5 minutes. Secondary antibody dilutions were made in 1XPBST (0.05% Tween 20) and 1% goat serum, added directly onto the slides and incubated for 1 hour at room temperature in the dark. The slides were then washed 5 times in 1XPBST (0.05% Tween 20) for 5 minutes, protected from the light. DAPI was diluted in 1XPBST (0.05% Tween 20) and 1% goat serum and added directly onto slides and incubated for 10 minutes protected from the light. Slides were washed 3 times in PBST (0.05% Tween 20) for 3 minutes, protected from the light.

The slides were then mounted using mounting medium and left to air dry overnight at 4°C protected from light. The slides were stored at 4°C. Slides were then visualised and photographed using the Nikon NiE upright microscope. Random regions of a section were captured at 20X making sure no overlaps took place. The images were recorded and processed using identical parameters of exposure and saturation between differentially treated and control samples. Analysis was performed using ImageJ. Analysis was performed blind.

2.12 Bioinformatics Tools

The following bioinformatics are available on-line and free for academic use:

- Gene sequences, with protein translations, gene structures and transcription products (intron-exon structures) are available with many graphic displays from NCBI and Ensembl: https://www.ncbi.nlm.nih.gov; www.ensembl.org
- Transcript sequences for *mstn and postn* were obtained from Ensembl (above)

- Homology between orthologue sequences was using SnapGene and EMBOSS Matcher. from the European Bioinformatics Institute: https://www.snapgene.com/academics/for-academics/ https://www.ebi.ac.uk/Tools/psa/emboss_matcher/nucleotide.html)
- For AON short sequence, off-target binding site searches, BLAST was performed over the nucleotide collection nr/nt database run under search parameters adjusted for 'short input sequences': https://blast.ncbi.nlm.nih.gov/Blast.cgi?PAGE_TYPE=BlastSearch
- Free energies of PMO binding to target and target free energy were calculated using RNAup server: http://rna.tbi.univie.ac.at/cgi-bin/RNAxs
- Secondary structures for portions of *mstn* mRNA were predicted with Mfold software: http://mfold.rna.albany.edu/?q=mfold
- Splice motifs were predicted using Human Splicing Finder and ESEfinder: http://www.umd.be/HSF3/HSF.shtml; http://krainer01.cshl.edu/cgi-bin/tools/ESE3/esefinder.cgi?process=home
- For a second method of predicting ESE sites RESCUE-ESE was used: http://genes.mit.edu/burgelab/rescue-ese/
- Oligonucleotide T_ms and %GC were calculated for PMOs using the IDT OligoAnalyzer tool: www.idtdna.com/tools/oligoanalyzer.

2.13 Statistics

All statistics for this project was carried out using Prism software. Where comparison of two groups was concerned a student t-test was performed between the groups. In the

case where multiple groups were compared One Way ANOVA was performed. T-test was used to compare groups after one-way ANOVA.

3. Design and *In-vitro* testing of antisense oligonucleotides targeting *MSTN* expression

3.1 Introduction

Myostatin downregulation has been suggested as an effective approach to decrease fibrosis and increase muscle mass, especially in dystrophic disease models (discussed in section 1.9). We have previously demonstrated that an AON-based exon-skipping strategy is particularly effective in decreasing myostatin expression by creating an out-of-frame transcript of the gene (Kang *et al.*, 2011b; Lu-Nguyen *et al.*, 2015). Here, we have speculated whether targeting other transcriptional signals regulating processing and maturation of mRNA (e.g. polyA signal) could also serve as an efficient method to downregulate myostatin expression. Therefore, PMOs against the myostatin polyA signal were designed and compared to the previously tested PMO (i.e., D30-PMO) that induces frameshift of the myostatin transcript.

3.1.1 Objectives

In this Chapter we designed new PMOs predicted to bind the polyA binding region of the *MSTN* gene, using bioinformatics tools. Three were selected based on various bioinformatic predictions: they were tested by transfecting cells, and measuring *MSTN* mRNA levels. Downregulation of myostatin mediated by three novel PMOs targeting the polyA signal was compared with downregulation achieved by the previously designed PMO which targeted exon 2 to cause a frame-shift of myostatin. It was anticipated that targeting the polyA control region of the gene might abrogate gene

transcription more severely than the previously designed oligonucleotide, and that this might be reflected in the mRNA levels as measured by RT-PCR and qPCR.

PMO chemistry was used in this *in vitro* study. PMOs are third generation antisense oligonucleotides with the main modification being on the furanose ring of the nucleotide (Chan, Lim and Wong, 2006). They have better target affinity, nuclease resistance, biostability and pharmacokinetics. PMOs are non-charged antisense oligonucleotides and are resistant to nucleases and proteases in biological systems making them very stable (Amantana and Iversen, 2005). The lack of charge on PMOs means they cannot be delivered efficiently across cells using cationic liposomes and therefore need to be used at high concentrations (Sazani *et al.*, 2001). Many different methods for the delivery of PMOs to cells have been studies such as conjugation of peptides to PMOs (P-PMOs or ARP-PMOs) (Nelson *et al.*, 2005), annealing of an anionic single-stranded nucleic acid molecule a 'leash'(Marsollier *et al.*, 2016) or the use of a transfection reagent called an Endo-Porter. Endo-Porter delivers substances into the cytosol by an endocytosis-mediated process and has been previously used and proved to be efficient. A previous study in the lab as well as a published study has shown that using the Endo-Porter reagent at 6µM is successful at delivering PMOs into cells (Summerton, 2005). Based on the mentioned, we used 6µM of the Endo-Porter in this study.

3.1.2 Choosing a target sequence common to mouse and human

In order to identify optimal target sequences for AON design, the homology between the human and mouse exon 3 sequences (where the polyA signal resides) were aligned using pairwise alignment, with EMBOSS Matcher. To predict off-target binding of the PMOs designed to target the 3'UTR of the *MSTN* transcript, a BLAST search of each of

the PMO sequences was run through the nucleotide collection nr/nt database run under search parameters adjusted for 'short input sequences' (NCBI Resource Coordinators, 2014). For BLAST, a very strong match for short sequences has an E-value (Expect value, where a score of 10 means that 10 hits will be found by chance, https://blast.ncbi.nlm.nih.gov/Blast.cgi?CMD=Web&PAGE_TYPE=BlastDocs&DOC_TYPE=BlastHelp#expect) of 1e-04 or smaller, whereas a poor match indicating that the PMO is less likely to bind to its target, is considered to be greater than the threshold of 1e-03.

3.1.3 Bioinformatic prediction of mRNA secondary structure as a design principle for antisense oligonucleotides

To design an antisense oligonucleotide that successfully hybridises with its target, several factors must be considered. The most likely structure of the folded, 3-dimensional target RNA molecule in the cell appears to affect binding; it is discovered by predictive software. Base pair interactions, as well as interactions with the environment, make the pre-mRNA polymers prone to formation of secondary and tertiary structures; these become one or more thermodynamically stable conformations (Mathews and Turner, 2006). During translation, this secondary structure is unwound by ribosomes (Qu *et al.*, 2011). Antisense oligonucleotides do not have an intrinsic ability to unwind mRNA, and therefore antisense-based downregulation is believed to be limited by the secondary structure of mRNA and the position of the target sequence within that structure (Popplewell *et al.*, 2009). Pre-mRNA secondary structures can be divided into several types of structural motifs, such as stems (i.e. double helices), internal loops, hairpin loops, bulge loops and pseudoknots (Qu *et al.*, 2011). Three-dimensional tertiary structures can also be produced as a result of the interaction between multiple secondary structural motifs (e.g. tRNA or G-quadruplexes).

Higher structural ordering inflicts changes in the free energy (kcal/mol) of the structure (Eddy, 2004). The measurement of free energy is indicated by the proportion of enthalpy (energy) and entropy (disorder) of the system. Chemical systems including nucleic acids show a tendency to minimise their free energy in order to maximise structural stability. The lower the free energy, the more stable is the predicted structure so, for an RNA molecule, the structure with the lowest free energy is determined. Mfold is the most widely utilised software for predicting secondary structure for an RNA molecule by finding energy minima and analyses sequences input in FASTA format (Zuker, 2003).

Knowing the most likely secondary structure of the pre-mRNA allows antisense oligonucleotides to be designed which target more accessible sequences. Previous research has shown that antisense oligonucleotides targeting sequences with little or no local structure are more effective (Vickers, Wyatt and Freier, 2000). In addition, a more recent study looking at PMO chemistry of AONs has shown that candidates designed to target sequences with less structure had better bioactivity (Popplewell *et al.*, 2009). Therefore, antisense oligonucleotides were designed so that both ends or at least one end of the antisense sequence is targeting an open conformation of the transcript to increase the efficacy of the AON.

3.1.4 Antisense oligonucleotide thermodynamics and its effects on bioactivity

Guanine-cytosine (GC) content, melting temperature (T_m) and energies of AON-target complexes have a profound effect on AON bioactivity. Generally, a GC content of around 30-40% and T_m around 50°C yield the most effective 2'OMe AON chemistry (Aartsma-Rus *et al.*, 2009). A higher theoretical total binding energy (ΔGi) of the AON to target sequence also results in a more effective drug in a biological system (Aartsma-Rus *et al.*,

2009; Popplewell *et al.*, 2009). The information needed to work out the theoretical total binding energy is: (1) opening energy of target sequence; (2) opening energy of the AON and (3) energy from duplex formation between target and AON. The theoretical binding energy of AON to tathe rget can be calculated following the formula below.

$$\Delta Gi = (Energy\ from\ duplex\ formation) - (opening\ energy\ of\ AO) - (Opening\ energy\ of\ target\ sequence)$$

It has also been suggested that longer PMOs have better binding energies and are more likely to bind to target its sequence (Pramono *et al.*, 2012). S-fold (http://sfold.wadsworth.org/cgi-bin/index.pl) is a software that has been used over the past two decades for bioinformatic prediction of antisense and siRNA given target sequences. S-oligo, a module of S-fold, produces a series of potential antisense sequences, each varying by one base pair, for an input sequence (Ding, Chan and Lawrence, 2004). S-oligo was therefore used to design a series of potential antisense oligonucleotides with a specified length (maximum 30nt), each varying by one base pair.

RNAup server is software that calculates the factors above to obtain the total theoretical binding energy and produce an optimal secondary structure predicted to occur upon hybridisation of AON to its target (Golshirazi *et al.*, 2018). RNAup server was therefore used to calculate the theoretical binding energies of the series of designed antisense oligonucleotides.

3.1.5 PMO bioactivity and transfection in an In-vitro model

PMO chemistry of antisense oligonucleotides has previously been tested for the restoration of dystrophin expression through exon skipping in the context of the DMD

disease model (details in section 1.6). In addition, PMOs were used to knock down myostatin through skipping of exon 2, producing an out of frame protein artefact (Kang *et al.*, 2011b; Lu-Nguyen *et al.*, 2015). Interestingly, PMO chemistries were also successfully used to downregulate the expression of a toxic gene, *DUX4,* by targeting its polyA signal in the 3'UTR of its pre-mRNA (Marsollier *et al.*, 2016).

The main chemical properties of PMO include high nucleic acid binding affinity, nuclease-resistance and high solubility in aqueous solutions (Alter *et al.*, 2006; Summerton and Weller, 1997). Compared to other AO chemistries, PMO shows particularly high bioactivity in restoring dystrophin expression in *mdx* mice and dystrophic dogs across various skeletal muscles (Yokota *et al.*, 2009). However, due to the lack of charge of the PMO molecules, their diffusion across cell membranes is limited and considerably high amounts of PMO have to be administered into cell cultures in order to achieve a biologically significant effect (Suwanmanee *et al.*, 2002; Sazani *et al.*, 2002).

Endo-Porter reagent provides an alternative way of effective PMO delivery into cultured cells (Summerton, 2005). Endo-Porter is a peptide-based reagent that mediates endocytosis, functions in the presence of serum and has the capacity to deliver a number of PMOs at various concentrations (Gene Tools, Manufacturer's manual, https://www.gene-tools.com/endo_porter). The process of PMO delivery by Endo-Porter requires both the AON and Endo-Porter to be taken up simultaneously from the media into the cell via endocytosis. The ionic properties of the Endo-Porter rupture the endosomal membrane inside the cell and release its contents into the cytoplasm. Endo-

Porter-mediated PMO delivery into various skeletal muscle cell line types, derived from both mouse and humans, have been effectively tested in numerous studies.

Changes in *MSTN* mRNA expression were assessed by transfection with the three PMOs targeting the polyA signal as well as the previously designed PMO targeting MSTN exon 2, MSTN-D30 PMO (Lu-Nguyen *et al.*, 2015). As a control PMO (presumed to bind at random) a Gene Tools scrambled PMO sequence was synthesised. PMO transfection was of rhabdomyosarcoma (RD) human immortalised myoblast cells from a line that expressed *MSTN*. Cells were transfected with 2 µM PMO and 6 µM of Endo-Porter in 2% (v/v) serum media. *MSTN* mRNA levels were assessed semi-quantitatively using multiplex RT-PCR and quantitatively using RT-qPCR. 18s and GAPDH were used as housekeeping genes for the multiplex RT-PCR and RT-qPCR, respectively. For semi-quantitative analysis products from the multiplex RT-PCR were ran on a 1.5 % (w/v) agarose gel and bands were quantified using the Gene Tool software.

3.1.6 Quantitative polymerase chain reaction

Quantitative polymerase chain reaction (qPCR) or real-time polymerase chain reaction (Real-Time PCR) quantify relative gene expression by detecting and quantifying the amplification products in real time (Gibson, Heid and Williams, 1996; Nolan, Hands and Bustin, 2006). Fluorescent reporter dyes are used to label PCR DNA products and aid their quantification (Tania *et al.,* 2006). The point where the fluorescence levels exceed a defined background threshold is recorded and given as a value called the C_t (threshold cycle) or C_p (crossing point) (Tania *et al.,* 2006). Therefore, the more abundant the target, the lower the C_t value. The C_t values obtained from a target gene is then normalised to C_t values of a housekeeping gene. The high sensitivity and quantitative

nature of qPCR have been found particularly useful in detecting small changes in gene expression levels that are not attainable by other conventional methods for gene expression detection (e.g. reverse transcription PCR products visualised on gels or *in-situ* hybridisation, Smith and Osborne, 2008).

3.2 Results

3.2.1 Comparison of human and mouse polyA signal and the surrounding sequence

PolyA signals were identified in both the human and mouse myostatin transcripts and using the NCBI nucleotide database (Figure 3.1). EMBOSS Matcher revealed sequences conserved between human and mouse in exon 3, which, combined with the polyA signal sequence could potentially indicate functional importance and serve as a candidate target for AON-based strategy to downregulate myostatin expression. The alignment analysis showed a high degree of homology between the mouse and human exon 3 (Figure 3.2). EMBOSS Matcher calculated a percentage similarity of 76.4% between the human and mouse exon 3. The 22 base pairs surrounding the polyA signal is completely homologous (highlighted in grey) showing conservation between species and suggesting that this region may be important in regulating *myostatin* expression if the two species regulate this gene in the same manner (Figure 3.2).

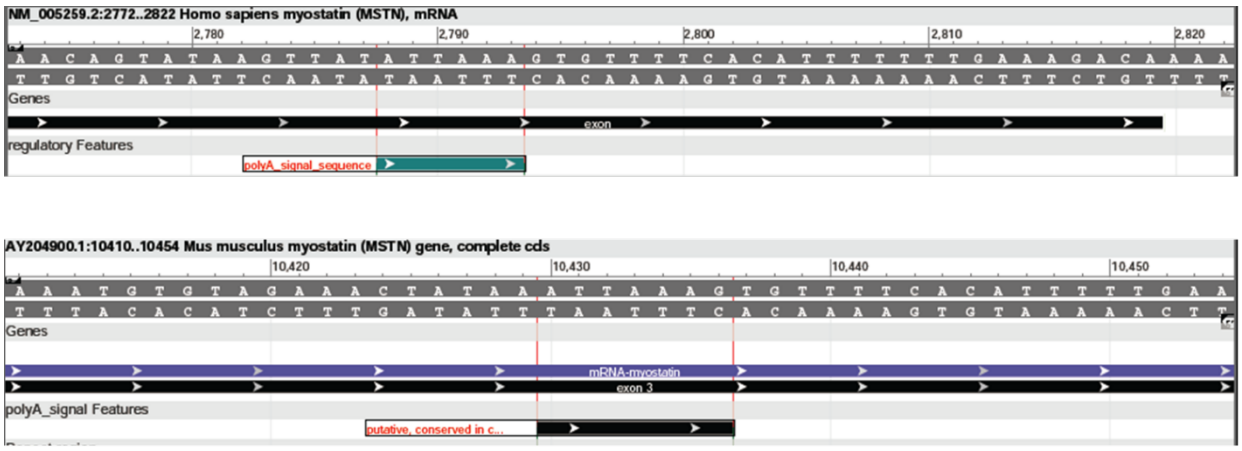

Figure 3.1 NCBI Nucleotide database output for human and mouse 3' MSTN transcript
The polyA signal (red writing on white) identified in the NCBI gene database which precede gene sequences (green for human and black in mouse).

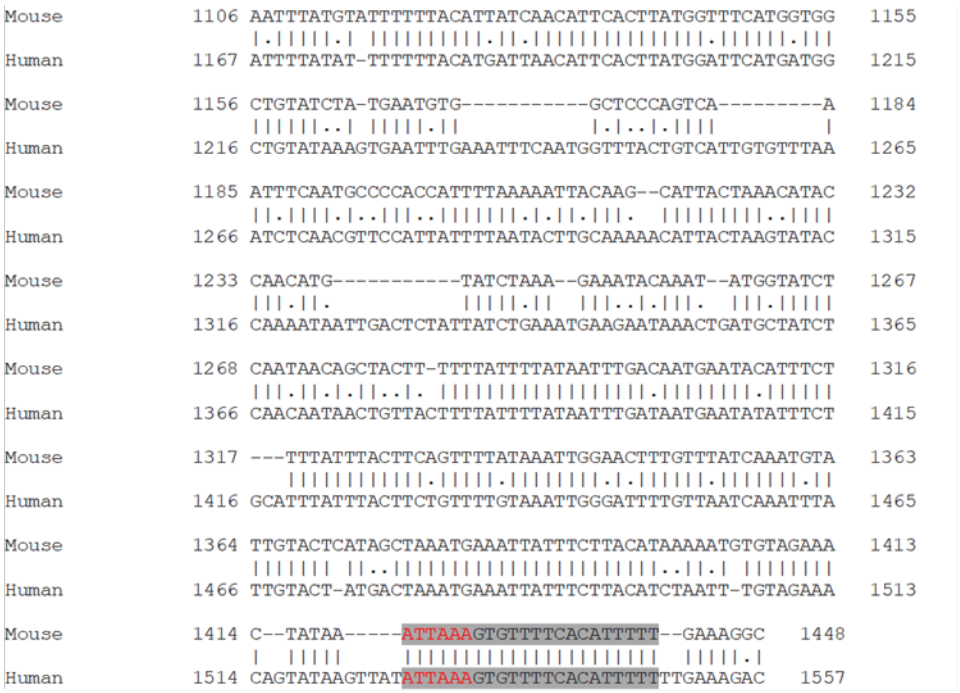

Figure 3.2 Alignment of Mstn 3' UTR in the human and mouse.

Alignment was carried out using EMBOSS Matcher with sequences obtained from Ensembl (http://www.ensembl.org). The polyA signal is indicated by a red font; a 22bp region with 100% homology between human and mouse (and including the polyA signal) is highlighted in grey.

3.2.2 Prediction of the secondary structure surrounding the human Mstn polyA signal and PMO design

Mfold was used to assess putative secondary structure of the transcript region surrounding the polyA signal. Mfold was given an input of 230 nucleotide sequence comprising exon 3 (and including the polyA signal previously identified). RNA secondary structure prediction indicated that 3 nucleotides of the polyA signal has an open configuration (Figure 3.3), consistent with it being a binding site for further processing.

S-fold was used to derive all potential PMO sequences targeting this polyA signal and the surrounding regions (Table 3.1). Due to the low GC content of the region containing the polyA signal, a series of longer PMO 30mers was designed. These include PMOs which were chosen and used for experiments: HpA1 and HpA2. The HpA1 PMO was predicted to bind the open conformation of the mRNA secondary structure, whereas the HpA2 targeted the closed conformation of the transcript but had a more optimal %GC and T_m values (Figures 3.4 & 3.5). Choosing PMOs with complementary binding targets allows investigation of the importance of binding to predicted secondary structures albeit complicated by the different thermodynamic properties of the PMO. In addition to the two 30mer PMOs, a 22-mer PMO, HMpA, was designed to target the polyA signal and the 22mer found to be conserved between mouse and human (Figure 3.2 & 3.4). The 3' end of HMpA spanned 7 nucleotides of the open conformation of the transcript, whereas its 5' end bound the part of the target that had a closed configuration (Figure 3.4).

The overall binding energy of the designed PMOs to their target sequence was assessed using RNAup server. The 3'UTR of human myostatin was submitted as the target

sequence and the PMO sequences as binding candidates. PMOs HpA1, HpA2 and HMpA all showed relatively low overall free-binding energies of -34.21kcal/mol, -34.01kcal/mol and -25.12kcal/mol, respectively, that is, exhibiting strong binding (Figure 3.5). As predicted, the longer PMOs (i.e. HpA1 and HpA2) have considerably lower binding free-energy compared with the shorter HMpA sequence so are predicted to bind better to the target (Figure 3.5).

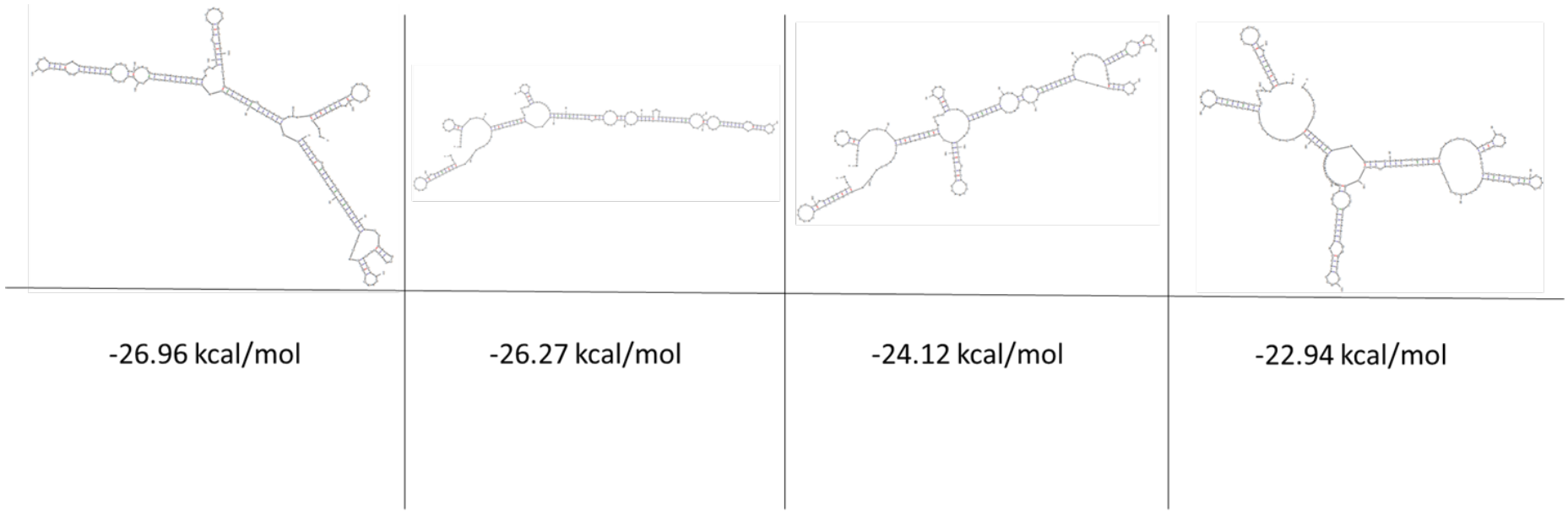

Figure 3.3 Secondary structure of the human *MSTN* polyA signal and its surrounding region predicted by Mfold.

The figure shows four predicted structures of the *MSTN* exon 3 sequence, along with their respective free-binding energies. The structures are shown in order of increasing free energy as indicated below each structure.

AON sequence (5'-3')(30 mer)	target sequence (5'-3')(30mer)	%GC	Tm (ºC)
TTTAATATAACTTATACTGTTTCTACAAAT	ATT TGT AGA AAC AGT ATA AGT TAT ATT AAA	16.7	48.4
CTTTAATATAACTTATACTGTTTCTACAAA	TTT GTA GAA ACA GTA TAA GTT ATA TTA AAG	20	48.9
ACTTTAATATAACTTATACTGTTTCTACAA	TTG TAG AAA CAG TAT AAG TTA TAT TAA AGT	20	49.6
CACTTTAATATAACTTATACTGTTTCTACA	TGT AGA AAC AGT ATA AGT TAT ATT AAA GTG	23.3	50.1
ACACTTTAATATAACTTATACTGTTTCTAC	GTA GAA ACA GTA TAA GTT ATA TTA AAG TGT	23.3	50.1
AACACTTTAATATAACTTATACTGTTTCTA	TAG AAA CAG TAT AAG TTA TAT TAA AGT GTT	20	49.6
AAACACTTTAATATAACTTATACTGTTTCT	AGA AAC AGT ATA AGT TAT ATT AAA GTG TTT	20	50.2
AAAACACTTTAATATAACTTATACTGTTTC	GAA ACA GTA TAA GTT ATA TTA AAG TGT TTT	20	49.6
GAAAACACTTTAATATAACTTATACTGTTT	AAA CAG TAT AAG TTA TAT TAA AGT GTT TTC	20	49.6
TGAAAACACTTTAATATAACTTATACTGTT	AAC AGT ATA AGT TAT ATT AAA GTG TTT TCA	20	50.3
GTGAAAACACTTTAATATAACTTATACTGT	ACA GTA TAA GTT ATA TTA AAG TGT TTT CAC	23.3	50.8
TGTGAAAACACTTTAATATAACTTATACTG	CAG TAT AAG TTA TAT TAA AGT GTT TTC ACA	23.3	50.8
ATGTGAAAACACTTTAATATAACTTATACT	AGT ATA AGT TAT ATT AAA GTG TTT TCA CAT	20	50.2
AATGTGAAAACACTTTAATATAACTTATAC	GTA TAA GTT ATA TTA AAG TGT TTT CAC ATT	20	49.6
AAATGTGAAAACACTTTAATATAACTTATA	TAT AAG TTA TAT TAA AGT GTT TTC ACA TTT	16.7	49.1
AAAATGTGAAAACACTTTAATATAACTTAT	ATA AGT TAT ATT AAA GTG TTT TCA CAT TTT	16.7	49.7
AAAAATGTGAAAACACTTTAATATAACTTA	TAA GTT ATA TTA AAG TGT TTT CAC ATT TTT	16.7	49.8
AAAAAATGTGAAAACACTTTAATATAACTT	AAG TTA TAT TAA AGT GTT TTC ACA TTT TTT	16.7	50.3
AAAAAAATGTGAAAACACTTTAATATAACT	AGT TAT ATT AAA GTG TTT TCA CAT TTT TTT	16.7	50.3
CAAAAAAATGTGAAAACACTTTAATATAAC	GTT ATA TTA AAG TGT TTT CAC ATT TTT TTG	20	50.2
TCAAAAAAATGTGAAAACACTTTAATATAA	TTA TAT TAA AGT GTT TTC ACA TTT TTT TGA	16.7	50.3
TTCAAAAAAATGTGAAAACACTTTAATATA	TAT ATT AAA GTG TTT TCA CAT TTT TTT GAA	16.7	50.3
TTTCAAAAAAATGTGAAAACACTTTAATAT	ATA TTA AAG TGT TTT CAC ATT TTT TTG AAA	16.7	50.8
CTTTCAAAAAAATGTGAAAACACTTTAATA	TAT TAA AGT GTT TTC ACA TTT TTT TGA AAG	20	51.2
TCTTTCAAAAAAATGTGAAAACACTTTAAT	ATT AAA GTG TTT TCA CAT TTT TTT GAA AGA	20	52.4

Table 3.1 Prediction of 30-mer PMOs spanning though the polyA signal region of the *MSTN*.

The list was generated by S-fold includes the GC content and Tm values for each PMO.

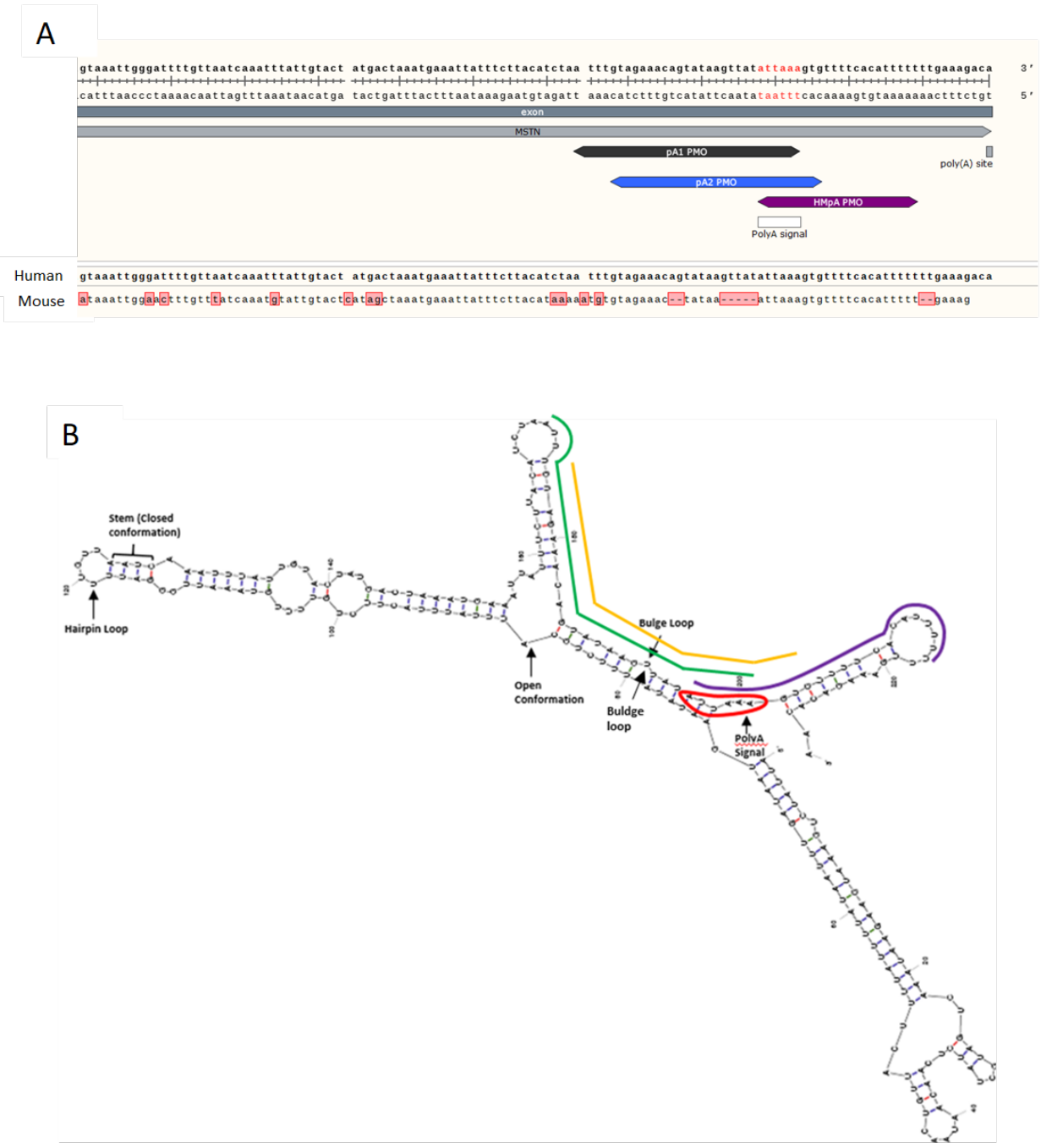

Figure 3.4 Positioning of designed PMOs on the human *MSTN* transcript

A) Placement of PMOs along exon 3 of the *MSTN* transcript. The polyA signal is shown with a red font and marked with a white box. The alignment of human and mouse sequence is shown with mismatches highlighted in red.

B) Position of designed PMOs on the human *MSTN* secondary structure targeting the polyA signal (circled in red). HpA1, HpA2 and HMpA PMOs are shown in green, orange and purple, respectively.

A

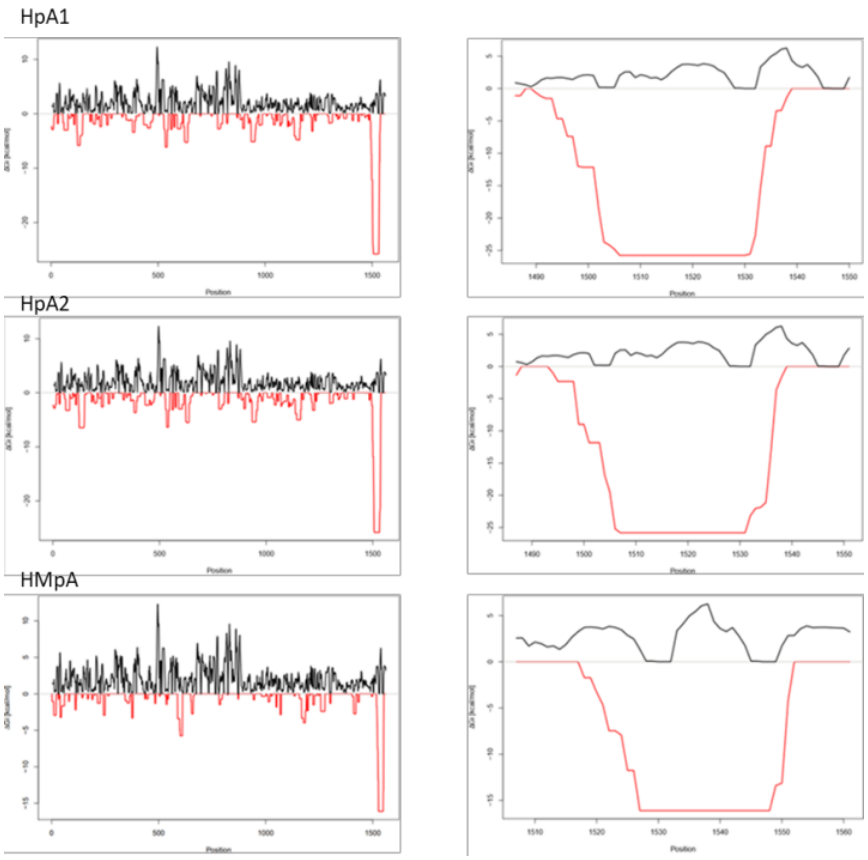

B

PMO Name	PMO Sequence	Target Sequence	ΔG (kcal/mol)	Opening energy of target (kcal/mol)	Opening energy of PMO (kcal/mol)	Overal ΔG (ΔGi)	%GC	TM
HpA1	TTTAATATAACTTATACTGTTTCTACAAAT	ATT TGT AGA AAC AGT ATA AGT TAT ATT AAA	-34.21	7.69	0.77	-25.75	16.7	48.4
HpA2	CACTTTAATATAACTTATACTGTTTCTACA	TGT AGA AAC AGT ATA AGT TAT ATT AAA GTG	-34.01	7.69	0.51	-25.81	23.3	50.1
HMpA	AAA AAT GTG AAA ACA CTT TAA T	A TTA AAG TGT TTT CAC ATT TTT	-25.12	7.20	1.80	-16.11	18.2	45.2

Figure 3.5 Thermodynamic properties of PMO calculated by RNAup server

A) The RNAup derived plot shows the overall free-binding energy between PMO and the target sequence along the transcript. In red, the free-binding energy of the PMO to the target sequence is indicated. The energy required to resolve the secondary structure of the target sequence is indicated in black. The y-axis shows the free energy in kcal/mol, while the x-axis indicates the nucleotide position in the sequence.

B) Summary of the thermodynamic properties of the PMO sequences designed to target the *MSTN* exon 3 polyA region (from RNAup).

3.2.3 Off target prediction of designed PMOs

The nr/nt BLAST search for off-target binding of the PMO sequences (Table 3.2) throughout the human genome For each of the PMO sequence analysed, two distinct gene target sequences were selected by the highest alignment scores as represented by smallest E-values (Table 3.2). For all the BLAST-analysed PMO sequences the predicted target sequences with the highest alignment score (i.e. lowest E-value) was the *MSTN* transcript (Table 3.2). Therefore, all designed PMOs were predicted to have a very strong binding to the *MSTN* transcript (E-value ≤ 7e-08), whereas the off-target gene candidates show markedly higher values, greater than 1e-03 (Table 3.2).

PMO Name	Target Name	E-Value	Query Cover	Orientation (strand)
HpA1	MSTN	7e-08	100%	Forward
	PDE8A	1.9	60%	Forward
HpA2	MSTN	8e-08	100%	Forward
	ITFG1	1.9	63%	Forward
HMpA	MSTN	0.009	100%	Forward
	DARS	2.2	81.8%	Forward

Table 3.2 PMO of off-target prediction

Each of the predicted series of PMOs was run through Ensembl BLASTN, under conditions for short input sequences and limited to human and nr/nt databases. E-values were generated which revealed these three PMOs have the highest probability of binding the *MSTN* transcript and a very low likelihood of binding any other gene.

3.2.4 In-vitro testing of PMOs targeting MSTn 3'UTR in RD cells

Having designed three specific PMOs based on the bioinformatic analysis, it was then important to test their effect on myostatin expression *in vitro*. RD cells are a human myoblast cell line that was previously used to study *MSTN* exon 2 skipping with one of the test (control) PMOs, MSTN-D30 (Nguyen *et al.*, 2015). *MSTN* message levels were assessed by PCR. Firstly, multiplex RT-PCR showed downregulation of *MSTN* by all PMOs tested, compared to the control PMO, a scrambled sequence (Figure 3.6). However, the reduction of *MSTN* by the HpA1 PMO was not statistically significant (Figure 3.6). Out of the three PMOs designed to target the polyA site, HMpA treatment resulted in the highest downregulation of the *MSTN* expression ($p<0.01$). Overall, the highest downregulation of *MSTN* mRNA, as measured by PCR, was that induced by MSTN-D30 targeting the *MSTN* exon 2 to induce exon skipping ($p<0.001$) (Figure 3.6). Multiplex PCRs are always complex because of interference between PCR products, so results are rarely quantitative and should be treated with caution.

To quantitatively assess the expression of the *MSTN* levels in the PMO treated cells, RT-qPCR was carried out. With this method, *MSTN* mRNA levels showed statistically significant downregulation with HpA1 treatment compared to the control ($p<0.01$), so that the relative sensitivity of the mono-PCR resulted in a greater sensitivity of RT-qPCR to changes in regulation, compared to the multiplex RT-PCR assay (Figure 3.7). The remaining PMO chemistries, showed a similar pattern of *MSTN* downregulation as measured by the RT-PCR. (Figures 3.6 & 3.7). However, the magnitude of statistical significance in RT-qPCR compared to the RT-PCR was increased by 10- fold for HpA2($p<0.001$) and MSTN-D30($p<0.0001$), and 100-fold for HMpA($p<0.0001$).

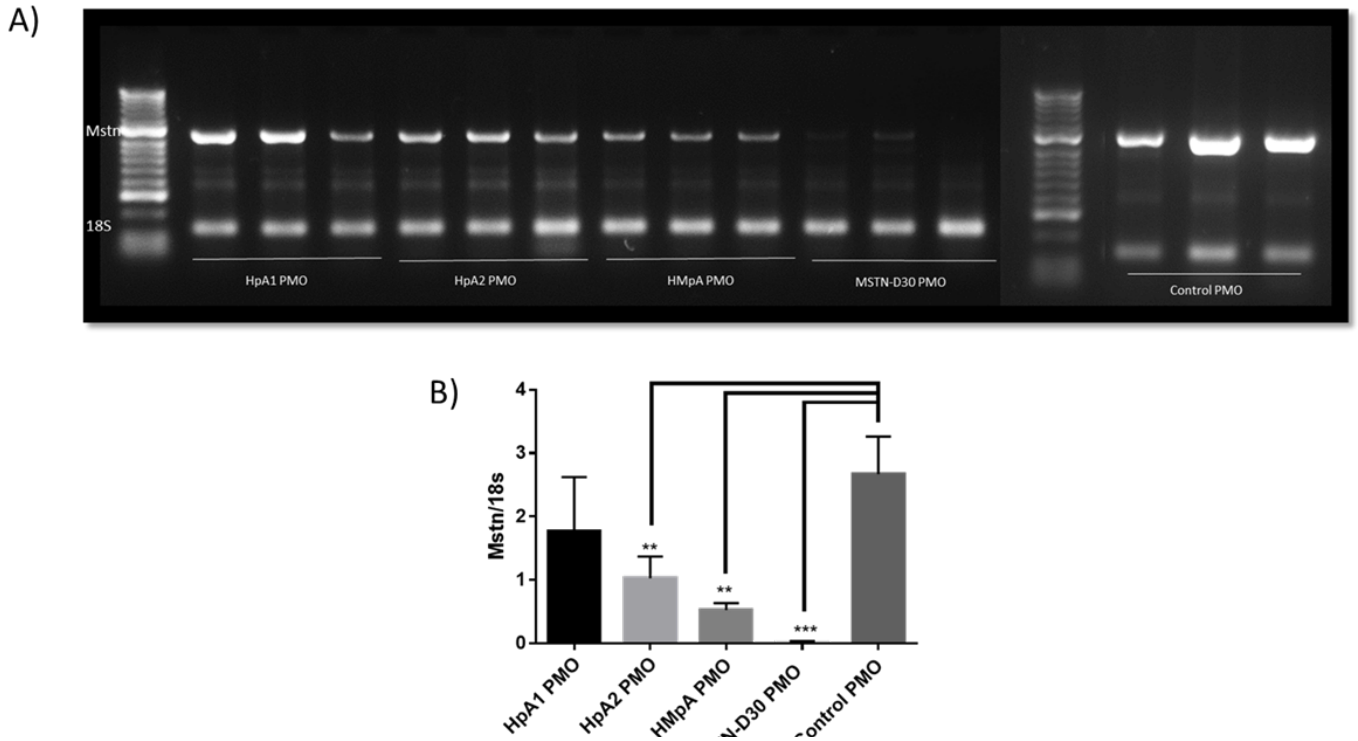

Figure 3.6 Myostatin expression following PMO transfection

RD cells were transfected with PMO: either HpA1, HpA2, HMpA or MSTN-D30-PMO; Mstn and 18S RNA primers were used together for PCR. A) Multiplex PCR was run using *MSTN* and 18S primers. The RT-PCR products were separated on a 2% agarose gel along with molecular weight markers. The strongest bands in the ladders are 1013 (marked Mstn) and 300bp (Hyperladder IV, Ecogen).

B) Intensities of the bands were quantified using GeneTools software. Expression is inhibited by all PMOs compared to the control, in order HpA1 < HpA2 < HMpA (polyA targetting) < MSTN-D30 (truncated product). Statistical comparison was using a one-way Anova test , N=3.

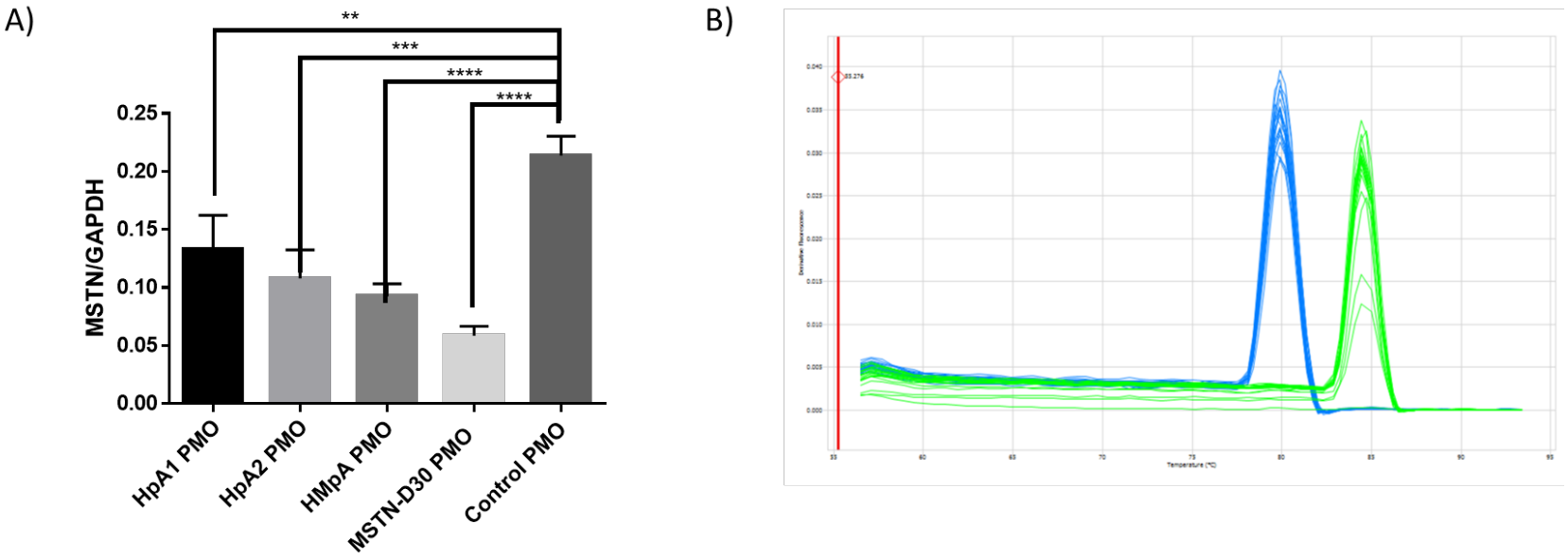

Figure 3.7qPCR assay of MSTN expression normalised to GAPDH.

RD cells were transfected with HpA1, HpA1, HMpA or MSTM-D30 PMOs. RT-qPCR of the cells was with primers to *MSTN* and *GAPDH* housekeeping gene. Replicate standard deviations are much smaller with this method. The same pattern of suppression of mRNA levels is seen as in Figure 3.6. A) *MSTN* expression relative to *GAPDH* was quantified and compared to levels in control PMO samples using a one-way ANOVA statistical test, N=3. B) Melting curves of *MSTN* and *GAPDH* showed two and only two distinct peaks (*MSTN* in blue and *GAPDH* in green) indicating primer specificity and absence of contamination arising from alternative PCR primer binding sites: only MSTN and GAPDH were amplified.

3.3 Discussion

Antisense oligonucleotides targeting the *MSTN's* polyA signal within the 3'UTR were designed, with a view to downregulating myostatin expression. Bioactivity of these PMOs was compared to MSTN-30D, the PMO inducing exon skipping which targets the *MSTN* exon 2 (Kang *et al.*, 2011b).

In order to design optimal PMO chemistries, bioinformatic tools can be used to predict the ability and specificity of a short DNA sequence binding to its target (Popplewell *et al.*, 2009; Golshirazi *et al.*, 2018). Extensive research has been carried out to assess how to design successful antisense oligonucleotides which induce exon exclusion (Mann *et al.*, 2002) to either disrupt or restore reading frames (Malerba *et al.,* 2012). Importantly, since they involve nucleotide sequences, the findings of these studies can be applied to the design of AON targeting other regulatory elements present within transcript sequences.

Polyadenylation of the 3' end of pre-mRNAs is essential for maturation of the message and its export from the nucleus (Chapter 1). The most important element determining the cleavage site is the polyA signal which consists of a six-nucleotide motif (Tian *et al.*, 2005b). In mammals, the consensus sequence AAUAAA or AUUAAA is recognised by cleavage and polyadenylation factors which demark a cleavage site 10-30 nt downstream of the polyA signal (Proudfoot, Furger and Dye, 2002b; Wada *et al.*, 2012). Previous studies have successfully targeted the polyA signal using PMO chemistry for antisense oligonucleotides, to downregulate gene expression (Marsollier *et al.*, 2016). In Marsollier's study, targeting of the polyA signal was more effective than targeting

other 3'UTR elements such as the DSE site where the pre-mRNA is cleaved. This is why targeting the polyA signal was used to downregulate myostatin in this study.

Many studies have been carried out to assess the 'hit rate' of AON oligonucleotides: thermodynamic stability, secondary structure of target mRNA, length of the AON and proximity of its hybridisation to a functional gene motif have all been found to affect the binding and effectiveness of synthetic 'drug' AONs (Chan, Lim and Wong, 2006; Aartsma-Rus, *et al.*, 2009; Popplewell *et al.*, 2009). It is widely accepted that the following four considerations are effective for increasing bioactivity of designed AONs: i) prediction of RNA secondary structure; ii) GC content; iii) T_m of AON (a prediction of how tightly it binds its target) and iv) total-free binding energy of AON to the target sequence. Bioinformatics tools are provided gratis to perform each of these calculations (Section 3.1). In this study, all the above factors were considered, and PMOs were designed as carefully as possible using bioinformatics alone, and the constraints of the target. The target itself was selected bioinformatically, based on homology between mouse and human sequences; homology indicates conservation of function. Given the very specific target sequence, it was necessary to work with PMOs where the percentage GC was below the ideal of 55%, suggested by Ho *et al.* (1996) as the minimum GC content for very stable AON binding. For this reason, the length of the newly designed PMOs was increased to 30 nucleotides, to increase the percentage GC as far as possible and increase the T_m of the PMO. An increase in length was found by Popplewell *et al.* (2009) to increase PMO bioactivity. The T_m of the designed PMOs were between 45-50°C which was shown to be optimal by Aartsma Rus *et al.* (2009) .

The role of secondary pre-mRNA structure in the efficacy of AONs has been studied, and there has been a general consensus that less local structure predicted at the target sequence, the more successful the AON (Bowen, Jenkins and Fraser, 2013). In the Popplewell study (Popplewell *et al.*, 2009), it was shown that when testing PMOs, the secondary structure of the target sequence does not significantly correlate with the success of the PMO, but when looking at successful PMOs, the ones that target sequences with less local structure are definitely more effective. PMOs in this study were therefore designed so that they bound different parts of the target, with respect to predicted secondary structures (Figure 3.4). The weakest PMO, HpA1, was predicted to bind the target sequence with both ends of the PMO in loops, one end being the open polyA signal sequence, but the other in the loop of a stem-loop structure. HpA2 was predicted to bind with both ends targeting stems or double helix, closed RNA conformation. However, it has better thermodynamic properties, with a higher GC content and higher overall binding energy. The best of the three PMOs, HMpA, had lower binding energy and GC content but targeted the polyA sequence with one end, where RNA is in the open conformation, and the other end of the PMO wraps around a stem-loop (like HpA1 but with the other end around the loop). These three combinations allowed some comparison of the putative effects of different factors; for a rigorous assessment of RNA secondary structure, every PMO would have had the same GC content and T_m/free binding energy.

Having designed three PMOs targeting the polyA signal they were tested in RD cells along with the *MSTN* exon 2 targeting PMO, MSTN-D30, which is also a 30-mer. Semi-quantitative analysis by RT-PCR showed that although all four PMOs caused a decrease in *MSTN* expression, the HpA2, HMpA and MSTN-D30 PMOs showed significant

downregulation; in our hands, MSTN-D30 PMO resulted in nearly no MSTN expression, while HMpA resulted in significant downregulation.

When semi-quantitative analysis was previously used to quantify the effect of exon skipping (Kinali *et al.*, 2009b; Popplewell *et al.*, 2009; Kang *et al.*, 2011b), both the skipped product and full-length product were amplified in the PCR reaction, products run on an agarose gel and the ratio of the full-length band and skipped band quantified. In our case, we only amplified the full-length Mstn. It is possible that more out-of-frame (exon-skipped) Mstn was produced using MSTN-D30, but as this was not quantified it was not possible to say whether the new polyA-targeted PMOs were more effective. In other words, MSTN-D30 may have resulted in aberrant Mstn production which was not measured. In the case of targeting the polyA signal, there was no secondary product expected, as messages lacking the polyA tail are not even transported out of the nucleus (section 1.10).

Although the multiplex PCR, optimised and used for this study, showed a clear downregulation of Mstn mRNA expression, the PCR amplification of *MSTN* mRNA was only semiquantitative, so not the most sensitive assay for our purposes. Due to this limitation, RT-qPCR was performed to more accurately quantitate *MSTN* mRNA. Predesigned primers were used to assess total RNA levels using, *GAPDH,* a housekeeping gene, for normalisation. It has previously been shown that RT-qPCR of total RNA is sensitive to mRNA loss by nonsense-mediated decay (NMD) (Pereverzev *et al.*, 2015): in the case of degradative exon skipping, the truncated mRNA missing an exon no longer has a reading frame, so the transcript is subject to NMD (Ward *et al.*, 2014). Using RT-qPCR is therefore ideal for quantifying gene expression with both polyA targeting PMOs

and the exon skipping PMO. This also suggests that semi-quantitative analysis may not be representative of the extent of knockdown by PMOs designed for degradative exon skipping.

RT-qPCR results showed a similar pattern to the semi-quantitative analysis. Knockdown by each PMO was significant, with MSTN-D30 PMO showing the greatest downregulation, followed by HMpA. This confirmed that exon skipping using the MSTN-D30 PMO is more effective for myostatin knockdown than polyA targeted PMOs.

HMpA was predicted to be least likely to bind its target as predicted by thermodynamic properties but proved to be the most effective in *vitro* assays. This could be due to the fact that HMpA completely targeted the putative 22-nucleotide sequence motif (presumably a control sequence) that are conserved between mouse and human. This result highlights the significance of this region in gene expression and the use of interspecies homologous motifs. Another factor contributing to the effectiveness of HMpA could be the fact that it binds to the predicted secondary structure at an open configuration *at the 5' end* (in the polyA signal motif). This, combined with it targeting a significant orthologous conserved region may compensate for the less optimal thermodynamic properties.

4. Design of antisense oligonucleotides to target out-of-frame exons and downregulate Periostin in human and mouse

4.1 Introduction

4.1.1 Objectives

PMOs have been made to target and downregulate Mstn (Chapter 3). This Chapter is concerned with designing PMO AONs targeting exons whose skipping will induce a reading frame shift in the human and mouse *POSTN1* gene mRNA. This involved identifying candidate exons in the *POSTN* gene, of both human and mouse, using different bioinformatic tools to design PMOs, targeting ESE sites within conserved regions between mouse and human, with the most ideal thermodynamic properties, then testing the PMOs in transfected cells for downregulation of POSTN1 message.

4.1.2 Modification of pre-mRNA splicing antisense oligonucleotides

AONs have been extensively used in a variety of fields to target sequences around the splice sites where they interfere with the splicing machinery, and so disrupt the splicing process. Depending on the sequence targeted this can lead to exon inclusion or exon exclusion. In the latter case this can lead to restoration of the open reading frame in a mutated gene or disruption of the natural open reading frame.

For DMD, a lot of effort has gone into designing AONs targeted to various exons of the *DMD* mRNA to restore the dystrophin reading frame, for several idiopathic mutations. The mRNA product is shorter because of skipping of the targeted exon, but in the

selected cases the ORF of flanking exons is in-phase and so the transcript is in-frame. In this way the final translation product is a shortened but functional dystrophin protein akin to those found in much milder BMD (Sherratt *et al.*, 1993; Aartsma-Rus *et al.*, 2002; Dickson, Hill and Graham, 2002). However, antisense mediated skipping of exons that are flanked by out-of phase exons will lead to a transcript where there is a frame shift downstream of the skip. In this situation the reading frame will not be open, and a nonsense codon will rapidly be encountered. Such "destructive" exon skipping will lead to translation termination and a truncated protein product which is most likely inactive or dysfunctional, and/or rapidly degraded. AON reagents of this nature thus carry potential to downregulate the functional activity of the target gene and its product. (Ralston and Shaw, 2008). Operationally, the triplet nature of codons mandates that only exons whose nucleotide length is divisible by 3 will have the in-phase flanking exons that are required for an in-frame skipped transcript (Popplewell *et al.*, 2009) and conversely, skipping of exons of a size non-divisible by 3 will yield a reading frame shift and a loss of function. Exon of this nature can thus be easily identified.

Although it has previously been shown that AON targeting of exon donor and acceptor splice site and branch point sequences successfully leads to exon exclusion (Mann *et al.*, 2002; Graham *et al.*, 2004; Wilton and Fletcher, 2005), there is no strong consensus (A Aartsma-Rus *et al.*, 2009) and there is also evidence that targeting acceptor/donor splice sites does not always lead to skipping (Wilton at al 2006). In contrast targeting ESE elements which function to facilitate recognition of exonic sequences and the recruitment of the spliceosome machinery to the pre-mRNA has been shown to yield more consistent successful activity in terms of antisense-mediated exon exclusion (Stojdl and Bell, 1999).

In previous studies on the DMD and MSTN genes, AONs have been used to target specific exons, and in both cases this reduces exon inclusion. In the case of DMD, where the mutated dystrophin mRNA often produces a frame-shift, targeting exons flanking mutation sites may lead to the restoration of the ORF and appearance of a semi-functional BMD-like dystrophin protein. In the case of myostatin the aim was to disrupt gene expression and so AON-mediated exon skipping was designed to induce frame-shifting, creating out-of-frame transcripts with premature termination codons and a reduction in the level and function of myostatin protein (Kang *et al.*, 2011a; Malerba *et al.*, 2012).

4.1.3 Predicting potential target ESE sites and designing PMOs

Popplewell *et al.* (2009) and Aartsma-Rus *et al.* (2009) both evaluated a range of parameters in the design and application of AONs for DMD exon skipping. Their studies showed that targeting exonic sequences gave more functional antisense effects than targeting intronic sequences. This could be due simply to the higher GC content of exons which allowed the design of AONs against GC-rich sequences, leading to stronger AON hybridising. These and other studies also showed that AON hybridising to and presumed to be blocking ESEs also led consistently to AONs with strong exon skipping activity(Caputi, Kendzior and Beemon, 2002; Cartegni and Krainer, 2002; Smith *et al.*, 2002). T

he number of ESE sites within the target sequence of AONs also showed a strong correlation with AON efficacy (Annemieke *et al.*, 2009): ESE sites in these studies were predicted and identified using algorithms linked to either the RESCUE-ESE database (Fairbrother *et al.*, 2002) or the Human Splicing Finder database (Desmet *et al.,* 2009).

Human Splicing Finder (HSF) uses other databases such as ESE-Finder (Cartegni *et al.*, 2003) and RESCUE-ESE (Fairbrother *et al.*, 2002) but as the title suggests is specific for human sequences. Targeting internal ESE sites by these means will imply operationally that exon-intron boundaries would not be precisely identified, as ESEs would not be recruited (Fairbrother *et al.*, 2002). This, in turn, leads to the exon being excluded from the transcript. As discussed previously in chapter 3, other factors such as the GC content, T_m, position of binding on the target RNA secondary structure and the overall binding energy should also be considered when designing AONs (Popplewell *et al.*, 2009).

ESE-Finder has an input of a specific nucleotide sequence and outputs 6-8 nucleotide predicted ESE binding sites for SR proteins. ESE-Finder does this by using different matrices relative to different SR protein motifs to search for possible ESE binding sites (Liu, Zhang and Krainer, 1998; Liu *et al.*, 2000). The sequence being examined at is pasted into the query interface or uploaded in FASTA format. A graphics output displays the exon sequence. Colour-coded bars on the graph represent the scores of different motifs above selected thresholds. The position of the bars on the X-axis (the breadth of the bar) shows the position and length of the motif on the exon sequence, whereas the height of the bar represents the motif score (Cartegni *et al.*, 2003).

RESCUE-ESE (http://genes.mit.edu/burgelab/rescue-ese/) is another bioinformatics tool used to predict ESE sites which uses a different method to find ESEs. In this case, ESE motifs are predicted by looking at the frequency of hexamers bound by weak or strong splice sites (Fairbrother *et al.*, 2002). ESEs are known to be used by weak splice sites, and so hexamers with weaker splice sites are more likely to be dependent on ESEs (Fairbrother *et al.*, 2002).

Human Splicing Finder (http://www.umd.be/HSF3/) and ESEfinder (http://krainer01.cshl.edu/cgi-bin/tools/ESE3/esefinder.cgi?process=home) were used in this Chapter to look at human and mouse ESE sites in Periostin (POSTN).

4.2 Results

4.2.1 Comparison of homology between exons whose skipping will cause a shift in the human and mouse POSTN transcript ORF

Results from Myostatin suggest that it would be ideal for identifying conserved sequences between the human and the mouse. Exons 3, 4, 7 and 16 were identified to be out-of-frame in the human and mouse *POSTN* transcript (below). In order to find conserved stretches within each exon sequence, pairwise alignment was used between the mouse and human sequences, using EMBOSS Matcher to calculate the percentage similarity for each exon (Figure 4.1). Exon 3 and 16 had the highest percentage similarity of 92.2% and 95.7% respectively. Exon 7 had a similarity of 91.5% while exon 4 and exon 10 similarity scores were 82.6% and 85.8% respectively. Finding homology between these orthologues not only increases chances of targeting significant sequences (see Chapter 3) but also allowed the design of PMO sequences to target mouse and human *POSTN* at identical sequences, making the clinical application of the AON likely to be more reliable as the sequence being tested in the mouse would be the exact same sequence as that being used against the human genome in patients.

The sequences for each exon were accessed on the NCBI nucleotide database and clearly show (for Exons 3 and 16 only) the ends of each exon amino acid codon, demonstrating that the exon does not begin or end with a complete triplet encoding an amino acid (Figures 4.2A1, 4.3A1, 4.4A1, 4.5A1, 4.6A1).

SnapGene software was then used to align the mouse and human exon sequences (Figures 4.2A2, 4.3A2, 4.4A2, 4.5A2, 4.6A2) and confirm the homologies found above (Figure 4.1).

Exon 3

```
Human          2 ACTGTGTTATATGAATGTTGCCCTGGTTATATGAGAATGGAAGGAATGAA 51
                 ||||||.||||||||||.||||||||.||||||||||||||||||.|||||
Mouse          2 ACTGTGCTATATGAATGCTGCCCTGGCTATATGAGAATGGAAGGGATGAA 51

Human         52 AGGCTGCCCAGCAG      65
                 |||||||||.||||
Mouse         52 AGGCTGCCCCGCAG      65
```

Exon 7

```
Human          1 GCAGCTGCCATCACATCGGACATATTGGAGGCCCTTGGAAGAGACGGTCA     50
                 |||||.||||||||.||.|||.|.||||||.||||||||||||||.|||||
Mouse          1 GCAGCCGCCATCACCTCTGACCTCTTGGAGTCCCTTGGAAGAGATGGTCA     50

Human         51 CTTCACACTCTTTGCTCCCACCAATGAGGCTTTTGAGAAACTTCCACGAG    100
                 ||||||.|||||||||||||||||||.|||||.||||||||.|||||||
Mouse         51 CTTCACGCTCTTTGCTCCCACCAATGAAGCTTTCGAGAAACTGCCACGAG    100

Human        101 GTGTCCTAGAAAGGATCATGGGAGACAAAGTGGCTTCCGAAG    142
                 |||||||||||||||||||||||||||||||||||||||.||||
Mouse        101 GTGTCCTAGAAAGGATCATGGGAGACAAAGTGGCTTCTGAAG    142
```

Exon 4

```
Human          4 TGCCCATTGACCATGTTTATGGCACTCTGGGCATCGTGGGAGCCACCACA     53
                 ||||.||||||||||||||||||.||||||||.||||||||||||.||.
Mouse          4 TGCCTATTGACCATGTTTATGGCACGCTGGGCATTGTGGGAGCCACTACC     53

Human         54 ACGCAGCGCTATTCTGACGCCTCAAAACTGAGGGAGGAGATCGAGGGAAA    103
                 ||.||||.|||.||.||.|.|||.||.||||||.||.||||||.||.|||||
Mouse         54 ACTCAGCACTACTCCGATGTCTCGAAGCTGAGAGAAGAGATTGAAGGAAA    103

Human        104 GGGATCCTTCACTTACTTTGCACCGAGTAATGAGGCTTGGGACAACTTGG    153
                 .||.||.|.|||.||||||.||.||||||||.||||||||||.|||.|||
Mouse        104 AGGGTCATACACGTACTTCGCGCCGAGTAACGAGGCTTGGGAGAACCTGG    153

Human        154 ATTCT    158
                 |||||
Mouse        154 ATTCT    158
```

Exon 10

```
Human          1 ATGATACTCTCAGCATGGATCAGCGCCTCCTTAAATTAATTCTGCAGAAT     50
                 ||||.|||||.||||||||.||.||||||.||||||..||||||||||.|||
Mouse          1 ATGACACTCTGAGCATGGACCAACGCCTTCTTAAGCTAATTCTGCAAAAT     50

Human         51 CACATATTGAAAGTAAAAGTTGGCCTTAATGAGCTTTACAACGGGCAAAT    100
                 ||||||||||||||||||||||||||||..||.||.|||||.||.||.||
Mouse         51 CACATATTGAAAGTAAAAGTTGGCCTTAGCGACCTCTACAATGGACAGAT    100

Human        101 ACTGGAAACCATCGGAGGCAAACAGCTCAGAGTCTTCGTATATCGTAC    148
                 ||||||||||||.||||||||||.|||.|||||||.||.||||||.||
Mouse        101 ACTGGAAACCATTGGAGGCAAACAACTCCGAGTCTTTGTGTATCGGAC    148
```

Exon 16

```
Human          1 TTTGTTCGTGGTAGCACCTTCAAAGAAATCCCCGTGACTGTCTATA     46
                 ||||||||||||.||||||||||||||||||||||.||||||||||||
Mouse          1 TTTGTTCGTGGCAGCACCTTCAAAGAAATCCCCATGACTGTCTATA     46
```

Figure 4.1 Alignments of mouse and human *POSTN* exons 3,4,7,10 and 16

Alignment was carried out using EMBOSS Matcher and sequences were obtained from Ensembl. Each exon is highly conserved with the highest percentage similarity being 95.7% in exon 16 and the lowest being 82.6% in exon 4 (see text). Dots represent mismatched nucleotides, bars homology.

4.2.2 Prediction of exon splicing enhancers (ESEs) and suppressors (ESSs) in exons 3, 4, 7, 10 and 16 of human and mouse POSTN genes

POSTN transcript ID ENSMUST00000107985.9 from Ensembl https://www.ensembl.org/index.html was used in the Human Splicing Finder programme (http://www.umd.be/HSF3/). Exons 3, 4 ,7, 10 and 16 were analysed individually. The outputs, shown in Figures 4.2B, 4.3B, 4.4B, 4.5B, 4.6B respectively**,** were a graph with the X-axis representing the sequence and scores for motifs on the Y-axis and. Putative splicing enhancer motifs ESE (hot colours) and splicer silencer (ESS) motifs (cold colours) were identified. Wherever a peak along the exon indicated a higher score on the Enhancer side of the Y-axis, an ESE site was predicted.

ESEs were predicted at the following positions (Figures 4.2B, 4.3B, 4.4B, 4.5B, 4.6B): on exon 3, two peaks were shown at nucleotide positions 4-11 and 53-65 of the exon sequence, with a score of ~10; exon 4 had two peaks at nucleotide positions 75-105 and 46-66 with scores of ~12 and 28, respectively; exon 7 had two peaks on the exon in positions 32-50 and 79-101, both with a score of ~10; exon 10 showed two peaks, one at 40-52 with a score of 20 and a smaller peak at 116-124 with a score of ~8. Exon 16 being merely 46bp in length showed only a very weak peak with a score of ~5 at position 1-31.

Human Splicing Finder predicted ESE sites in the human genome only. In order to confirm the findings and also compare ESE sites between the human and mouse to identify conserved ESE motifs, ESEfinder was used. The human and mouse exon sequences were inserted into the ESEfinder software query box individually, and output generated (Figures 4.7, 4.8, 4.9, 4.10, 4.11). Putative human and mouse ESE sites were

compared, to look for conservation between the two species. Quite similar patterns in positions of some of the SR motifs suggested that ESE sites could be found in the same location in both the human and mouse POSTN exons. This allowed the design of PMOs to the same sequence on both human and mouse

An Mfold prediction of the secondary structures is also shown for each, isolated exon sequence (Figures 4.2C, 4.3C, 4.4C, 4.5C, 4.6C). In each case, the exon exhibits a structure which could be folded so that the exon is 'pinched out' of the pre-mRNA during splicing, with the 3' and 5' ends located naturally adjacent to one another.

A1)

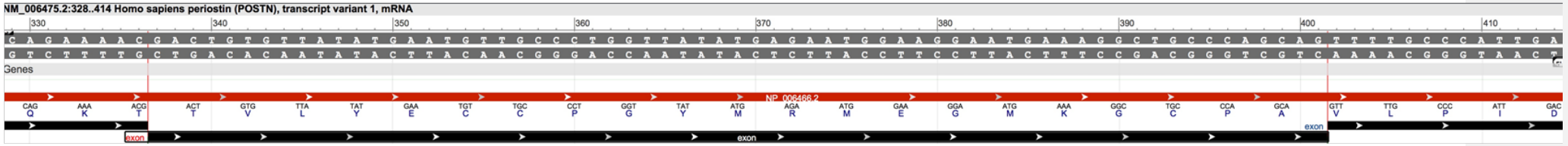
NM_006475.2:328..414 Homo sapiens periostin (POSTN), transcript variant 1, mRNA
Genes
NP_006466.2
exon

A2)

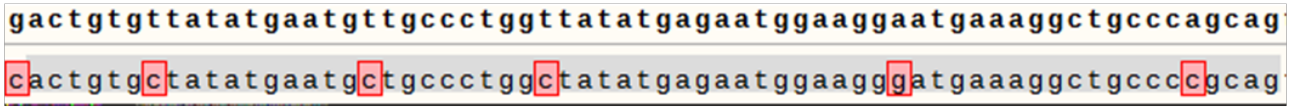
gactgtgttatatgaatgttgccctggttatatgagaatggaaggaatgaaaggctgcccagcag
cactgtgctatatgaatgctgccctggctatatgagaatggaaggatgaaaggctgccccgcag

B)

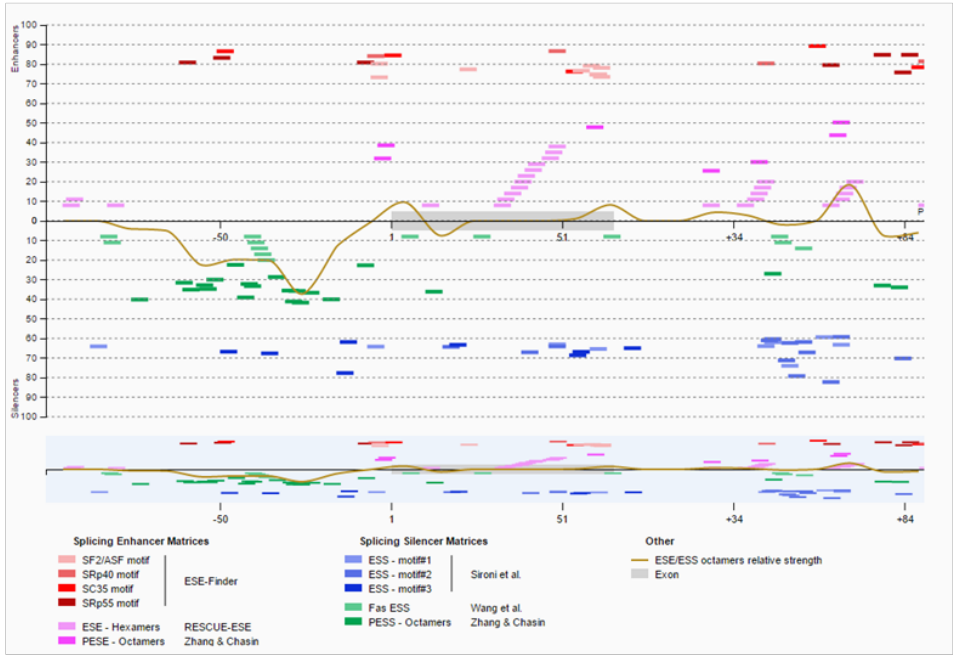
Enhancers
Silencers
Splicing Enhancer Matrices
SF2/ASF motif
SRp40 motif
SC35 motif
SRp55 motif
ESE-Finder
ESE - Hexamers
PESE - Octamers
RESCUE-ESE
Zhang & Chasin
Splicing Silencer Matrices
ESS - motif#1
ESS - motif#2
ESS - motif#3
Sironi et al.
Fas ESS
PESS - Octamers
Wang et al.
Zhang & Chasin
Other
ESE/ESS octamers relative strength
Exon

C)

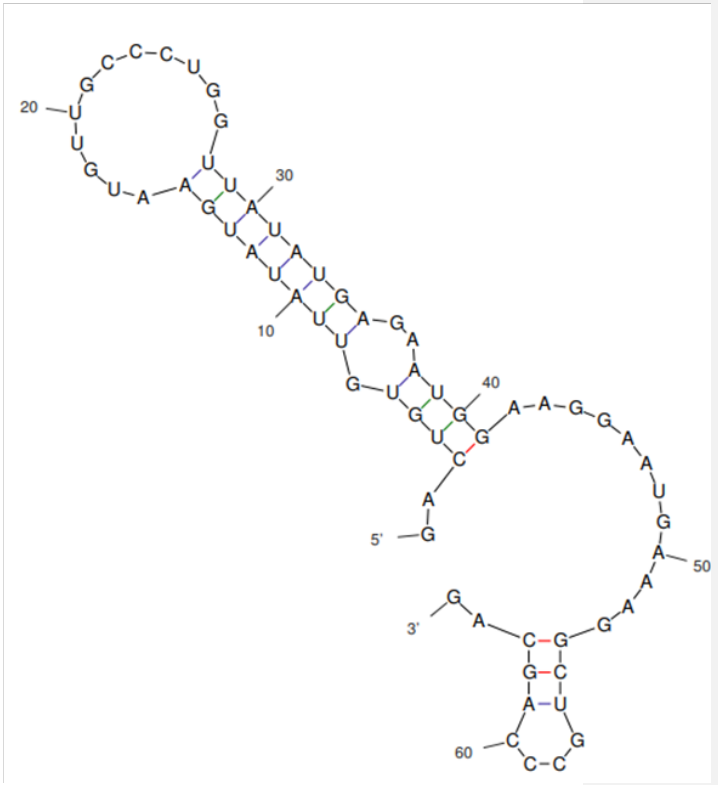
5'
3'

Figure 4.2 Analysis of human *POSTN* exon 3 for homology, ESE sites and secondary structure.

(A1) Output from NCBI nucleotide database showing human *POSTN* exon 3 (lower black line, with nucleotide sequence top).

(A2) Output from SnapGene aligning exon 3 of human (upper) and mouse (highlighted in grey). Mismatches are highlighted with red boxes.

(B) Human Splicing Finder output for exon 3 (highlighted in grey). Different red and pink coloured bars show different Splicing Enhancer Matrices and green and blue bars show different Splicing Silencer Matrices as labelled (below). The Y axis displays the score for presence of the particular motif above a set threshold, with stronger motifs represented by higher scores. In this case exon 3 is predicted to have two ESE sites at the beginning and end of the exon.

(C) Secondary structure of human *POSTN* exon 3 in isolation, as predicted by Mfold.

A1)

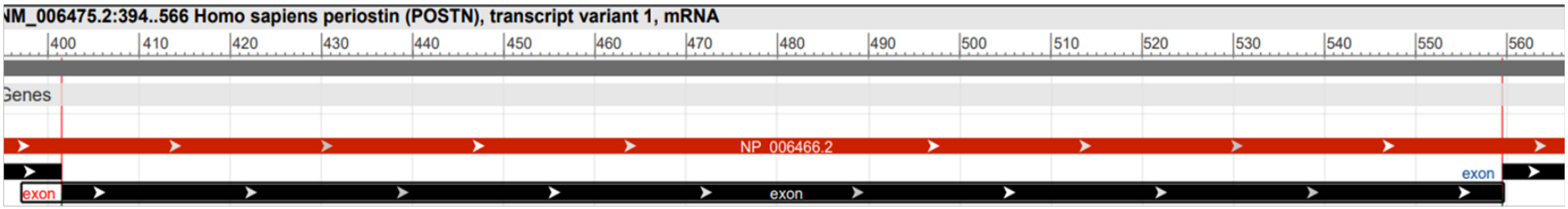
NM_006475.2:394..566 Homo sapiens periostin (POSTN), transcript variant 1, mRNA
400
410
420
430
440
450
460
470
480
490
500
510
520
530
540
550
560
Genes
NP_006466.2
exon
exon
exon

A2)

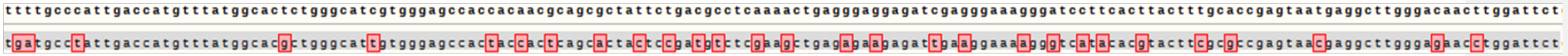

B)

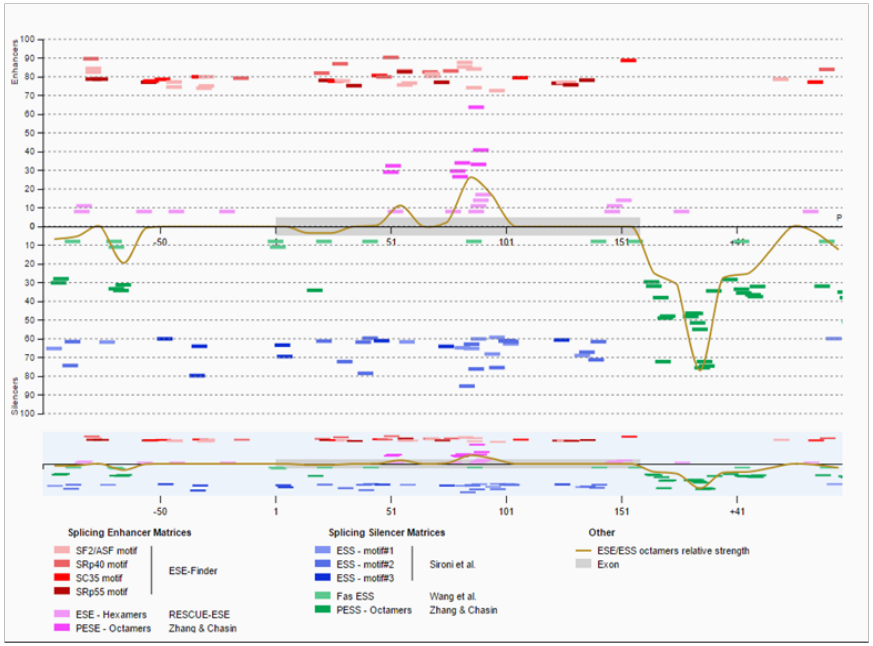
Enhancers
Silencers
-50
1
51
101
151
+41
Splicing Enhancer Matrices
SF2/ASF motif
SRp40 motif
SC35 motif
SRp55 motif
ESE-Finder
ESE - Hexamers
PESE - Octamers
RESCUE-ESE
Zhang & Chasin
Splicing Silencer Matrices
ESS - motif#1
ESS - motif#2
ESS - motif#3
Sironi et al.
Fas ESS
PESS - Octamers
Wang et al.
Zhang & Chasin
Other
ESE/ESS octamers relative strength
Exon

C)

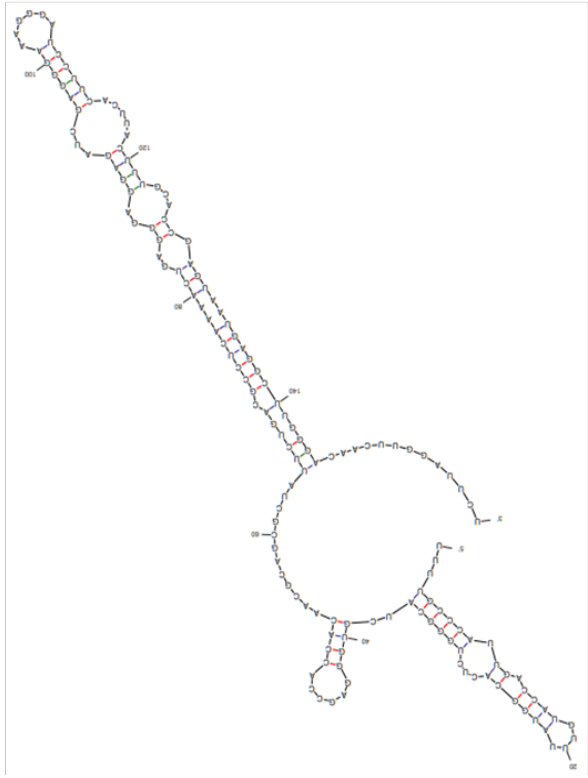

Figure 4.3 Analysis of human *POSTN* exon 4 for homology, ESE sites and secondary structure.

(A1) Output from NCBI nucleotide database showing human *POSTN* exon 4 (lower black line, with nucleotide sequence top).

(A2) Output from SnapGene aligning exon 4 of human (upper) and mouse (highlighted in grey). Mismatches are highlighted with red boxes.

(B) Human Splicing Finder output for exon 4 (highlighted in grey). Different red and pink coloured bars show different Splicing Enhancer Matrices and green and blue bars show different Splicing Silencer Matrices as labelled (below). The Y axis displays the score for presence of the particular motif above a set threshold, with stronger motifs represented by higher scores.

(C) Secondary structure of the human POSTN exon 4 predicted by Mfold.

A1)

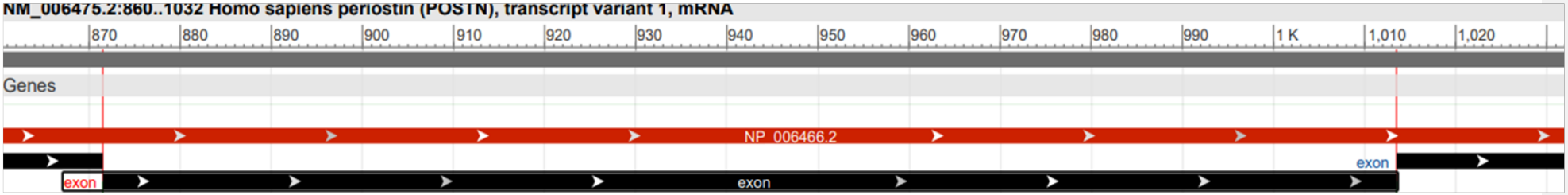
NM_006475.2:860..1032 Homo sapiens periostin (POSTN), transcript variant 1, mRNA
870
880
890
900
910
920
930
940
950
960
970
980
990
1 K
1,010
1,020
Genes
NP_006466.2
exon
exon
exon

A2)

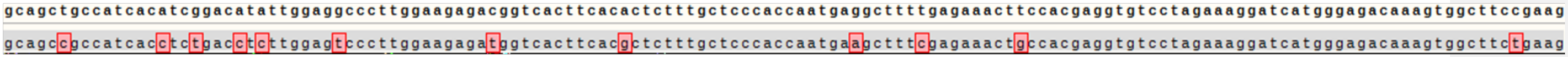
gcagctgccatcacatcggacatattggaggcccttggaagagacggtcacttcacactctttgctcccaccaatgaggcttttgagaaacttccacgaggtgtcctagaaaggatcatgggagacaaagtggcttccgaag
gcagccgccatcacctctgacctcttggagtcccttggaagagatggtcacttcacgctctttgctcccaccaatgaagctttcgagaaactgccacgaggtgtcctagaaaggatcatgggagacaaagtggcttctgaag

B)

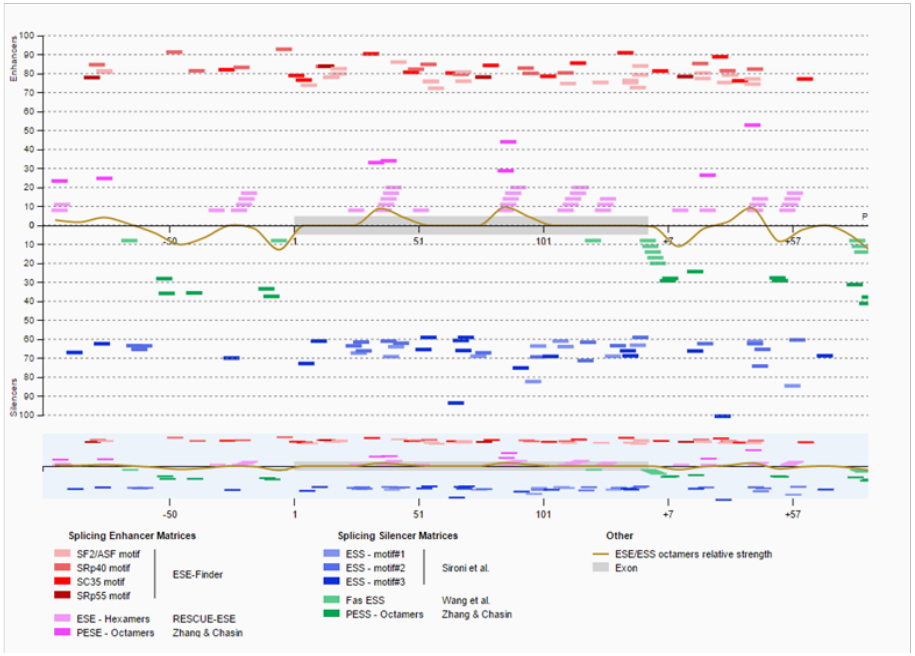
Enhancers
Silencers
-50
1
51
101
+7
+57
Splicing Enhancer Matrices
SF2/ASF motif
SRp40 motif
SC35 motif
SRp55 motif
ESE-Finder
ESE - Hexamers
PESE - Octamers
RESCUE-ESE
Zhang & Chasin
Splicing Silencer Matrices
ESS - motif#1
ESS - motif#2
ESS - motif#3
Sironi et al.
Fas ESS
PESS - Octamers
Wang et al.
Zhang & Chasin
Other
ESE/ESS octamers relative strength
Exon

C)

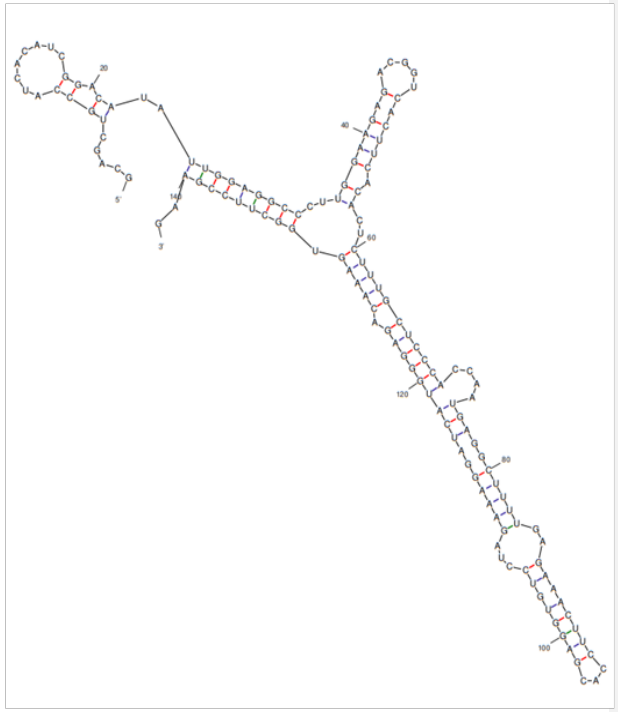

Figure 4.4 Analysis of human *POSTN* exon 7 for homology, ESE sites and secondary structure.

(A1) Output from NCBI nucleotide database showing human *POSTN* exon 7 (lower black line, with nucleotide sequence top).

(A2) Output from SnapGene aligning exon 7 of human (upper) and mouse (highlighted in grey). Mismatches are highlighted with red boxes.

(B) Human Splicing Finder output for exon 7 (highlighted in grey). Different red and pink coloured bars show different Splicing Enhancer Matrices and green and blue bars show different Splicing Silencer Matrices as labelled (below). The Y axis displays the score for presence of the particular motif above a set threshold, with stronger motifs represented by higher scores. In this case exon 7 is predicted to have two ESE sites at the beginning and end of the exon.

(C) Secondary structure of the human *POSTN* exon 7 as predicted by Mfold.

A1)

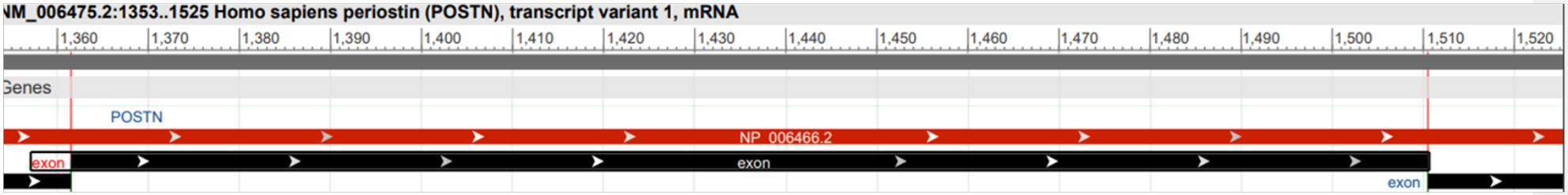
NM_006475.2:1353..1525 Homo sapiens periostin (POSTN), transcript variant 1, mRNA
1,360
1,370
1,380
1,390
1,400
1,410
1,420
1,430
1,440
1,450
1,460
1,470
1,480
1,490
1,500
1,510
1,520
Genes
POSTN
NP_006466.2
exon
exon
exon

A2)

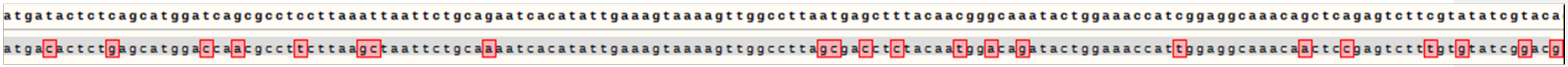
atgatactctcagcatggatcagcgcctccttaaattaattctgcagaatcacatattgaaagtaaaagttggccttaatgagctttacaacgggcaaatactggaaaccatcggaggcaaacagctcagagtcttcgtatatcgtaca
atgacactctgagcatggaccaacgcctcttaagctaattctgcaaaatcacatattgaaagtaaaagttggccttagcgacctctacaatggacagatactggaaaccattggaggcaaacaactccgagtcttttgtgtatcggacg

B)

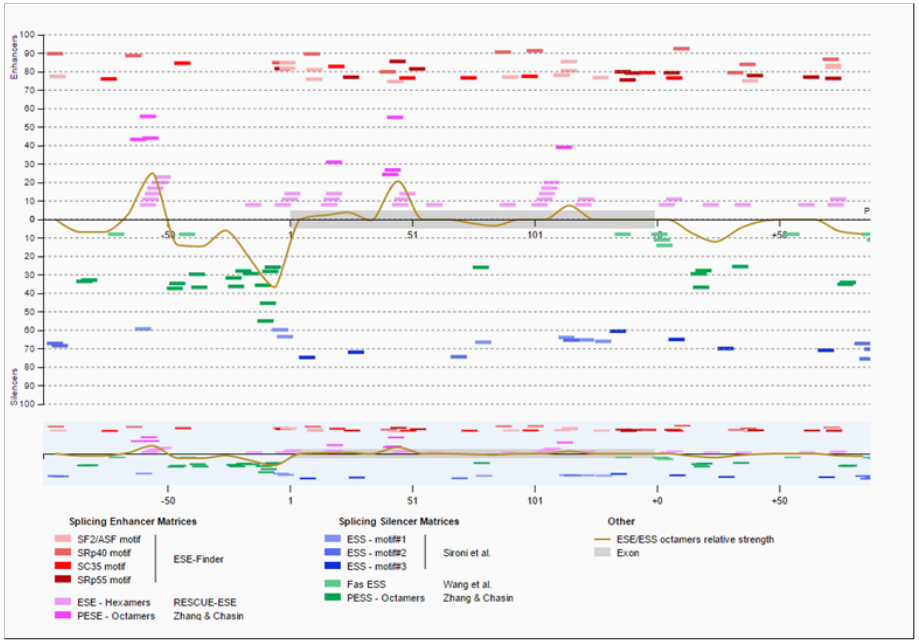
Enhancers
Silencers
-50
1
51
101
+0
+50
Splicing Enhancer Matrices
SF2/ASF motif
SRp40 motif
SC35 motif
SRp55 motif
ESE-Finder
ESE - Hexamers
PESE - Octamers
RESCUE-ESE
Zhang & Chasin
Splicing Silencer Matrices
ESS - motif#1
ESS - motif#2
ESS - motif#3
Sironi et al.
Fas ESS
PESS - Octamers
Wang et al.
Zhang & Chasin
Other
ESE/ESS octamers relative strength
Exon

C)

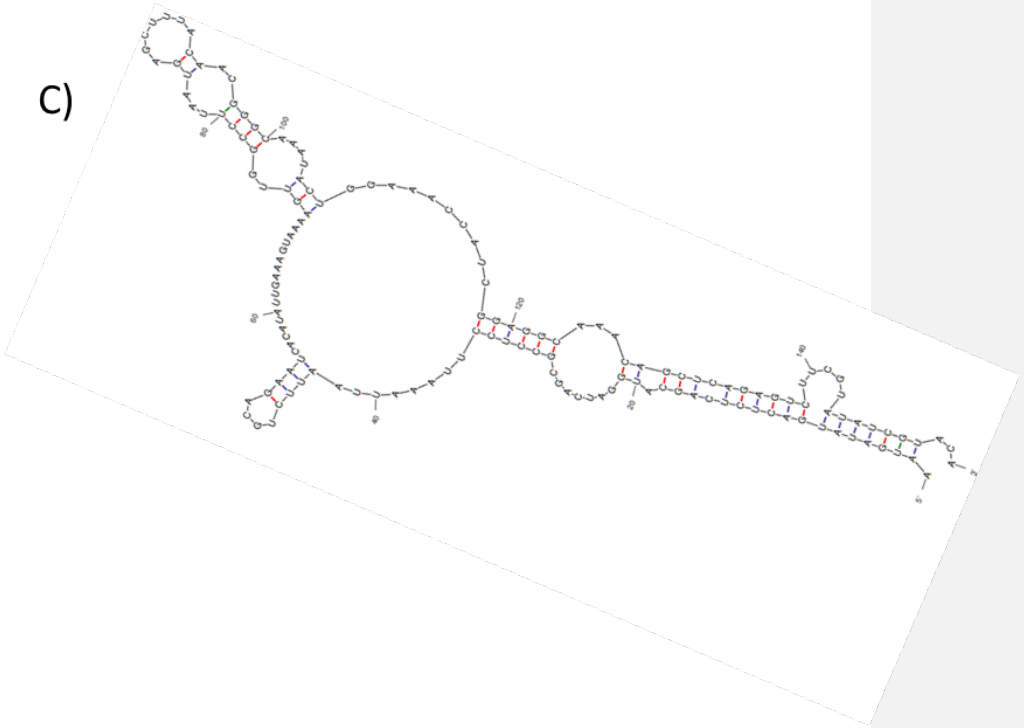

Figure 4.5 Analysis of human *POSTN* exon 10 for homology, ESE sites and secondary structure.

(A1) Output from NCBI nucleotide database showing human *POSTN* exon 10 (lower black line, with nucleotide sequence top).

(A2) Output from SnapGene aligning exon 10 of human (upper) and mouse (highlighted in grey). Mismatches are highlighted with red boxes.

(B) Human Splicing Finder output for exon 10 (highlighted in grey). Different red and pink coloured bars show different Splicing Enhancer Matrices and green and blue bars show different Splicing Silencer Matrices as labelled (below). The Y axis displays the score for presence of the particular motif above a set threshold, with stronger motifs represented by higher scores. In This case exon 10 is predicted to have two ESE sites at the beginning and end of the exon.

(C) Secondary structure of human *POSTN* exon 10 as predicted by Mfold.

A1)

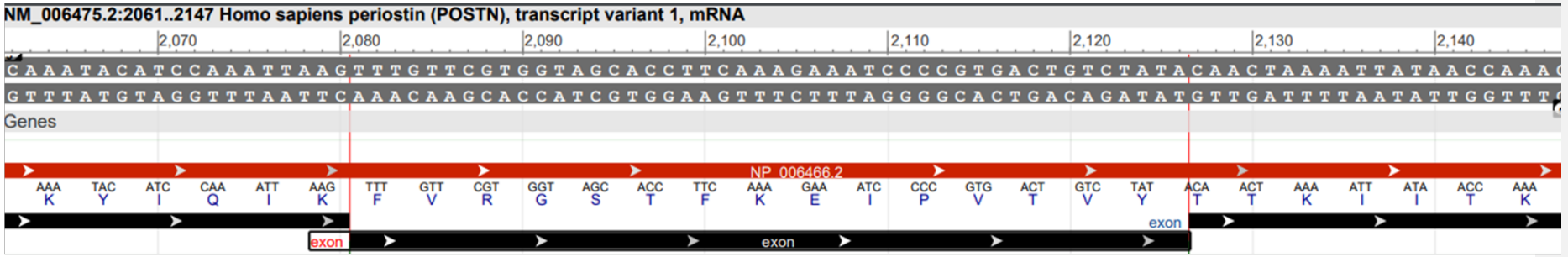
NM_006475.2:2061..2147 Homo sapiens periostin (POSTN), transcript variant 1, mRNA
2,070
2,080
2,090
2,100
2,110
2,120
2,130
2,140
Genes
NP_006466.2
exon
exon
exon

A2)

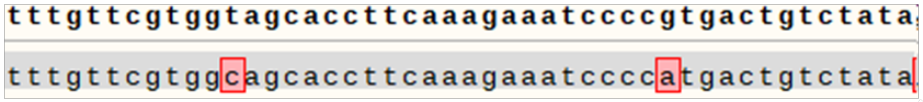
tttgttcgtggtagcaccttcaaagaaatccccgtgactgtctata
tttgttcgtggcagcaccttcaaagaaatccccatgactgtctata

B)

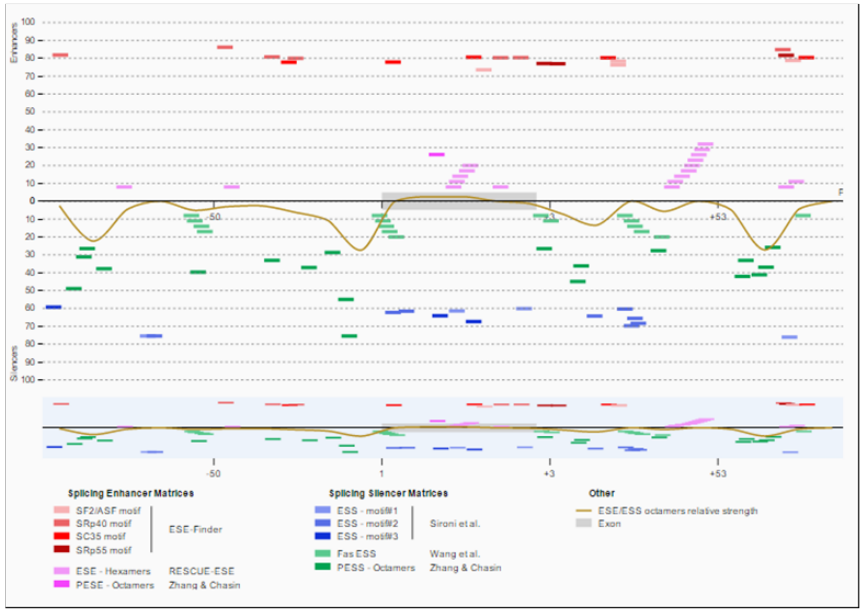
Enhancers
Silencers
Splicing Enhancer Matrices
SF2/ASF motif
SRp40 motif
SC35 motif
SRp55 motif
ESE-Finder
ESE - Hexamers
PESE - Octamers
RESCUE-ESE
Zhang & Chasin
Splicing Silencer Matrices
ESS - motif#1
ESS - motif#2
ESS - motif#3
Sironi et al.
Fas ESS
PESS - Octamers
Wang et al.
Zhang & Chasin
Other
ESE/ESS octamers relative strength
Exon

C)

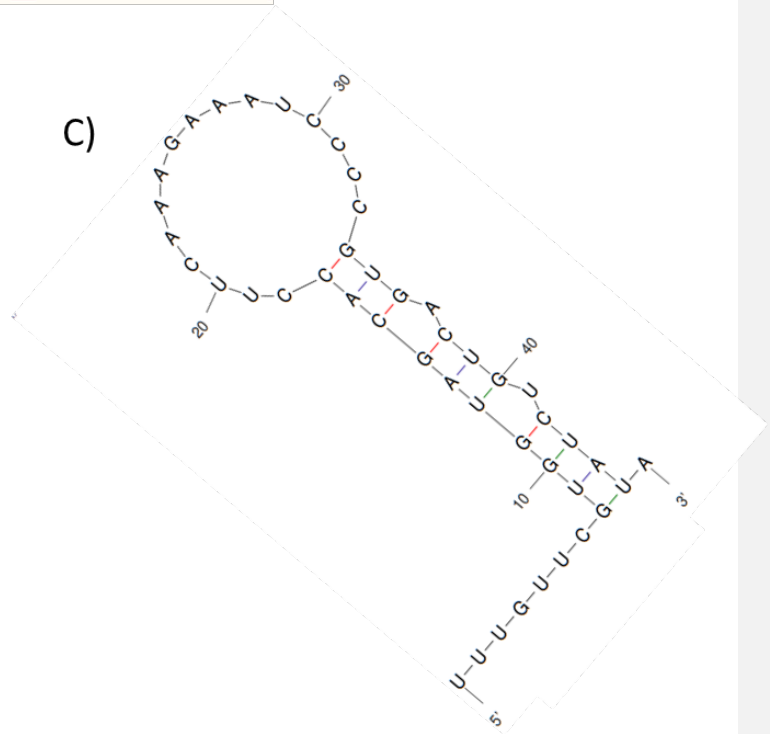

Figure 4.6 Analysis of human *POSTN* exon 16 for homology, ESE sites and secondary structure.

(A1) Output from NCBI nucleotide database showing human *POSTN* exon 16 (lower black line, with nucleotide sequence top).

(A2) Output from SnapGene aligning exon 16 of human (upper) and mouse (highlighted in grey). Mismatches are highlighted with red boxes.

(B) Human Splicing Finder output for exon 16 (highlighted in grey). Different red and pink coloured bars show different Splicing Enhancer Matrices and green and blue bars show different Splicing Silencer Matrices as labelled (below). The Y axis displays the score for presence of the particular motif above a set threshold, with stronger motifs represented by higher scores. In this case exon 16 is predicted to have two ESE sites at the beginning and end of the exon.

(C) Secondary structure of the human *POSTN* exon 16 as predicted by Mfold.

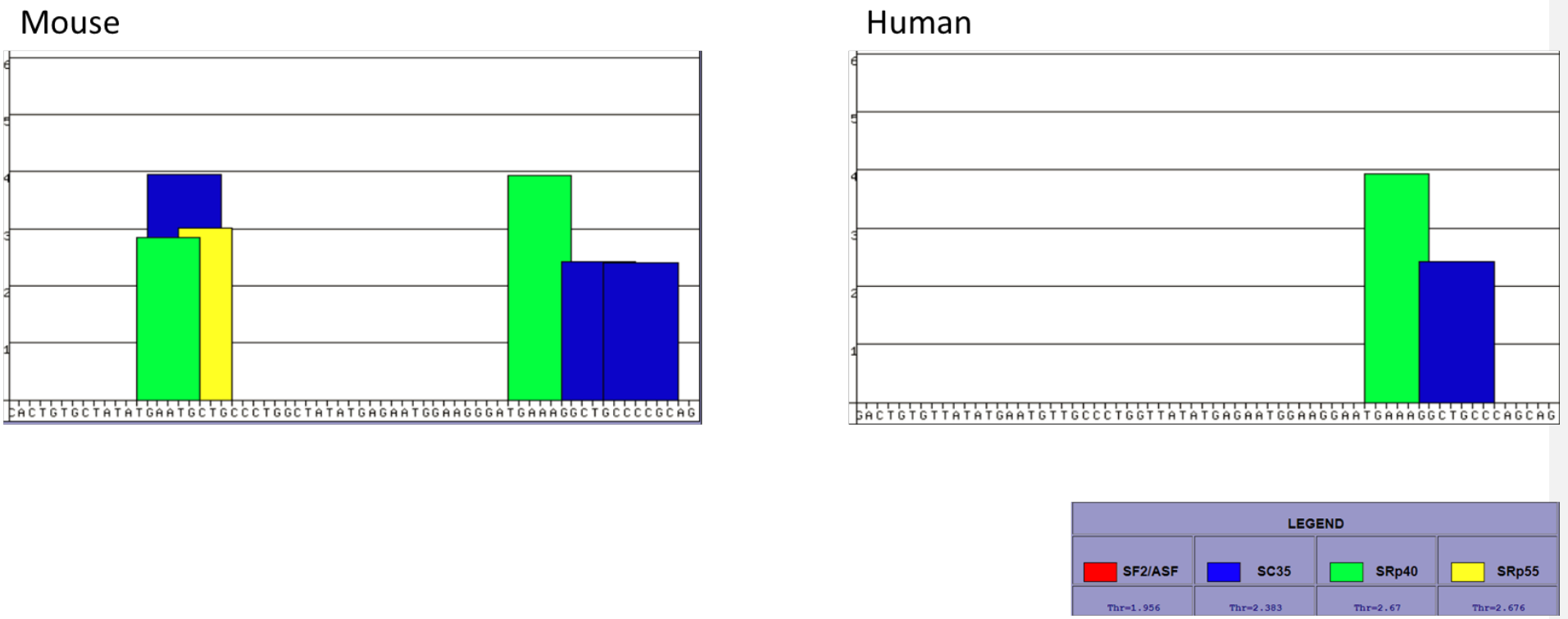

Figure 4.7 Comparison of ESE sites predicted in exon 3 of human and mouse *POSTN*.

ESEfinder output for mouse and human *POSTN* exon 3. The width of each column displays the location where the motif may be present. The X axis shows the sequence of the exon. The height of each bar depicts the score of the predicted motif above a set threshold. The higher the score the more likely the motif is present in that particular position on the X axis.

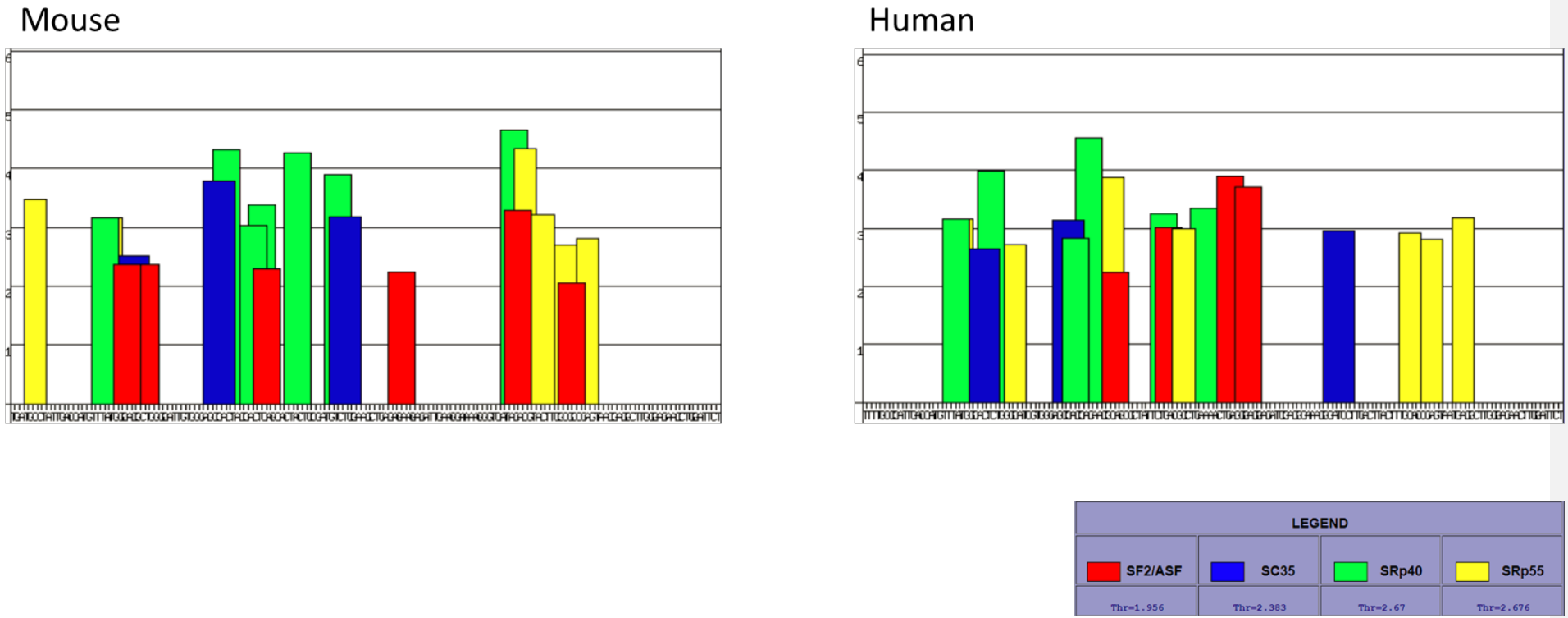

Figure 4.8 Comparison of ESE sites predicted in exon 4 of human and mouse *POSTN.*

ESEfinder output for mouse and human *POSTN* Exon 4. The width of each column displays the location where the motif may be present. The X axis shows the sequence of the exon. The height of each bar depicts the score of the predicted motif above a set threshold. The higher the score the more likely the motif is present in that particular position on the X axis

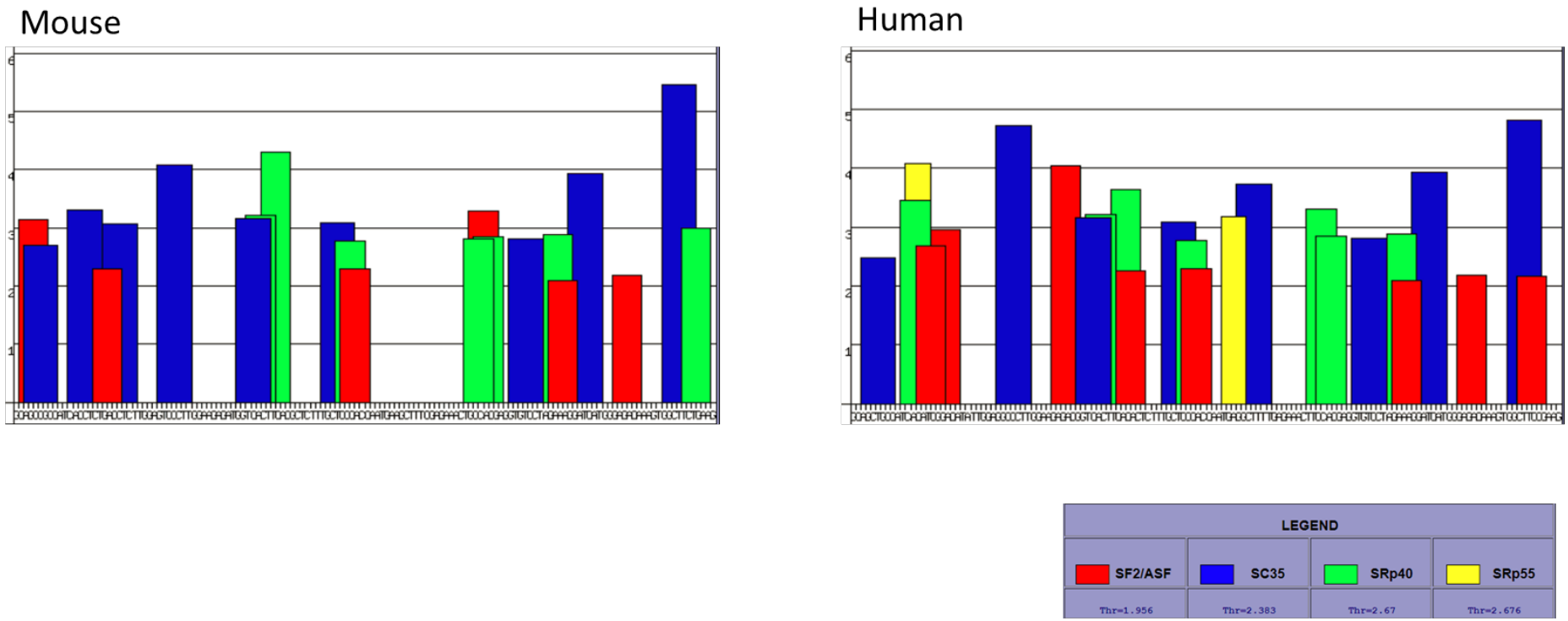

Figure 4.9 Comparison of ESE sites predicted in exon 7 of human and mouse *POSTN.*

ESEfinder output for mouse and human *POSTN* Exon 7. The width of each column displays the location where the motif may be present. The X axis shows the sequence of the exon. The height of each bar depicts the score of the predicted motif above a set threshold. The higher the score the more likely the motif is present in that particular position on the X axis.

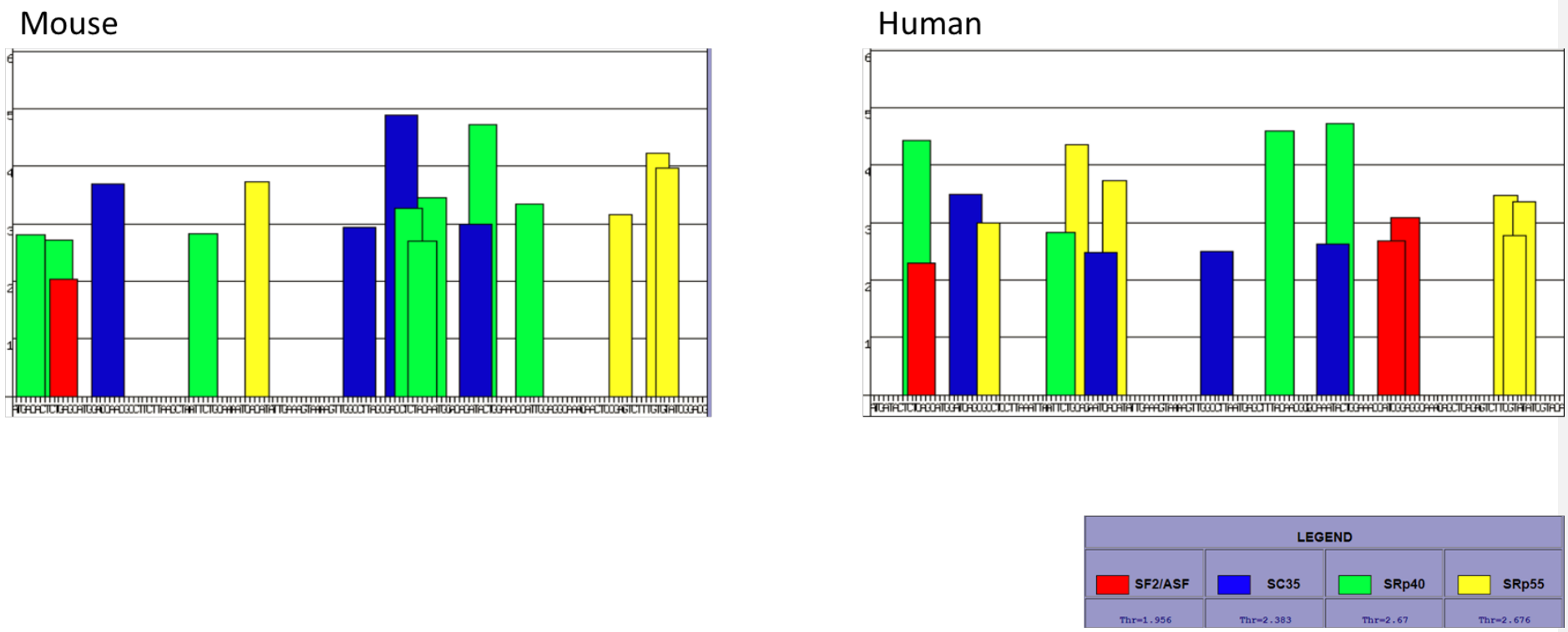

Figure 4.10 Comparison of ESE sites predicted in exon 10 of human and mouse *POSTN.*

ESEfinder output for mouse and human *POSTN* Exon 10. The width of each column displays the location where the motif may be present. The X axis shows the sequence of the exon. The height of each bar depicts the score of the predicted motif above a set threshold. The higher the score the more likely the motif is present in that particular position on the X axis.

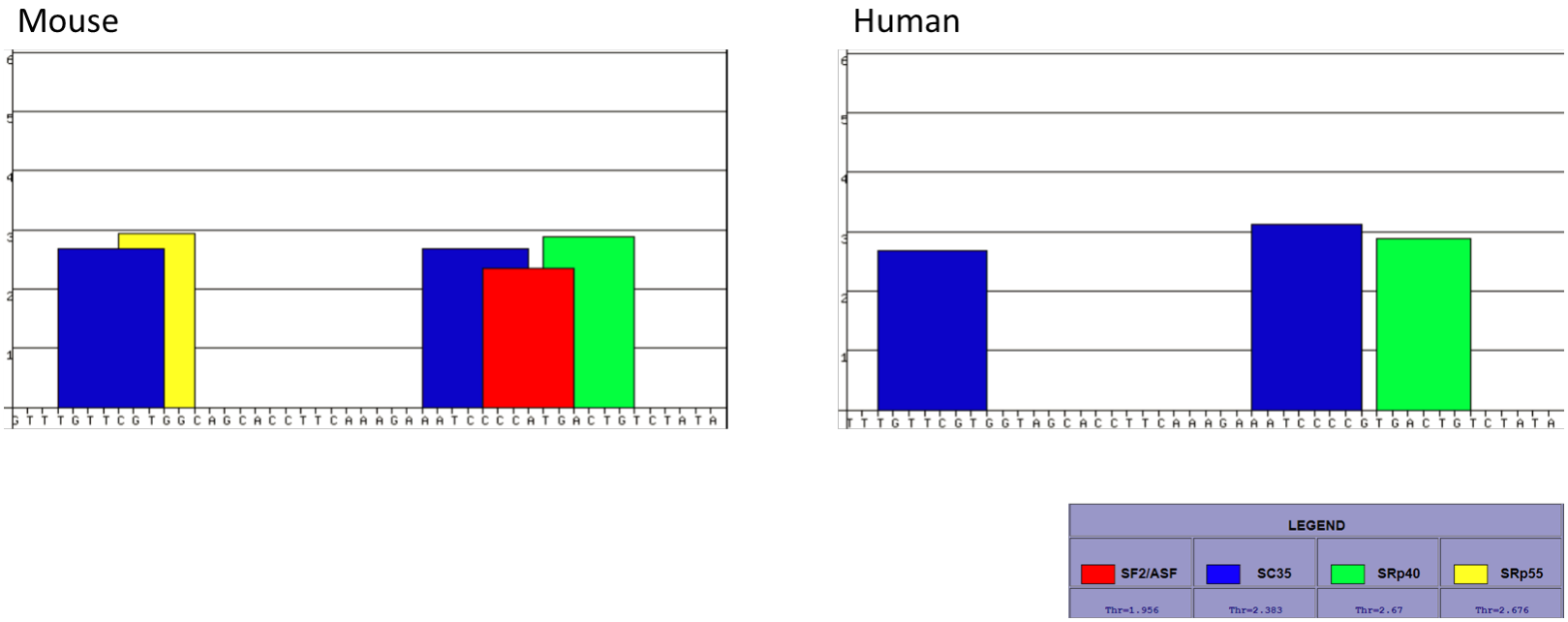

Figure 4.11 Comparison of ESE sites predicted in exon 16 of human and mouse *POSTN.*

ESEFinder output for mouse and human *POSTN* Exon 16. The width of each column displays the location where the motif may be present. The X axis shows the sequence of the exon. The height of each bar depicts the score of the predicted motif above a set threshold. The higher the score the more likely the motif is present in that particular position on the X axis

4.2.3 Relationship of selected ESEs and designed AON PMOs to the predicted RNA secondary structure of targeted POSTN exons

PMOs were designed to target conserved regions of exon 3, 7, 10 and 16 at regions containing ESE sites and avoiding ESS sites. They were designed considering overall binding energy and GC content of the PMO. For exon 3, one 25mer PMO sequence was designed to target the predicted ESE shared between the mouse and human in the conserved region of the exon (Figure 4.12). Exon 7 contained longer stretches of the sequence where there was only one mismatch between the mouse and human, which also contained ESE motifs. In order to cover these regions of interest, two 30mer PMOs were designed as well as one 25mer PMO (Figure 4.13). In the same way, three overlapping 30mer PMOs were designed for exon 10 (Figure 4.14) and two overlapping 25mer PMOs for exon 16 (Figure 4.15).

Mfold was used to predict the secondary structure of each exon within the pre-mRNA for human and mouse genes. This allowed investigation of conservation between the human and mouse on the level of secondary structure. Each exon sequence along with 100nt of intron on either side was pasted, in FASTA format, as input into the Mfold software. Secondary structures showed identical secondary structures for exon 3 from human and mouse. Very similar structures were predicted for exons 7, 10 and 16, but a very different structure for mouse versus human exon 4 (Figures 4.16, 4.17, 4.18, 4.19, 4.20). The very different secondary structure for exon 4 was probably due to the fact that exon 4 had more mismatches in sequence between the human and mouse; therefore it was eliminated for PMO design and further investigation as it would have been not possible to confidently design a single PMO for both human and mouse. The

position on which the newly designed PMOs (above) bind on the secondary structure of both human and mouse are shown (Figures 4.16, 4.17, 4.18, 4.19, 4.20).

A)

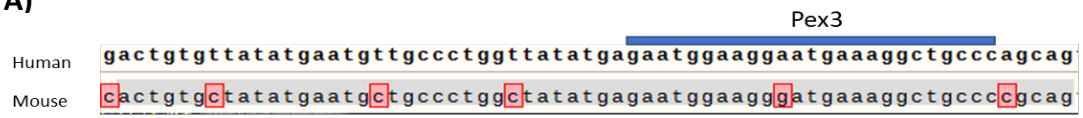

B)

PMO Name	PMO Sequence	Target Sequence	ΔG (kcal/mol)	Opening energy of target (kcal/mol)	Opening energy of PMO (kcal/mol)	Overal ΔG (ΔGi)	%GC	TM
Pex3	TTTAATATAACTTATACTGTTTCTACAAAT	ATT TGT AGA AAC AGT ATA AGT TAT ATT AAA	-50.01	4.28	1.57	-44.15	52	60.4ºC

Figure 4.12 Overview of PEX3 AON targeting exon 3 in the human and mouse POSTN gene transcript

A) Human and mouse *POSTN* exon 3 alignment generated by SnapGene. Mismatches are highlighted in red. Binding position of Pex 3 PMO is shown in blue.

B) PEX3 PMO sequence and thermodynamic properties outlined in the table. Overall binding energy calculated using RNAup server. T_m and %GC were calculated using OligoAnalyzer.

A)

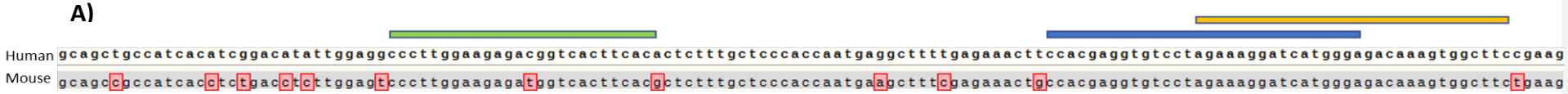

B)

PMO Name	PMO Sequence	Target Sequence	ΔG (kcal/mol)	Opening energy of target (kcal/mol)	Opening energy of PMO (kcal/mol)	Overal ΔG (ΔGi)	%GC	TM
Pex7.1	TCCCATGATCCTTTCTAGGACACCTCGTGG	CCACGAGGUGUCCUAGAAAGGAUCAUGGGA	-51.81	9.47	6.93	-35.41	53.3	63.8ºC
Pex7.2	GAAGCCACTTTGTCTCCCATGATCCTTTCT	AGAAAGGAUCAUGGGAGACAAAGUGGCUUC	-27.1	0.97	5.84	-20.30	46.7	61.7ºC
Pex7.3	GTGAAGTGACCGTCTCTTCCAAGGG	CCCUUGGAAGAGACGGUCACUUCAC	-49.70	3.11	2.77	-43.83	56	61ºC

Figure 4.13 Overview of PEX7.1, 7.2 and 7.3 AON targeting exon 7 in the human and mouse POSTN gene transcript.

A) Human and mouse *POSTN* exon 7 alignment generated by SnapGene. Mismatches are highlighted in red. Binding position of Pex 7.1, Pex7.2 and Pex7.3 PMO are shown in blue, yellow and green respectively.

B) Pex7.1, Pex7.2 and Pex7.3 PMO sequences and thermodynamic properties outlined in the table. Overall binding energy calculated using RNAup server. T_m and %GC were calculated using OligoAnalyzer

A)

B)

PMO Name	PMO Sequence	Target Sequence	ΔG (kcal/mol)	Opening energy of target (kcal/mol)	Opening energy of PMO (kcal/mol)	Overal ΔG (ΔGi)	%GC	TM
Pex10.1	TTTTACTTTCAATATGTGATTCTGCAGAAT	AUUCUGCAGAAUCACAUAUUGAAAGUAAAA	-40.61	1.32	0.73	-38.56	26.7	54.1ºC
Pex10.2	CCAACTTTTACTTTCAATATGTGATTCTGC	GCAGAAUCACAUAUUGAAAGUAAAAGUUGG	-36.61	0.98	0.76	-34.87	33.3	55.3ºC
Pex10.3	TAAGGCCAACTTTTACTTTCAATATGTGAT	AUCACAUAUUGAAAGUAAAAGUUGGCCUUA	-41.11	1.42	0.83	-38.86	30	55.4ºC

Figure 4.14 Overview of PEX10.1,10.2 and 10.3 AON targeting exon 10 in the human and mouse POSTN gene transcript.

A) Human and mouse *POSTN* exon 10 alignment generated by SnapGene. Mismatches are highlighted in red. Binding position of Pex 10.1, Pex10.2 and Pex10.3 PMO are shown in blue, yellow and green respectively.

B) Pex10.1, Pex10.2 and Pex10.3 PMO sequences and thermodynamic properties outlined in the table. Overall binding energy calculated using RNAup server. T_m and %GC were calculated using OligoAnalyzer.

A)

B)

PMO Name	PMO Sequence	Target Sequence	ΔG (kcal/mol)	Opening energy of target (kcal/mol)	Opening energy of PMO (kcal/mol)	Overal ΔG (ΔGi)	%GC	TM
Pex16.1	GGGGATTTCTTTGAAGGTGCTACCA	UGGUAGCACCUUCAAAGAAAUCCCC	-46.41	2.85	1.22	42.34	48%	59.1ºC
Pex16.2	TATAGACAGTCACGGGGATTTCTTT	AAAGAAAUCCCCGUGACUGUCUAUA	-42.31	2.00	0.19	-40.11	40%	55.5ºC

Figure 4.15 Overview of PEX16.1 and 16.2 AON targeting exon 16 in the human and mouse POSTN gene transcript.

A) Human and mouse *POSTN* exon 16 alignment generated by SnapGene. Mismatches are highlighted in red. Binding positions of Pex 16.1 and Pex16.3 PMOs are shown in blue and yellow respectively.

B) Pex16.1 and Pex16.2 PMO sequences and thermodynamic properties are listed in the table. Overall binding energy was calculated using RNAup server. T_m and %GC were calculated using OligoAnalyzer.

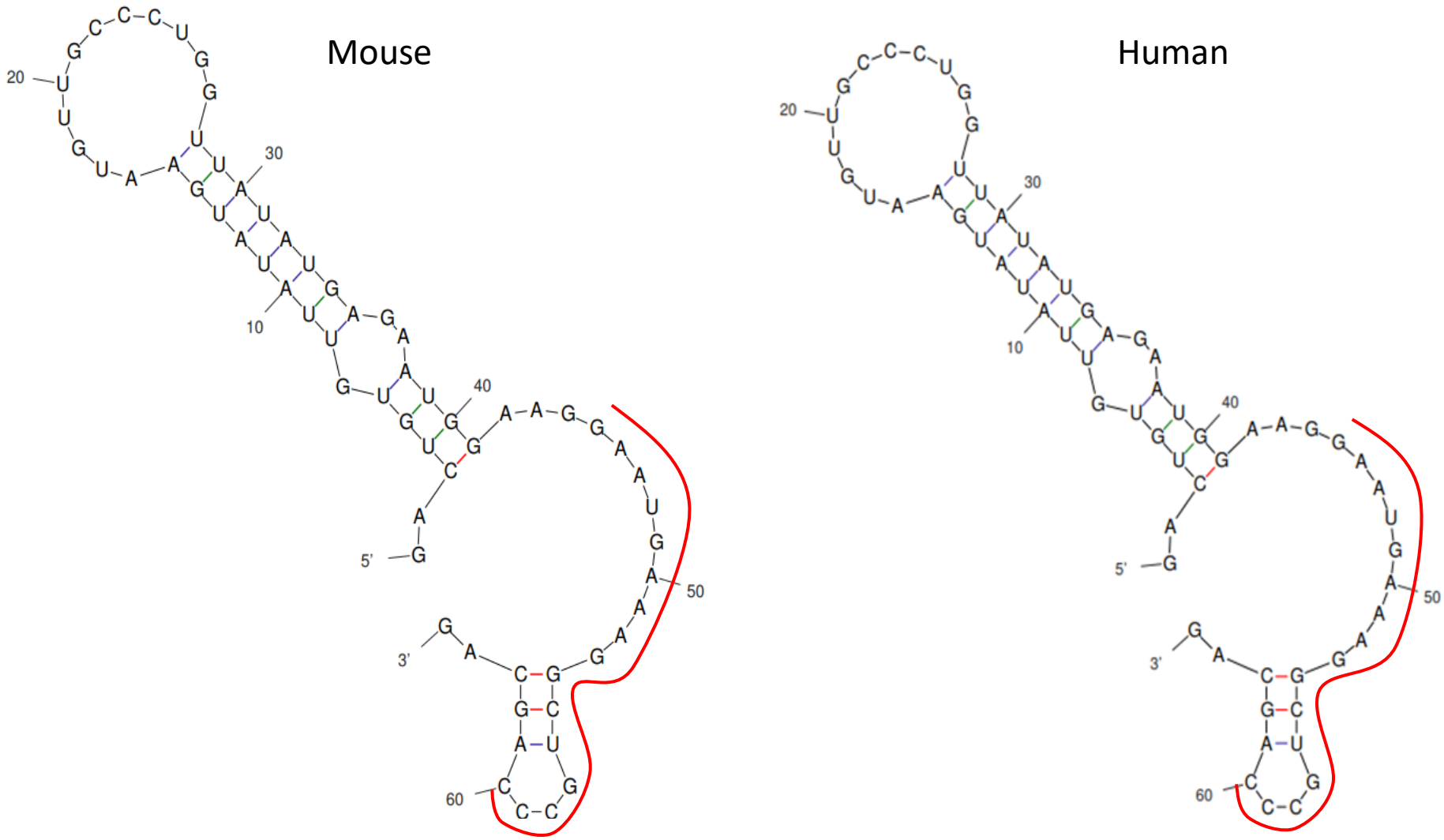

Figure 4.16 Predicted RNA secondary structure around exon 3 of mouse and human *POSTN* gene transcript

Secondary structures were predicted using Mfold Both mouse and human exon 3 are 65 nucleotides long and the numbers indicate the position of the specific nucleotide in the exon. Binding position of PEX3 PMO designed to target exon 3 is shown in red. Both ends of the PMO bind the secondary structure in open conformation.

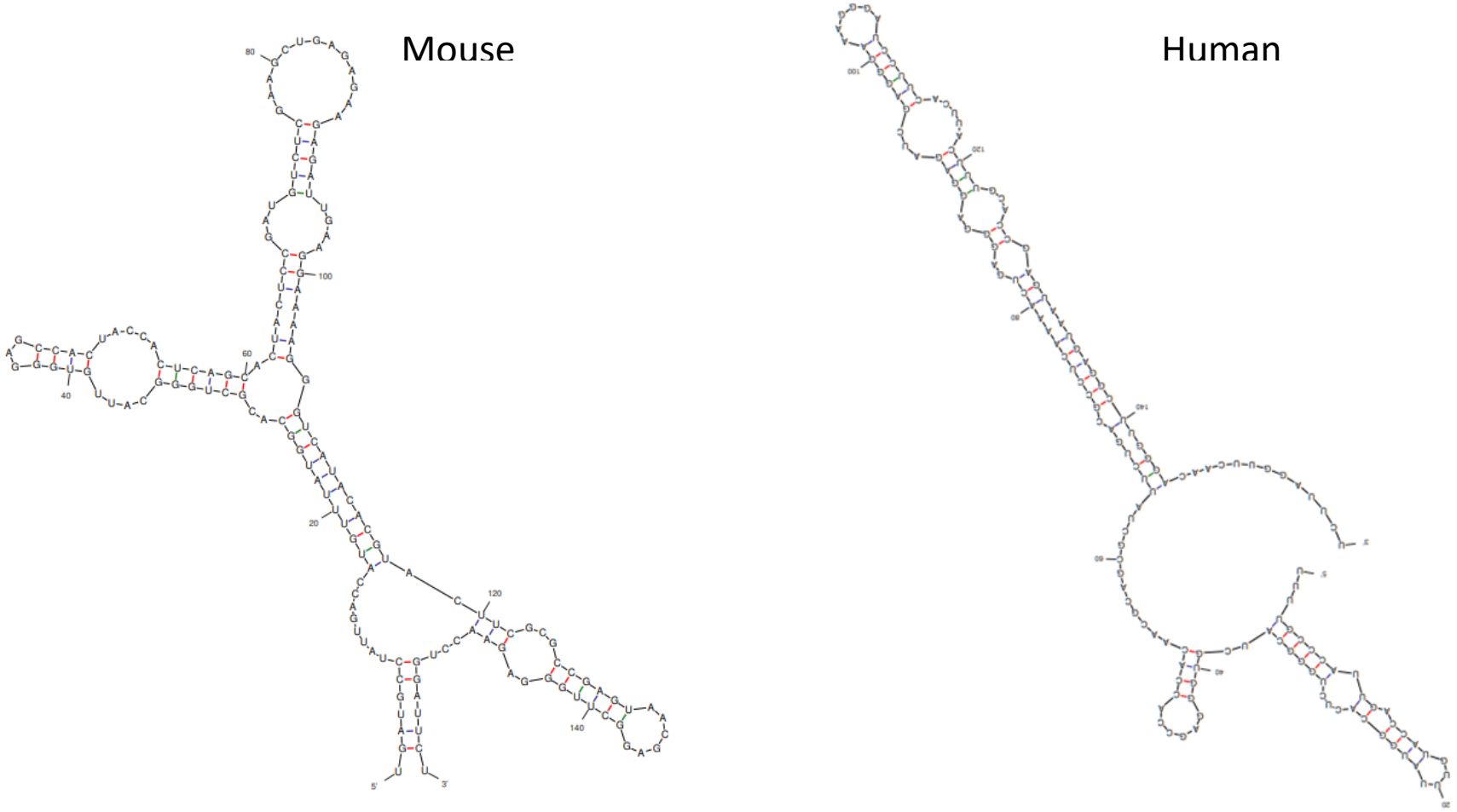

Figure 4.17. Predicted RNA secondary structure around exon 4 of mouse and human *POSTN* gene transcript

Secondary structures were predicted using Mfold. Secondary structure of mouse and human *POSTN* exon 4 as predicted by Mfold. Both mouse and human exon 4 are 158 nucleotides long and the numbers indicate the position of the specific nucleotide in the exon.

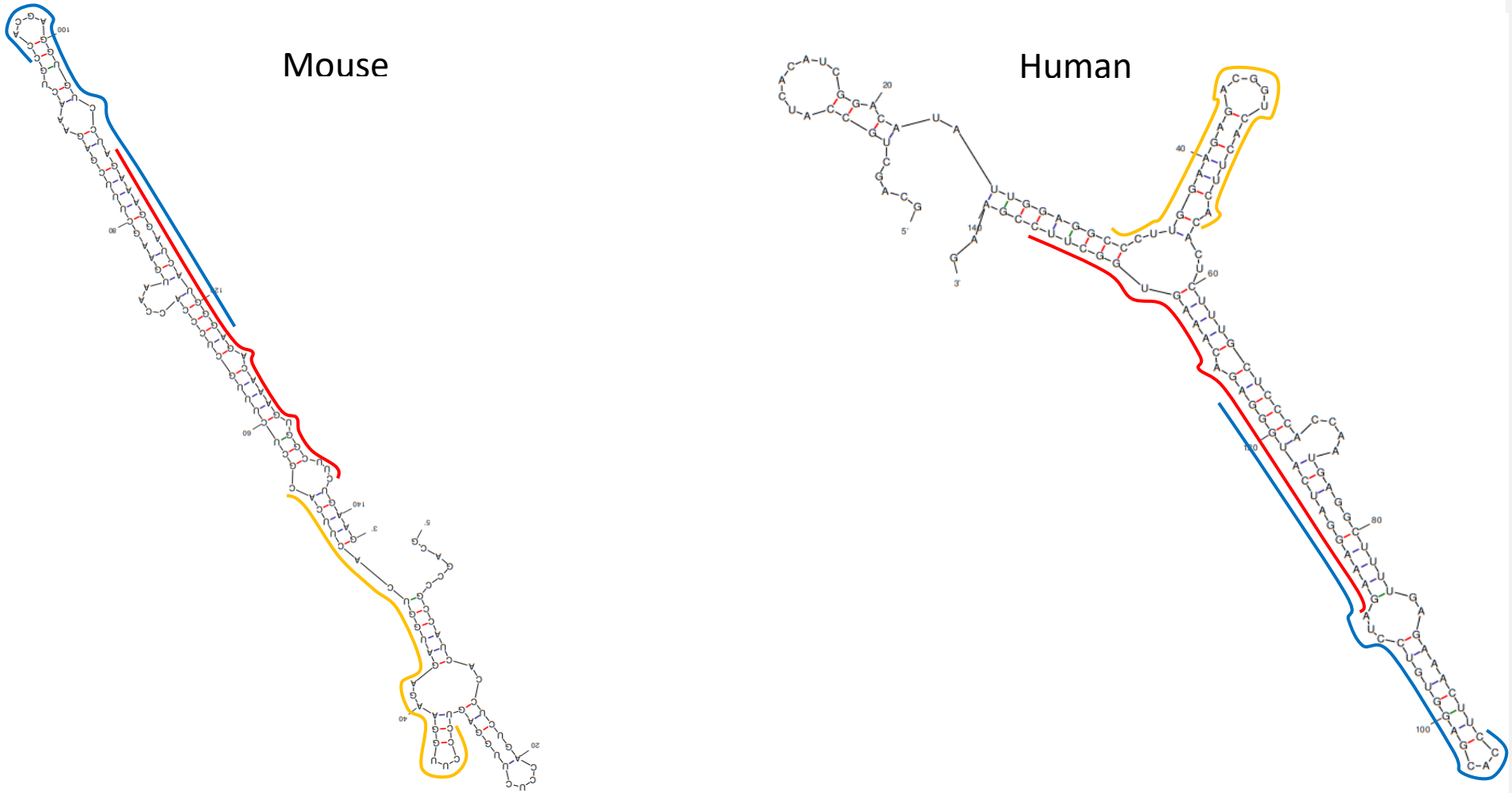

Figure 4.18 Predicted RNA secondary structure around exon 7 of mouse and human *POSTN* gene transcript

Secondary structures were predicted using Mfold. Both mouse and human exon 7 are 142 nucleotides long and the numbers indicate the position of the specific nucleotide in the exon. Binding position of PEX7.1, PEX7.2 and PEX7.3 PMOs designed to target exon 7 are shown in blue, red and yellow respectively

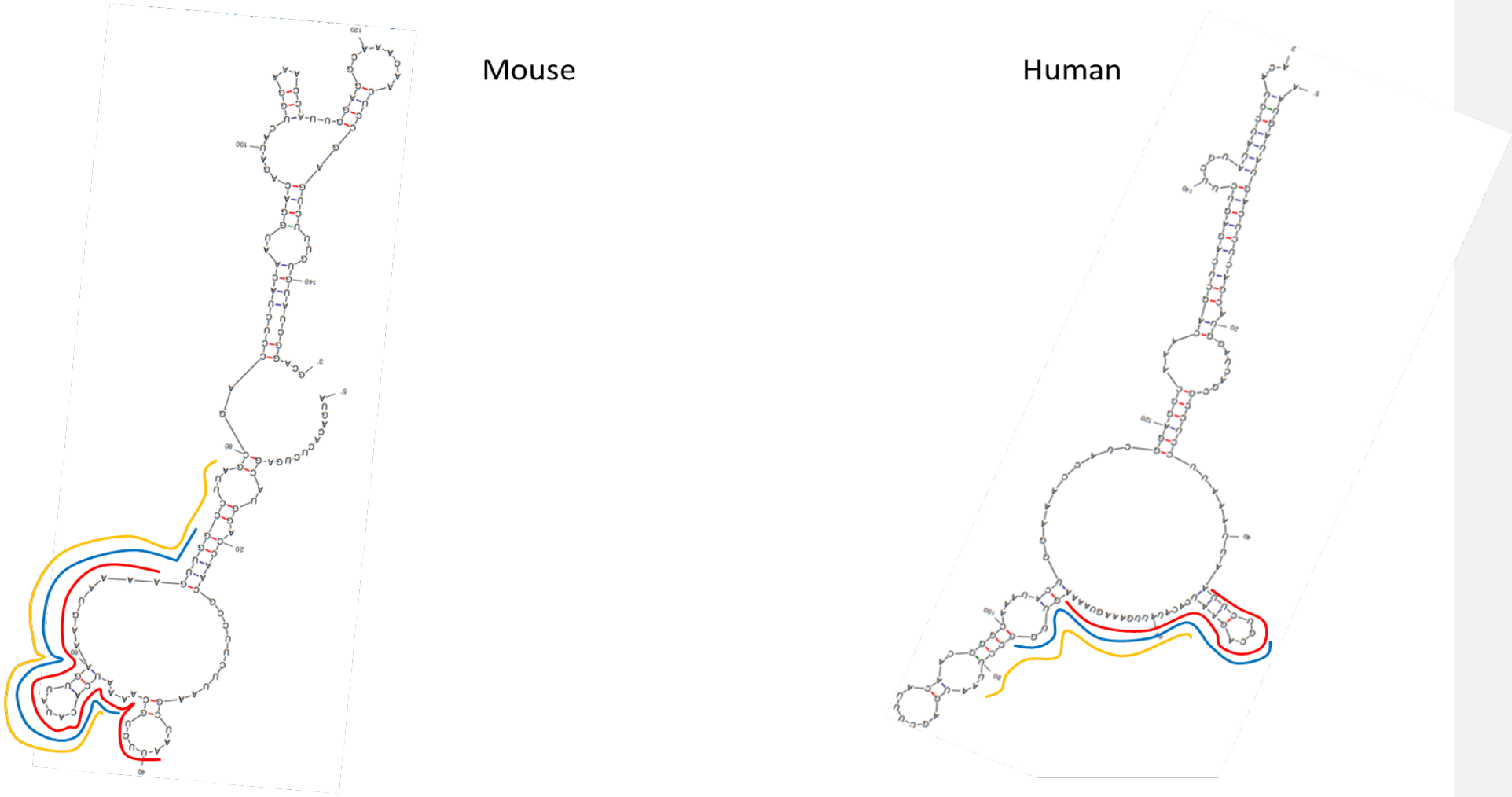

Figure 4.19 Predicted RNA secondary structure around exon 10 of mouse and human *POSTN* gene transcript

Secondary structures were predicted using Mfold. Both mouse and human exon 10 are 149 nucleotides long and the numbers indicate the position of the specific nucleotide in the exon. Binding position of PEX10.1, PEX10.2 and PEX10.3 PMOs designed to target exon 10 are shown in red, blue and yellow respectively.

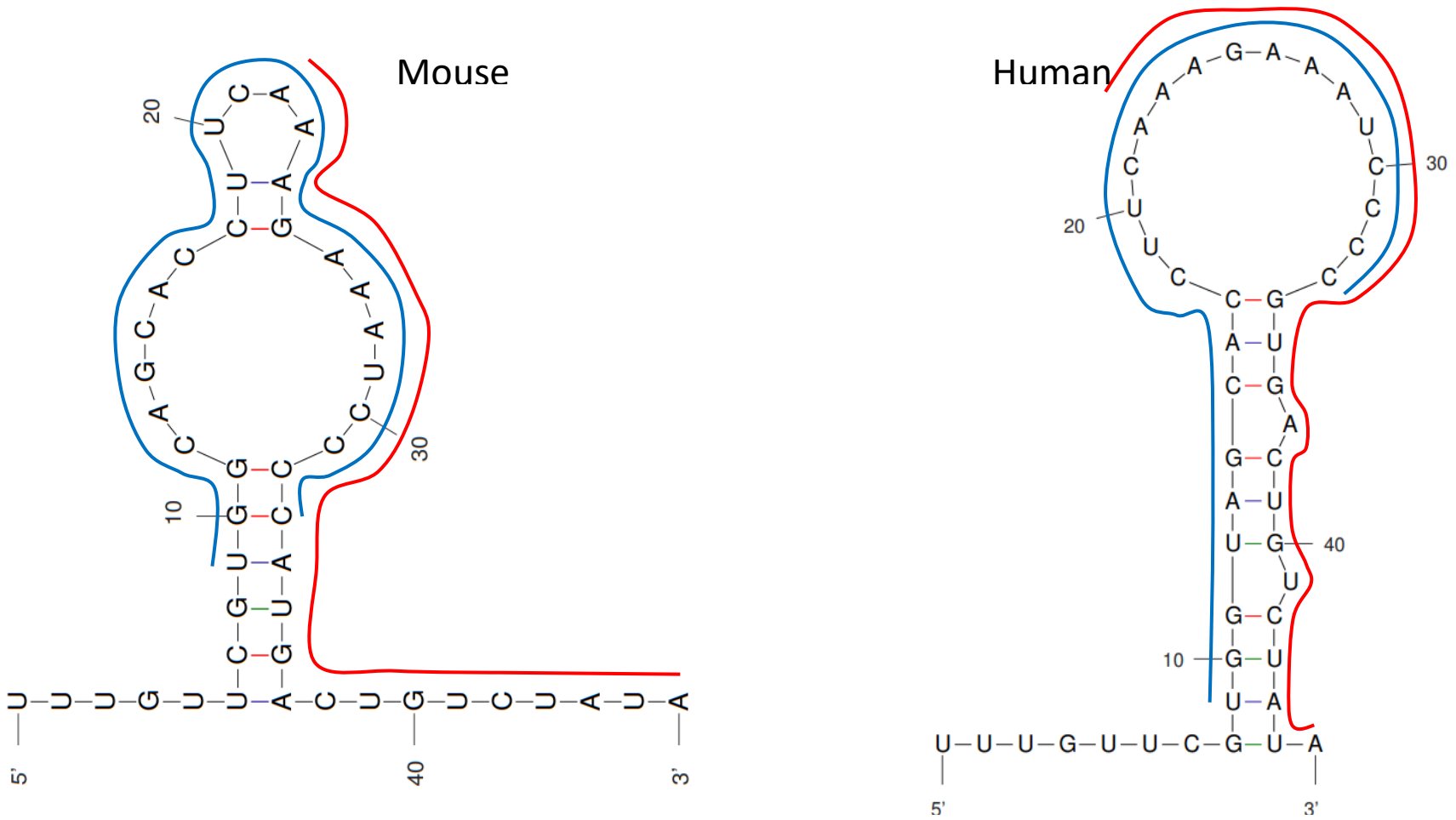

Figure 4.20 Predicted RNA secondary structure around exon 16 of mouse and human *POSTN* gene transcript

Secondary structures were predicted using mfold. Both mouse and human exon 16 are 46 nucleotides long and the numbers indicate the position of the specific nucleotide in the exon. Binding position of PEX16.1 and PEX16.2 designed to target exon 16 are shown in blue and red respectively.

4.3 Discussion

In this Chapter, nine AONs for synthesis by PMO chemistry (Chapter 5) were designed to target *POSTN* and deliver a message with out-of-frame exons; this should result, *in vivo*, in a reduction of *POSTN* mRNA due to NMD. Targeting ESE motifs has been explored extensively and targeting ESE motifs with antisense oligonucleotides and more specifically PMO chemistries has been shown to be successful in exon exclusion in DMD (Malerba, Kang, McClorey, Saleh, Popplewell, Gait, Matthew Ja Wood, *et al.*, 2012).

To design the oligonucleotides, bioinformatics tools were used to identify ESE motifs, the mouse and human exons were compared to find homology and appropriate thermodynamic properties were considered. AONs were mostly designed with alternative overlapping binding sites on the RNA secondary structure. Bioinformatics software are commonly used in the literature to predict the position of ESE motifs, so for this work, recommended software included RESCUE-ESE (Fairbrother *et al.*, 2002, 2004) and ESEfinder (Cartegni *et al.*, 2003). Human Splicing Finder (HSF) uses both RESCUE-ESE and ESEfinder algorithms but only human sequences (Desmet *et al.*, 2009). Here, HSF was used to predict ESE motifs in the human *POSTN* sequences, and ESEfinder used to look at both human and mouse sequences. The combined data from HSF and ESE finder were used to compare and find overlapping predicted ESE motifs across the two species, and AONs were designed targeting selected ESE motifs which are present in both the human and mouse. Previously we found that targeting mouse-human homologous regions gave better downregulation of target gene (Chapter 3).

One of the downsides of evaluating AON-mediated exon skipping in mouse and other in-vivo animal models is that human-specific AONs generally cannot be validly tested

since sequence homology may be limited. Thus while mouse models for example allow general studies on the proof of concept of therapeutic exon skipping strategies, the testing of precise human medicinal product AON going into clinical application or clinical trials may not be feasible unless humanised models have been developed(Veltrop *et al.*, 2018). In order to tackle this problem, this study focused on regions of exons where human-mouse homology is high. This has the added advantage of adding evolutionary conservation to our knowledge-base for the PMO, and conservation of sequence may indicate conservation of function. Nine PMOs were designed to either have no mismatches in the human and mouse or have a maximum of one mismatch with the mouse. Prior to clinical studies, human-specific AONs have been screened in-silico against the human genome *for off-target hybrisation sites,* and hits within genes with one, two or three mismatches tested for AON-mediated changes in mRNA transcript levels (Kamola *et al.*, 2015; Schoch and Miller, 2017). These studies indicate that the presence of 1 or 2 base mismatches do not stop an AON being effective at inducing exon skipping or changing mRNA levels. The success in this test, of the PMOs designed in this study, when tested *in vitro* in the mouse C2C12 cell line allowed proof of concept for *postn* exon skipping and allowed moving on towards further testing of these AONs which are specific to the human gene.

As previously discussed (Chapter 3, Discussion), factors affecting bioactivity of AONs have been widely researched. Previous studies by Vickers, Wyatt and Freier (2000) argue that local secondary structure of the precise region of the mRNA where AONs are targeted may be critical for bioactivity of an AON: targeting unstructured sites gives better results and increases AON efficacy. On the other hand, a more recent study by Popplewell *et al.* (2009) showed that when it comes to designing PMOs for exon skipping

the predicted overall binding energy of PMO to target sequence is the most important factor along with PMO length. Long oligonucleotides bind more tightly and specifically as their T_m and %GC can be dramatically increased. Popplewell *et al.* also show that the position of PMO binding with respect to RNA secondary structure does not have a significant effect on bioactivity unless choosing between successful PMOs, where the more bioactive PMOs show binding to targets with an open conformation. In this Chapter, PMOs were designed focusing on the overall binding energy of PMO to target and increasing the length of the PMO to increase binding energy where necessary. The secondary structure of mRNA was also considered and where possible PMOs were designed to target open confirmations or sequences where there is less putative local structure, but this factor was not seen to be detrimental. Percentage GC of the designed PMOs was kept at around 50% as recommended by Ho *et al.* (1996). However, %GC was lower in some PMOs due to the low GC content of the exon sequence.

5. In vitro analysis of antisense oligonucleotide targeting human and mouse *POSTN* out-of-frame exons

5.1 Introduction

As discussed in Chapter 4, splicing of pre-mRNA results in the production of functional mRNA with only protein coding sequences and the consequent production of biochemically active protein (Proudfoot, Furger and Dye, 2002b). The use of AONs to mask an exon and produce a shorter, out-of-frame transcript, that is consequently degraded through NMD, is well established in the literature (Kang *et al.*, 2011a; Lu-Nguyen *et al.*, 2017; Golshirazi *et al.*, 2018). AONs were designed in the previous chapter to target four out-of-frame exons in the mouse and human *POSTN1* pre-mRNA. The PMOs were designed to bind their target and prevent a specific exon from being included in the transcript, making the resulting mRNA shorter and lacking the correct reading frame (Aartsma-Rus and van Ommen, 2007). Successful PMOs should, in theory, decrease the amount of in-frame transcript produced since AON reagents do not work to 100% efficiency and because the half-life of mRNAs ranges from minutes to hours (Chen, Ezzedine and Shyu, 2008), but they do effectively reduce the amount of functional protein in the cell.

Following the design of AONs targeting exons 3, 7, 10 and 16 of *POSTN1* in both human and mouse sequences, they were synthesised with PMO chemistry (Chapters 1, 2). it was important to demonstrate the capability of the PMOs in inducing specific exon

skipping in both human and mouse cell culture systems. This process is well established in the laboratory.

Prior to transfection, muscle cells and fibroblasts were treated with TGF-β1 to stimulate POSTN expression; this mimics the transcriptional and translational process that occurs following injury (Chapter 1, March *et al.*, 2018). The effect of TGF-β treatment on POSTN and Collagen I expression was assessed prior to transfection with PMO, to determine a dose at which the pathways related to damage and fibrosis are activated.

A suitable TGF-β dose was tested in two cell lines: human muscle cells from DMD patients; and mouse C2C12 cells. Then these cell lines were therefore treated with TGF-β and then transfected with the newly designed PMOs, using Endo-Porter as the transfection reagent (Chapter 2). Initially, semi-quantitative analysis of *POSTN1* transcripts was used to compare the efficiency of each PMO in its ability to induce exon skipping.

The most successful PMO, based on full-length transcript reduction (the PCR primers bound to the start and end of full-length POSTN1 transcripts), was then chosen to test in the mouse fibroblast cell system as these cells are believed to have a major burst in POSTN production in the event of fibrosis (Crawford *et al.*, 2015). RT-qPCR and Western blots were then used to more accurately investigate the efficiency of the most successful PMO in the mouse cell system at mRNA and protein levels, respectively.

5.2 Results

5.2.1 Effect of TGF-β on Periostin and Collagen expression

An important consideration for the transfection of AONs designed for exon skipping is that they need to be transfected at the stage of target gene transcription. TGF-β activates POSTN expression as well as other genes involved in regeneration and repair, such as collagen-I (March *et al.*, 2018). In order to determine that TGF-β stimulates POSTN expression and mimics a fibrotic pathway, C2C12 cells were plated in six-well plates, and when confluent, cultures were treated with 2ng or 10ng of TGF-β. 24 hours after treatment, RNA was harvested and subjected to RT-qPCR to detect POSTN message expression levels (Figure 5.1). To normalise the expression (effectively to get a clear percentage reduction per cell) RT-qPCR of GAPDH was used; GAPDH is a constantly expressed housekeeping gene. Levels of POSTN message were normalised to the GAPDH expression by a division sum.

The purity of the PCR products (discrimination of the PCR primers) was assessed by a melting curve, which showed two distinct peaks, one for the POSTN transcript and the other, GAPDH. Two clean peaks indicated no issues with the two sets of primers and no contamination in the samples or reagents (Figure 5.1A).

The normalised qPCRs show an increase in POSTN expression at both 2ng and 10ng treatments of TGF-β. At 10ng there is a threefold increase in expression relative to no treatment, with a statistical significance ($p<0.001$) using one-way ANOVA (Figure 5.1B); using 2ng gave only a two-fold increase with no statistical significance.

RT-qPCR was also used to look at the effect of TGF-β on Collagen I expression. This was to confirm the activation of fibrotic pathways, not just POSTN (Figure 5.2). The melting curve for these sets of primers revealed two distinct, clean peaks, one for GAPDH and one for *POSTN*, indicating functional primers with no contaminating binding sites (Figure 5.2A). Despite the low activation of POSTN expression at 2ng of TGF-β, collagen I was significantly increased by four-fold at both 2ng and 10ng of TGF-β treatment with a significance of $p<0.01$ (Figure 5.2B). This result shows that TGF-β treatment activates the fibrotic pathways and concomitantly stimulates POSTN transcription. As 10ng shows a significant increase in POSTN expression, it was decided to treat cell cultures with 10ng of TGF-β for our experiments with AONs.

To measure the effect of AON on POSTN1 expression induced by TGF-β, it was decided to treat cells with TGF-β just 1 hour prior to transfection with AONs. After that, cells were left for 24h before harvesting, as above.

A

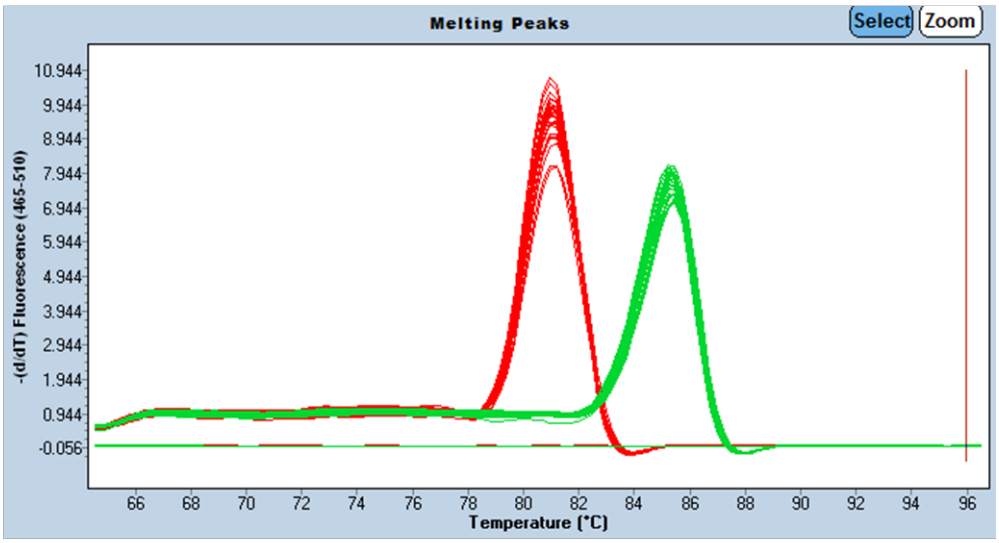

B

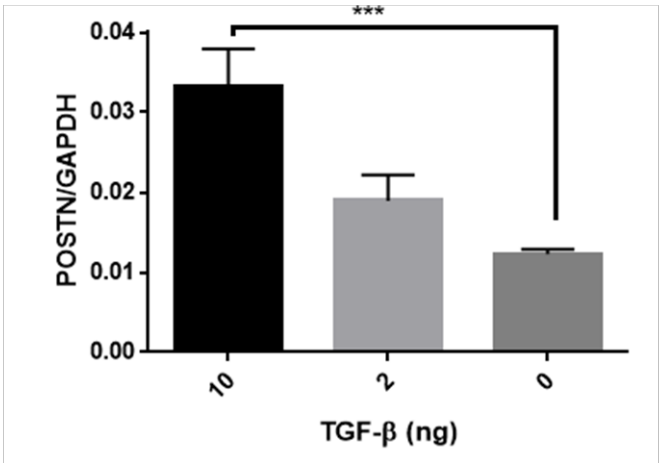

Figure 5.1 Treatment of C2C12 cells with TGF-β and quantification of POSTN expression

C2C12 cells were treated with 2ng or 10ng of TGF-β, or no TGF-β as negative control. 24 hours after treatment RNA was extracted followed by qPCR to quantify POSTN. GAPDH was quantified and used as housekeeping gene for normalisation.

A) Melting curve from the qPCR reaction showing two distinct peaks indicating two specific distinct products with no overlap: POSTN (green); GAPDH (red).

B) Quantification of POSTN expression normalised to GAPDH expression. Dose dependent increase is seen upon TGF-β treatment with statistical significance calculated for 10ng treatment using one-way Anova test. (***$p<0.001$, N=3).

A

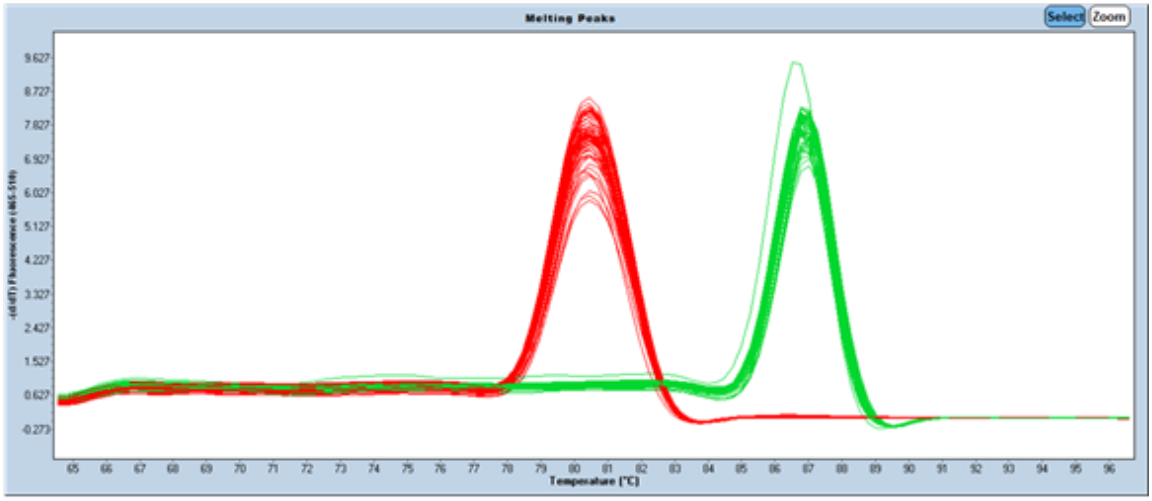

B

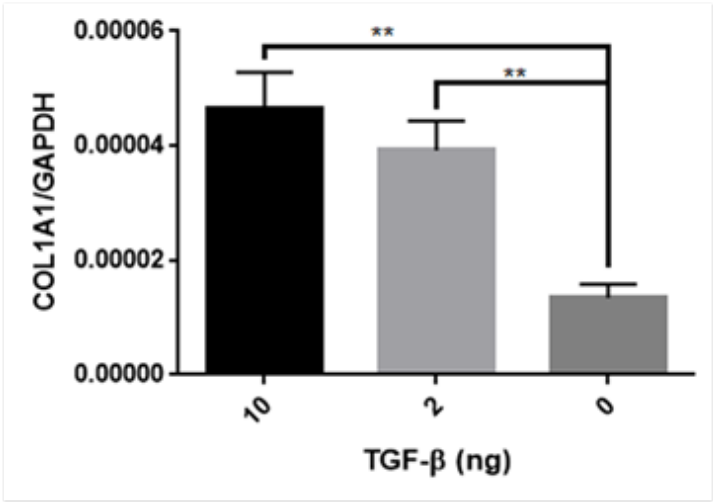

Figure 5.2 Treatment of C2C12 cells with TGF-β and quantification of type I Collagen expression

C2C12 cells were treated with 2ng or 10ng TGF-β, or no TGF-β as negative control. 24 hours after treatment RNA was extracted followed by qPCR to quantify type I Collagen. GAPDH was quantified and used as housekeeping gene for normalisation.

A) Melting curve from the qPCR reaction showing two distinct peaks indicating specific distinct products with no overlap: Collagen (green); GAPDH (red).

B) Quantification of Collagen expression normalised to GAPDH expression from qPCR. Dose dependent increase is seen upon both TGF-β treatments, with statistical significance calculated for both 2ng and 10ng treatment using one-way Anova test. (**$p<0.01$, N=3).

5.2.2 PMO induced skipping of POSTN

5.2.2.1 Determination of optimal conditions for Endo-Porter as transfection reagent

As previously discussed (Chapter 3), Endo-Porter is a peptide-based reagent that mediates endocytosis allowing the uptake of peptides, proteins and neutral PMOs in the presence of serum and has been shown to deliver PMOs at various concentrations.

Recent work in our laboratory has shown that the concentration of Endo-Porter used may have significant impact on the effect of AONs designed for exon skipping (Popplewell, L. 2009, personal communication, 2019). The length of time for which cells are incubated with Endo-Porter has also been shown to be a crucial factor. Both these factors were therefore investigated to determine the best concentration at which to use Endo-Porter and to verify that cells remain viable after 24 hours of incubation with Endo-Porter present in the media.

Initially, C2C12 cells were seeded in 6-well plates and allowed to grow to confluency. 8µM of Endo-Porter was then added to 3 of the 6 wells along with fresh media. A time course of the treated and control cells was made, counting the number of floating cells (this cell line normally adheres to the bottom) and live cells (using Trypan blue) by microscopic observation, at time intervals of 24h, 48h and 72h and percentage cell death was calculated (Figure 5.3A). This shows that Endo-Porter has a toxic effect on the cells with approximately 20% +/- 0.3 cell death at 24 hours. This cell death doubles at 48 hours to 40% +/-0.2. It was therefore decided that the previously practised protocol of harvesting RNA 24 hours after transfection with Endo-Porter is best practice: a 24 hour period was needed to get a significant upregulation of POSTN message (above).

In order to determine the optimal concentration of transfection reagent, C2C12 cells were seeded in six-well plates and transfected with a 10µM solution of a PMO that targets exon 7 of *POSTN1,* with 6µM or 8µM Endo-Porter; the Endo-Porter website, Genetools, suggests 6µM as the optimum concentration for transfection and 8µM the maximum concentration to use. RNA was harvested 24 hours following transfection at these two concentrations (Figure 5.3B). The fragment of *POSTN* amplified in the nested RT-PCR is exons 5-8 which is 643bp in length. Exclusion of exon 7 results in an RT-PCR product of 402 bp. The results show a visually stronger and more consistent skip band when using 8µM of Endo-Porter, indicating a more effective transport of PMO into cells. Semi-quantitative densitometric analysis of the gel using Image J (Figure 5.3B) also confirmed that stronger skipping seen in samples with 8µM of Endo-Porter. It was decided to use 8µM of Endo-Porter for all transfections.

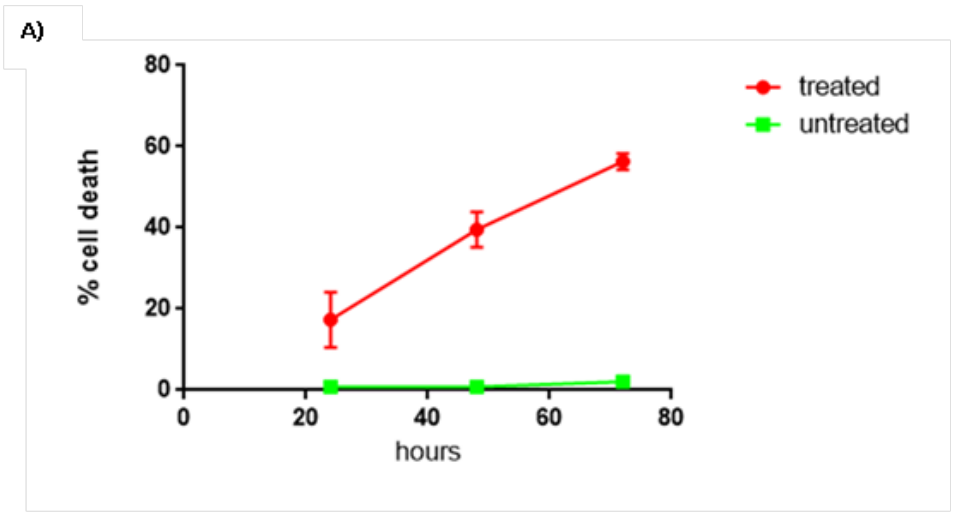
A)
80
60
40
20
0
% cell death
0
20
40
60
80
hours
treated
untreated

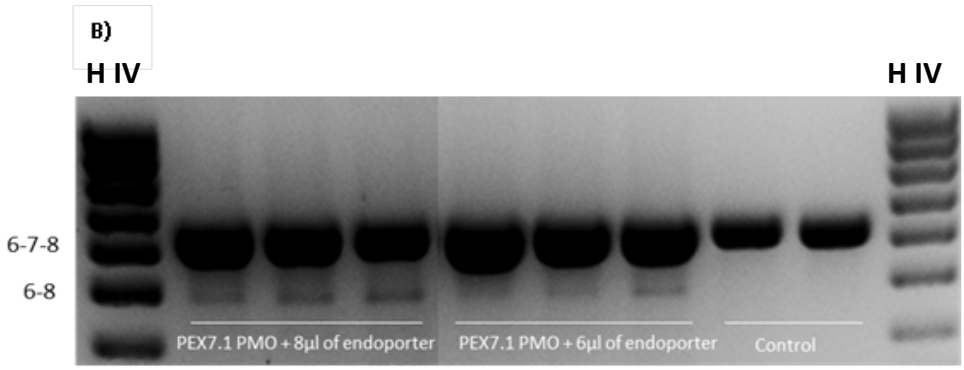
B)
H IV
H IV
6-7-8
6-8
PEX7.1 PMO + 8µl of endoporter
PEX7.1 PMO + 6µl of endoporter
Control

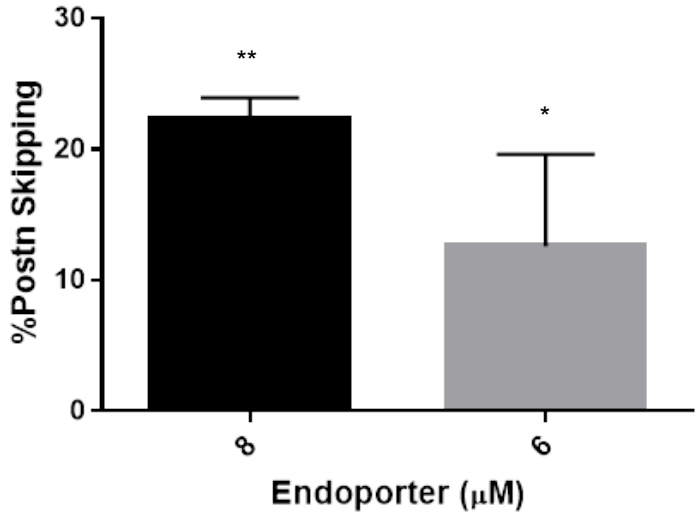
30
20
10
0
%Postn Skipping
**
*
8
6
Endoporter (µM)

Figure 5.3 Evaluation of optimal conditions for Endo-Porter as transfection reagent

A) C2C12 cells were plated and allowed to grow and divide. Media was exchanged for fresh media and three of the six wells were treated with 8µM of Endo-Porter and another three wells were untreated. Floating/dead cells and live cells were then counted at 24h, 48h and 72h and percentage cell death calculated: treated cells (green); untreated cells (red). N = 3

B) C2C12 cells were plated and allowed to grow and divide. Cells were then transfected with PEX7.1 PMO, for exon 7 exclusion, using 6µM or 8µM of Endo-Porter. RNA was harvested 24 hours after transfection and subjected to RT-PCR amplifying the *POSTN* exon 6-8. A 3% agarose gel of the RT-PCR products is shown along with Hyperladder IV (H IV). Full length product was present in all lanes including the control lane at 643bp in length. The exon skipped band is 402 bp, present in treated lanes and stronger in the 8µM Endo-Porter treated samples. Semi-quantitative analysis of the gel image, using GeneTools, shows nearly twice as much skipping in the 8µM treated samples. This analysis was carried out by comparing the intensity of the skipped band to the intensity of skipped + full length band. Significance was calculated relative to control samples using one way ANOVA. (*$p<0.05$, **$p<0.01$, N=3).

5.2.2.2 PMO induced exclusion of Periostin exon 3,7,10 and 16 in patient cells

PEX3, PEX7.1, PEX7.2, PEX7.3, PEX10.1, PEX10.2, PEX10.3, PEX16.1 and PEX16.2 are the nine PMOs designed as AONs in Chapter 4 (Figures 4.12-4.20). To see how they perform in DMD patient cell lines, cells were pre-treated with TGF-β. Each PMO was transfected into these DMD patient cell systems treated with 10ng of TGF-β 1 hour prior to transfection, at a concentration of 10μM using 8μM of Endo-Porter transfection reagent (above, see Chapter 2 for details of Endo-Porter function). Control AON treated samples were included with the Endo-Porter reagent, and a control PMO was supplied from GeneTools which has no target and very little biological activity.

RNA was harvested 24 hours after transfection and subjected to nested RT-PCR to amplify specific exons of *POSTN*, dependant on the PMO used (exons skipped). For RNA harvested from PEX3-transfected cells, exon 2-4 was amplified. The longest PCR product which contains all exons is expected to be 149bp in length. The exclusion of the 65bp exon 3 results in an 84bp product. This is a size difference that is very difficult to resolve on a 3% TAE agarose gel and bands were instead resolved on a high-resolution, 10% polyacrylamide TBE gel. TBE gels were semi-quantitatively analysed as described. The results (Figure 5.4A) show the smaller band lacking exon 3 in the lanes treated with PEX3 and absent in the control samples. Semi-quantitative analysis of the gel showed 37% +/- SD skipping (Figure 5.4B).

In the case of PEX7.1, PEX7.2 and PEX7.3, exons 5-8 were amplified. The full-length product is 544bp in length. The exclusion of the 142bp exon 7 results in a 402bp product. This size difference was efficiently resolved on a 2**%** agarose gel. Results (Figure 5.5A) show the smaller band lacking exon 7 to be evident only after transfection with PEX7.1.

Both PEX7.2 and PEX7.3 showed the full-length 544bp product but lacked the smaller skipped product, as do control samples. Semi-quantitative analysis (Figure 5.5B) showed that 18% of POSTN was the skip product using PEX7.1 PMO; there was no skipping evident using PEX7.2 and PEX7.3 PMO.

In the case of PEX10.1-PEX10.3 transfected cells RNA, exons 8-12 were amplified. The full-length product is 521bp in length. The exclusion of the 149bp exon 10 resulted in a 372bp product, a size difference that is resolved on a 2% agarose gel. Results (Figure 5.6) showed the presence of the full-length 521bp band in all lanes, but no evidence of the shorter 149bp skipped band indicating no successful skipping.

In the case of PEX16.1- and PEX16.2-transfected cell RNA, exons 14-18 were amplified in the first round of the nested RT-PCR and exons 15-17 were amplified in the second round of PCR. The full-length product is 168bp in length. The exclusion of the 46bp exon 16 results in a 122bp product, a size difference that is resolved on a 10% polyacrylamide TBE gel. Results (Figure 5.7A) show the smaller 122bp product lacking exon 16 to be evident in lanes transfected with both PEX16.1 and PEX16.2. Semi-quantitative analysis of the gel shown in Figure 5.7B showed a 41% skip for PEX16.1-transfection and a lower, 8% skip for PEX16.2 transfection.

The results show successful skipping of *POSTN1* in DMD patient cells when transfected with 10µM of four AONs, PEX3, PEX7.1, PEX16.1 and PEX16.2. PEX7.1 showed the poorest skip at below 20% of full-length product. In the case of exon 16 skipping, PEX16.1 was more successful. It was therefore decided to take two AONs, PEX3 and PEX16.1, both of which showed over 30% skipping, and test them in murine muscle cells

since the mouse is the *in vivo* model used for testing successful PMOs for therapeutic use

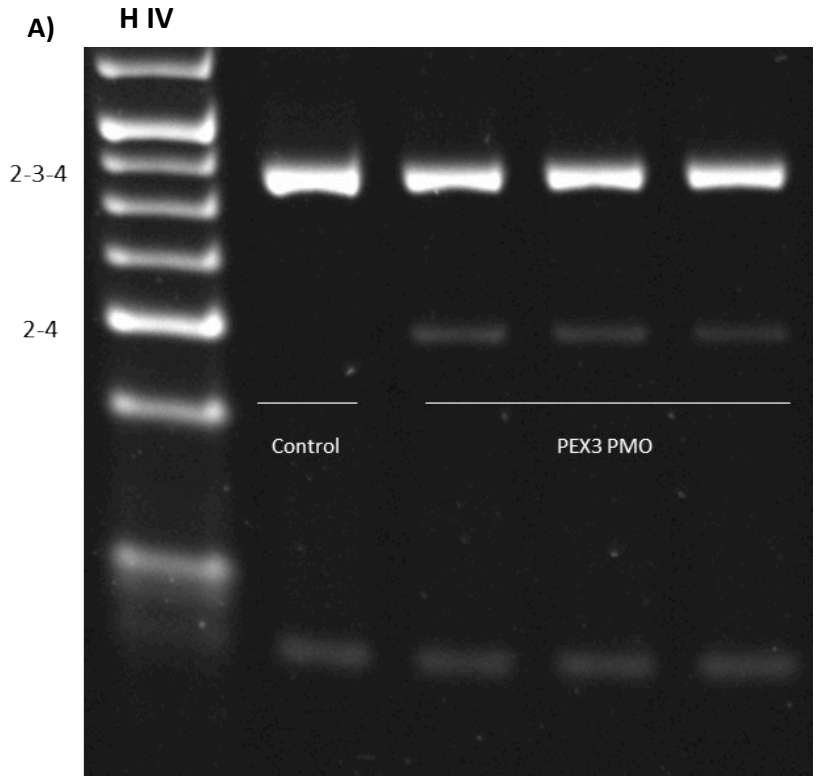
A)
H IV
2-3-4
2-4
Control
PEX3 PMO

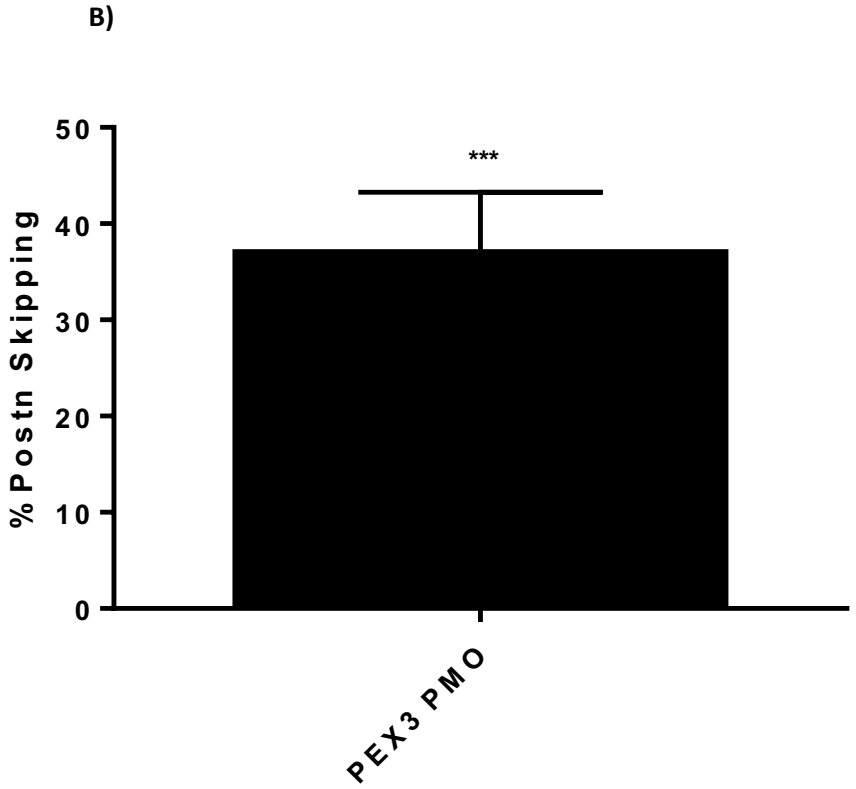
B)
% Postn Skipping
50
40
30
20
10
0
***
PEX3 PMO

Figure 5.4 Transfection of PEX3 PMO targeting exon 3 in DMD patient muscle cells

DMD patient muscle cells were transfected after reaching confluency, with PEX3 PMO at 10µM using 8µM of Endo-Porter. RNA was extracted 24 hours after transfection and subjected to RT-PCR amplifying exons 2-4 of *POSTN* mRNA.

A) 10% Polyacrylamide TBE gel of the RT-PCR products from amplification of exon 2-4 of *POSTN* from patient cells transfected with 10µM of PEX3. Control sample was transfected with the GeneTools-supplied control PMO at 10µM. Full length exon 2-3-4 product at 149bp, containing exon 3, is present in all lanes. The smaller product, without exon 3, at 84bp is present in the three lanes transfected with PEX3 PMO. There is also a very short band in all wells. Hyperladder VI (H IV) was used.

B) Semi-quantitative analysis of the gel using GeneTools software showing 37% skipping of *POSTN* exon 3 in patient muscle cells. Significance was calculated compared to the control sample using a t-test (***$p<0.001$, N=3).

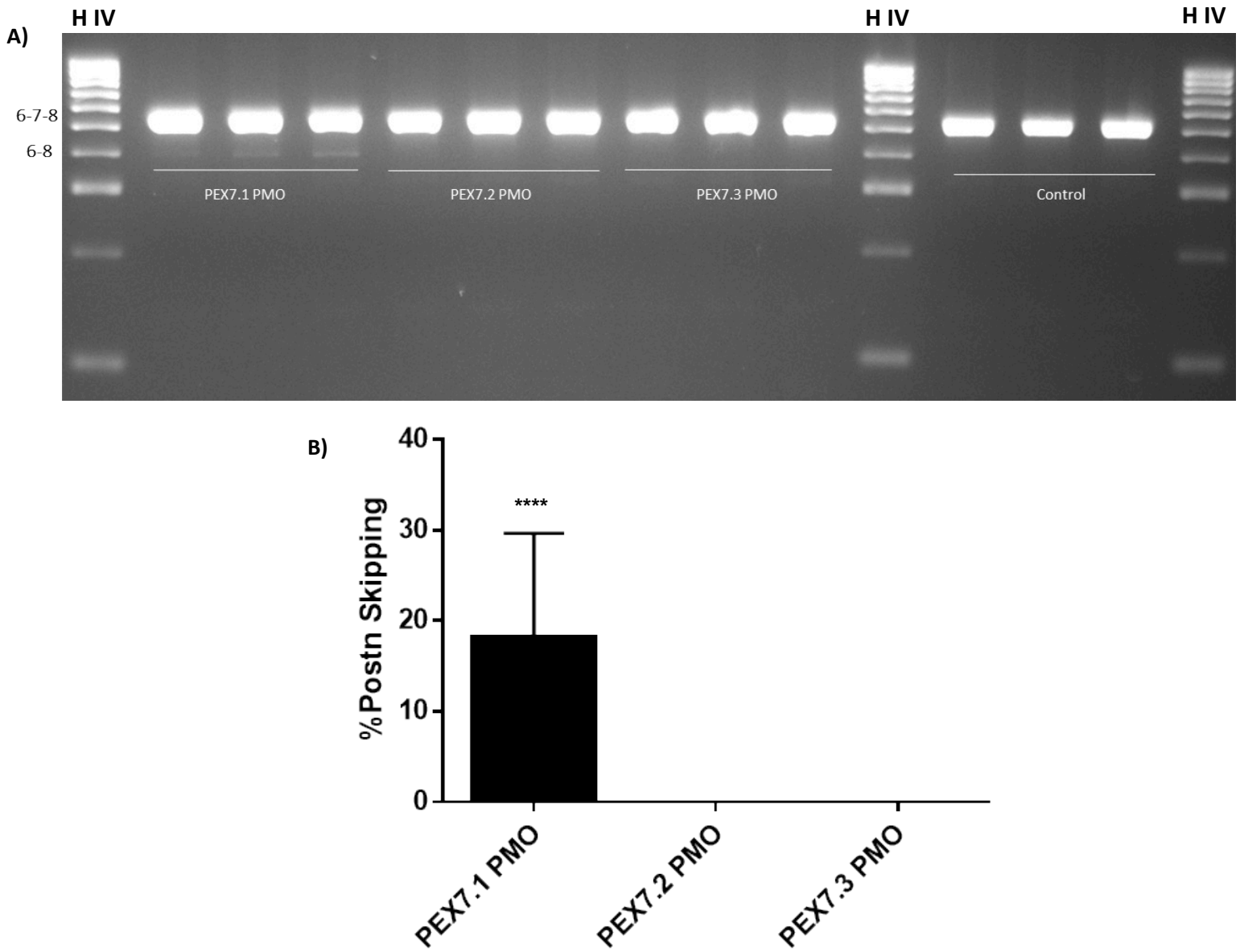
A)
H IV
H IV
H IV
6-7-8
6-8
PEX7.1 PMO
PEX7.2 PMO
PEX7.3 PMO
Control
B)
%Postn Skipping
40
30
20
10
0
****
PEX7.1 PMO
PEX7.2 PMO
PEX7.3 PMO

Figure 5.5 Transfection of PEX7.1, PEX7.2, PEX7.3 PMOs targeting exon 7 in DMD patient muscle cells

DMD patient muscle cells were transfected after reaching confluency, with PEX7.1, PEX7.2 and PEX7.3 PMO at 10µM using 8µM of Endo-Porter transfection reagent. Control samples were transfected with the GeneTools PMO control at 10µM. RNA was extracted 24 hours after transfection and subjected to RT-PCR to amplify exons 6-8 of *POSTN* mRNA.

A) 2% agarose gel of the RT-PCR products from amplification of exons 6-8 of *POSTN* from patient cells transfected with 10µM of PEX7.1, PEX7.2 and PEX7.3 PMO. Full length product at 544bp containing exon 7 is present in all lanes. The smaller product at 402bp is present in the three lanes transfected with PEX7.1 but is not present in other lanes. Hyperladder IV (HP IV) was used.

B) Semi-quantitative analysis of the gel using GeneTools showing 18% skipping of *POSTN* exon 7 in patient cells and no skipping in other samples. Significance was calculated with respect to the control sample using one way Anova (****$p<0.0001$, N=3).

H IV

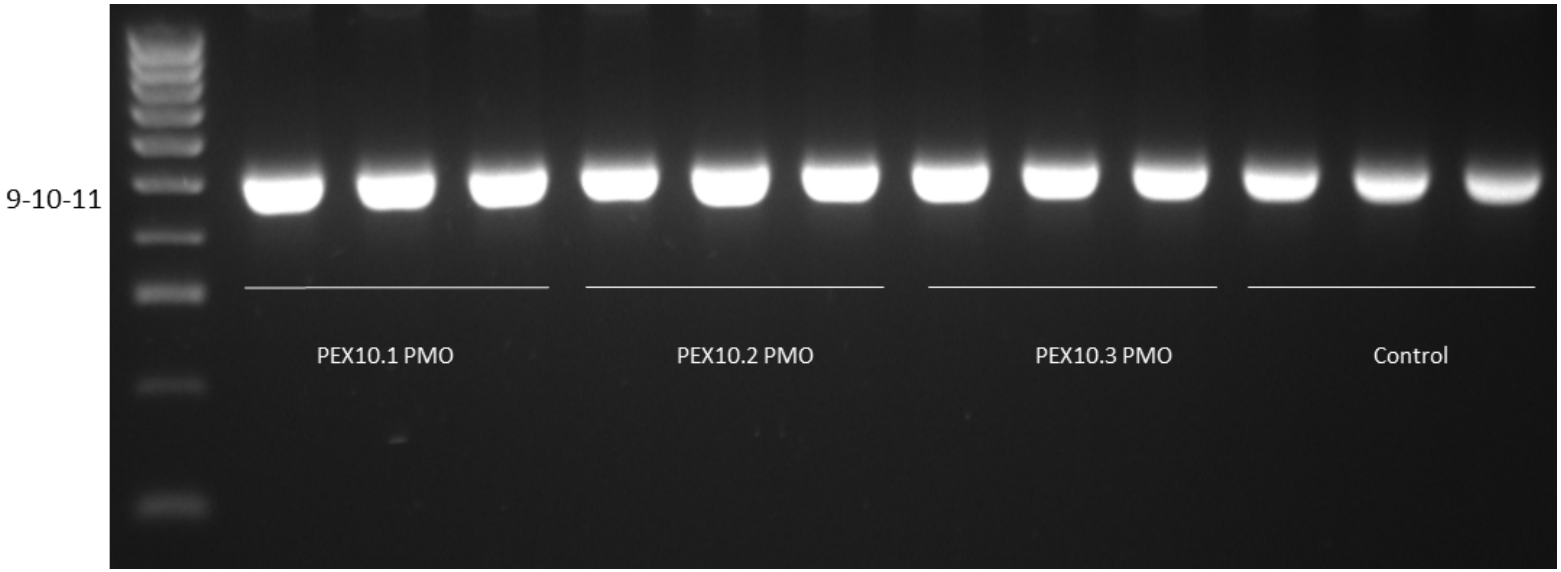

Figure 5.6 Transfection of PEX10.1, PEX10.2 and PEX10.3 PMO targeting exon 10 in DMD patient muscle cells.

DMD patient muscle cells were allowed to reach confluency then transfected with PEX10.1, PEX10.2 or PEX10.3 PMO at 10µM using 8µM of Endo-Porter. Control samples were transfected with the GeneTools control PMO at 10µM. RNA was extracted 24 hours after transfection and subjected to RT-PCR to amplify exons 8-12 of *POSTN* mRNA.

A) A 2% agarose gel of the RT-PCR products from amplification of exon 8-12 of *POSTN* from patient cells transfected with 10µM of PEX10.1, PEX10.2 or PEX10.3. Full length product containing exon 10 at 521bp is present in all lanes. The expected smaller product at 372bp is not present in any lane (N=3). Hyperladder IV (HP IV) was used.

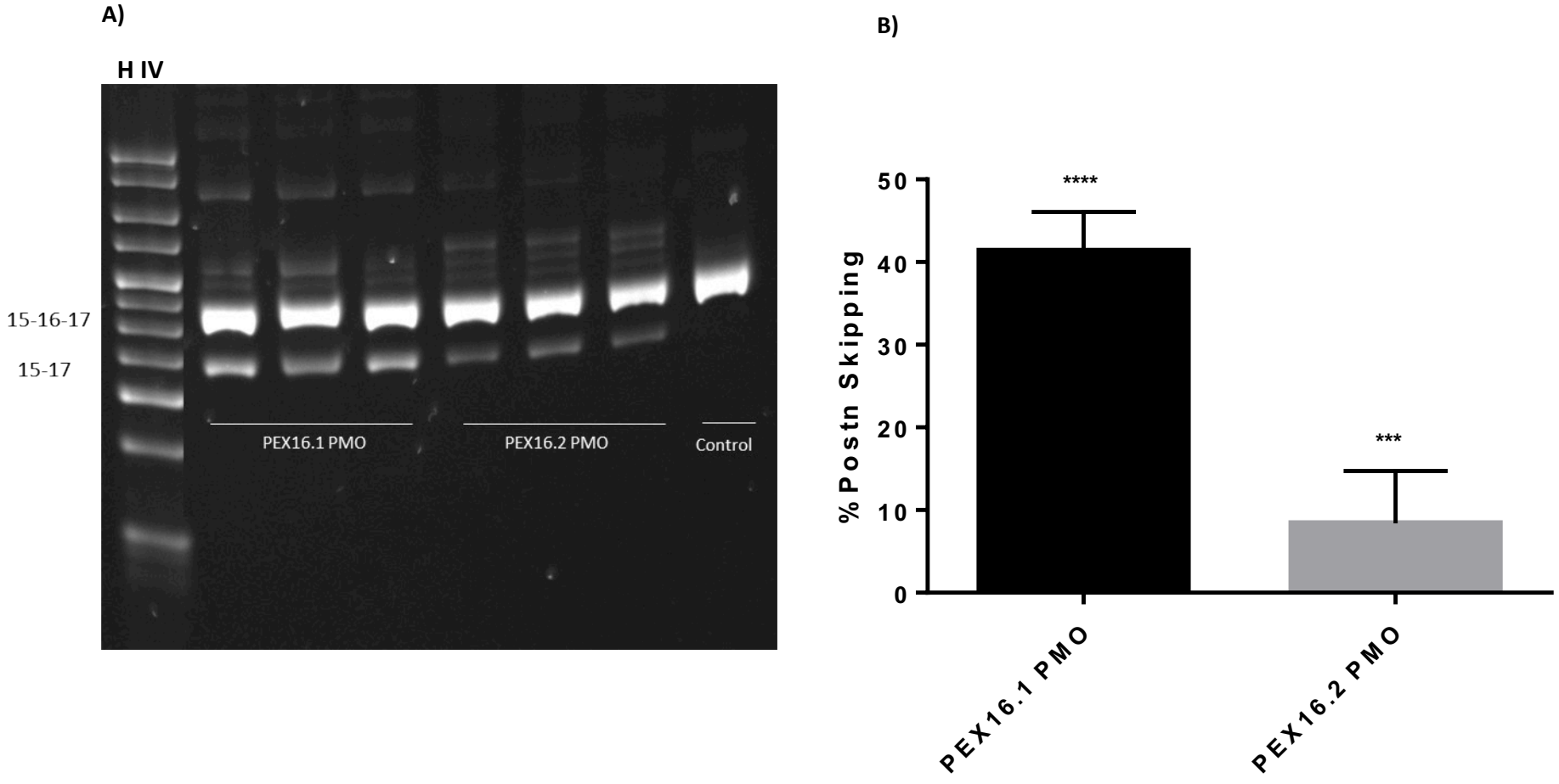
A)
H IV
15-16-17
15-17
PEX16.1 PMO
PEX16.2 PMO
Control
B)
% Postn Skipping
50
40
30
20
10
0
****
***
PEX16.1 PMO
PEX16.2 PMO

Figure 5.7 Transfection of PEX16.1, PEX16.2 targeting exon 16 in DMD patient muscle cells

DMD Patient muscle cells were allowed to reach confluency then transfected with PEX16.1 or PEX16.2 PMO at 10µM using 8µM of Endo-Porter. Control samples were transfected with the GeneTools PMO control at 10µM. RNA was extracted 24 hours after transfection and subjected to RT-PCR to amplify exon 15-17 of *POSTN* mRNA.

A) 10% Polyacrylamide TBE gel of the RT-PCR products from amplification of exon 15-17 of *POSTN* from patient cells transfected with 10µM of PEX16.1, and PEX16.2 PMO. Full length product at 168bp containing exon 16 was present in all lanes. The smaller product at 122bp was present in cells transfected with PEX16.1 as well as cells transfected with PEX16.2. Hyperladder IV (HP IV) was used.

B) Semi-quantitative analysis of the gel using GeneTools software showed 41% skipping of *POSTN* exon 16 in samples transfected with PEX16.1 and 8% skipping in samples transfected with PEX16.2. Significance was calculated using One way Anova with respect to control samples with no skipping. (***$p<0.001$, ****$p<0.0001$, N=3).

5.2.2.3 PMO induced exclusion of Periostin exon 3 and 16 in C2C12 cells

C2C12 cells are a murine muscle-derived cell line (YAFFE and SAXEL, 1977) that are an established myogenic cell line. C2C12 cells have also been extensively used in the laboratory to test AON reagents including PMOs (Kang *et al.*, 2011a; Malerba, Kang, McClorey, Saleh, Popplewell, Gait, Matthew JA Wood, *et al.*, 2012; Lu-Nguyen *et al.*, 2015; Golshirazi *et al.*, 2018). The next experiments were designed to investigate the bioactivity of the successful PMOs in this mouse *in-vitro* model, i.e. PMOs were transfected into C2C12 cells. Dose-response analysis was used to identify the minimal effective transfection concentration of the PMOs shown to be effective in previous experiments (above).

C2C12 cells were seeded in six-well plates and treated with TGF-β for an hour prior to being transfected with different PMOs. Initially, cells were transfected with PMOs at concentrations of 10µM, 5µM and 2µM (Figure 5.8 and Figure 5.10) with 8µM of Endo-Porter for maximum efficacy of transfection (above). As shown in Figure 5.4, RNA was harvested 24 hours after transfection and subjected to nested RT-PCR. The most successful PMO was then transfected into C2C12 cells, as before, but at a wider range of concentrations: 10µM, 5µM. 2µM, 0.5 µM and 0.2 µM (Figure 5.12).

The harvested RNA from all transfections was also subjected to RT-qPCR to give a more accurate quantitative result of skipping (Figures 5.9, 5.11 and 5.13) using the predesigned primers outlined in section 2.4.3.2. GAPDH was used as the housekeeping gene, and all results were normalised to GAPDH. Primers for GAPDH were also predesigned as outlined in section 2.4.3.2.

In the case of PEX3 transfection, exons 2-4 were amplified. The full-length product was 169bp in length. The exclusion of the 65bp exon 3 results in a 104bp product, a size difference that

was resolved on a 3% (w/v) agarose gel (Figure 5.8A). Semi-quantitative analysis of the gel image showed skipping at 56% +/- 0.2 at 10µM, 40% skipping at 5µM and 25% at 2µM (Figure 5.8B). RT-qPCR analysis of mRNA from the PEX3-transfected cells (Figure 5.9) confirmed the trend seen on the agarose gel but showed a much more significant effect of the PMO, with statistically significant downregulation of *POSTN* at all concentrations of PEX3 transfection; $p<0.05$ at 2µM and $p<0.01$ at 10µM and 5µM; (calculated by one-way ANOVA).

In the case of PEX16.1, exons 15-17 were amplified. The full-length product was 131bp in length and exclusion of the 46bp exon 16 results in an 85bp product, a size difference that was resolved on a 10% TBE polyacrylamide gel (Figure 5.10A). Semi-quantitative analysis of the gel using GeneTools software (Chapter 2) revealed 28% at 2µM, 40% skipping at 5µM and 35% skipping at 10µM (Figure 5.10B). The qPCR analysis of the PEX16.1 transfection RNA shown in Figure 5.11 showed a relatively similar downregulation of *POSTN* at all transfection concentrations all of which showed statistical significance using a one-way ANOVA analysis $p<0.01$.

PEX 3 was the more successful PMO and so used for the dose-response analysis, transfected at concentrations of 0.2, 0.5, 2, 5 and 10µM. As before, exons 2-4 +/- exon 3 were amplified by RT-PCR and the products resolved on a 3% agarose gel resolving the full length, 169bp, and the skipped, 104bp, products (Figure 5.12A). Semi-quantitative analysis of the gel image using GeneTools showed a dose-dependent response to PEX3 with skipping of 9.2% at 0.2µM and 53% at 10µM. qPCR analysis of the RNA showed a statistically significant downregulation of *POSTN* ($p<0.005$) at all concentrations, with a dose-dependent pattern confirming the trend observed on the gel. Transfection at 0.2µM PMO was the anomaly, showing a greater

decrease in *POSTN* expression than that seen at 0.5, 1 and 2µM although this difference was not found to be statistically significant (Figure 5.13).

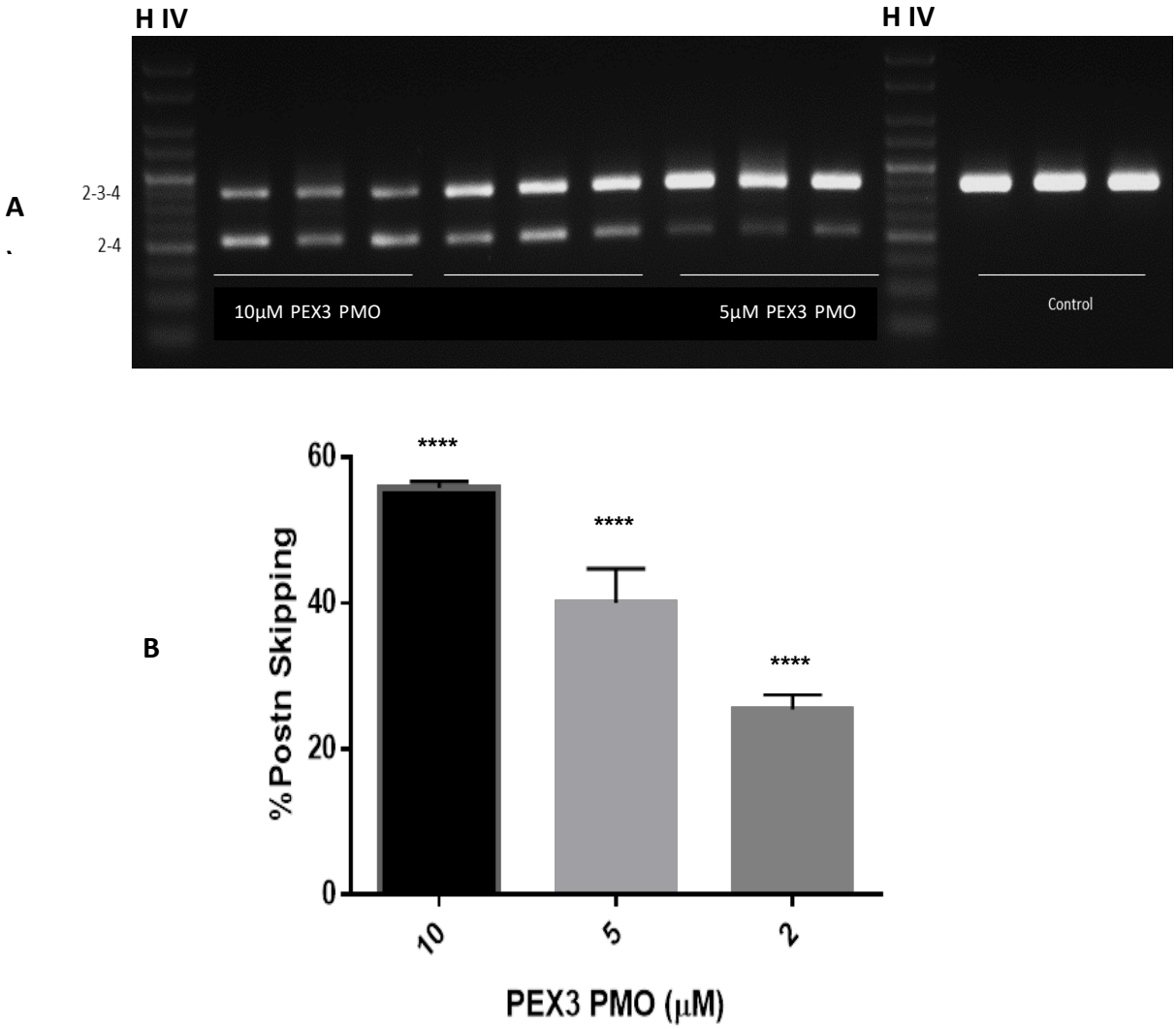

Figure 5.8 Transfection of PEX3 PMO targeting exon 3 in C2C12 cells

C2C12 cells, after reaching confluency, were transfected with PEX3 at 2, 5 and 10µM using 8µM of Endo-Porter. Control samples were transfected with the GeneTools control PMO at 10µM. RNA was extracted 24 hours after transfection and RT-PCR used to amplify exons 2-4 of *POSTN* mRNA.

A) 3% agarose gel of the RT-PCR products from amplification of exon 2-4 of *POSTN* from C2C12 transfected with 10, 5 and 2µM of PEX3..Full length product at 149bp containing exon 3 is present in all lanes. The smaller product at 84bp is present in all three concentrations of the transfection. Hyperladder IV (H IV) was used.

B) Semi-quantitative analysis of the gel in section A using GeneTools showing 25% skipping at 2µM, 40% at 5µM and 56% skipping at 10µM. (****$p<0.0001$, N=3).

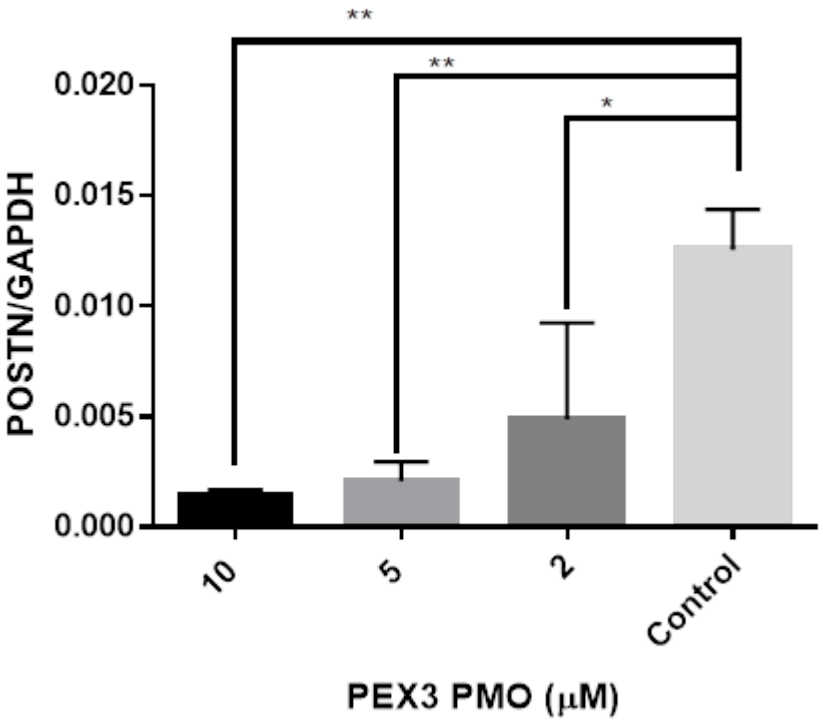

Figure 5.9 Quantification of POSTN expression in PEX3 transfected C2C12 cells

C2C12 cells after reaching confluency were transfected with PEX3 at 2, 5 and 10μM using 8μM of Endo-Porter. RNA was extracted 24 hours after transfection and qPCR used to amplify *POSTN* mRNA. GAPDH was co-amplified and used as a housekeeping gene to normalise quantified *POSTN* expression levels. Statistical significance was calculated using a one-way ANOVA test. (*p<0.05, **p<0.01, N=3).

H IV

A

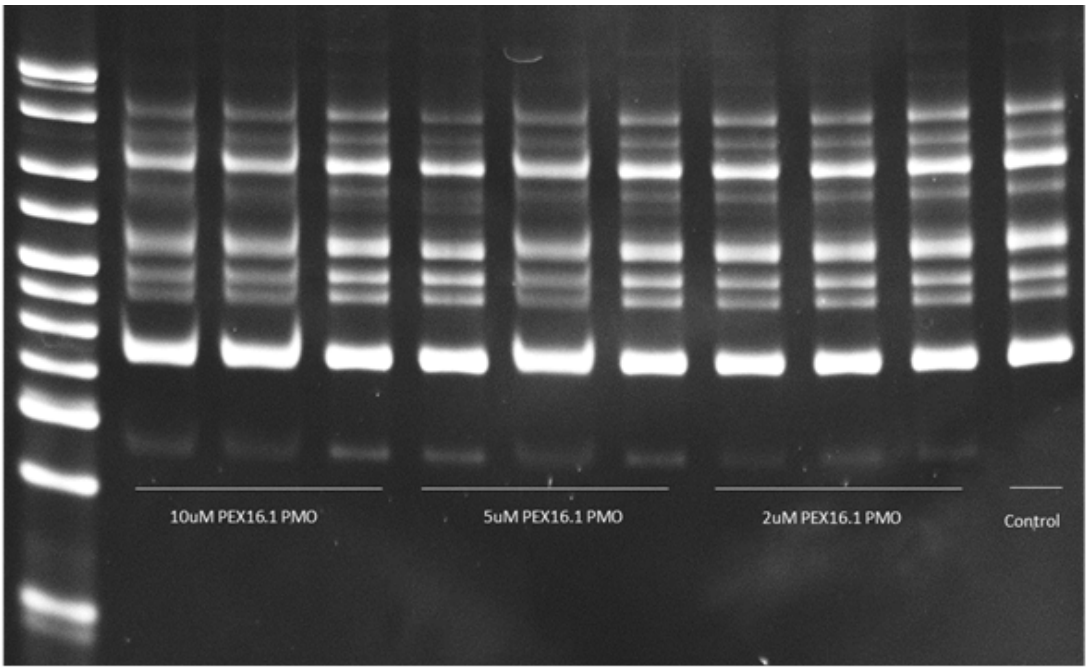
15-16-17
15-17
10uM PEX16.1 PMO
5uM PEX16.1 PMO
2uM PEX16.1 PMO
Control

B

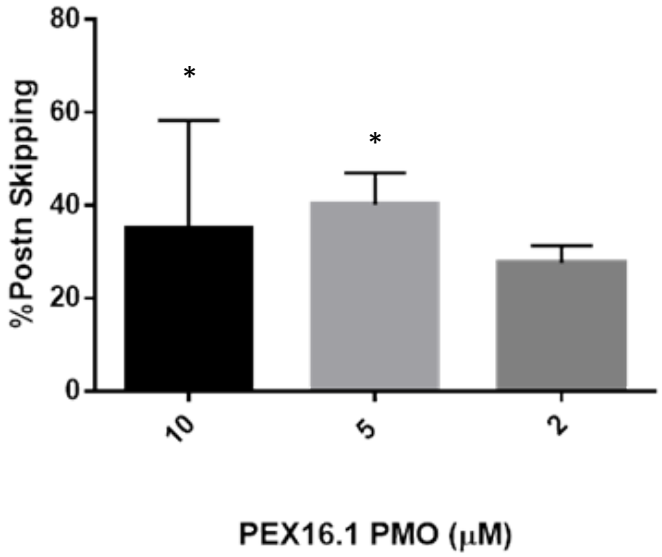
% Postn Skipping
80
60
40
20
0
*
*
10
5
2
PEX16.1 PMO (μM)

Figure 5.10 Transfection of PEX16.1 PMO targeting exon 16 in C2C12 cells

C2C12 cells after reaching confluency were transfected with PEX16.1 at 2, 5 and 10µM using 8µM of Endo-Porter. Control samples were transfected with the GeneTools PMO control at 10µM. RNA was extracted 24 hours after transfection and RT-PCR used to amplify exons 2-4 of *POSTN* mRNA.

A) 10% polyacrylamide TBE gel of the RT-PCR products from amplification of exon 15-17 of *POSTN* from C2C12 transfected with 2, 5 and 10µM of PEX16.1. Full length product at 168bp containing exon 16 is present in all lanes. The smaller product at 122bp is present in all three concentrations of the transfection. Due to the sensitivity of the gel various small unspecific bands were also visualised. Hyperladder IV (H IV) was used

B) Semi-quantitative analysis of the gel in section A using GeneTools software showing 28% skipping at 2µM, 40% at 5µM and 35% skipping at 10µM. Statistical analysis was carried out using one way ANOVA with respect to control samples with no skipping (*$p<0.05$, N=3).

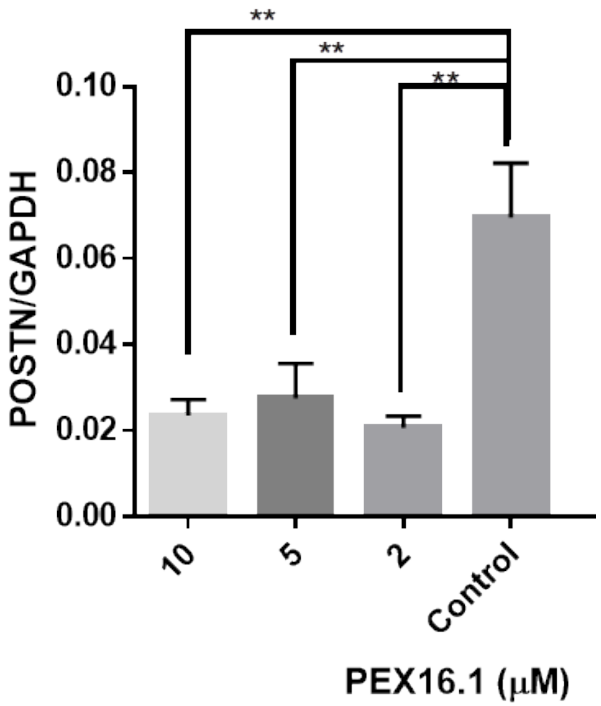

Figure 5.11 Quantification of *POSTN* expression in PEX16.1 transfected C2C12 cells

C2C12 cells after reaching confluency were transfected with PEX16.1 PMO at 10μM, 5 μM and 2 μM using 8μM of Endo-Porter. RNA was extracted 24 hours after transfection and subjected to RT-qPCR to amplify *POSTN* mRNA. GAPDH was co-amplified and used as a housekeeping gene to normalise quantified *POSTN* expression levels. Statistical significance of normalised POSTN transcript levels were calculated using a one-way ANOVA test. (**$p<0.01$, N=3).

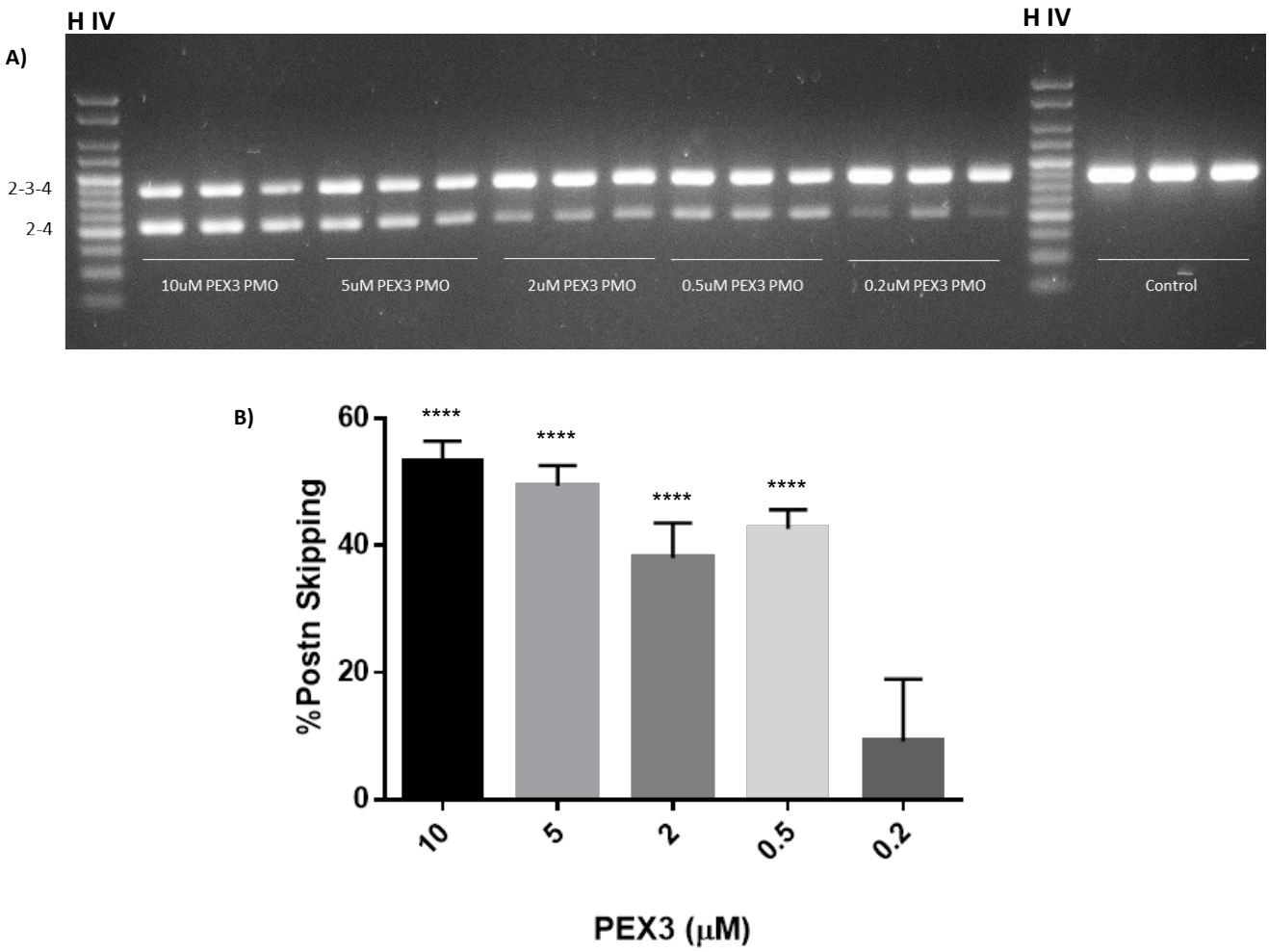

Figure 5.12 Dose response analysis of PEX3 PMO targeting exon 3 in C2C12 cells.

C2C12 cells after reaching confluency were transfected with PEX3 PMO at 10µM, 5 µM, 2, 0.5 and 0.2 µM using 8µM of Endo-Porter. Control samples were transfected with the GeneTools PMO control at 10µM. RNA was extracted 24 hours after transfection and subjected to RT-PCR to amplify exons 2-4 of *POSTN* mRNA.

A) A 3% agarose gel of the RT-PCR products from amplification of exon 2-4 of *POSTN* from C2C12 transfected with 0.2, 0.5, 2, 5 and 10µM of PEX3. Full length product containing exon 3 at 149bp is present in all lanes. The smaller product at 84bp is present in all six concentrations of the transfection. B) Semiquantitative analysis of the gel in section A using GeneTools showing 9% skipping at 0.2µM, 42% at 0.5µM, 38% at 2µM, 49% at 5µM and 53% skipping at 10µM (****$p<0.0001$, N=3). Hyperladder IV (H IV) was used

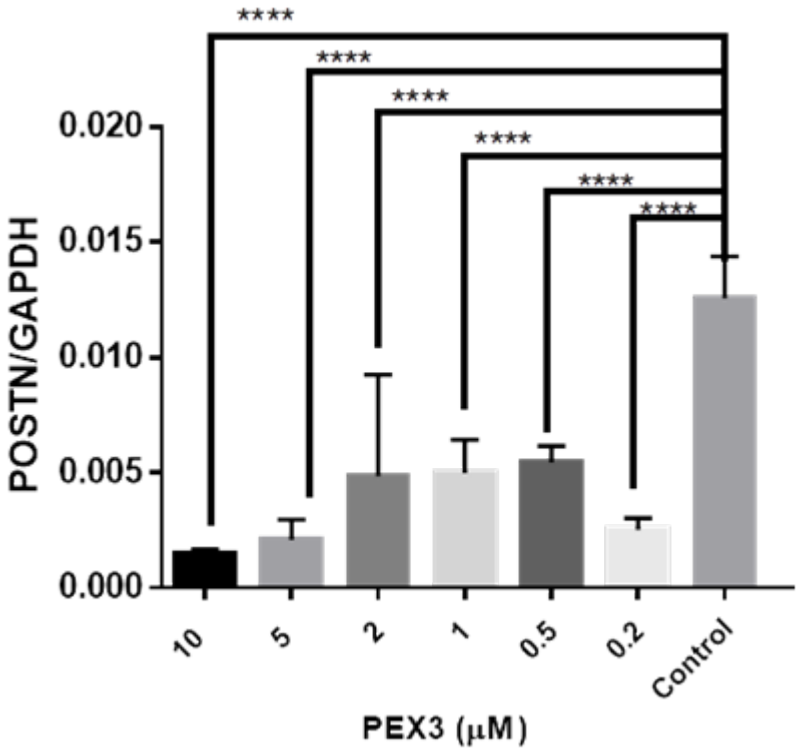

Figure 5.13 Quantification of *POSTN* expression in dose analysis of PEX3 transfected C2C12 cells

C2C12 cells after reaching confluency were transfected with PEX3 PMO at 0.2, 0.5, 2, 5 and 10μM using 8μM of Endo-Porter. RNA was extracted 24 hours after transfection and subjected to qPCR to amplify *POSTN* mRNA. GAPDH was co-amplified and used as a housekeeping gene to normalise *POSTN* expression levels. Statistical significance was calculated using a one-way ANOVA test. (****$p<0.0001$, N=3).

5.2.2.4 PMO induced exclusion of POSTN exon 3 using 28mer PMOs

The 25mer PEX3 showed promising skipping in the C2C12 cell system with a (non-significant) 9% skip at 0.2µM and as much as 53% at 10µM ($p<0.0001$). As previously mentioned, it has been shown in the literature that the longer the PMO, the more successful at it is at skipping (Popplewell *et al.*, 2009). The longest PMO that can be synthesised for *in vivo* purposes is 28 nucleotides. It was therefore decided to extend the PEX3 PMO by three bases and design some 28mer PMOs. Two PMOs were designed, PEX3.28.1 and PEX3.28.2. both targeting the secondary structure of exon 3 with the 3' end of the PMO binding an open loop (Figure 5.14). Pex3.28.1 and Pex3.28.2 were predicted to have overall binding energy of -48.31 and -50.81 respectively (Figure 5.15)

As before, C2C12 cells were seeded in six-well plates and treated with TGF-β an hour prior to being transfected with one of the two PMOs. The cells were transfected at concentrations of 0.2, 0.5, 2, 5 and 10µM (Figures 5.16, 5.18) to allow a dose-response analysis as carried out for PEX3 above. RNA was harvested 24 hours after transfection and subjected to nested RT-PCR amplifying exons 2-4 as before, giving a full-length product of 169bp and a skipped product of 104bp; PCR products were resolved on a 3% agarose gel.

The harvested RNA was subjected to RT-qPCR using the same primers as before for PEX3 analysis. outlined in section 2.4.3.2. *POSTN* message expression was quantified using RT-qPCR (Figures 5.17 and 5.19) and all expression normalised to GAPDH expression.

The result for PEX3.28.1 (Figure 5.14) shows a clear dose-dependent decrease with 4% skipping at 0.2µM and 80% skip at 10µM, the best seen so far. RT-qPCR analysis of the

RNA also showed a clear dose response to the PMO with significant downregulation shown at 1, 2, 5 and 10µM but not 0.2 and 0.5µM (Figure 5.17).

The results for PEX3.28.2 (Figure 5.18A) also showed a clear dose-response very similar to that of PEX3.28.1. Semi-quantitative analysis showed very similar results to PEX3.28.1 with 6% exon skipping at 0.2 µM going up to an 80% skip at 10 µM (Figure 5.18B). qPCR analysis of the RNA showed a much more significant effect of the PEX3.28.2 PMO. Even concentrations as low as 0.2µM showed highly significant downregulation of POSTN with $p<0.00001$ (Figure 5.19).

To determine if the treatment of C2C12 cells with PEX3.28.2 had an effect on POSTN protein expression *in-vitro*, protein was extracted from cells transfected with 0.2, 5 and 10µM PMO 48 hours after transfection. Whole cell extracts were subjected to Western blotting to detect Periostin expression with POSTN-specific polyclonal antibody ab1404 and α-tubulin as a loading control for normalisation of protein expression (Figure 5.20).

POSTN has previously been shown to be detected using this antibody, running at a molecular weight of 90-100kda (Semba *et al.*, 2018a). Low POSTN protein expression was found even in control samples which confirms the low expression found in qPCR analysis on the RNA level. Quantification of the image showed reduced POSTN expression in a dose-dependent manner with PEX3.28.2 transfection. No statistical significance was seen.

Fibronectin protein expression was also assessed as a fibrotic marker and to investigate whether POSTN protein downregulation had a downstream effect on fibronectin expression. Fibronectin was detected using fibronectin-specific polyclonal antibody ab2413. Vinculin was used as its loading control, to normalise expression (Figure 5.21)

The fibronectin Western blot (Figure 5.21) showed high fibronectin expression in the control samples in comparison to POSTN expression. The results, with the expected band at 280kDa, shows a dose-dependent decrease in fibronectin expression upon PEX3.28.2 transfection. This is a similar pattern to that of POSTN protein expression described above. Statistical significance was barely noted at 10µM when analysed using a one-way ANOVA test (*$p<0.05$, N=3).

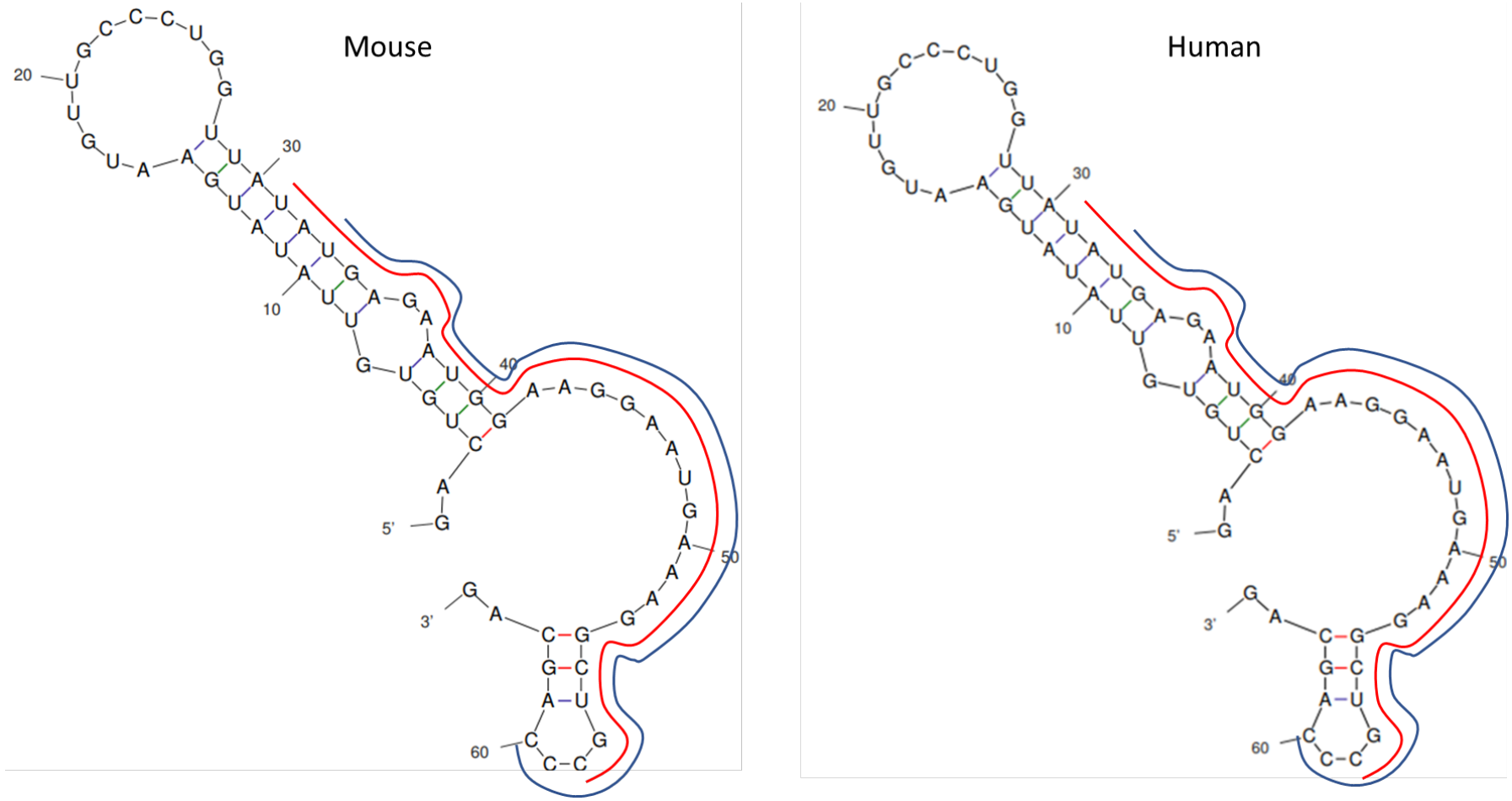

Figure 5.14 Secondary structure of mouse and human *POSTN* exon 3 and binding position of Pex3.28.1 and Pex3.28.2

Secondary structures were predicted using Mfold. Both mouse and human exon 3 are 65 nucleotides long; numbers indicate the position of the nucleotide in the exon. Binding position of PEX3.28.1 (red) and Pex3.28.2 (blue) were designed to target exon 3. The 3' end of each PMO binds the secondary structure in open conformation.

A)

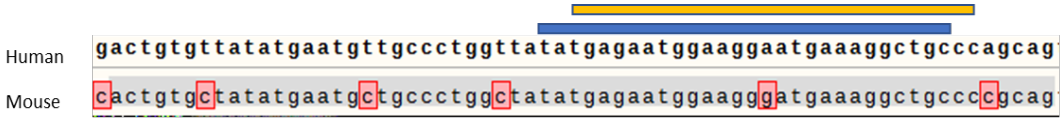

B)

PMO Name	PMO Sequence	Target Sequence	ΔG (kcal/mol)	Opening energy of target (kcal/mol)	Opening energy of PMO (kcal/mol)	Overal ΔG (ΔGi)	%GC	TM
Pex3.28.1	GCA GCC TTT CAT TCC TTC CAT TCT CAT A	TAT GAG AAT GGA AGG AAT GAA AGG CTG C	-48.31	4.53	0	-43.77	42.9	58.9ºC
Pex3.28.2	GGG CAG CCT TTC ATT CCT TCC ATT CTC A	TGA GAA TGG AAG GAA TGA AAG GCT GCC C	-50.81	4.28	1.58	-44.95	50	62.5

Figure 5.15 Exon 3 targeting 28mer PMOs

A) Human and mouse Postn exon 3 alignment generated by SnapGene. Mismatches are highlighted in red. Binding position of Pex 3.28.1 and Pex3.28.2 are shown in blue and yellow respectively. B) Pex 3.28.1 and Pex3.28.2 PMO sequences and thermodynamic properties outlined in the table. Overall binding energies were calculated using the RNAup server. T_m and %GC were calculated using IDT OligoAnalyser.

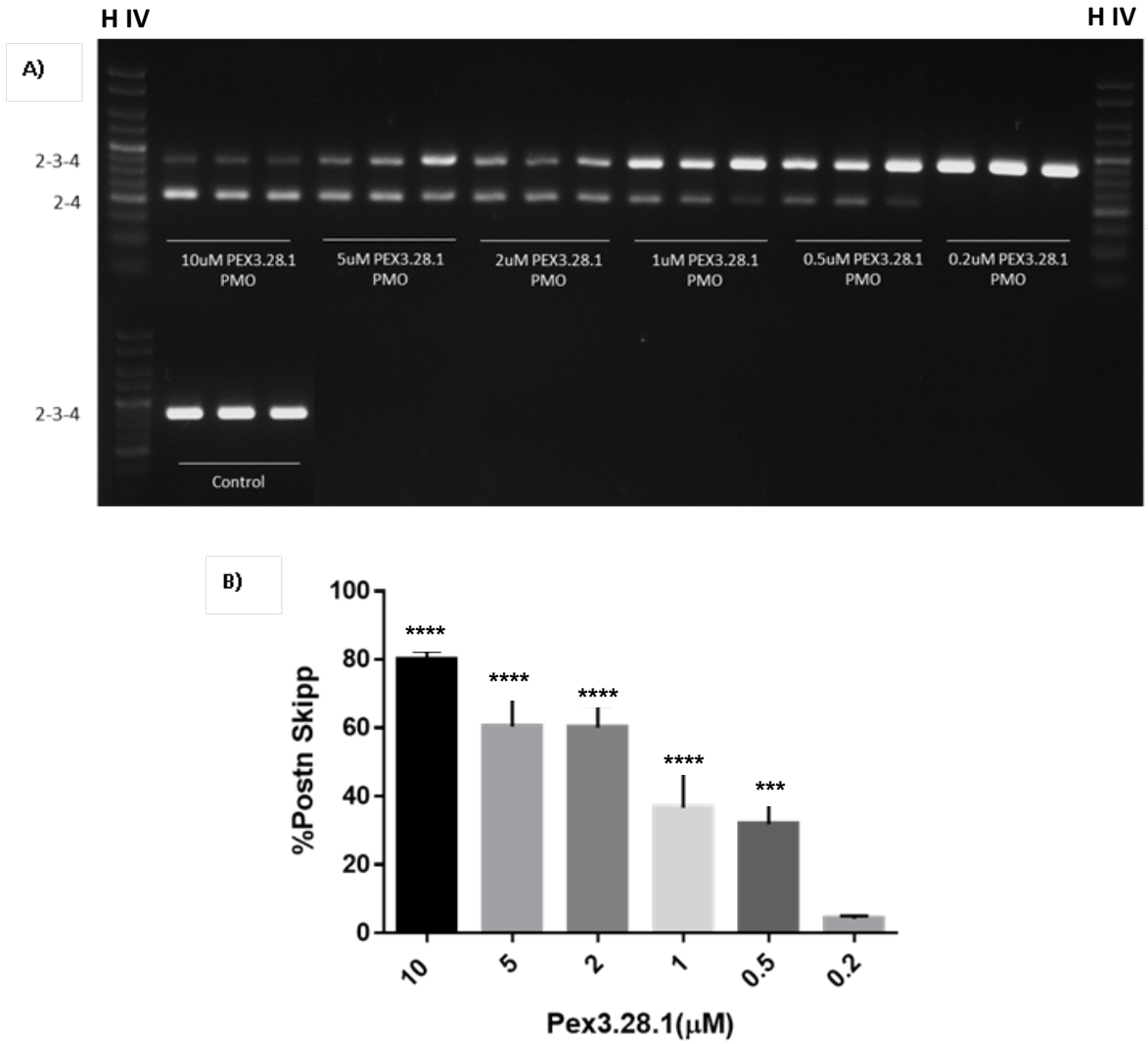
H IV
H IV
A)
2-3-4
2-4
10uM PEX3.28.1 PMO
5uM PEX3.28.1 PMO
2uM PEX3.28.1 PMO
1uM PEX3.28.1 PMO
0.5uM PEX3.28.1 PMO
0.2uM PEX3.28.1 PMO
2-3-4
Control
B)
%Postn Skipp
100
80
60
40
20
0
****
****
****
****
***
10
5
2
1
0.5
0.2
Pex3.28.1(μM)

Figure 5.16 Dose response analysis of PEX3.28.1 PMO targeting exon 3 in C2C12 cells. C2C12 cells after reaching confluency were transfected with PEX3.28.1 PMO at 0.2, 0.5, 2, 5, and 10µM using 8µM of Endo-Porter. Control samples were transfected with the GeneTools PMO control at 10µM. RNA was extracted 24 hours after transfection and subjected to RT-PCR to amplify exons 2-4 of *POSTN* mRNA.

A) 3% agarose gel of the RT-PCR products from amplification of exons 2-4 of *POSTN* from C2C12 transfected with PEX3.28.1..Full length product at 149bp containing exon 3 is present in all lanes. The smaller product at 84bp is present at all six concentrations of PMO transfection. Hyperladder IV (H IV) was used.

B) Semi-quantitative analysis of the gel in section A using GeneTools software measures 4% skipping at 0.2µM, 32% at 0.5µM, 37% at 1µM, 60% at 2 and 5µM and 80% skipping at 10µM. Statistical significance was calculated using one way ANOVA with respect to control samples (****$p<0.0001$,***$p<0.001$, N=3).

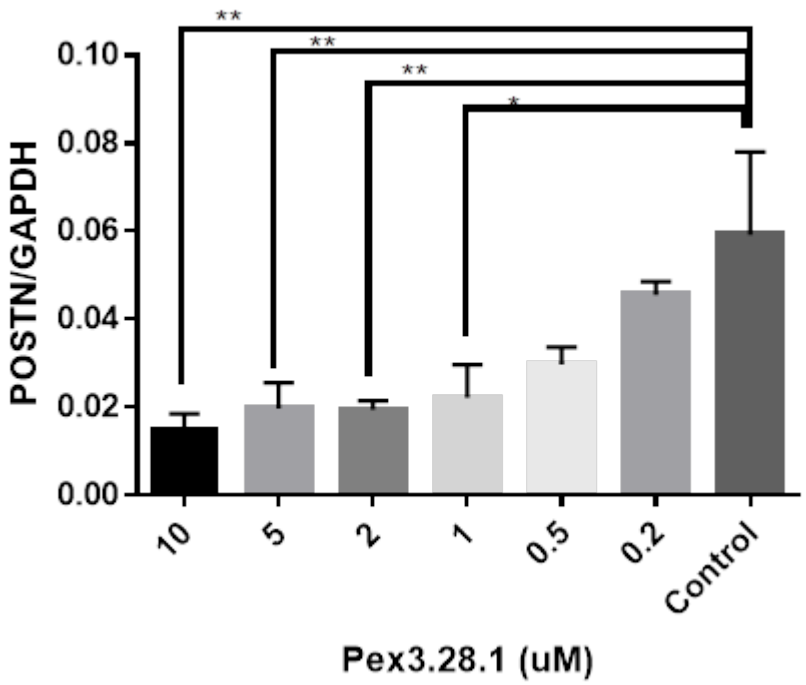

Figure 5.17 Quantification of *POSTN* expression in dose analysis of PEX3.28.1 transfected C2C12 cells

C2C12 cells after reaching confluency were transfected with PEX3.28.1 at 0.2, 0.5, 2, 5 and 10µM using 8µM of Endo-Porter. RNA was extracted 24 hours after transfection and subjected to qPCR to amplify *POSTN* mRNA. GAPDH was co-amplified and used as a housekeeping gene to normalise quantified *POSTN* expression levels. Statistical significance was calculated using a one-way ANOVA test. (**p<0.01, *p<0.05, N=3).

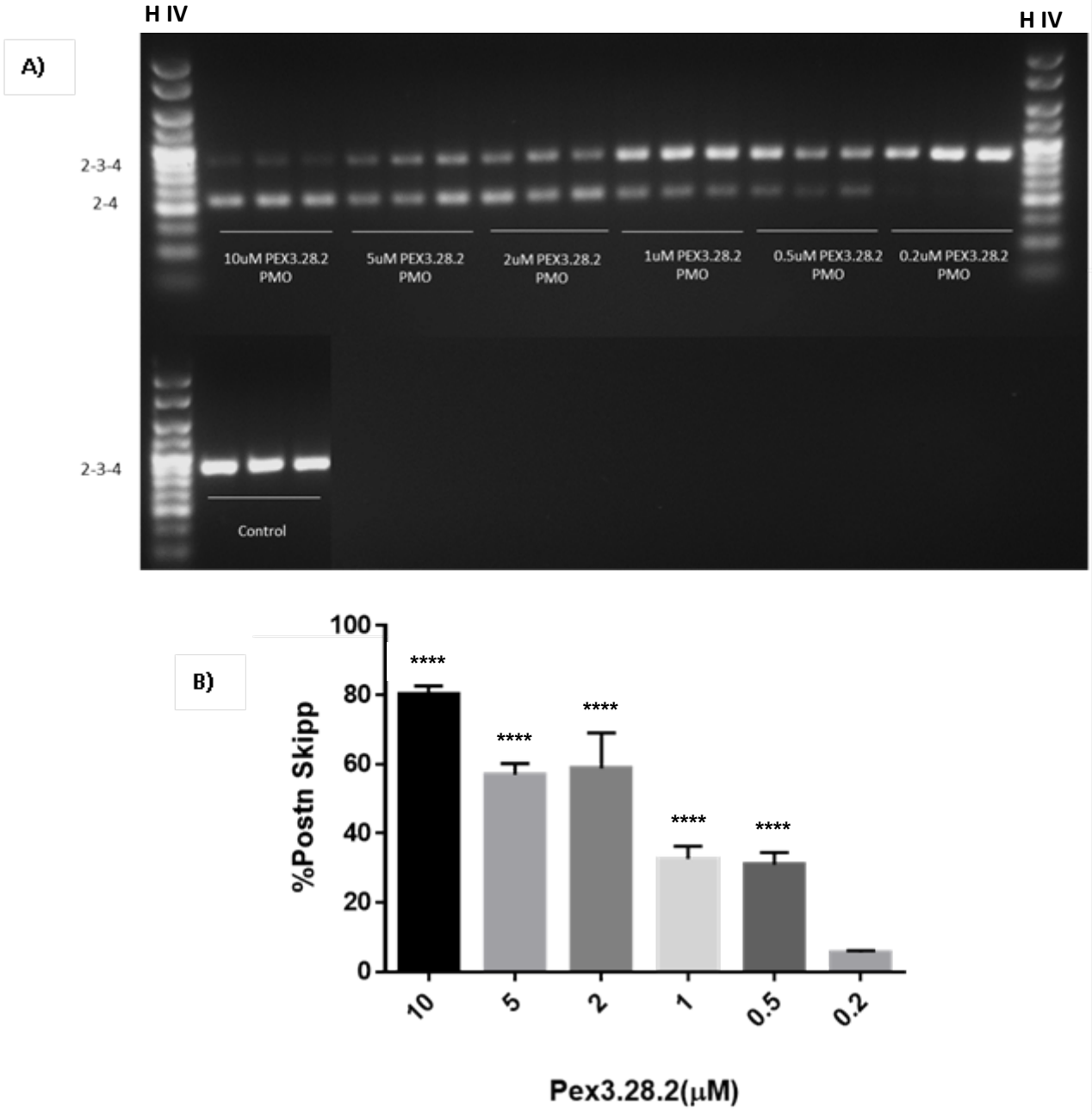
H IV
H IV
A)
2-3-4
2-4
10uM PEX3.28.2 PMO
5uM PEX3.28.2 PMO
2uM PEX3.28.2 PMO
1uM PEX3.28.2 PMO
0.5uM PEX3.28.2 PMO
0.2uM PEX3.28.2 PMO
2-3-4
Control
B)
%Postn Skipp
100
80
60
40
20
0
****
****
****
****
****
10
5
2
1
0.5
0.2
Pex3.28.2(μM)

Figure 5.18 Dose response analysis of PEX3.28.2 PMO targeting exon 3 in C2C12 cells.

C2C12 cells after reaching confluency were transfected with PEX3.28.2 PMO at 0.2, 0.5, 1, 2, 5 and 10µM using 8µM of Endo-Porter. Control samples were transfected with the GeneTools PMO control at 10µM. RNA was extracted 24 hours after transfection and subjected to RT-PCR to amplify exons 2-4 of *POSTN* mRNA.

A) A 3% agarose gel of the RT-PCR products from amplification of exons 2-4 of *POSTN* from C2C12 transfected with PEX3.28.2. Full length product at 149bp containing exon 3 is present in all lanes. The smaller product at 84bp is present in all six concentrations of the transfection although very faint in the 0.2µM PMO transfected cells. Hyperladder IV (H IV) was used.

B) Semi-quantitaitve analysis of the gel in section A using GeneTools software showing skipping at 6% at 0.2µM, 31% at 0.5µM, 33% at 1µM, 59% at 2µM, 57% at 5µM and 80% skipping at 10µM. Statistical significance was calculated using one way ANOVA with respect to control samples with no skipping (****$p<0.0001$, N=3).

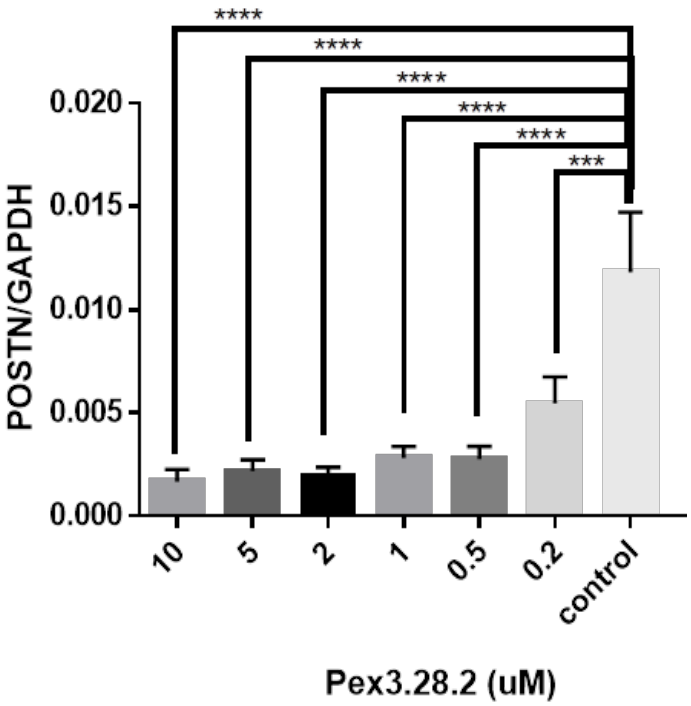

Figure 5.19 Quantification of *POSTN* expression in dose analysis of PEX3.28.3 transfected C2C12 cells

C2C12 cells after reaching confluency were transfected with PEX3.28.2 PMO at 0.2, 0.5, 1, 2, 5 and 10µM using 8µM of Endo-Porter. RNA was extracted 24 hours after transfection and subjected to qPCR to amplify *POSTN* mRNA. GAPDH was co-amplified and used as a housekeeping gene to normalise quantified *POSTN* expression levels. Statistical significance was calculated using a one-way ANOVA test. (***p<0.001, ****p<0.00001, N=3).

A)

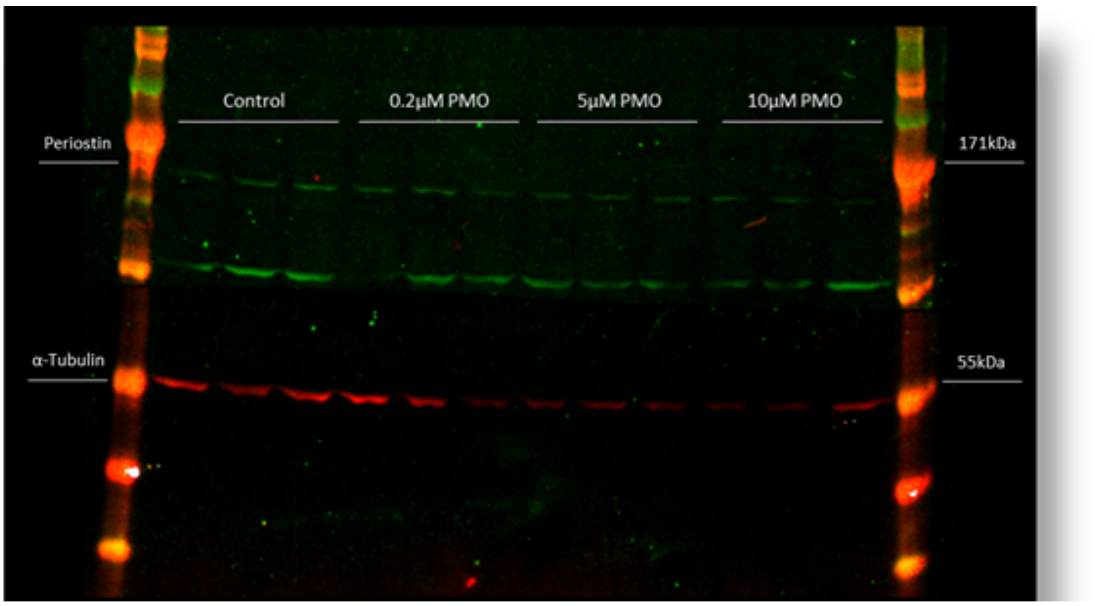
Control
0.2μM PMO
5μM PMO
10μM PMO
Periostin
171kDa
α-Tubulin
55kDa

B)

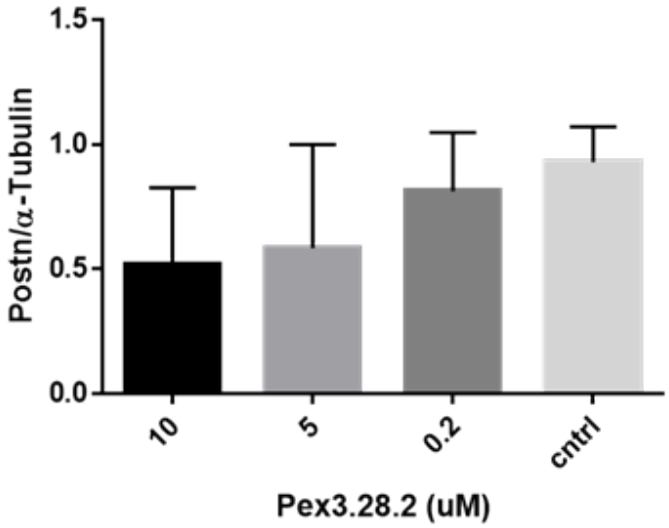
1.5
1.0
0.5
0.0
Postn/α-Tubulin
10
5
0.2
cntrl
Pex3.28.2 (uM)

Figure 5.20 Western Blot analysis to detect POSTN protein expression from PEX2.28.2 PMO transfected C2C12 cells.

C2C12 cells were plated in 6 well multiplates and allowed to grow to confluency before being transfected with 0.2, 5 and 10µM of PEX3.28.2 PMO using 8µM Endo-Porter. Control samples were treated with gene tools PMO at 10µM. Protein was extracted 48 hours after transfection and POSTN expression analysed with Western blotting using fluorescently tagged secondary antibodies and imaged using NIR fluorescence imaging Odyssey as described in Methods and Materials.

A) Western blot of protein extracted from PEX3.28.2 transfected C2C12 cells. POSTN expression was probed with POSTN specific polyclonal antibody ab1404. Secondary antibodies with green fluorescence was used to show POSTN expression. α-tubulin was used as loading control, to normalise POSTN expression. Red fluorescently-tagged secondary antibody was used to probe tubulin. Bands corresponding to POSTN (100kDa) and tubulin (50kDa) are labelled (predicted molecular weights).

B) Semi-quantitative analysis of the Odyssey image shown in A using Image Studio showed a dose dependent decrease in POSTN expression. No statistical significance was seen when analysed using a one-way ANOVA test (N=3).

A)

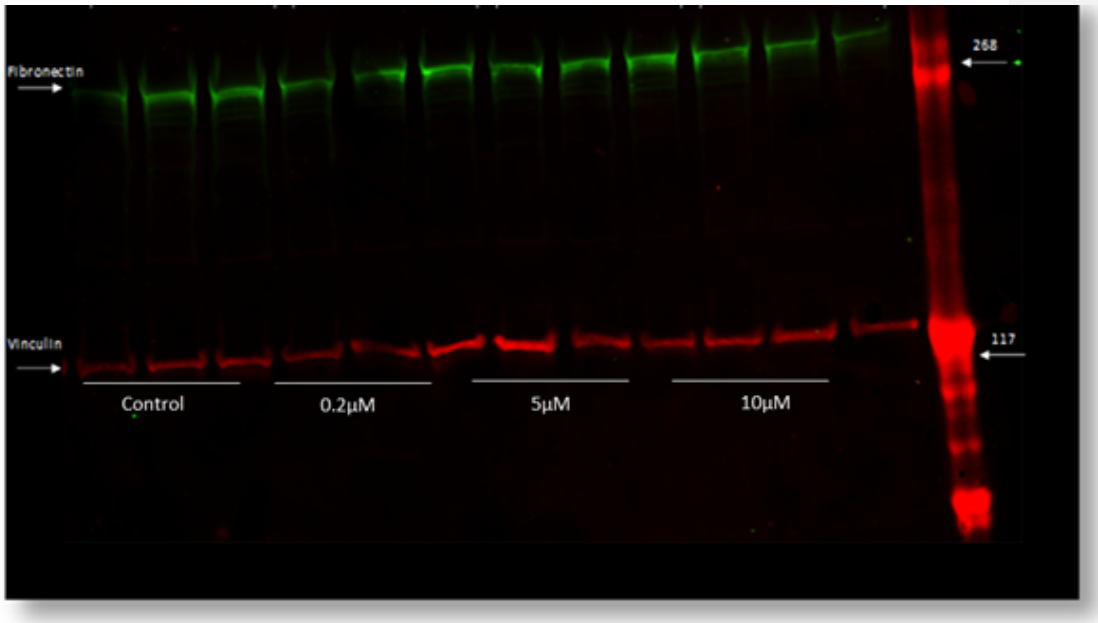
Fibronectin
Vinculin
268
117
Control
0.2µM
5µM
10µM

B)

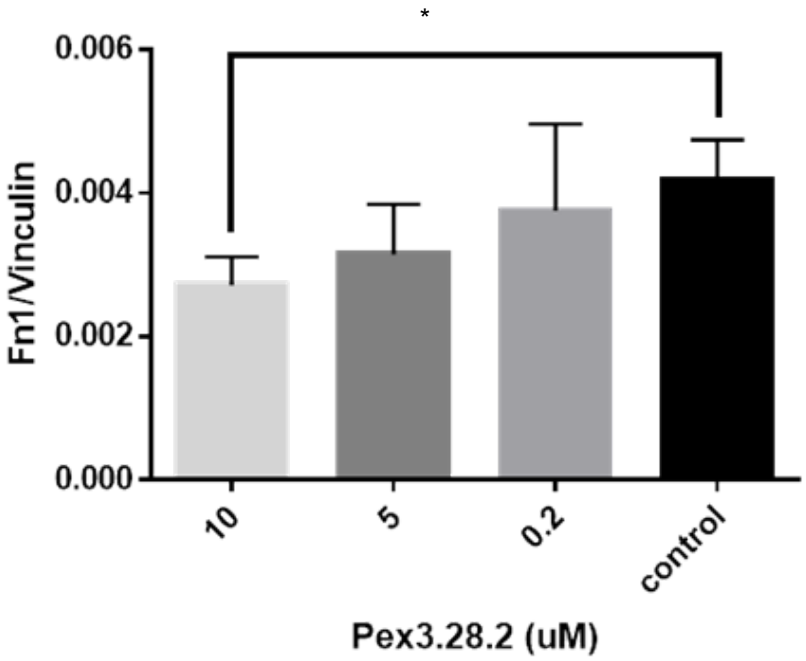
*
0.006
0.004
0.002
0.000
Fn1/Vinculin
10
5
0.2
control
Pex3.28.2 (uM)

Figure 5.21 Western Blot analysis to detect Fibronectin protein expression from PEX2.28.2 PMO transfected C2C12 cells.

C2C12 cells were plated in 6-well plates and allowed to grow to confluency before being transfected with 0.2, 5 or 10µM of PEX3.28.2 PMO using 8µM Endo-Porter. Control samples were transfected with the GeneTools control PMO at 10µM. Protein was extracted 48 hours after transfection. Fibronectin expression was analysed by Western blotting using fluorescently tagged secondary antibodies and imaged using Odyssey Image Studio.

A) Western blot of proteins extracted from PEX3.28.2 (transfected as described above). Fibronectin expression was probed with fibronectin-specific polyclonal antibody ab2413. Secondary antibody with green fluorescence was used to visualise fibronectin. Vinculin was used as a loading control and to normalise fibronectin expression. Red fluorescently-tagged secondary antibody was used to visualise vinculin. Fibronectin (280kDa) and vinculin (124kDa) are labelled (predicted molecular weights).

B) Semiquantitative analysis of the Odyssey image shown in A. Dose dependent decreases in fibronectin expression are visible but there is arguable statistical significance at 10µM when analysed using a one-way ANOVA test (*$p<0.05$, N=3).

5.2.2.5 PEX3.28.2 Transfection in cultured murine fibroblast cells

To investigate the bioactivity of PEX3.28.2 in mouse fibroblasts, cells were treated with PEX3.28.2 in order to abrogate POSTN expression which is a big contributor to fibrosis (Katsuragi *et al.*, 2004). Fibroblasts were seeded in 6-well plates, treated with TGF-β as before and an hour afterwards transfected with 0.5, 1, 5 or 10μM of PEX3.28.2 using 8 μM of Endo-Porter. Control samples were transfected with 10 μM of the GeneTools control PMO and mock samples were not treated with either TGF-β, PMO or Endo-Porter. RNA harvesting and nested RT-PCR as well as RT-qPCR for exon 3 was carried out as for C2C12 cells (above).

Initially, the effect of TGF-β on POSTN protein expression in fibroblasts was assessed, as before, by Western blotting; as expected, TGF- β treatment caused a significant increase in POSTN protein expression (Figure 5.22).

Nested RT-PCR (Figure 5.23) showed production of both the full-length 169bp product and the smaller, skipped 104bp product. There was a clear dose response to PEX3.28.2. Semi-quantitative analysis of the agarose gel using GeneTools software (Figure 5.23B) verified this: no skipping was measurable at 0.2μM, while 17% was observed at 1μM, 33% at 5μM and 10μM transfection show 38% skipping. RT-qPCR analysis (Figure 5.24) confirmed those semi-quantitative results in terms of trend, but showed a much more significant effect of the PMO, with close to no periostin expression at 10 μM and statistically significant downregulation at 1, 5 and 10 μM.

To determine whether the PEX3.28.2 treatment of the fibroblast cells has an effect on periostin (POSTN) and fibronectin protein expression, Western blotting was

carried out (Figure 5.25). Fibroblast cells were treated in the same way, transfected with 0.2, 1, 5 or 10μM PEX3.28.2 or controls. Protein was harvested, and Western blotting carried out for POSTN as above. Similarly, for fibronectin 1, 5 or 10 μM and control transfections were carried out and whole cell protein samples used on the Western blot (these concentrations were chosen based on the results from the POSTN Western). Figure 5.25 shows a dose-dependent downregulation of POSTN at 1, 5 and 10 μM with no downregulation seen at 0.2 μM, confirming the trend seen at the RNA level. Fibronectin Western blotting is shown in Figure 5.26 and shows dose-dependent downregulation of fibronectin with statistical significance seen at 5 and 10 μM transfection with $p<0.05$ (N=3).

A)

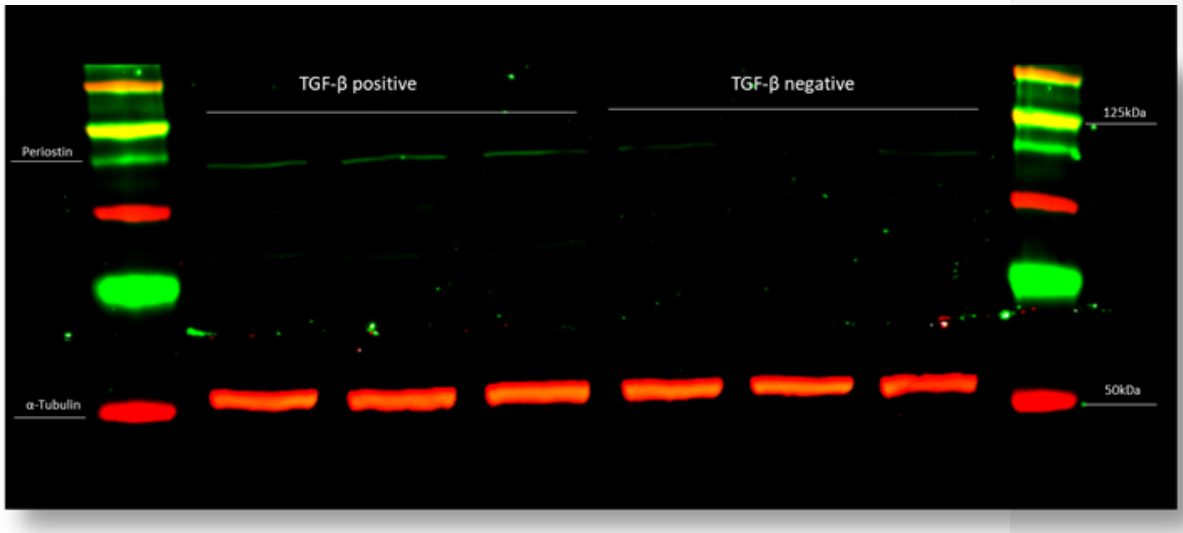
TGF-β positive
TGF-β negative
Periostin
α-Tubulin
125kDa
50kDa

B)

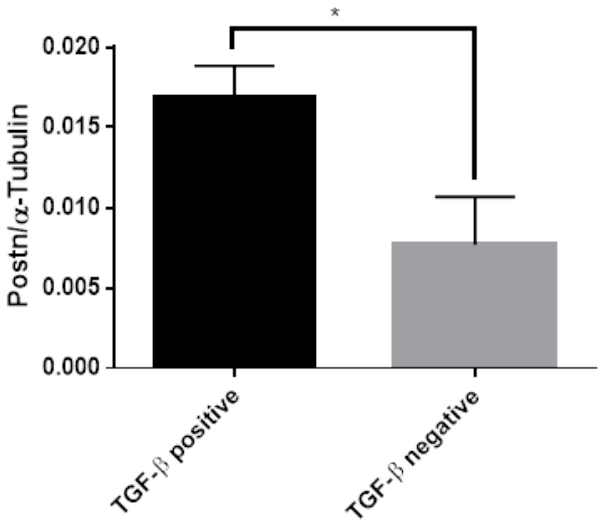
*
0.020
0.015
0.010
0.005
0.000
Postn/α-Tubulin
TGF-β positive
TGF-β negative

Figure 5.22 Western Blot analysis to detect POSTN protein expression from TGF-β treated fibroblast cells.

Fibroblast cells were plated in 6 well multi-plates and allowed to grow to confluency before being treated with 10ng of TGF-β. Control samples were not treated with TGF-β. Protein was extracted 48 hours after transfection and POSTN expression analysed with western blotting using fluorescently tagged secondary antibodies and imaged using Odyssey as described in Methods and Materials. A) Western blot of protein extracted from TGF-β treated fibroblast cells at 10ng. Periostin expression probed with POSTN specific polyclonal antibody ab1404. Secondary antibody with green fluorescence was used to show POSTN expression. α-tubilin was used as loading control and to normalise POSTN expression. Red fluorescently tagged secondary antibody was used to probe tubulin. The bands corresponding to POSTN and tubulin are labelled. POSTN has a predicted weight of 100kDa and α-tubilin has a predicted weight of 50kDa. B) Image Studio, provided by Odyssey clx, was used for semiquantitative analysis of the Odyssey image shown in section A statistically significant increase in POSTN protein levels was calculated using a one-way ANOVA test. (*$p<0.05$, N=3).

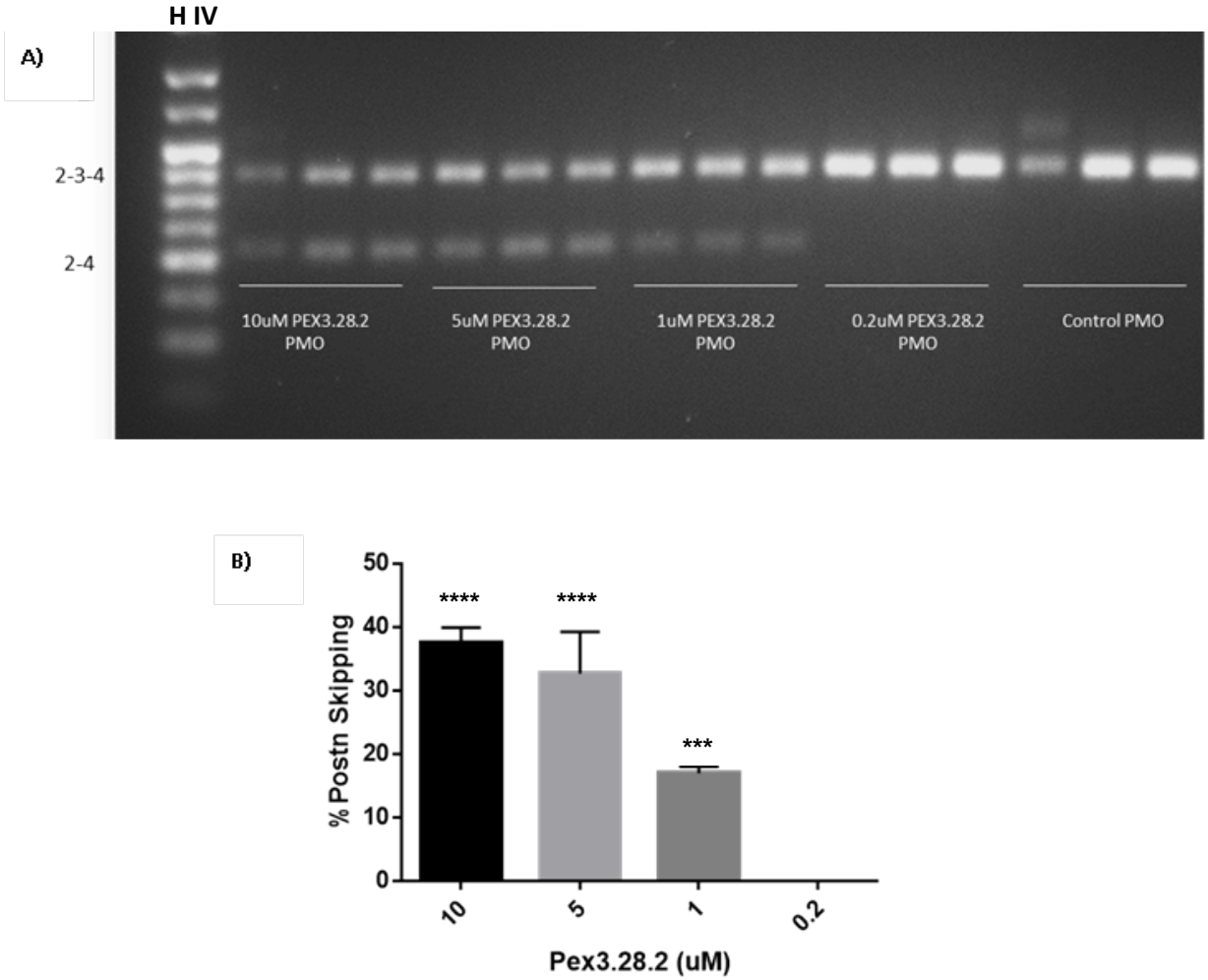
H IV
A)
2-3-4
2-4
10uM PEX3.28.2 PMO
5uM PEX3.28.2 PMO
1uM PEX3.28.2 PMO
0.2uM PEX3.28.2 PMO
Control PMO
B)
% Postn Skipping
50
40
30
20
10
0
****
****
***
10
5
1
0.2
Pex3.28.2 (uM)

Figure 5.23 Dose response analysis of PEX3.28.2 PMO targeting exon 3 in murine fibroblast cells.

Fibroblast cells after reaching confluency were transfected with PEX3.28.2 at 0.2, 1, 5 and 10µM PMO using 8µM of Endo-Porter. Control samples were transfected with the GeneTools control PMO at 10µM. RNA was extracted 24 hours after transfection and subjected to RT-PCR.

A) A 3% agarose gel of the RT-PCR products from amplification of exons 2-4 of *POSTN*. Full length product at 149bp containing exon 3 is present in all lanes. The smaller product at 84bp is present in lanes transfected with 1, 5 and 10µM. Hyperladder IV (H IV) was used.

B) Semi-quantitative analysis of the gel in A using GeneTools, shows 17% skipped product at 1µM, 33% at 5µM and 37% skipping at 10µM with no skipping detectable at 0.2µM. Statistical significance was calculated using one way ANOVA with respect to control samples with no skipping (****$p<0.0001$,***$p<0.001$, N=3).

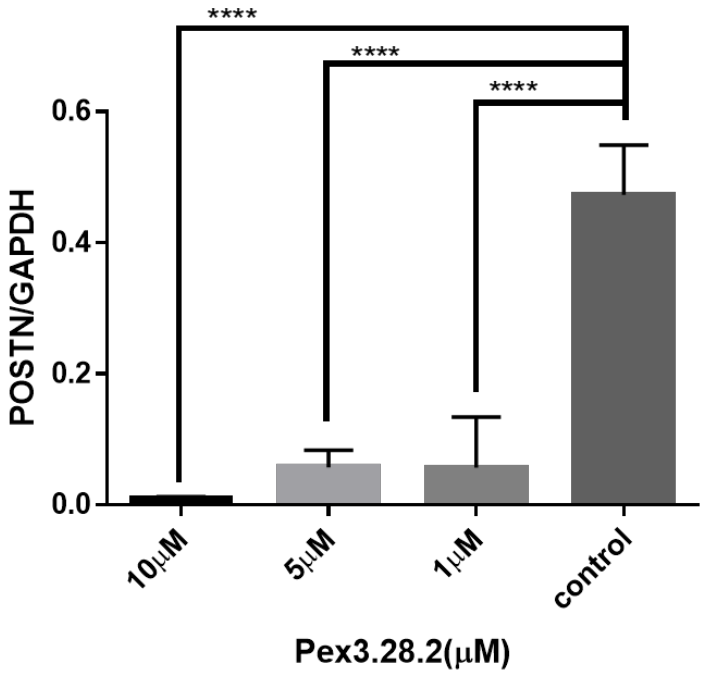

Figure 5.24 Quantification of *POSTN* expression in dose analysis of PEX3.28.2 transfected fibroblast cells

Fibroblast cells after reaching confluency were transfected with PEX3.28.2 PMO at 1, 5 and 10μM using 8μM of Endo-Porter. RNA was extracted 24 hours after transfection and subjected to qPCR to amplify *POSTN* mRNA. GAPDH was also amplified and used as a housekeeping gene to normalise quantified *POSTN* expression levels. Statistical significance was calculated using a one-way ANOVA test (****$p<0.00001$, N=3).

A)

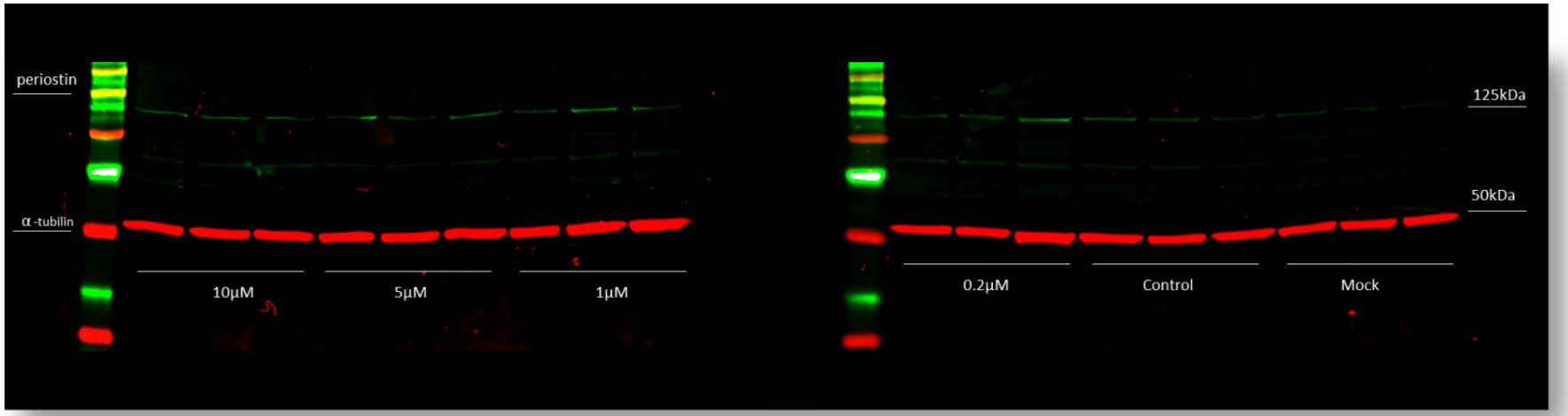
periostin
α-tubilin
125kDa
50kDa
10μM
5μM
1μM
0.2μM
Control
Mock

B)

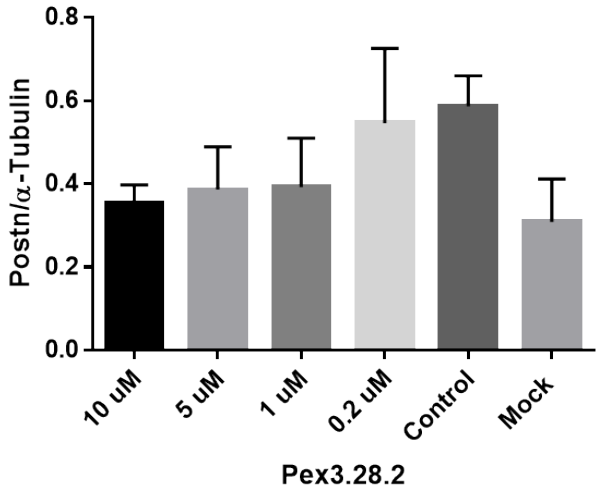
Postn/α-Tubulin
0.8
0.6
0.4
0.2
0.0
10 uM
5 uM
1 uM
0.2 uM
Control
Mock
Pex3.28.2

Figure 5.25 Western Blot analysis to detect POSTN protein expression from PEX2.28.2 PMO transfected fibroblast cells.

Fibroblast cells were plated in 6-well plates and allowed to grow to confluency before being transfected with 0.2, 1, 5 or 10µM of PEX3.28.2 PMO using 8µM Endo-Porter. Control samples were treated with the GeneTools negative control PMO at 10µM. Mock samples were untreated cells with no TGF-β treatment. Protein was extracted 48 hours after transfection and POSTN expression analysed by Western blotting using fluorescence-tagged secondary antibodies and imaged using Odyssey.

A) Western blot of proteins from PEX3.28.2 transfected fibroblast cells probed for POSTN expression with POSTN-specific polyclonal antibody. Secondary antibodies with green fluorescence show POSTN expression. α-tubulin was used as loading control and to normalise POSTN expression. Tubulin was probed with anti-tubulin and picked out with red fluorescence-tagged secondary antibodies. Bands corresponding to POSTN (100kDa) and tubulin (50kDa, predicted molecular weights) are labelled.

B) Semiquantitative analysis of the digital image in A was with Image Studio. Dose dependent decreases in POSTN expression is visible but no statistical significance was found upon analysis using a one-way ANOVA test (N=3).

A)

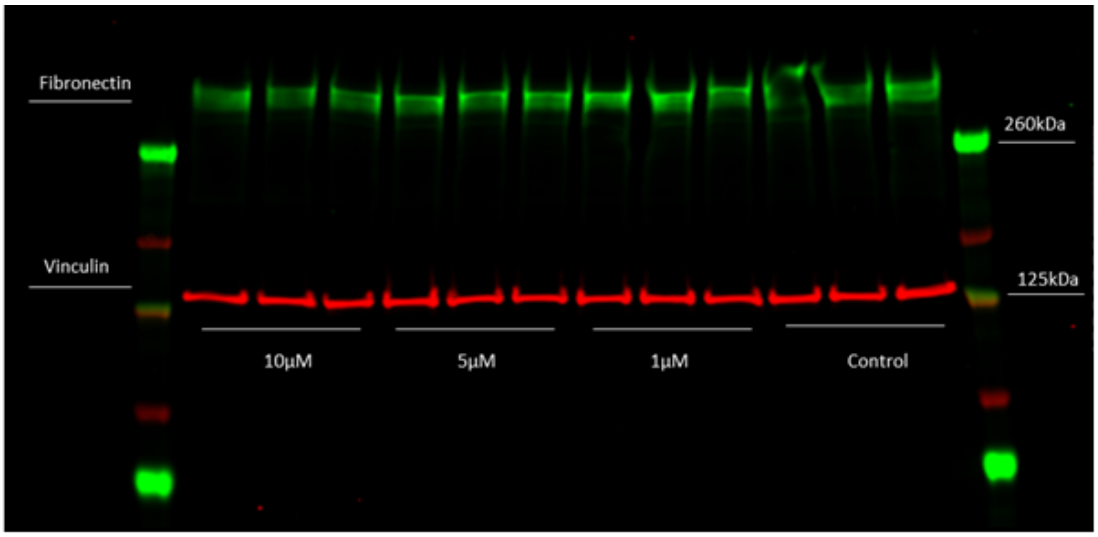
Fibronectin
Vinculin
260kDa
125kDa
10µM
5µM
1µM
Control

B)

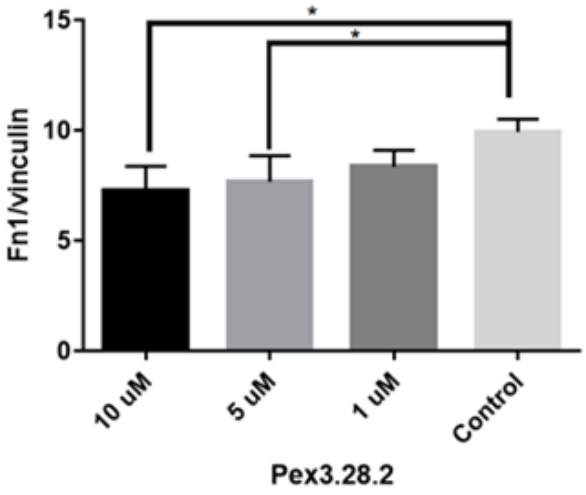
15
10
5
0
Fn1/vinculin
*
*
10 uM
5 uM
1 uM
Control
Pex3.28.2

Figure 5.26 Western Blot analysis to detect Fibronectin protein expression from PEX2.28.2 PMO transfected fibroblast cells.

Fibroblast cells were plated in 6 well plates and allowed to grow to confluency before being transfected with 1, 5 and 10µM of PEX3.28.2 PMO using 8µM Endo-Porter. Control samples were treated with the GeneTools negative control PMO at 10µM. Protein was extracted 48 hours after transfection and fibronectin expression analysed by Western blotting, visualising using fluorescence-tagged secondary antibodies, imaged using Odyssey.

A) Western blot of protein extracted from PEX3.28.2 transfected fibroblast cells. Fibronectin-specific polyclonal antibody ab2413 and secondary antibody with green fluorescence was used to probe fibronectin expression. Vinculin, a loading control and to normalise fibronectin expression was probed with anti-vinculin and visualised with red fluorescence-tagged secondary antibody. Bands corresponding to fibronectin (280kDa) and vinculin (124kDa predicted molecular weights) are labelled.

B) Semi-quantitative analysis of the Odyssey image in A was with Image Studio. Dose dependent decreases in fibronectin expression are visible. Statistical significance was calculated at 5 and 10µM PMO transfection using a one-way ANOVA test (*$p<0.05$ N=3).

5.3 Discussion

As discussed in Chapter 1 section 1, fibroblasts have been shown to be a major source of POSTN expression and a big contributor to fibrosis (Katsuragi *et al.*, 2004). To prevent fibrosis we wished to find a way to abrogate the upregulation of the mechanisms that give rise to this debilitating infilling of muscle tissue with non-muscle components. Therefore in this study, AONs aimed at interacting with the pre-mRNA to promote the production of out-of-frame, exon-skipped nonsense mRNAs which are likely downregulated by NMD, were designed, synthesised and tested in various cell systems for their effect on mRNA and protein downregulation. Mouse and human candidate sequences were compared so that AONs could be tested in the mouse and then potentially used on human patients without alteration; conserved regions are also more likely regulatory.

5.3.1 Effect of TGF-β on POSTN expression in muscle cells

The fibrotic pathway is stimulated through the TGF-β signalling pathway (March *et al.*, 2018). TGF-β has been shown to be directly responsible for upregulating POSTN in various tissues as well as cell lines (Bowen, Jenkins and Fraser, 2013; Özdemir *et al.*, 2014; March *et al.*, 2018).

In this Chapter, we initially looked at the effect of TGF-β treatment on murine muscle cells, C2C12, as well as myofibroblasts. Our findings showed that POSTN is expressed at relatively low amounts *in vitro* (Figure 5.1) and increased significantly upon TGF-β treatment, as previously shown in other cell lines (Litvin, Selim and Montgomery, 2004; Li *et al.*, 2006). Protein readout in fibroblasts also confirmed close to no POSTN protein

expression in cells not treated with TGF-β and a significant increase upon treatment (Figure 5.20). This finding confirmed the need to stimulate POSTN expression in cells, prior to transfection with antisense oligonucleotides, to activate transcription of POSTN, allowing the PMO to bind the newly abundantly produced pre-mRNA, interacting with it to promote successful exon skipping.

5.3.2 PMO induced skipping of Periostin

AONs have been used to successfully target and downregulate POSTN expression in a variety of targets such as the lung, kidney and tumours, in order to diminish fibrosis (Tomaru *et al.*, 2017; Semba *et al.*, 2018a). Targeting out-of-frame exons, to remove them from transcripts producing an out-of-frame read, leads to exon exclusion, out-of-frame regions of the transcript and downregulation of the targeted gene at the RNA level by NMD leading to subsequent downregulation at the protein level (Kang *et al.*, 2011a).

PMOs designed to the out-of-frame exons 3, 7, 10 and 16 were initially tested in a human DMD muscle cell line in order to confirm skipping before being tested in murine muscle cells. The PMOs being tested in cell lines from different species are nonetheless targeting the same sequences, and it was important for skipping to be confirmed in both. PMOs targeting exon 10 showed no skipping in the human cell line and were therefore eliminated from the further investigation. The most successful PMOs were tested in a C2C12 murine muscle cell line and a dose-response analysis performed, with POSTN expression assessed both semi-quantitatively and quantitatively. PEX3 showed significant exon skipping and POSTN downregulation at 0.5-10μM concentrations. Interestingly PEX3 proved to be more successful in the C2C12 cell line, where there is

actually a mismatch between the target sequence and the PMO, than in human patient cells where the PMO is designed with no mismatches. This could be due to toxicity effects of the transfection on the cell line as C2C12 are much easier to grow and transfect and are not as sensitive.

It has previously been shown in our laboratory that longer PMOs are more effective at inducing exon skipping (Popplewell *et al.*, 2009) so the maximum length (for human therapy) of 28mer PMOs targeting exon 3 were designed and tested: they were found indeed to be more effective, with PMO PEX3.28.2 showing significant downregulation of POSTN at concentrations as low as 0.2 μM. Protein readout from C2C12 cells transfected with PEX3.28.2 also confirmed downregulation of POSTN protein in a dose-dependent manner although statistical significance was not achieved. The less significant downregulation on the protein level compared to RNA level could be due to that fact that protein was harvested 48 hours following transfection: this was shown to be cytotoxic, resulting in the death of about 20% of cells per 24 hours (above), thus reducing protein levels! In addition, this may be too short a time for protein turnover so that protein already made is being seen, although we had demonstrated a good increase in POSTN production following 24h of TGF- β exposure. Another reason could be the high variability between samples and the relatively low expression of Periostin in these cells, so more replicates could be run or a more sensitive assay developed.

Interestingly, fibronectin protein expression was also found to be downregulated in a dose-dependent manner in response to POSTN downregulation, with statistical significance seen at 10μM. This is in agreement with the literature where it has been reported that POSTN is involved in fibronectin secretion (Kii, Nishiyama and Kudo, 2016).

Secreted fibronectin is therefore a good marker of POSTN downregulation under these conditions, since it is much more abundant and easily analysed by Western blot, whereas antibodies to POSTN are less sensitive compared to the normalisation proteins and the immunosensitivity remains to be improved: in our hands the Western blotting for POSTN was not as straight forward.

PEX3.28.2 also showed successful skipping in the robust murine fibroblast cells, with detectable skipping at concentrations as low as 1µM and significant downregulation at the RNA level when assessed by qPCR. Protein readout also confirmed the results of the RNA analysis, showing a dose-dependent downregulation of POSTN; however, the results were not significant. Despite this, a significant downregulation of secreted fibronectin was observed at 5 and 10µM indicating acceptable downregulation of POSTN. Fibronectin is downstream of POSTN in the fibrotic pathway.

The results, therefore, suggest that PMO PEX3.28.2, which removes exon 3 from the POSTN pre-mRNA producing a significant quantity of exon skipped message compared to full length, could be a successful candidate to take on to *in vivo* investigations in mice.

5.3.3 Comparison between the bioinformatic prediction of PMO bioactivity with in-vitro results of the PMO bioactivity

Using bioinformatics is essential for the intelligent design of AONs and the uses of various parameters to predict bioactivity has been widely studied (Sun, Peng and He, 2008; Popplewell *et al.*, 2009; Schoch and Miller, 2017) as discussed in Chapters 3 and 4. Popplewell *et al.* reported that the most significant thermodynamic property in PMO bioactivity is the energy of binding, while, although the binding site did not determine PMO bioactivity, amongst successful PMOs those that targeted open structures were

more successful . The binding energy is critically affected by another PMO parameter cited to be of high significance, i.e. oligonucleotide length with 30mer PMOs more successful than their 25mer counterparts. This study confirms the findings above. PMOs that lead to successful exon skipping had a minimum overall binding energy of -40 kcal/mol, with the exception of PEX7.3 PMO which had binding energy of -48.83 kcal/mol yet was still not successful at promoting exon skipping. This could be due to the nature of the target sequence of PEX7.3 rather than the lack of PMO binding, although it is not yet possible to see oligonucleotides bind to pre-mRNA targets in cells: an *in vitro* experiment with a synthetic RNA target may show whether PEX7.3 actually binds its putative target. From the exon 3 and exon 16 PMOs, PEX3 and PEX16.1, PEX16.2, which initially all showed good POSTN mRNA exon skipping, it was PEX3 that showed significantly better bioactivity. This correlated with the better energy of binding of PEX3 at -44.15 kcal/mol as well as its predicted binding to open loops at *both* ends of the PMO, confirming that increased binding energy and targeting sequences with less secondary structure can enhance PMO bioactivity. Increasing the length of Pex3 from a 25mer to 28mers, in this study, also confirmed that PMO length is a parameter of high significance. By an increase in the length of just 3 bases, the bioactivity of the PMO increased from 33% skipping to 80% skipping.

It is worth mentioning that the GC content of all the designed PMOs with the exception of Pex10.1 was below 55% as suggested to be ideal by Ho et al. (Ho *et al.*, 1996).

6. Antisense modulation of Periostin pre-mRNA splicing in the C57 mouse model

6.1 Introduction

Investigations in control mouse myoblasts (C2C12 cell line), murine skeletal muscle fibroblasts (MH cell line) and immortalised DMD patient myoblasts were used to assess the bioactivity of the PMOs designed to affect exon skipping, specifically of exon 3. They demonstrated that PMO PEX3.28.2 was the most effective at promoting exon skipping, inducing exclusion of exon 3.

To move to an *in vivo* system, previous work in the laboratory was considered. Intramuscular injection of 25µg of 2OMe-P-AON induced *de novo* expression of dystrophin in the *mdx* mouse model (Graham *et al.*, 2004). Also, 20µg intramuscular injection of AON with "vivo-PMO" chemistry induces expression of dystrophin in the *mdx* mouse model (Akpulat *et al.*, 2018)

POSTN isoforms have been shown to be involved in the regeneration and healing of muscle (Morita and Komuro, 2016), as well as fibrosis. There is concern that reducing POSTN expression may interfere with the regeneration and healing process. In skin healing studies, Nishiyama *et al.* (2011) demonstrated defects in re-epithelialisation in *Postn-/-* mice (Nishiyama *et al.*, 2011). In cardiac muscle research, *Postn-/-* mice were found to have significantly decreased survival rates after induction of myocardial infarction (Shimazaki *et al.*, 2008). This was attributed to impaired ECM deposition in the healing cardiac muscle (Periostin is in the ECM). Studies like this highlight the importance of POSTN upregulation following acute injury to quickly restore ECM and tissue homeostasis. In skeletal muscle, POSTN is expressed at extremely low levels under

normal circumstance but is upregulated upon mechanical stress or damage when it is expressed by infiltrating cells such as macrophages and fibroblasts as well as regenerating myofibres (Özdemir *et al.*, 2014). It has been shown that in the case of *sgcd-/- postn-/-* double knockouts, the pathology of the dystrophic mouse was a lot less severe due to a decrease in fibrosis (Lorts *et al.*, 2012). It is important to achieve POSTN downregulation such that fibrotic tissue is reduced but regeneration and healing can still take place.

Therefore, work in this Chapter is concerned with assessing the bioactivity of the PEX3.28.2 PMO *in vivo* and the effect of POSTN downregulation by PEX3.28.2 on skeletal muscle regeneration in damaged C57 mice, after having the TA muscle injected with $BaCl_2$.

6.2 Results

6.2.1 $BaCl_2$ induced muscle damage in 24month old C57 mice

The first experiment was to assess damage and fibrosis in the TA of mice that had been subjected to the intramuscular injection of $BaCl_2$ (Hardy *et al.*, 2016). The left TA of 4 female 24-month-old C57/B10 mice were injected with 50µl of 1.2% (w/v) $BaCl_2$. The right TA was used as a non-injected control. Animals were sacrificed at 1, 3, 7 and 14 days after injection and tissue collected as described in section 2.9.

6.2.1.1 Sirius red staining

Sections from TA muscle injected with $BaCl_2$ and controlled TA were stained with Sirius red as described in Materials and Methods and the results are shown in Figure 6.1. Sirius

red staining is one of the most widely used techniques for looking at collagen histochemistry (Puchtler, Waldrop and Valentine, 1973; Junqueira, Bignolas and Brentani, 1979). Picro-Sirius red dyes have specific reactivity to collagen I and III are therefore used for quantitative estimation of tissue fibrosis (Sweat, Puchtler and Rosenthal, 1964). Collagen is stained red, and muscle fibres and cytoplasm are stained yellow (Figure 6.1A). The staining revealed a peak in collagen I and III 3 days after $BaCl_2$ treatment, where a 30% increase in red stain, measured using ImageJ, relative to control TA, was quantified. This was reduced to a 10% increase at 14 days after injection when normal muscle morphology is restored, as indicated by the presence of healthy muscle architecture (Figure 6.1B).

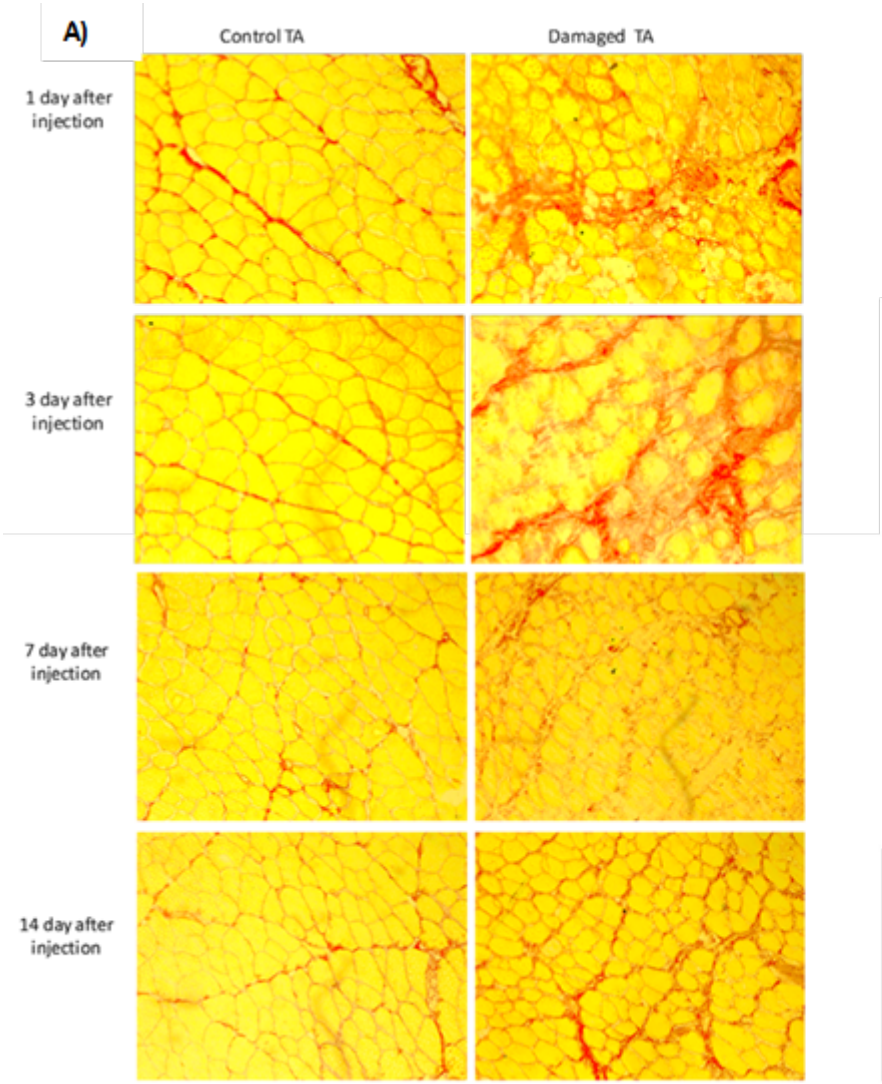
A)
Control TA
Damaged TA
1 day after injection
3 day after injection
7 day after injection
14 day after injection

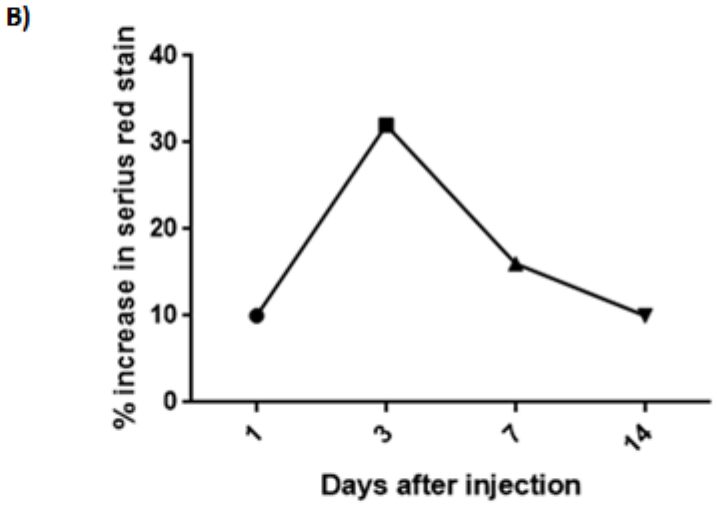
B)
% increase in serius red stain
40
30
20
10
0
1
3
7
14
Days after injection

Figure 6.1 Sirius red staining of C57 TA

24 month old C57 mice were treated in one thigh with a damage reagent and the other untreated, as control (see text).

A) Microscope images of sections from treated and untreated TAs harvested 1, 3, 7 or 14 days after Ba_2Cl injection into the test TA, stained with Sirius red. Visually, there is a clear increase in collagen (red) staining from 1 day after injection to 3 days after injection. After this the muscle morphology begins to be restored and collagen expression (red) becomes limited to the ECM of the regenerated fibres. Magnification X20

B) Collagen (red stain) in three random fields of each section was quantified using ImageJ to calculate the percentage increase in red stain in Ba_2Cl injected samples compared to the control. A steep increase in collagen expression is seen between 1 day and 3 day after Ba_2Cl injection after which a more gradual decrease in collagen levels is measured. N=1,

6.2.1.2 Immunohistochemistry for Periostin, Fibronectin, Collagen VI, and α-SMA

Sections from TA muscle injected with $BaCl_2$ and control TA were stained for POSTN, fibronectin, collagen VI or α-SMA, as described in Materials and Methods (Chapter 2). Results are shown in Figures 6.2, 6.3, 6.4 and 6.5 respectively. Fibronectin, collagen VI and α-SMA are commonly used to look at tissue fibrosis (Specks *et al.*, 1995; Veerasamy *et al.*, 2009; To and Midwood, 2011). All slides were co-stained with laminin to outline skeletal muscle fibres and Dapi to visualise the nuclei. The staining reveals necrosis induced by $BaCl_2$ followed by regeneration of the muscle fibres (Caldwell, Mattey and Weller, 1990). As observed by the laminin and Dapi stains, in the first 7 days after the injection there is an abundance of mononuclear cells, mostly leukocytes and macrophages as well as activated satellite cells (Casar, 2004) in the enlarged intercellular space between the necrotic fibres. At day 7, regenerated fibres can be seen with nuclei in a central position but with heterogenous diameters. Fibres continue to regenerate, and by 14 days after injection, the tissue has recovered to normal morphology but still showed central nuclei and increased interstitial spaces.

POSTN has been shown to be expressed in low amounts in healthy skeletal muscle, upregulated upon damage within regenerating fibres and finally restricted to the ECM following restoration of skeletal muscle morphology (Özdemir *et al.*, 2014). As discussed in Chapter 1, POSTN is important in regeneration and repair of damaged muscle. In accordance with previous data, Figure 6.2 shows upregulation of POSTN protein 3 days after injection with POSTN clearly observed inside the newly forming fibres. At 7 days, when fibres were clearly regenerating, POSTN protein levels were at their peak; interestingly the fibres were devoid of POSTN, which was heavily localised to the

endomysial space. At 14 days after injection where regenerating fibres had mostly recovered their normal morphology, POSTN protein expression was reduced, though still high relative to control TA, being limited mainly to the interstitial space deposited in the ECM lining the rim of fibres.

Collagen VI is heavily involved in maintaining skeletal muscle integrity and function (Chu *et al.*, 1988; Knupp and Squire, 2001). Collagen I, II, III as well as Collagen V and VI are extracellular proteins and localised in the endomysium and perimysium; they are upregulated upon damage (Specks *et al.*, 1995; Ricard-Blum and Ruggiero, 2005). Figure 6.3 shows collagen VI was indeed restricted to the perimysium and endomysium in healthy TA. In the injected TA, collagen was upregulated and present in the necrotic tissue. Seven days after $BaCl_2$ injection when the fibres were regenerating, collagen was highly expressed in the intercellular space. Fourteen days after injection, muscle morphology was restored and collagen expression reduced (in comparison to 7 days), and its distribution was that of healthy muscle cells, visible in the endomysium and perimysium though the perimysium is enlarged.

Fibronectin protein is expressed at extremely low levels in the ECM of healthy skeletal muscle and is upregulated upon tissue damage aiding in ECM remodelling and fibrosis (Kharraz *et al.*, 2014; Kii, Nishiyama and Kudo, 2016). Figure 6.4 shows that fibronectin expression was relatively low in control TA but upregulated upon damage with $BaCl_2$ injection. Fibronectin protein was upregulated and expressed in the necrotic tissue, being restricted to the intercellular space in regenerating fibres 7 days after injection and to the interstitial space 14 days after injection where normal morphology was seen. Fibronectin and collagen showed the same patterns of expression in the necrotic and

regenerating fibres (Figures 6.3 and 6.4). Figure 6.5 shows upregulation of α-SMA in the necrotic tissue 3 days after $BaCl_2$ injection. Expression was at its peak in the regenerating fibres 7 days after injection. At 14 days post-injection, α-SMA was downregulated with minimum expression in the centrally nucleated fibres.

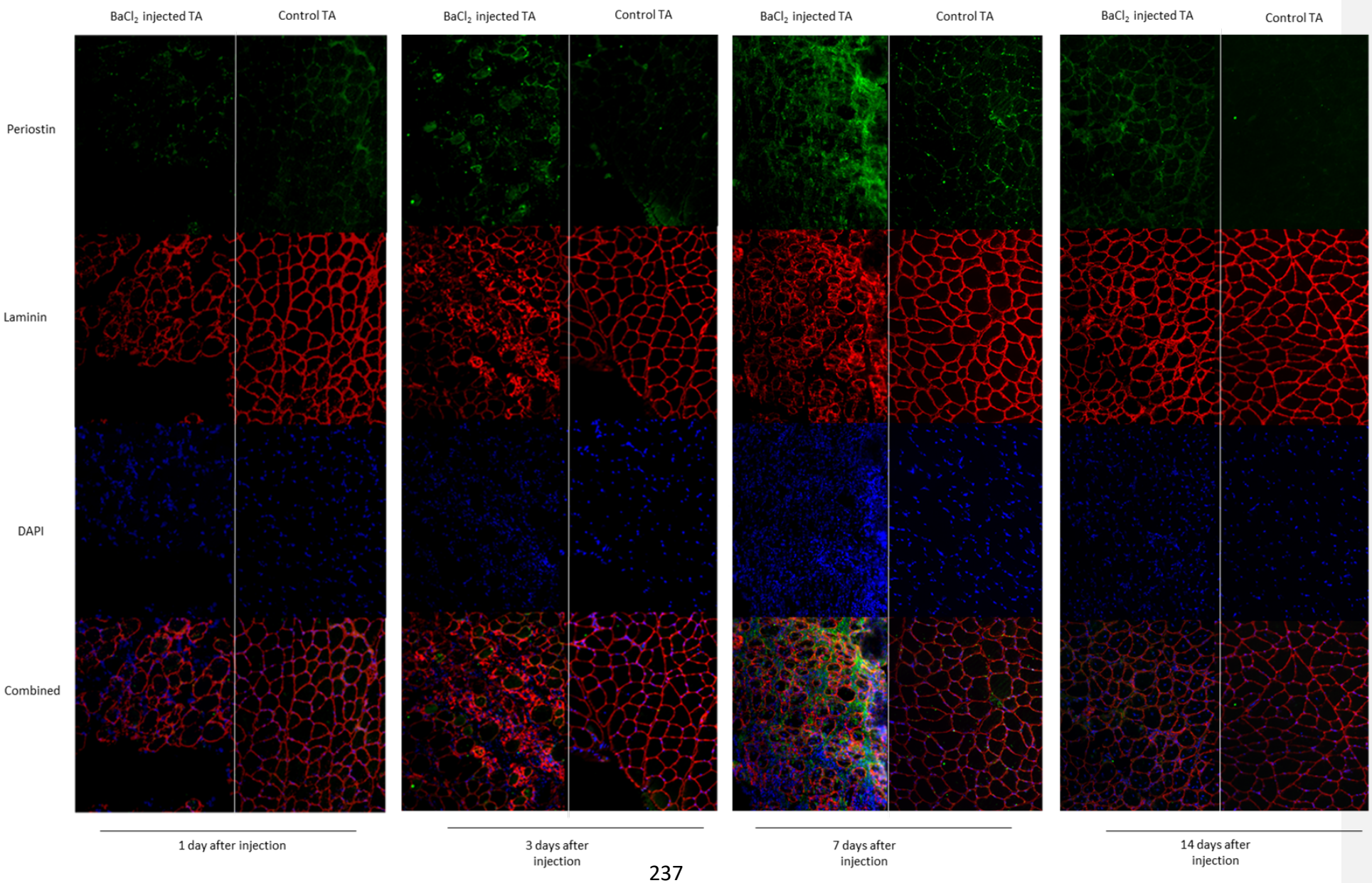
BaCl2 injected TA
Control TA
BaCl2 injected TA
Control TA
BaCl2 injected TA
Control TA
BaCl2 injected TA
Control TA
Periostin
Laminin
DAPI
Combined
1 day after injection
3 days after injection
7 days after injection
14 days after injection

Figure 6.2 Analysis of POSTN expression in TA Muscles treated with$BaCl_2$

C57 mice were injected with $BaCl_2$ in one TA and the other was left undamaged as control. Both TA of each mouse was recovered 1,3,7 and 14 days after injection. Cryosections (10µm) of TA muscle were prepared and stained for POSTN, DAPI and laminin as described (see text). Primary polyclonal antibody ab1404.was used for POSTN. Magnification X20.

Fluorescently tagged secondary antibody was used showing POSTN (green), laminin (red) and DAPI (blue). Combined images with all three stains overlaid are shown (bottom row).

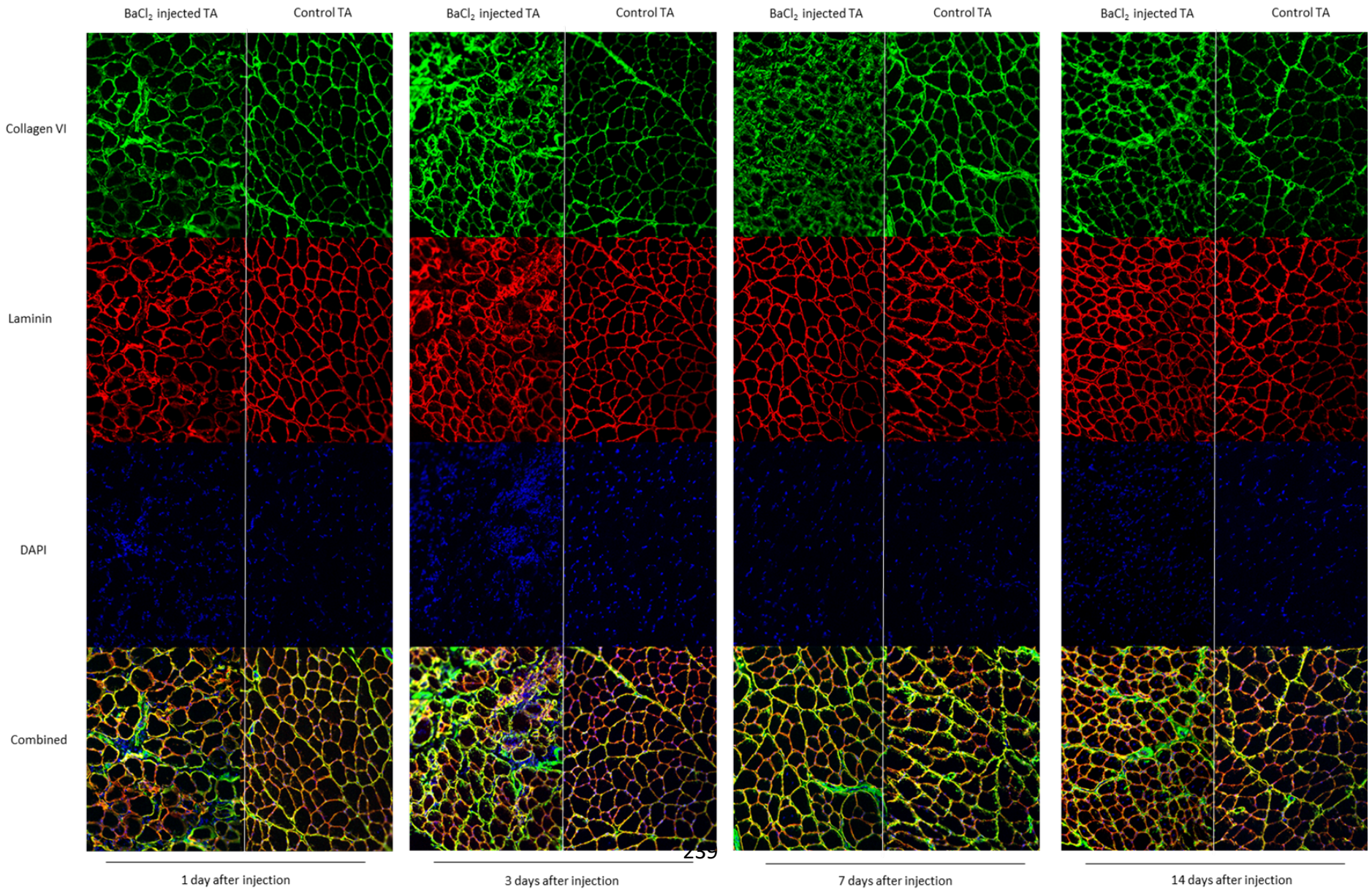
$BaCl_2$ injected TA
Control TA
$BaCl_2$ injected TA
Control TA
$BaCl_2$ injected TA
Control TA
$BaCl_2$ injected TA
Control TA
Collagen VI
Laminin
DAPI
Combined
1 day after injection
3 days after injection
7 days after injection
14 days after injection

Figure 6.3 Analysis of Collagen VI expression in TA muscle treated with $BaCl_2$

C57 mice were injected with $BaCl_2$ in one TA and the other was left undamaged as control. Both TA of each mouse wer recovered 1, 3, 7 and 14 days after injection (see text). Cryosections (10µm thick) of TA muscle were prepared and stained for Collagen VI, DAPI and laminin as described. Magnification is x20. Fluorescently tagged secondary antibody was used showing collagen VI (green), laminin (red) and DAPI (blue). Combined images with all three stains overlaid is also shown (bottom row).

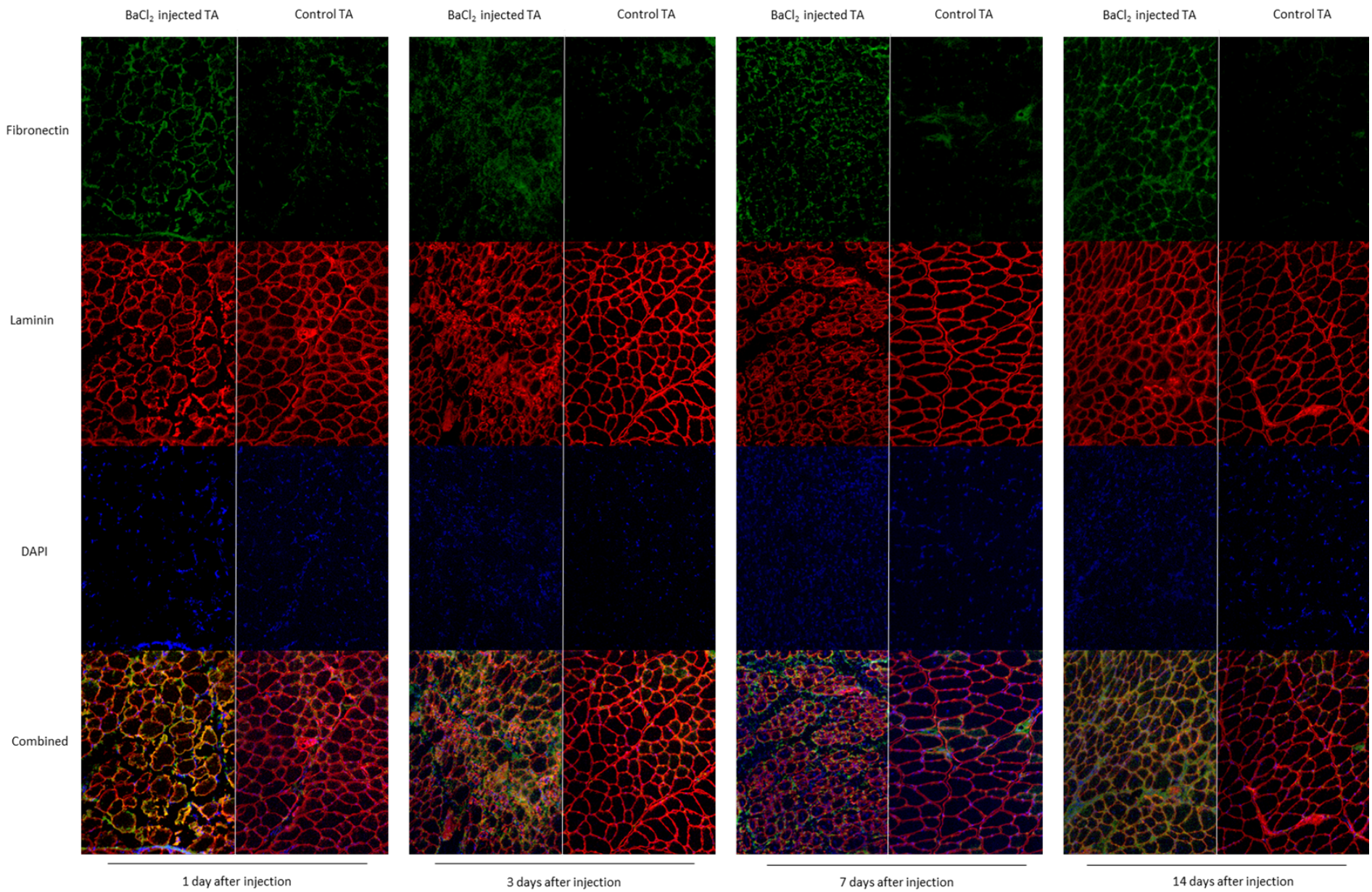
$BaCl_2$ injected TA
Control TA
$BaCl_2$ injected TA
Control TA
$BaCl_2$ injected TA
Control TA
$BaCl_2$ injected TA
Control TA
Fibronectin
Laminin
DAPI
Combined
1 day after injection
3 days after injection
7 days after injection
14 days after injection

Figure 6.4 Analysis of Fibronectin expression in TA muscle treated with $BaCl_2$

C57 mice were injected with $BaCl_2$ in one TA and the other was left undamaged as control. Both TA of each mouse was recovered 1, 3, 7 and 14 days after injection. Cryosections (10µm) of TA muscle were prepared and stained for Collagen VI, DAPI and laminin as described in Materials and Methods. Fluorescently tagged secondary antibody was used showing collagen VI (green), laminin (red) and DAPI (blue). Combined images with all three stains overlaid is also shown (bottom row). Magnification x20.

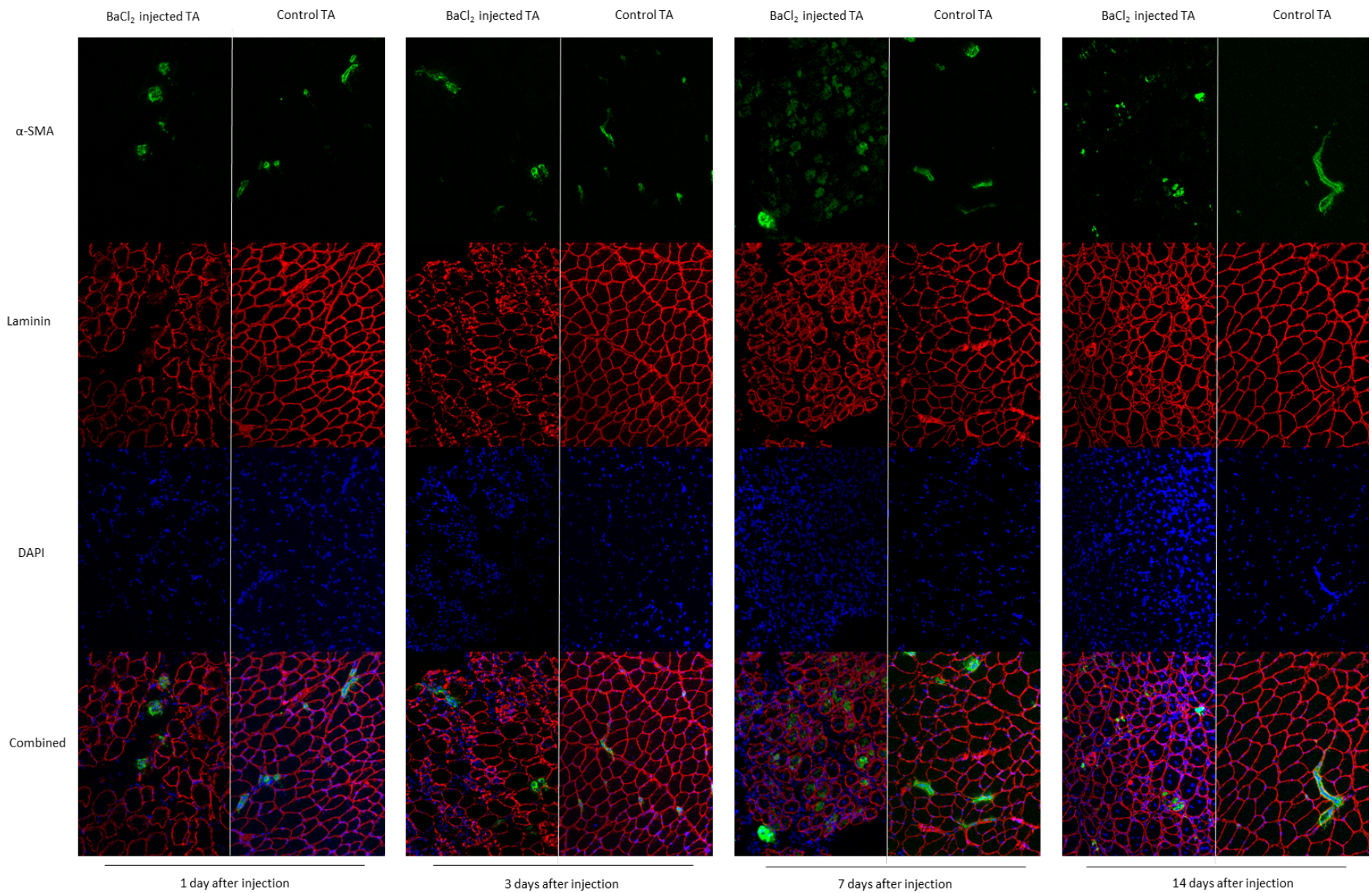
$BaCl_2$ injected TA
Control TA
$BaCl_2$ injected TA
Control TA
$BaCl_2$ injected TA
Control TA
$BaCl_2$ injected TA
Control TA
α-SMA
Laminin
DAPI
Combined
1 day after injection
3 days after injection
7 days after injection
14 days after injection

Figure 6.5 Analysis of α-SMA expression in TA muscles treated with$BaCl_2$

C57 mice were injected with $BaCl_2$ in one TA and the other was left undamaged as control. Both TA of each mouse was recovered 1,3,7 and 14 days after injection. Cryosections (10µm) of TA muscle were prepared and stained for α-SMA, DAPI and laminin as described in Materials and Methods. Fluorescently tagged secondary antibody was used showing α-SMA (green), laminin (red) and DAPI (blue). Combined images with all three stains overlaid is also shown (last row). Magnification x20.

6.2.1.3 RT-PCR of Periostin in $BaCl_2$ injected TA of C57 mice

Total RNA was extracted from TA sections as described in Materials and Methods. RNA extracts were subjected to a multiplex RT-PCR to amplify *POSTN* exon 2-4 and 18S (Figure 6.6A). The *POSTN* mRNA expression was semi-quantitatively analysed as described in Materials and Methods and normalised to 18S expression. The *POSTN* mRNA expression of the damage TA was then calculated relative to the healthy TA (Figure 6.6b).

POSTN mRNA expression peaked 14 days after $BaCl_2$ injection. In order to reveal when *POSTN* expression began decreasing, mice injected with $BaCl_2$ and harvested 28 days and 6 weeks after injection was investigated. RNA was extracted, and RT-PCR was performed for all samples 1, 3, 7, 14, 28 and 42 days post-injection. Products were separated on a 3% agarose gel (Figure 6.6A). It can be seen that at 28 days the *POSTN* RNA levels began to decrease. At 6 weeks *POSTN* expression is only 20% above that of the healthy TA (Figure 6.6B).

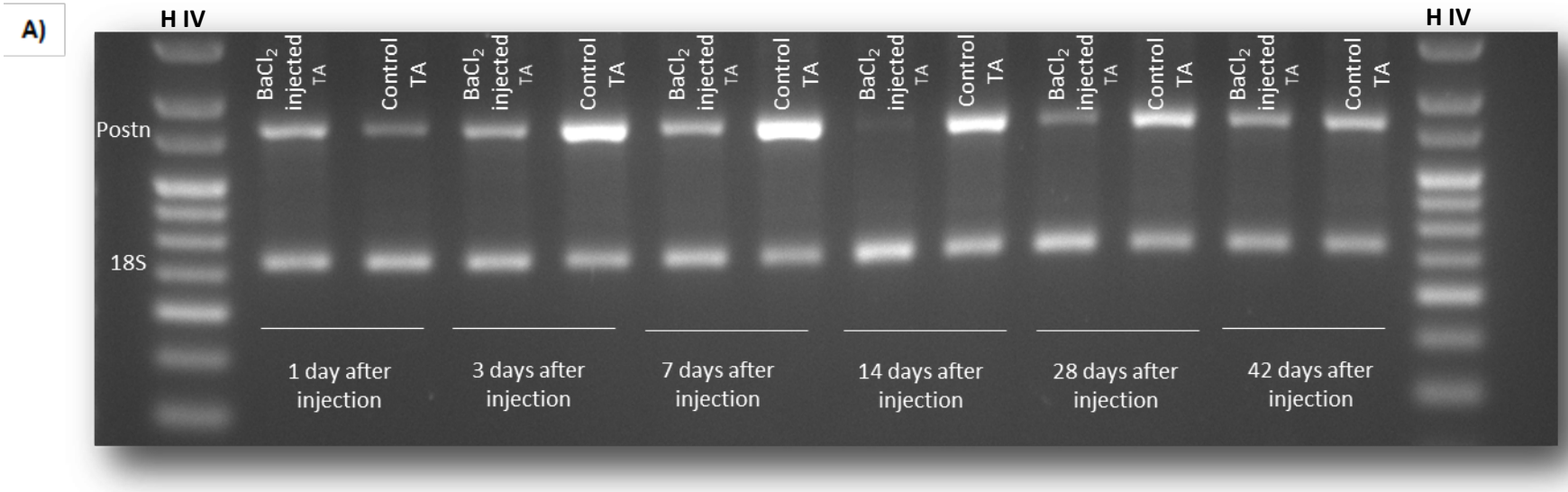
A)
H IV
H IV
Postn
18S
BaCl2 injected TA
Control TA
1 day after injection
3 days after injection
7 days after injection
14 days after injection
28 days after injection
42 days after injection

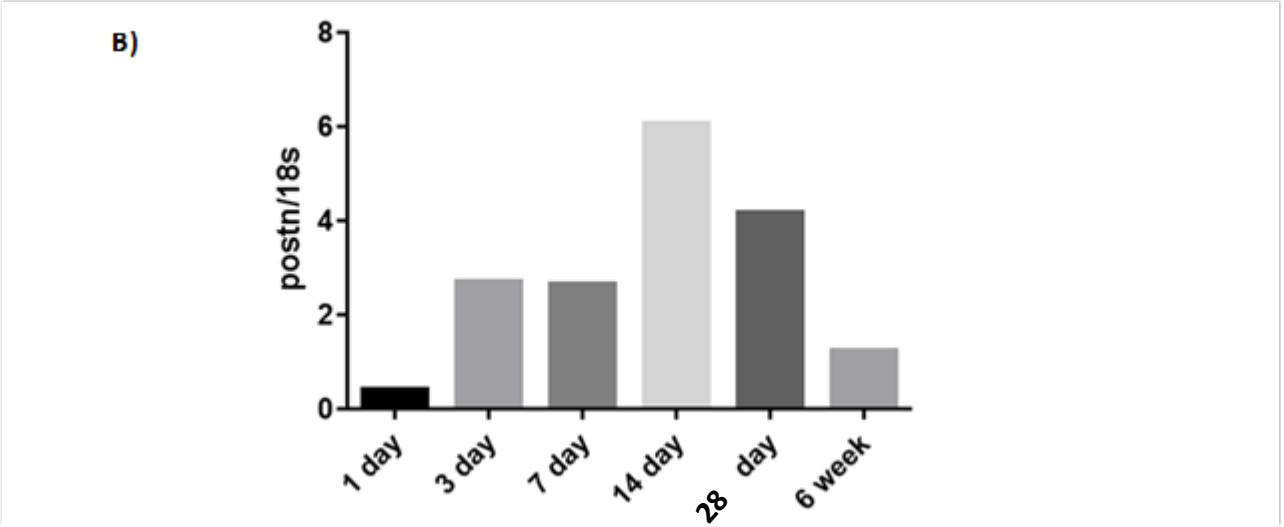
B)
postn/18s
0
2
4
6
8
1 day
3 day
7 day
14 day
28 day
6 week

Figure 6.6 RT-PCR of C57 TA RNA

24 month old C57 mice were used. One TA was injected with Ba_2Cl and the opposite TA was not injected as a matched control. Tissue was harvested 1, 3, 7, 14, 28 and 42 days after injection and sectioned. RNA was harvested and subjected to multiplex RT-PCR amplifying exons 2-4 of *POSTN* mRNA and PCR of 18S mRNA. was included as a normalisation product. N=1

A) A 3% agarose gel of the RT-PCR products from the amplification of *POSTN* exons 2-4 and 18S RNA from samples injected with $BaCl_2$ next to matched control samples with no injection. In controls there was a clear increase in *POSTN* message during tissue damage; however there was a decrease in *POSTN* expression relative to control TA 1 day after injection. The levels significantly increase between 1 day and 14 days after injection in the control TAs, after which they decrease to normal levels (relative to control samples) at 42 days after injection.

B) Intensity of the products on the 3% agarose gel was quantified using GeneTools software. Periostin expression in $BaCl_2$ injected TA samples were normalised to 18S expression. The semi-quantitative analysis showed an increase in *POSTN* expression peaking at 14 days after injection after which *POSTN* levels decrease.

6.2.2 Effect of Pex3.28.2 induced Periostin skipping in $BaCl_2$ injected TA of C57 mice

Assessing the traumatising effect of $BaCl_2$ in the TA of 24-month-old C57 mice (section 6.2.1) confirmed that intramuscular injection of 50µl of 1.2% $BaCl_2$ caused significant damage in the TA leading to an upregulation of POSTN expression. Upregulation of POSTN was particularly pronounced in regenerating fibres, 7 days after injection, confirming the role and importance of POSTN in the regeneration of muscle fibres and healing of damage (March *et al.*, 2018).

In order to test the bioactivity of PEX3.28.2 PMO *in vivo*, and assess the consequent effect of PMO induced POSTN downregulation in regenerating fibres, 1-month-old mice were injected with 50 µl of 1.2% $BaCl_2$ in both TA. 4 days after $BaCl_2$ injection, when fibres were shown to be regenerating and POSTN expression upregulated (section 6.2.1), the left TA was injected with 20µg in 50 µl of PEX2.28.2 and the right TA with 50µl of saline. Tissue was then harvested at 7, 14, 28 days and 6 weeks after PMO injection, to investigate levels of message and protein by RT-qPCR and Western.

6.2.2.1 q-PCR of Periostin and fibronectin in $BaCl_2$ /PMO and in $BaCl_2$/saline injected TA of C57 mice

As found in Chapter 5, RT-qPCR analysis of harvested RNA was able to efficiently detect downregulation of POSTN in PMO treated samples. Total RNA was therefore extracted from TA sections as described in Materials and Methods. RNA extracts were subjected to RT-qPCR to amplify POSTN and fibronectin message (Figures 6.7, 6.8, 6,9, 6.10). Predesigned primers (described in Chapter 2) were used for amplification. GAPDH was

used as a housekeeping gene for normalisation. The primers for GAPDH were also predesigned and outlined in section 2.

There was an overall decrease in POSTN RNA expression as assessed by RT-qPCR, in TA muscle following PMO or saline injection, showing successful exon exclusion although this was not statistically significant (Figure 6.7A). Fibronectin was also tested by RT-PCR (Figure 6.7B). There was very little decrease of fibronectin in the PMO injected samples with no statistical significance.

After 14 days the same RT-qPCR tests were performed. Figure 6.8A shows that POSTN RNA expression showed an obvious decrease in POSTN expression. Figure 6.8B revealed that at 14 days after injection there was still no change in fibronectin RNA levels after PMO treatment.

At 21 days, POSTN RNA levels were still lower in the PMO injected samples than the saline-injected TA (Figure 6.9A). This time, a statistically significant decrease ($p=0.02$) in fibronectin RNA levels was detected in the PMO injected samples in comparison to the saline-injected samples (Figure 6.9B).

At 6 weeks after PMO and saline injection, the POSTN levels were too low to quantitatively measured, as expected from their diminishing role by that time. Fibronectin levels still showed no change (Figure 6.10), and no statistical difference in expression levels between the PMO injected, and saline-injected samples.

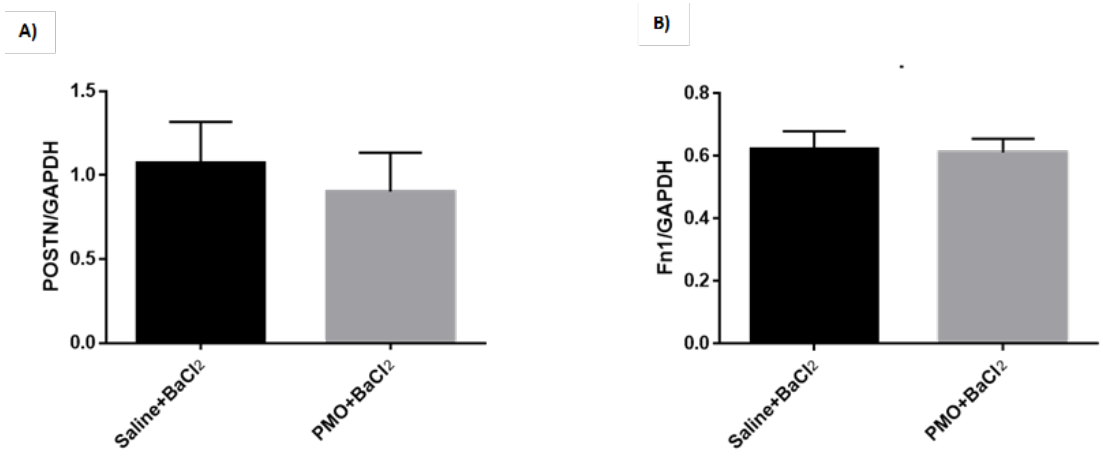

Figure 6.7 Quantification of *POSTN* and Fibronectin mRNA expression in PEX3.28.2 injected C57Bl10 mice 7 days after $BaCl_2$ injection

1 month old C57 mice were injected with 50µl of 1.2% $BaCl_2$ in both TA. Three days after $BaCl_2$ injection the left TA was injected with 20µg of PEX3.28.2 PMO and the right TA with saline as control. TA of mice was harvested 7 days after PMO injection. RNA was harvested from sectioned samples and subject to qPCR amplifying *POSTN* and fibronectin along with GAPDH a house keeping gene. A) Periostin expression was quantified and normalised to GAPDH expression. A decrease in *POSTN* RNA levels is observed in the PMO injected samples .N=3

B) Fibronectin expression was quantified and normalised to GAPDH. No change in fibronectin RNA level was seen upon PMO injection. N=3

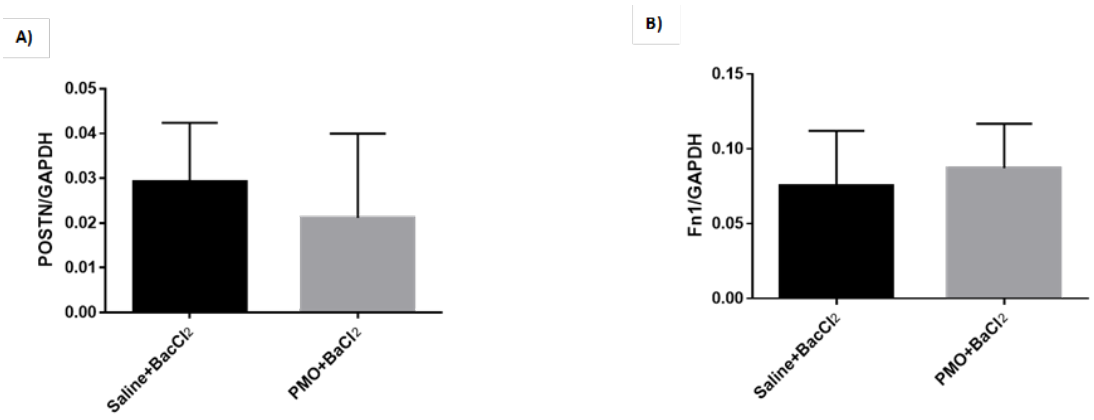

Figure 6.8 Quantification of *POSTN* and Fibronectin mRNA expression in PEX3.28.2 injected C57Bl10 mice 14 days after Ba_2Cl injection

1 month old C57 mice were injected with 50µl of 1.2% $BaCl_2$ in both TA. Three days after $BaCl_2$ injection the left TA was injected with 20µg of PEX3.28.2 PMO and the right TA with saline as control. Both TA of each of the mice was harvested 14 days after PMO injection. RNA was harvested from sectioned samples and subject to qPCR amplifying *POSTN* and fibronectin along with GAPDH.

A) Periostin expression was quantified and normalised to GAPDH expression. A decrease in Postn RNA levels is observed in the PMO injected samples (N=3)

B) Fibronectin expression was quantified and normalised to GAPDH. No change in fibronectin RNA level was seen upon PMO injection (N=3).

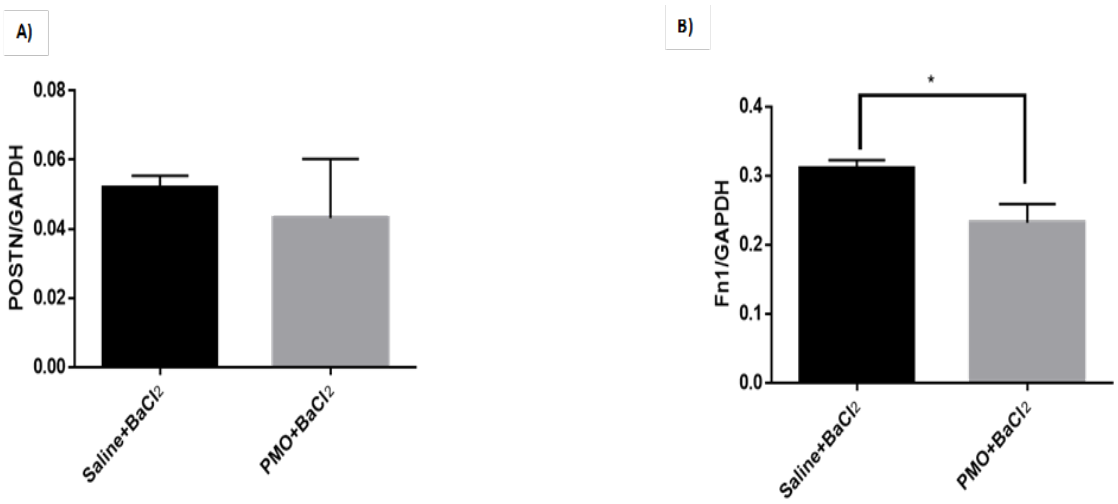

Figure 6.9 Quantification of *POSTN* and fibronectin mRNA expression in PEX3.28.2 injected C57Bl10 mice 28 days after $BaCl_2$ injection

1 month old C57 mice were injected with 50µl of 1.2% $BaCl_2$ in both TA. Three days after $BaCl_2$ injection the left TA was injected with 20µg of PEX3.28.2 PMO and the right TA with saline as a matched control. TA were harvested 14 days after PMO injection. RNA harvested from sectioned samples was subject to RT-qPCR amplifying *POSTN* and fibronectin message along with GAPDH.

A) Periostin message expression was quantified and normalised to GAPDH expression. A maintained decrease in *POSTN* RNA levels is observed in the PMO injected samples at this time point (N=3).

B) Fibronectin expression was quantified and normalised to GAPDH. PMO-injected samples showed a marginally significant decrease in fibronectin RNA levels in comparison to the saline treated samples (*$p<0.05$, N=3).

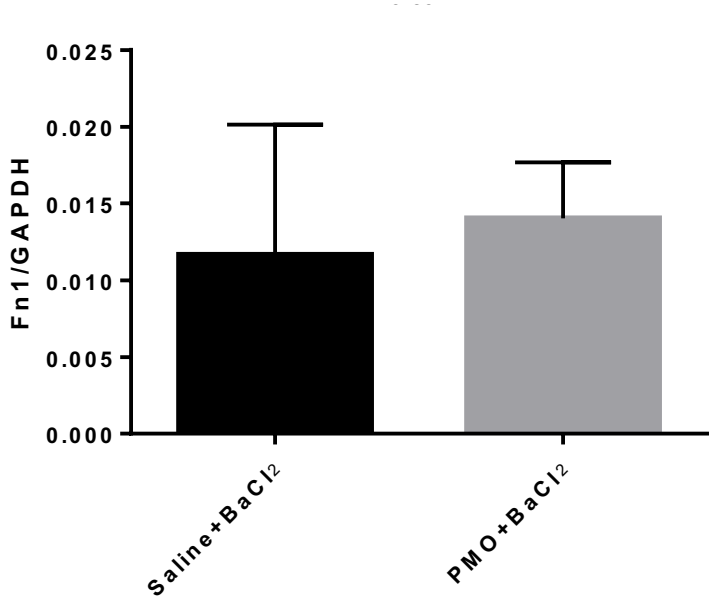

Figure 6.10 Quantification of POSTN and Fibronectin mRNA expression in PEX3.28.2 injected C57BI10 mice 6 weeks after $BaCl_2$ injection

1 month old C57 mice were injected with 50µl of 1.2% $BaCl_2$ in both TA. Three days after $BaCl_2$ injection the left TA was injected with 20µg of PEX3.28.2 PMO and the right TA with saline as a control. TA of mice were harvested 14 days after PMO injection. RNA was harvested from sectioned samples and subject to qPCR amplifying POSTN and fibronectin along with GAPDH. POSTN expression could not be quantified presumably because RNA levels were too low which is the situation in normal muscle. Fibronectin expression was quantified and normalised to GAPDH. PMO injected samples and saline injected samples showed no significant difference in fibronectin RNA levels both samples showing very low levels of expression.

6.2.2.2 Western blotting of periostin and fibronectin in $BaCl_2$ /PMO and in $BaCl_2$/saline injected TA of C57 mice

To determine whether PEX3.28.2 PMO affects protein expression in damaged muscle *in vivo,* Western blotting was carried out. Protein was extracted from sections of TA, as described in Methods and Materials (Chapter 2), from PMO injected and saline-injected samples at 7, 14, 28 days and 6 weeks after injection. Protein samples were then Western blotted to detect POSTN protein, and α-tubulin was used as a loading control and to normalise expression. Fibronectin protein was also visualised and vinculin used as the loading control. NIR fluorescence imaging or Odyssey was used to visualise the blot and the Odyssey software, Image Studio, was used to quantify the image.

Figures 6.11A, 6.12B, 6.13A and 6.14a show that there was reduced Periostin protein expression in PMO injected samples compared to the saline-injected samples, indicating that PEX3.28.2 PMO induced exon exclusion successfully, leading in turn to a decrease in POSTN protein levels that is visible even at 6 weeks after injection (unlike the RNA message which has become undetectable by 6 weeks). The largest difference between PMO injected, and saline-injected samples were seen 14 days after injection (Figure 6.12A), and the lowest difference between PMO injected, and saline-injected samples at 7 days after injection (Figure 6.11A) when Postn message is at its height (above). Although differences in protein expression were observed between control and PMO treated mice, these were not found to be statistically significant.

Fibronectin protein levels were also reduced by PMO injection (Figures 6.11B, 6.12B, 6.13B, 6.14B) at 7, 14 and 28 days but there was no statistical significance due to the large error bars as also seen in both Periostin Western blots and POSTN q-PCR. As for

Periostin, the largest difference in fibronectin levels, between PMO and saline-injected samples, was 7 days after injection (Figure 6.11B). At 6 weeks (Figure 6.14B), fibronectin protein levels in the PMO injected samples were no longer lower than the saline-injected samples.

A)

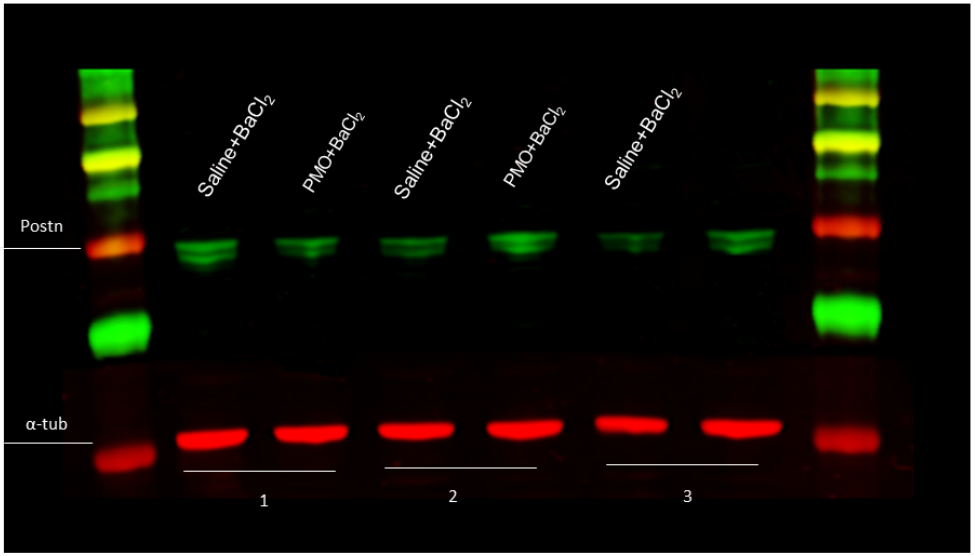
Saline+BaCl2
PMO+BaCl2
Saline+BaCl2
PMO+BaCl2
Saline+BaCl2
Postn
α-tub
1
2
3

B)

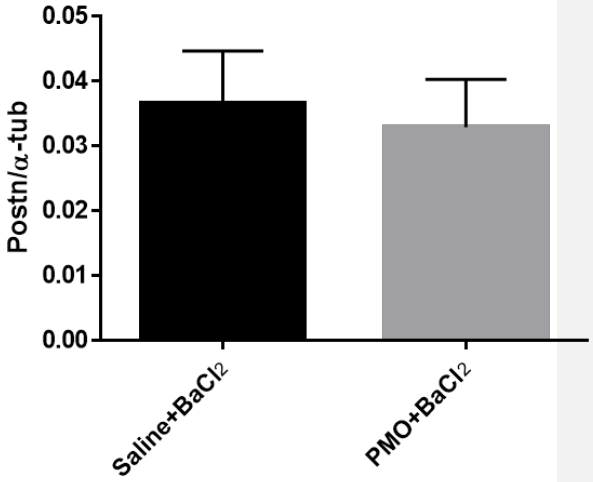
0.05
0.04
0.03
0.02
0.01
0.00
Postn/α-tub
Saline+BaCl2
PMO+BaCl2

C)

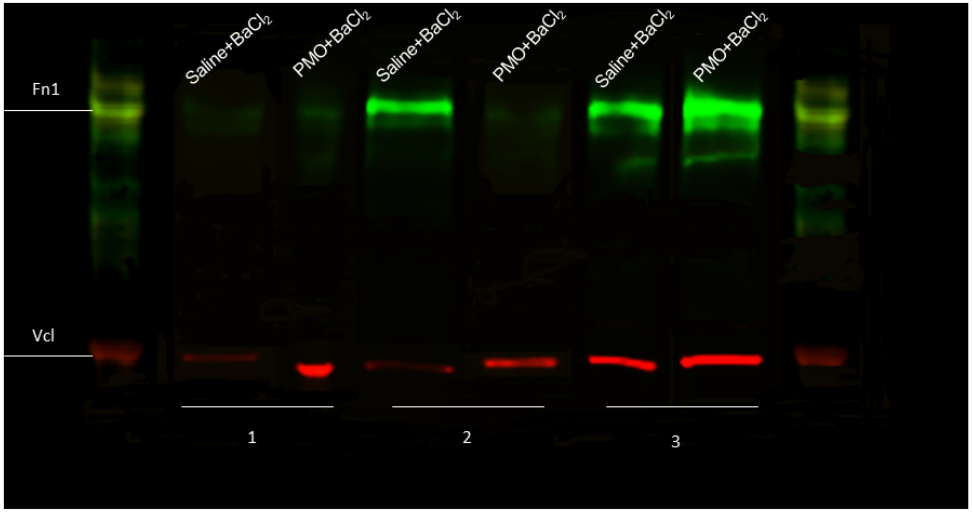
Saline+BaCl2
PMO+BaCl2
Saline+BaCl2
PMO+BaCl2
Saline+BaCl2
PMO+BaCl2
Fn1
Vcl
1
2
3

D)

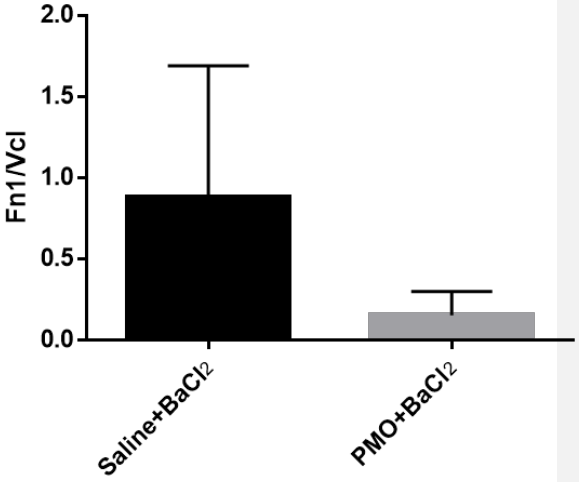
2.0
1.5
1.0
0.5
0.0
Fn1/Vcl
Saline+BaCl2
PMO+BaCl2

Figure 6.11 Analysis of POSTN and fibronectin protein in PEX3.28.2 injected C57 mice 1 weeks after PMO injection

C57 mice were injected with Ba_2Cl in both TA, and later with PMO in the left TA and saline right. TA of mice were taken and tissue harvested for Western blotting as described in Methods and Materials (Chapter 2). POSTN was detected with rabbit polyclonal antibody ab1404, and fibronectin with rabbit polyclonal ab2413. α-tubulin and vinculin were used as loading controls and for semi-quantitative analysis. Fluorescently tagged secondary antibodies allowed blots to be imaged using Odyssey and analysed in Image Studio.

A) Western Blot of protein extracts from TA muscle developed with antibodies for POSTN and α-tubulin. Each pair of lanes (3 pairs) represent biological repeats: each pair consists of PMO injected and saline injected TA. Periostin (green), and tubulin (red). Periostin had a predicted weight of 100kDa and has been reported to appear between 90-100kDa from *in vivo* samples. Tubulin has a predicted weight of 50kDa.

B) Semiquantitative analysis of the Odyssey image in A . A decrease in total POSTN protein levels is seen in PMO injected samples, without statistical significance due to large error bars, because one of three replicates showed no change in POSTN levels (N=3).

C) Western Blot of protein extracts from TA muscle developed with antibodies against fibronectin and vinculin. Each pair of lanes (3 pairs) represent biological repeats: each pair consists of PMO injected and saline injected TA. Fibronectin (green) and vinculin (red). Fibronectin has a predicted weight of 100kDa but has been reported to run at 280kDa from *in vivo* samples. Vinculin has a predicted weight of 124kDa**.**

D) Semiquantitative analysis of image in C. Fibronectin protein levels decreased in PMO injected samples (N=3).

A)

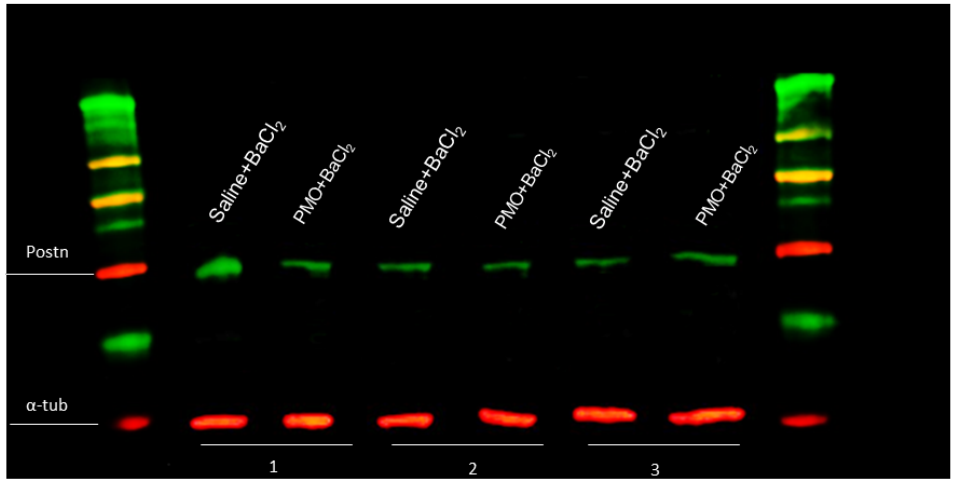
Saline+BaCl2
PMO+BaCl2
Saline+BaCl2
PMO+BaCl2
Saline+BaCl2
PMO+BaCl2
Postn
α-tub
1
2
3

B)

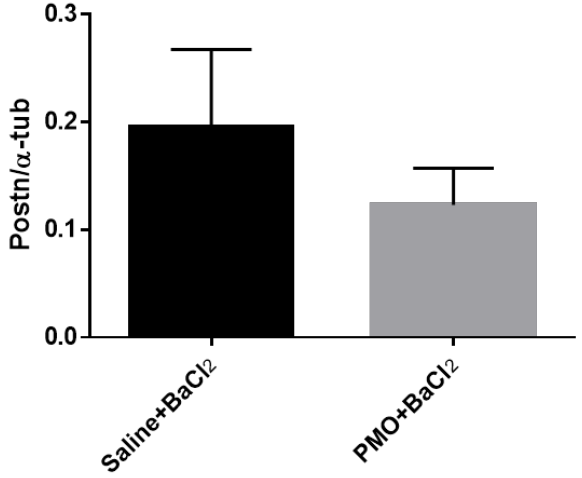
Postn/α-tub
0.3
0.2
0.1
0.0
Saline+BaCl2
PMO+BaCl2

C)

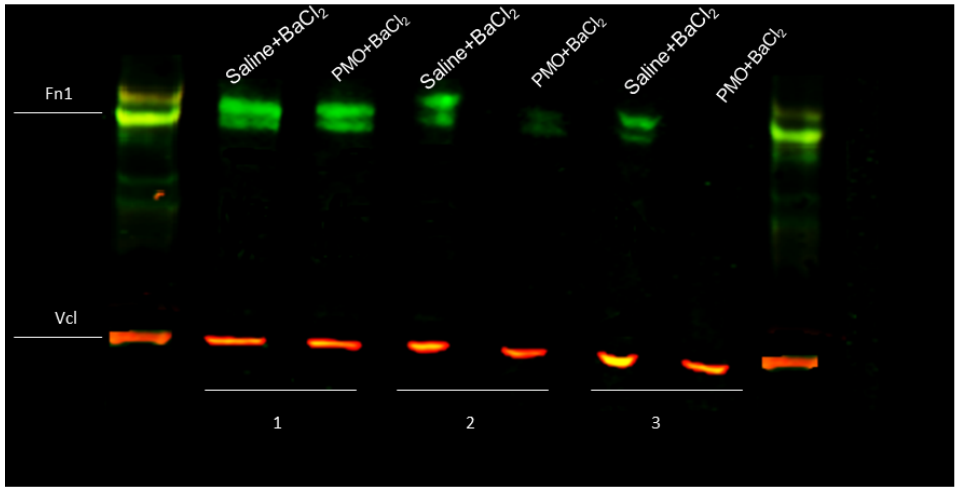
Saline+BaCl2
PMO+BaCl2
Saline+BaCl2
PMO+BaCl2
Saline+BaCl2
PMO+BaCl2
Fn1
Vcl
1
2
3

D)

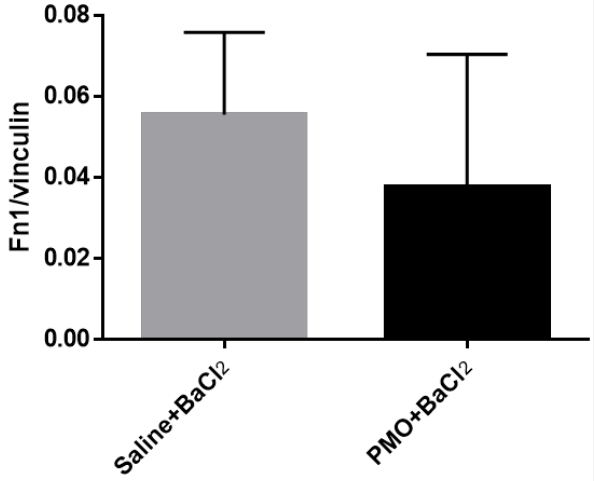
Fn1/vinculin
0.08
0.06
0.04
0.02
0.00
Saline+BaCl2
PMO+BaCl2

Figure 6.12 Analysis of POSTN and Fibronectin protein in PEX3.28.2 injected C57 mice 2 weeks after PMO injection

C57 mice were injected with Ba_2Cl in both TA then with PEX3.28.2 PMO in the left and saline, right, as control. After two weeks, TA of mice were recovered and tissue harvested from sectioned samples for Western Blotting. POSTN was detected with rabbit polyclonal antibody ab1404, and fibronectin with rabbit polyclonal ab2413. α-tubulin and vinculin were used as loading controls. Fluorescently tagged secondary antibodies were used and blots imaged using Odyssey and analysed with Image Studio as described in Methods and Materials (Chapter 2).

A) Western Blot of protein extracts from TA muscle developed with antibodies against POSTN and α-tubulin. Each pair of lanes (3 pairs) represent biological repeats: each pair consists of PMO injected and saline injected TA. POSTN (green), tubulin (red). Periostin had a predicted weight of 100kDa and has been reported to appear between 90-100kDa from *in vivo* samples. Tubulin has a predicted weight of 50kDa.

B) Semiquantitative analysis of the image in A . Decreased POSTN protein levels were seen in PMO injected samples, but there was no statistical significance (N=3).**C)** Western Blot of protein extracts from TA muscle developed with antibodies against fibronectin and vinculin. Each pair of lanes (3 pairs) represent biological repeats: each pair consists of PMO injected and saline injected TA. Fibronectin (green), vinculin (red). Fibronectin (100kDa) and has been reported to run at 280kDa from *in vivo* samples. Vinculin has a predicted weight of 124kDa.

D) Semiquantitative analysis of the image in C. A decrease in total fibronectin protein levels is seen in PMO injected samples, without statistical significance (N=3).

A)

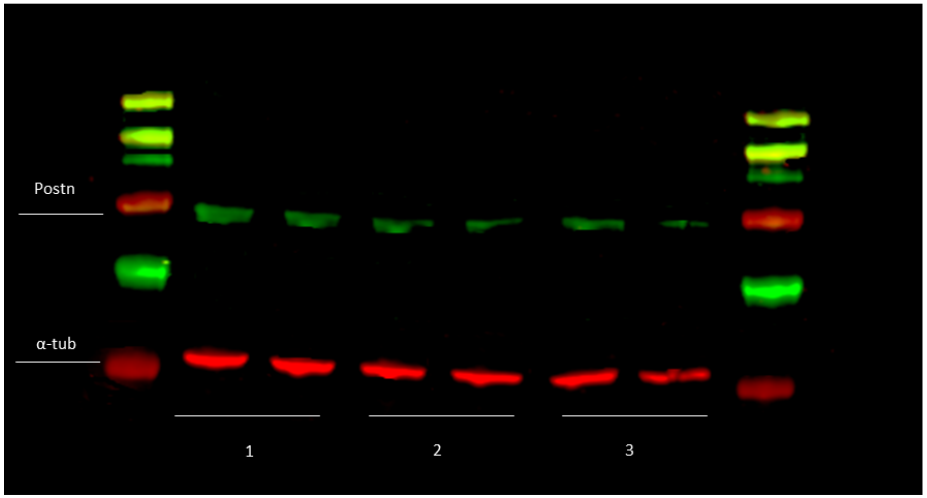
Postn
α-tub
1
2
3

B)

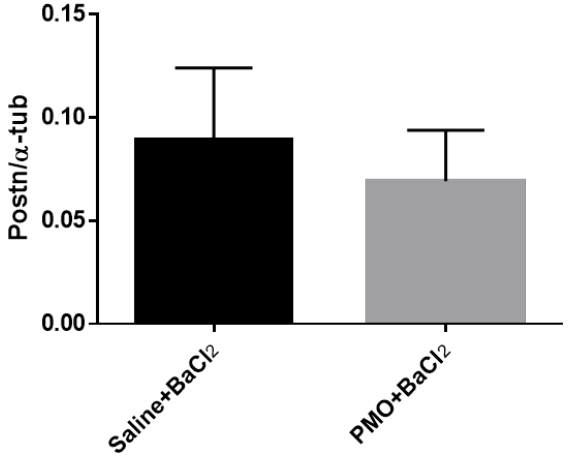
0.15
0.10
0.05
0.00
Postn/α-tub
Saline+BaCl2
PMO+BaCl2

C)

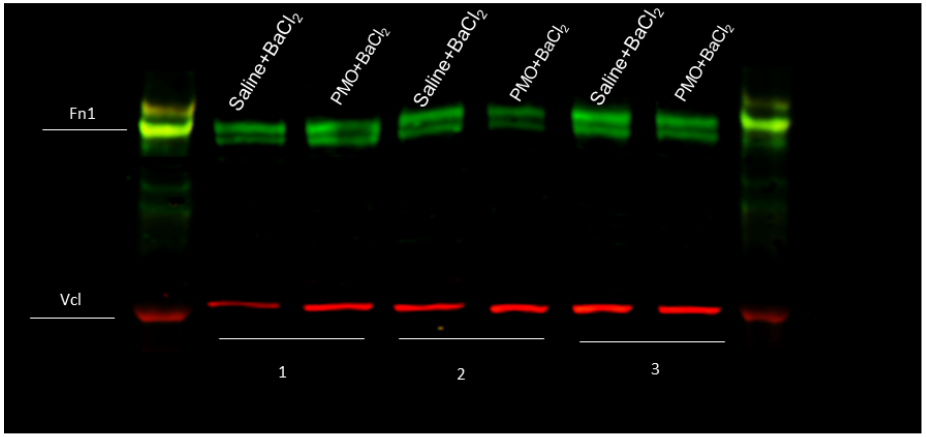
Saline+BaCl2
PMO+BaCl2
Saline+BaCl2
PMO+BaCl2
Saline+BaCl2
PMO+BaCl2
Fn1
Vcl
1
2
3

D)

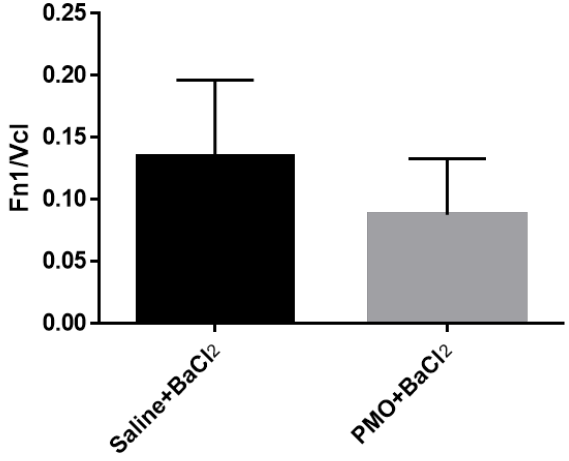
0.25
0.20
0.15
0.10
0.05
0.00
Fn1/Vcl
Saline+BaCl2
PMO+BaCl2

Figure 6.13 Analysis of POSTN and Fibronectin protein in PEX3.28.2 injected C57 mice 4 weeks after PMO injection

C57 mice were injected with Ba_2Cl in both TA then with PEX3.28.2 PMO in the left and saline, right, as control. After two weeks, TA of mice were recovered and tissue harvested from sectioned samples for Western Blotting. POSTN was detected with rabbit polyclonal antibody ab1404, and fibronectin with rabbit polyclonal ab2413. α-tubulin and vinculin were used as loading controls. Fluorescently tagged secondary antibodies were used and blots imaged using Odyssey and analysed with Image Studio as described in Methods and Materials (Chapter 2).

A) Western Blot of protein extracts from TA muscle developed with antibodies against POSTN and α-tubulin. Each pair of lanes (3 pairs) represent biological repeats: each pair consists of PMO injected and saline injected TA. POSTN (green), tubulin (red). Periostin had a predicted weight of 100kDa and has been reported to appear between 90-100kDa from *in vivo* samples. Tubulin has a predicted weight of 50kDa.

B) Semiquantitative analysis of the image in A . Decreased POSTN protein levels were seen in PMO injected samples, but there was no statistical significance (N=3).

C) Western Blot of protein extracts from TA muscle developed with antibodies against fibronectin and vinculin. Each pair of lanes (3 pairs) represent biological repeats: each pair consists of PMO injected and saline injected TA. Fibronectin (green), vinculin (red). Fibronectin (100kDa) and has been reported to run at 280kDa from *in vivo* samples. Vinculin has a predicted weight of 124kDa**.**

D) Semiquantitative analysis of the image in C. A decrease in total fibronectin protein levels is seen in PMO injected samples, without statistical significance (N=3).

A)

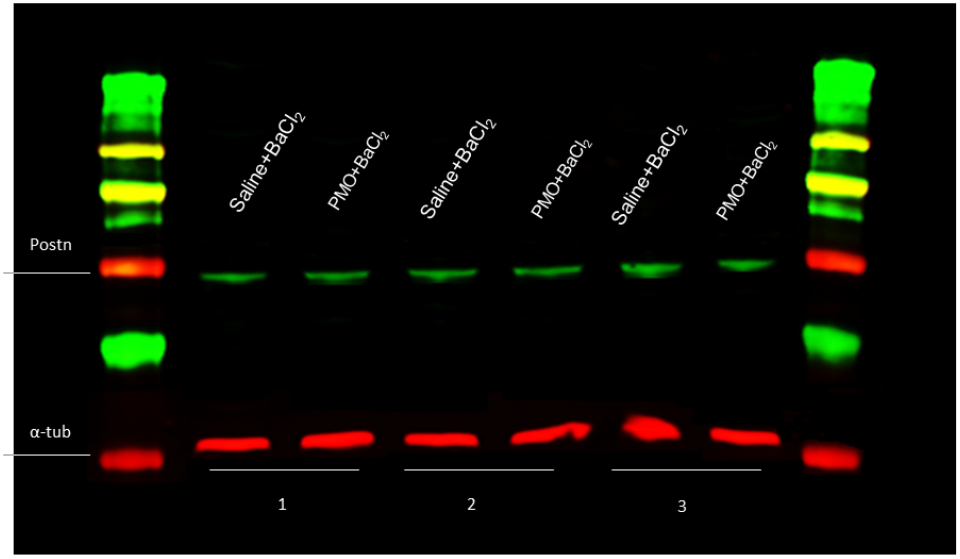
Saline+BaCl2
PMO+BaCl2
Saline+BaCl2
PMO+BaCl2
Saline+BaCl2
PMO+BaCl2
Postn
α-tub
1
2
3

B)

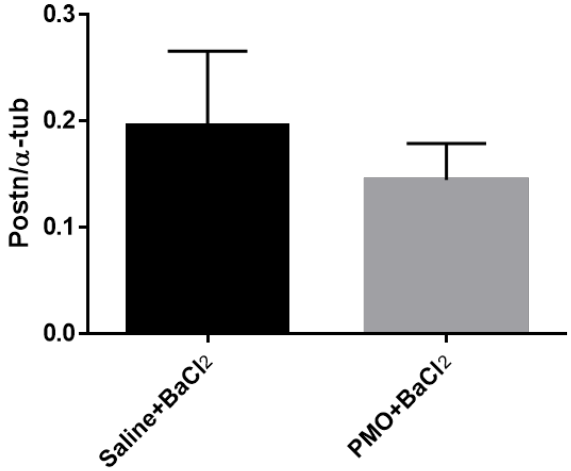
Postn/α-tub
0.3
0.2
0.1
0.0
Saline+BaCl2
PMO+BaCl2

C)

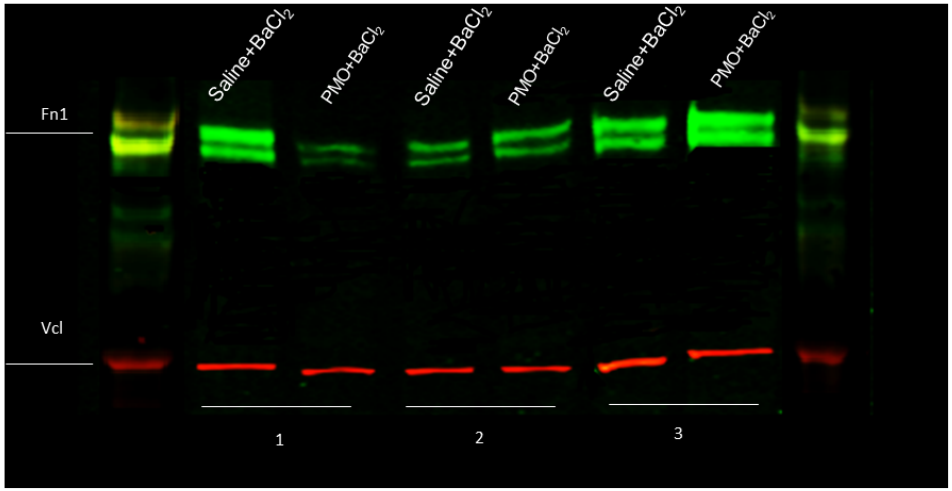
Saline+BaCl2
PMO+BaCl2
Saline+BaCl2
PMO+BaCl2
Saline+BaCl2
PMO+BaCl2
Fn1
Vcl
1
2
3

D)

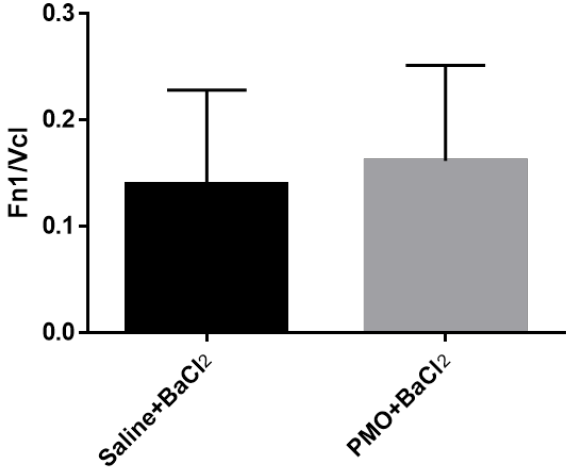
Fn1/Vcl
0.3
0.2
0.1
0.0
Saline+BaCl2
PMO+BaCl2

Figure 6.14 Analysis of POSTN and fibronectin protein in PEX3.28.2 injected C57 mice 6 weeks after PMO injection

C57 mice were injected with Ba_2Cl in both TA then with PEX3.28.2 PMO in the left and saline, right, as control. After two weeks, TA of mice were recovered and tissue harvested from sectioned samples for Western Blotting. POSTN was detected with rabbit polyclonal antibody ab1404, and fibronectin with rabbit polyclonal ab2413. α-tubulin and vinculin were used as loading controls. Fluorescently tagged secondary antibodies were used and blots imaged using Odyssey and analysed with Image Studio as described in Methods and Materials (Chapter 2).

A) Western Blot of protein extracts from TA muscle developed with antibodies against POSTN and α-tubulin. Each pair of lanes (3 pairs) represent biological repeats: each pair consists of PMO injected and saline injected TA. POSTN (green), tubulin (red). Periostin had a predicted weight of 100kDa and has been reported to appear between 90-100kDa from *in vivo* samples. Tubulin has a predicted weight of 50kDa.

B) Semiquantitative analysis of the image in A . Decreased POSTN protein levels were seen in PMO injected samples, but there was no statistical significance (N=3).

C) Western Blot of protein extracts from TA muscle developed with antibodies against fibronectin and vinculin. Each pair of lanes (3 pairs) represent biological repeats: each pair consists of PMO injected and saline injected TA. Fibronectin (green), vinculin (red). Fibronectin (100kDa) and has been reported to run at 280kDa from *in vivo* samples. Vinculin has a predicted weight of 124kDa**.**

D) Semiquantitative analysis of the image in C. No significant difference in fibronectin protein levels is seen in PMO injected samples (N=3).

6.2.2.3 Sirius red staining

The effect of PMO injection on collagen distribution during muscle injury was examined by Picro-Sirius red staining of tissue sections. Sections were taken from TA muscle injected with $BaCl_2$/PEX3.28.2 PMO or $BaCl_2$/saline, stained as described in Materials and Methods (Chapter 2) and the results showed (Figure 6.15). Picro-Sirius red dyes have specific reactivity to collagen I and III are therefore used for quantitative estimation of tissue fibrosis (section 6.2.1). Collagen is stained red, and muscle fibres and cytoplasm are stained in yellow. At 1 and 2 weeks after PMO/saline injection the saline-injected TA showed significantly higher expression of collagen I/III in comparison to PMO injected TA ($p<0.01$). The lowered expression levels in PMO injected sections was still seen at 4 weeks after PMO injection, but at 6 weeks this difference was no longer observable.

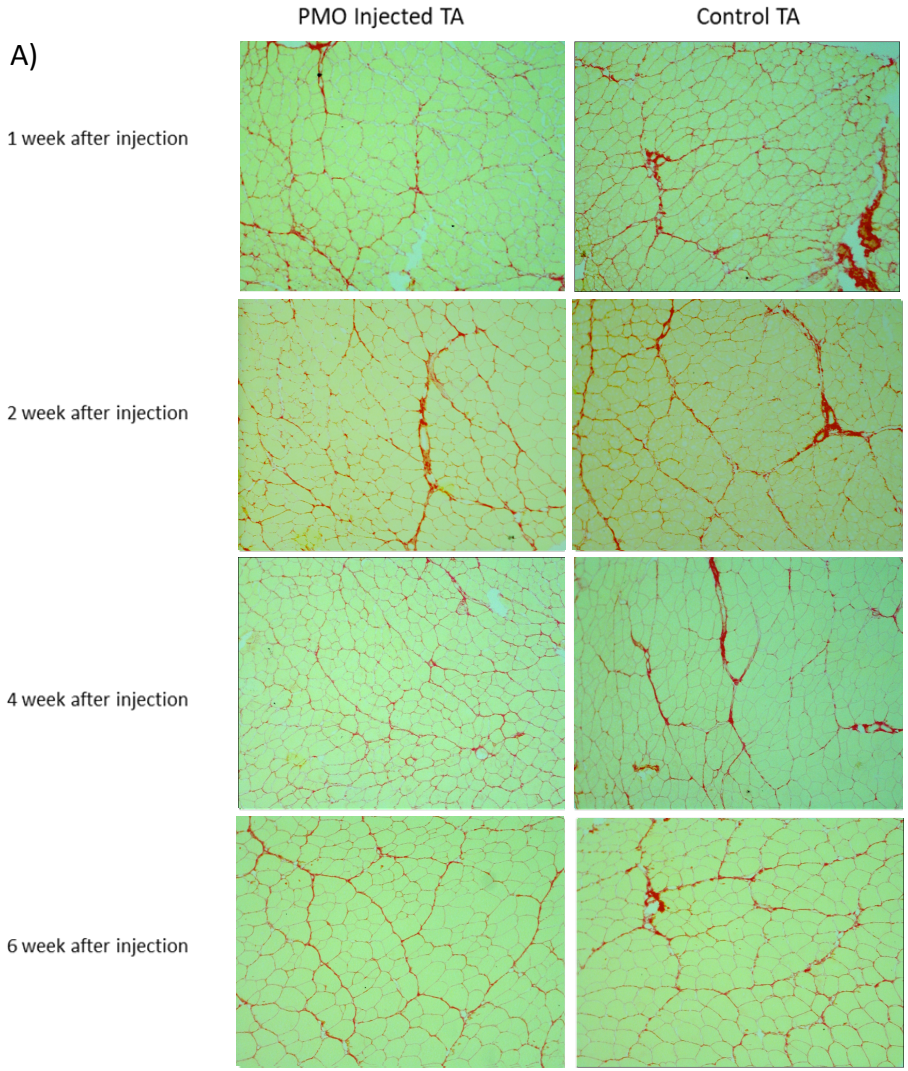
PMO Injected TA
Control TA
A)
1 week after injection
2 week after injection
4 week after injection
6 week after injection

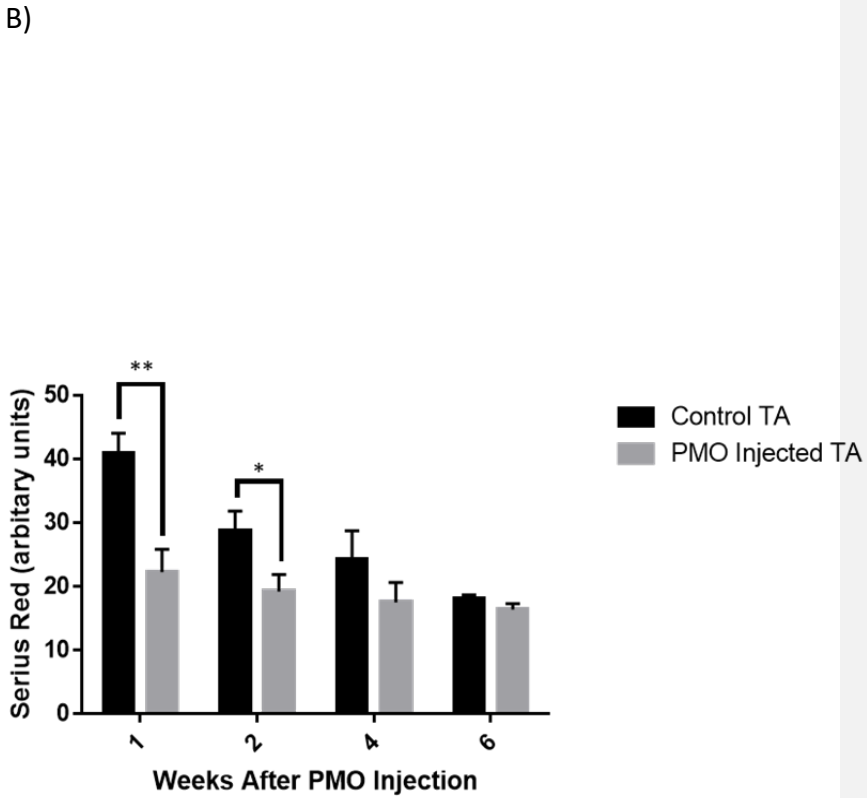
B)
**
*
Serius Red (arbitary units)
0
10
20
30
40
50
1
2
4
6
Weeks After PMO Injection
Control TA
PMO Injected TA

Figure 6.15 Analysis of Collagen I/III expression in TA muscles treated with$BaCl_2$ and PEX3.28.2 PMO

C57 mice were injected with $BaCl_2$ in both TA. 3 days after Ba_2Cl injection the left TA was injected with PEX3.28.2 PMO and the right TA with saline as a matched control. TA of mice were recovered 1, 2, 4 and 6 weeks after PMO injection. Cryosections (10µm) of TA muscle were prepared and stained for Collagen I and III using Sirius red staining.

A) Representative image of each time point in both control and PMO injected TA samples. Collagen I/III e shown in red (Magnification x10)

B) Red staining on sections was measured using image J and shown using arbitrary units. Statistical Significance was calculated using a T test (*p<0.05,**p<0.01, N=3).

6.2.2.4 Immunohistochemistry for Periostin, Fibronectin, Collagen VI and α-SMA

Tissue fibrosis was investigated in PMO treated mouse muscle, an *in vivo* model. Sections from TA muscle injected with $BaCl_2$ / Pex3.28.2 PMO and $BaCl_2$ /saline were stained for POSTN, fibronectin, collagen VI, and α-SMA as described in materials and methods and results are shown in Figures 6.16, 6.17, 6.18 and 6.19 respectively. Fibronectin, collagen VI and α-SMA are commonly used to look at tissue fibrosis (Specks *et al.*, 1995; Shi-Wen *et al.*, 2009; To and Midwood, 2011). All slides were co-stained with laminin to outline skeletal muscle fibres and Dapi to visualise nuclei. The staining revealed that there was no longer any necrosis at one week after PMO/saline injection, (3 days after $BaCl_2$ injection), but instead, the presence of regenerating fibres with centrally nucleated fibres was seen. These fibres appear narrow with heterogenous diameters. The fibres continued to regenerate up to six weeks after PMO/saline injection when the tissue had recovered mostly to normal morphology but showing central nuclei and varying fibre diameters.

As shown in section 6.2.1, POSTN is expressed in low amounts in healthy skeletal muscle and upregulated upon damage within regenerating fibres. It is restricted to the ECM upon recovery of muscle tissue to normal morphology (Özdemir *et al.*, 2014). 7 days after PMO injection (3 days after $BaCl_2$ injection) so 10 days after injury, POSTN was seen to be upregulated and mainly localised to the endomysial space (Figure 6.16), though this appeared to be more significant in control TA without PMO. POSTN levels gradually decreased in both control and PMO injected samples up until 6 weeks, showing visibly lower POSTN in PMO injected tissue at each time point; there were extremely low levels

in both control and PMO injected samples at 6 weeks, where muscle morphology was restored, as expected for healthy muscle.

Fibronectin protein is also expressed at extremely low levels in healthy muscle (section 6.2.1). Figure 6.17 shows fibronectin levels were upregulated and restricted to intracellular space in regenerating tissue at 1 week after PMO injection. At 14 days after injection fibronectin was limited to the interstitial space lining the regenerating fibres. Between 1 and 6 weeks after injection, fibronectin levels were seen to gradually reduce in both control and PMO injected sections but appear to be at a lower level in the PMO injected tissue. This mirrors the expression pattern seen in the POSTN stained sections.

Collagen VI (Figure 6.18) was upregulated and restricted to the enlarged interstitial space in the regenerating fibres. At 4 weeks and 6 weeks after PMO injection collagen VI staining intensity was visibly lower in the PMO treated samples in comparison to controls. At 6 weeks after injection both control and PMO injected samples showed close to normal morphology with healthy expression patterns of Collagen VI.

Figure 6.19 shows upregulation of α-SMA inside the regenerating fibres with visually higher levels seen in control sections compared to the PMO injected sections. This expression in both control and PMO injected samples is absent from 2 weeks after injection onwards with α-SMA only seen lining vessels. This suggests that tissue repair may be occurring in controls but is repressed by the PMO.

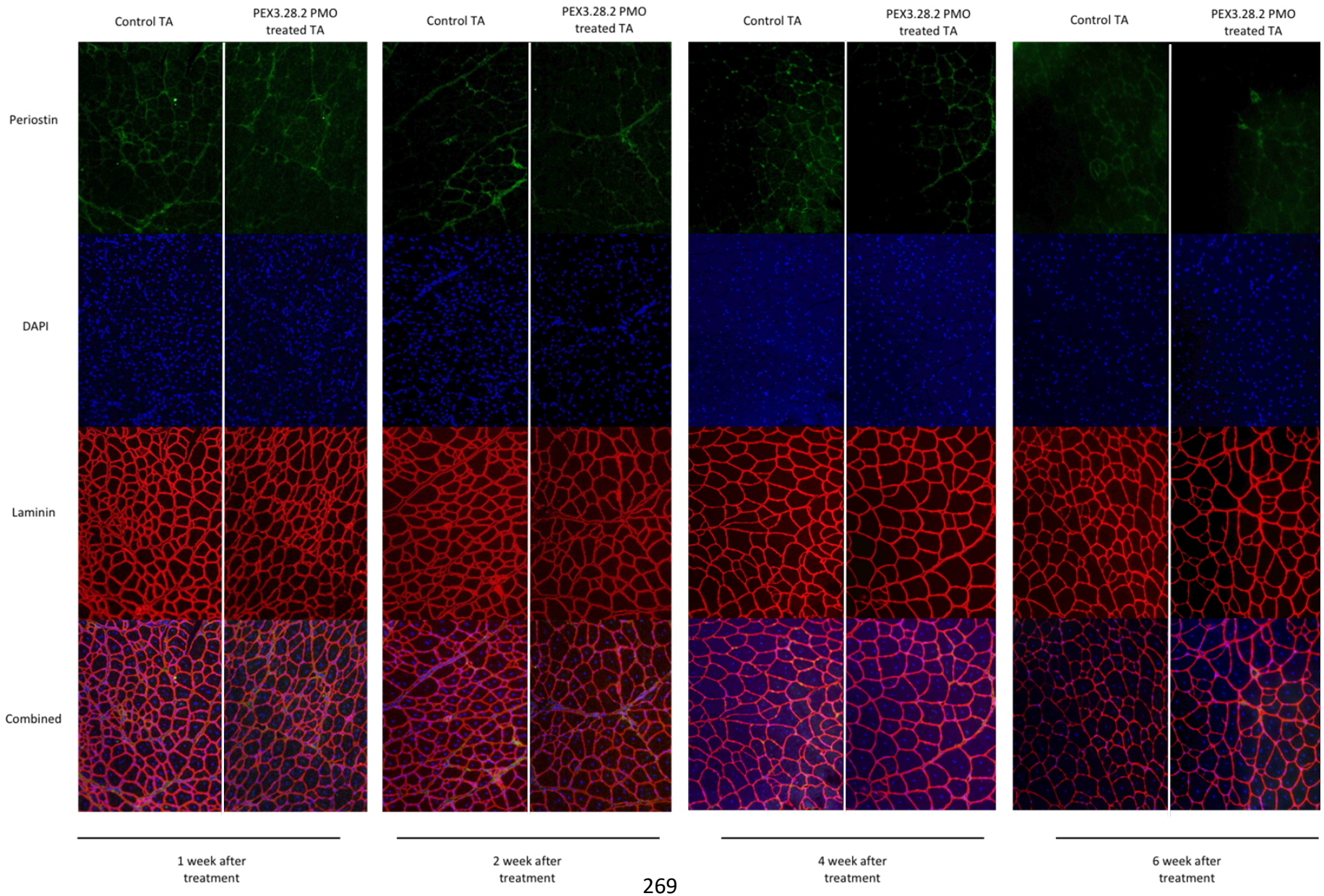
Control TA
PEX3.28.2 PMO treated TA
Control TA
PEX3.28.2 PMO treated TA
Control TA
PEX3.28.2 PMO treated TA
Control TA
PEX3.28.2 PMO treated TA
Periostin
DAPI
Laminin
Combined
1 week after treatment
2 week after treatment
4 week after treatment
6 week after treatment

Figure 6.16 Analysis of POSTN expression in TA Muscles treated with$BaCl_2$ and PEX3.28.2 PMO

C57 mice were injected with $BaCl_2$ in both TA. 3 days after Ba_2Cl injection the left TA was injected with PEX3.28.2 PMO and the right TA with saline as a control. TA of mice were recovered 1, 2, 4 and 6 weeks after PMO injection. Cryosections (10µm) of TA muscle were prepared and stained for POSTN, DAPI and laminin as described in Materials and Methods. Primary polyclonal antibody ab1404.was used for POSTN. Fluorescence-tagged secondary antibodies was used showing POSTN (green), laminin (red); DAPI (blue). Combined images with all three stains overlaid is shown (last row). (Magnification x20)

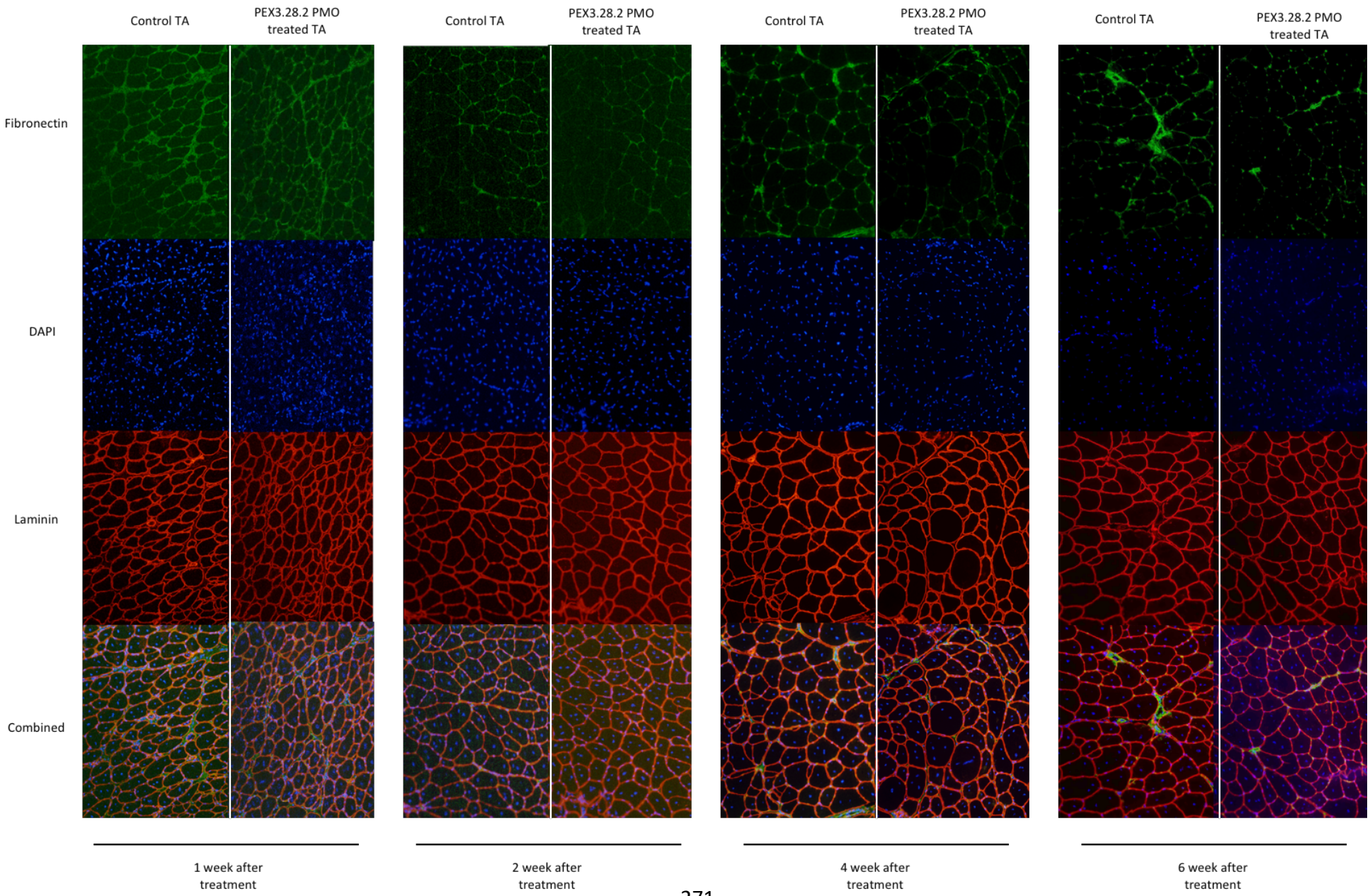
Control TA
PEX3.28.2 PMO treated TA
Control TA
PEX3.28.2 PMO treated TA
Control TA
PEX3.28.2 PMO treated TA
Control TA
PEX3.28.2 PMO treated TA
Fibronectin
DAPI
Laminin
Combined
1 week after treatment
2 week after treatment
4 week after treatment
6 week after treatment

Figure 6.17 Analysis of Fibronectin expression in TA Muscles treated with$BaCl_2$ and PEX3.28.2 PMO

C57 mice were injected with $BaCl_2$ in both TA. 3 days after $BaCl_2$ injection the left TA was injected with PEX3.28.2 PMO and the right TA with saline as control. TA of mice were recovered 1, 2, 4 and 6 weeks after PMO injection. Cryosections (10µm) of TA muscle were prepared and stained for fibronectin, DAPI and laminin as described in Materials and Methods. Primary polyclonal antibody ab2413was used for fibronectin. Fluorescence tagged secondary antibodies was used to anti-fibronectin (green), laminin (red); DAPI (blue). Combined images with all three stains overlaid is also shown (last row). (Magnification x20)

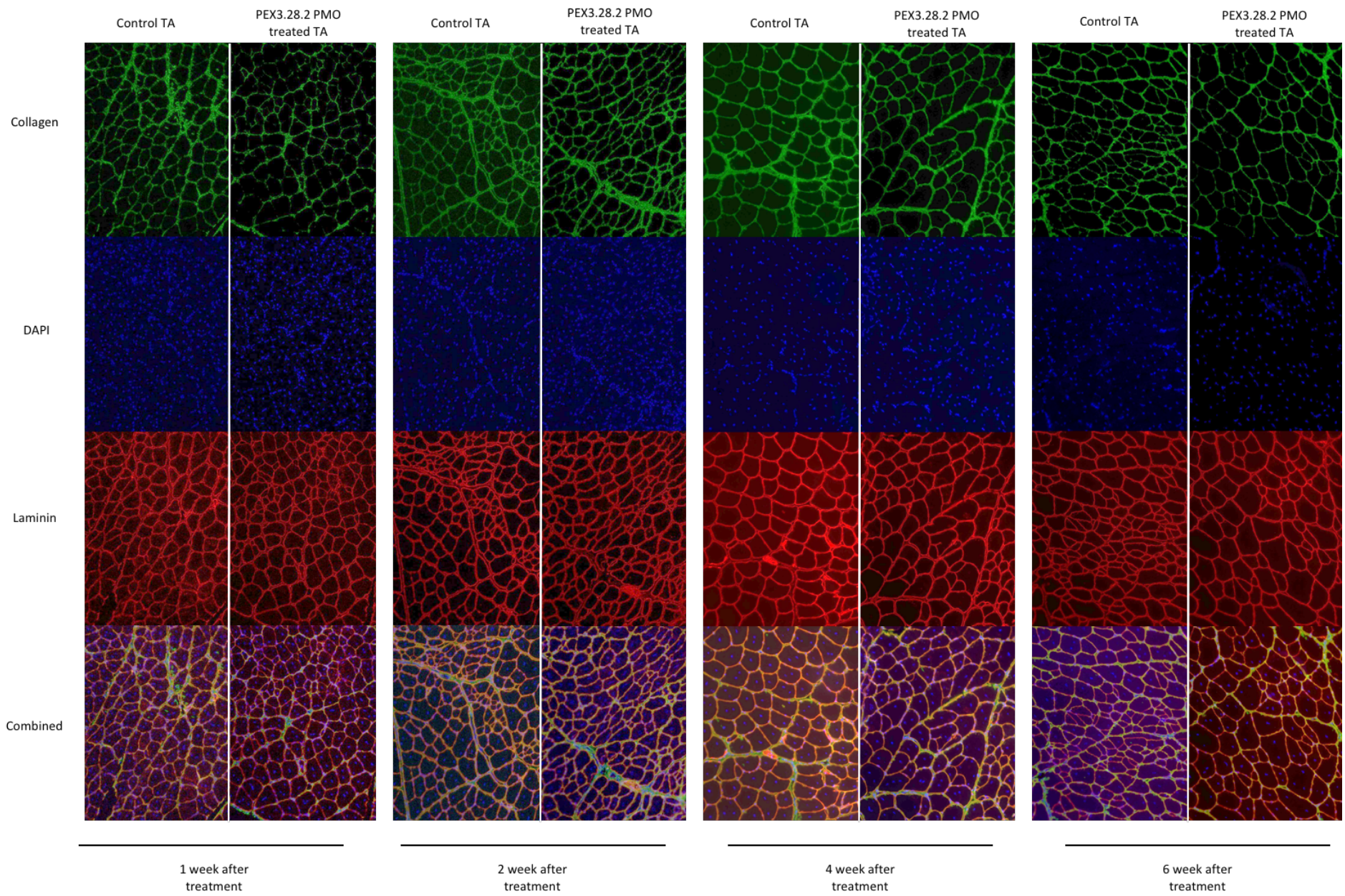
Control TA
PEX3.28.2 PMO treated TA
Control TA
PEX3.28.2 PMO treated TA
Control TA
PEX3.28.2 PMO treated TA
Control TA
PEX3.28.2 PMO treated TA
Collagen
DAPI
Laminin
Combined
1 week after treatment
2 week after treatment
4 week after treatment
6 week after treatment

Figure 6.18 Analysis of Collagen VI expression in TA Muscles treated with$BaCl_2$ and PEX3.28.2 PMO

C57 mice were injected with $BaCl_2$ in both TA. 3 days after $BaCl_2$ injection the left TA was injected with PEX3.28.2 PMO and the right TA with saline as a control. TA of mice were recovered 1, 2, 4 and 6 weeks after PMO injection. Cryosections (10µm) of TA muscle were prepared and stained for collagenVI, DAPI and laminin as described in Materials and Methods. Fluorescence-tagged secondary antibody was used showing Collagen (green), laminin (red); DAPI (blue). Combined images with all three stains overlaid is also shown (last row). (Magnification x20)

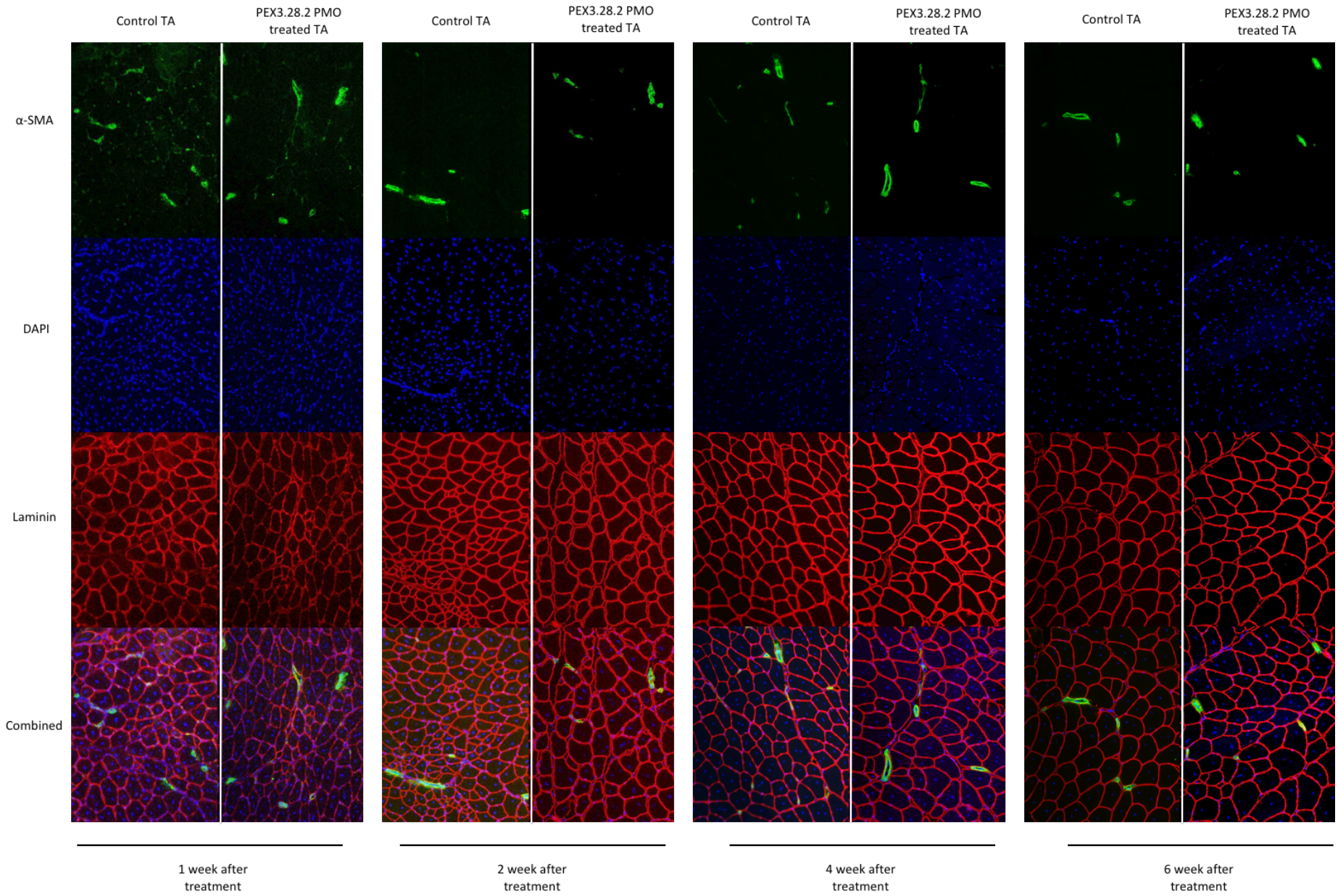
Control TA
PEX3.28.2 PMO treated TA
Control TA
PEX3.28.2 PMO treated TA
Control TA
PEX3.28.2 PMO treated TA
Control TA
PEX3.28.2 PMO treated TA
α-SMA
DAPI
Laminin
Combined
1 week after treatment
2 week after treatment
4 week after treatment
6 week after treatment

Figure 6.19 Analysis of α-SMA expression in TA muscles treated with$BaCl_2$ and PEX3.28.2 PMO

C57 mice were injected with $BaCl_2$ in both TA. 3 days after $BaCl_2$ injection the left TA was injected with PEX3.28.2 PMO and the right TA with saline as a control. TA of mice were recovered 1, 2, 4 and 6 weeks after PMO injection. Cryosections (10µm) of TA muscle were prepared and stained for α-SMA, DAPI and laminin as described in Materials and Methods. Primary polyclonal antibody ab5694 was used for α-SMA. Fluorescence-tagged secondary antibodies were used showing α-SMA (green), laminin (red); DAPI (blue). Combined images with all three stains overlaid is also shown (last row). (Magnification x20)

6.3 Discussion

6.3.1 Effect of $BaCl_2$ on TA of 24month old C57 mice

$BaCl_2$ intramuscular injection leads to necrosis of skeletal muscle tissue followed by regeneration and restoration of muscle morphology (Caldwell, Mattey and Weller, 1990; Hardy *et al.*, 2016). In this Chapter, we initially looked at the effect of intramuscular injection of $BaCl_2$ in TA of 24-month-old C57 mice which are more likely to exhibit a fibrotic phenotype. Our findings confirmed that $BaCl_2$ induces necrotic damage in the injected tissue, which then regenerates, after which normal morphology is restored with no scar tissue left behind. Interestingly, contrary to findings by Özdemir *et al.* (2014) where POSTN RNA levels were shown to be at their highest 7 days after $BaCl_2$ injection in rats, we show that in mice, POSTN RNA levels are at their peak 14 days after $BaCl_2$ injection. This may be a difference in the animal models and the age of the animals: the mice used in our study were 24 months old whereas the Sprague Dawley rats used by Özdemir were young, at 3 months old.

Immunohistochemistry studies of samples were also in agreement with protein expression results from the study on rats by Özdemir *et al.*; we demonstrated that POSTN protein expression in C57 mice was reduced, in comparison to control samples with healthy TA, one day after $BaCl_2$ injection when tissue is necrotic. At 3 days after injection, POSTN protein levels were increased in comparison to control samples and continued increasing to a peak at 7 days after injection. Contrary to the Özdemir studies in rats, where POSTN protein levels were restored to normal at day 10, in our hands, the 24-month-old mice showed elevated POSTN protein levels at day 14. This might be due

to the old age of the mice leading to slower regeneration and healing (di Schiaffino, Gorza and Parry, 1993; Joanisse *et al.*, 2016).

Collagen and fibronectin staining also confirmed that the effects of $BaCl_2$ injection were necrosis, regeneration then restoration of normal muscle morphology. Since POSTN has a role in the localisation of fibronectin and collagen to the ECM, the correlation between POSTN expression pattern and fibronectin and collagen expression patterns is as expected (Takayama, Arima and Kanaji, 2006; Butcher *et al.*, 2007; Kii *et al.*, 2010).

α SMA staining was successfully used to identify regenerating muscle as it is reported to be upregulated in activated myofibroblasts and repairing fibres and it is indeed seen to be expressed within regenerating fibres 7 days after injection (March *et al.*, 2018). It is worth mentioning that the limitation to this study was the limited sample size of 1.

The findings from this study show firstly, that POSTN is temporally expressed in regenerating and differentiating C57 TA muscle when damaged using intramuscular injection of $BaCl_2$. This made damage by $BaCl_2$ a suitable model upon which to induce POSTN expression and test exon skipping, using the PEX3.28.2 PMO designed and tested in previous chapters.

6.3.2 PEX3.28.2 induced Periostin exon 3 exclusion in $BaCl_2$ injected C57 mice

Having confirmed the effects of $BaCl_2$ intramuscular injection in C57 TA muscle and looked at changes in POSTN expression in response to $BaCl_2$ injected tissue, we looked at the effect of PEX3.28.2 PMO in damaged, $BaCl_2$ injected TA. PMO was injected into the damaged TA muscle 3 days after $BaCl_2$ injection when the fibres were regenerating and POSTN expression upregulated (section 6.3.1). We confirmed that PEX3.38.2 lead

to a successful reduction of POSTN expression at the RNA and protein levels. RNA levels quantified by RT-qPCR showed reduced POSTN levels in PMO injected samples compared to saline-injected samples, with reduced RNA levels in PMO injected samples maintained for up to 21 days after injection. 6 weeks after injection, POSTN levels could no longer be quantified, this could be due to very low levels of POSTN expression in the recovered muscle tissue, as expected. Protein expression patterns were examined by Western blots, which on the other hand show consistently reduced POSTN levels in the PMO injected samples; this effect remains even 6 weeks after injection.

Fibronectin RNA expression was not affected by PMO injection, but there was a reduction in protein level by Western blot. This work confirms literature showing that POSTN is involved in the transport of fibronectin protein to the ECM (Kudo, 2011) but suggests POSTN downregulation has no effect on fibronectin transcription *in vivo*, but at the protein level, translation of fibronectin is reduced (by the lower levels of Postn); Chapter 5 also suggests that reducing POSTN levels *in vitro* had a transcriptional effect on fibronectin transcription reducing fibronectin RNA levels. The work *in vivo* (this Chapter) indicates that the reduction in POSTN levels, achieved by PEX3.28.2 PMO, had no detrimental effect on muscle regeneration and repair as muscle morphology was restored in PMO injected samples no later, if not sooner, than control saline injected samples.

Fibronectin, Collagen I/III and Collagen VI levels were all reduced towards normal levels earlier in the PMO injected samples than the saline-injected samples in correlation with the appearance of normal muscle morphology indicating improved muscle recovery. This finding is in agreement with work by Lorts *et al.* (2012a) where sgcd -/-,postn-/-

mice showed enhanced regeneration. Hara *et al.* (2018) also showed improved muscle recovery after partial laceration injuries in samples treated with Postn-monoclonal antibody and suggested this was due to reduced fibroblast migration to the site of injury.

Statistical significance was not seen *in* vivo in response to PMO injection; however only 3 sets of control/experimental samples were generated and often one out of three showed a different result. This is to be expected *in vivo* as different mice will have different physiological responses to insult or the application of PMO may have been different in our hands. This could be due to loss of PMO in the regenerating fibres (Aoki *et al.*, 2013). The effect of PMO is likely transient due to protein turnover, and a weekly injection of PMO could be necessary in order to see a significant downregulation of POSTN.

It can, therefore, be concluded, secondly, that PEX3.28.2 was successful at decreasing POSTN expression both at RNA and protein levels *in vivo* after injection into TA muscle in old mice. Also, thirdly, that PMO application had no negative impact on tissue regeneration and repair. It also indicated that the reduction in POSTN levels using the PEX3.28.2 PMO lead to reduced localisation of fibrotic proteins such as Collagen and Fibronectin to the ECM, confirming that the downstream processing by POSTN was compromised by the PMO.

Though this *in vivo* model allows examination of the bioactivity of PEX3.28.2 and its safety, it is limited in that it is based on acute injury rather than chronic and so does not result in permanent fibrotic replacement of muscle tissue. The effect of POSTN downregulation on fibrosis and the fibrotic pathway is therefore yet to be assessed. In addition to this, though *POSTN* targeted PMOs shows an effect it may not be strong

enough to affect the regeneration/fibrosis pathways significantly and so it would be beneficial to test more potent knock down such as use of AAV-shRNAs for POSTN.

7. General discussion and conclusion

7.1 Summary of findings

7.1.1 Targeting PolyA signal to downregulate MSTN mRNA expression

In this thesis PMO AONs were designed to target the polyA signal in the Myostatin (MSTN) 3'UTR. The PMOs were tested in the RD cell system to see that they decreased MSTN mRNA expression; the bioactivity of the designed PMOs were compared to that of a published PMO targeting exon 3 of MSTN. The results from this experiment demonstrated that targeting the PolyA signal lead to successful downregulation of MSTN; however, targeting exon 3 to create an out-of-frame transcript of MSTN led to a more significant downregulation of total MSTN mRNA expression.

The experiments in Chapter 3 indicate that targeting gene expression through disruption of transcript reading frame is a more efficient method than targeting polyadenylation through binding to the polyA signal. Use of PMOs to target polyA signals was investigated in the FSHD disease model where DUX4 expression was altered through targeting of the polyadenylation process (Marsollier *et al.*, 2016). The potential disadvantage of targeting the polyA signal for expression knockdown is the ability of many human genes to use more than one polyA / cleavage site (Vickers *et al.*, 2001; Raz *et al.*, 2014); blocking one polyA signal could lead the cell to use an alternative. Another concern with targeting 3'UTR elements is the specificity of the designed PMOs as these elements are highly conserved between genes and also species (Verrotti *et al.*, 1996). It

is therefore likely that inducing an exon skip to disrupt the transcript reading frame using an AON is a more specific and efficient way to knockdown gene expression.

7.1.2 Designing PMO AONs to target out of frame exons in POSTN

In Chapter 4, AONs were created aimed at generating POSTN out-of-frame transcription products by exon skipping, in both human and mice. PMOs were designed bioinformatically, to exclude one of the out-of-frame exons 3, 7, 10 or 16. Human and mouse conserved sequences and position of ESE binding motifs within those conserved regions of the transcript were taken into consideration when designing the AON. Human Splicing Finder and ESEfinder were both used to identify and compare ESE binding motifs. Mfold was used to determine the secondary structure of the target sequence, whereas RNAup was utilised to analyse the binding position and the thermodynamic properties of the designed PMOs as well as their overall binding energy. As a result, 11 PMOs were designed.

7.1.3 PMO mediated exon exclusion of POSTN in-vitro

In Chapter 5, POSTN expression was stimulated using TGF-β treatment in *vitro* models: DMD human patient muscle cells; the murine C2C12 cell system and murine myofibroblast cells. Bioactivity of the designed PMOs was assessed in these cell systems and the PMO targeting exon 3 was shown to the most successful in human and mouse muscle cells as well as mouse fibroblast cells, showing statistical significance in both quantitative and semi-quantitative PCR analysis. The PMO was increased in length to a 28mer in order to increase binding energy and improve the efficiency of exon skipping. qPCR analysis of POSTN total mRNA expression proved to be a better read out of PMO

effectiveness in downregulation of POSTN mRNA. This also showed that POSTN downregulation *in vitro* leads to downregulation of fibronectin mRNA.

TGF-β treatment has been shown to stimulate POSTN expression (March *et al.*, 2018). Özdemir *et al.* (2014) also showed that POSTN expression in C2C12 cells is very low and increased significantly 48 hours after differentiation. In order for an AON to be effective, transcription of its target gene needs to be active for pre-mRNA to be produced and the AON to bind (Popplewell *et al.*, 2009; Mael-ainin *et al.*, 2014). It is therefore of importance to stimulate POSTN expression *in vitro* in order to investigate AON bioactivity. This is perhaps a limitation in testing POSTN targeted molecules *in vitro*. On the other hand, POSTN is stimulated in acute injury, making it a method for study in *in vivo* systems. It remains to be seen how closely a stimulated system matched the DMD model for POSTN expression.

Previous studies have shown overall binding energy to target and the length of PMO (which affects the former) to be the two most important factors affecting PMO bioactivity (Marsollier *et al.*, 2016). We confirmed these findings showing that the local position of binding of the PMO to the secondary structure to be less decisive in PMO success in exon exclusion, whereas the length of PMO significantly increased the success of PMO (Popplewell *et al.*, 2009).

POSTN is alternatively spliced with 6 protein-coding variants (Viloria and Hill, 2016) with additional isoforms expressed during foetal development. The role of these different splice variants is yet to be discovered, but it has been shown that the choice of C terminal, which is affected by alternative splicing, has functional significance. Highly tissue-specific expression patterns of POSTN have been reported (Wahab, Brinkman and

Mason, 2001; Morra and Moch, 2011) with isoform 1 expressed in heart tissue (Ensembl, accessed March 2016). POSTN expression *in vitro* and *in vivo* is therefore likely to be regulated in different ways and this should be taken into consideration when investigating POSTN downregulation *in vitro*.

7.1.4 Antisense modulation of POSTN expression in $BaCl_2$ injected C57 TA.

Chapter 6 explored the efficacy of the PMO in tissue repair *in vivo.* Healthy muscle tissue expresses low levels of POSTN as the TGF-β induced expression is not active (Özdemir *et al.*, 2014). In order to activate POSTN expression, muscle damage in mice was induced using $BaCl_2$ intramuscular injection. This study showed POSTN expression decreased one day after injection caused necrotic muscle tissue and then rose as myotubes began maturing. These findings were also reported by Özdemir *et al.* (2014) in rats injected with $BaCl_2$, so we confirmed that this pattern of expression of POSTN in regenerating muscle is conserved between the two species.

Following confirmation that POSTN expression significantly increases in maturing myotubes following $BaCl_2$ damage, data in Chapter 6 showed that injecting the damaged TA with the 28mer PMO, 3 days after $BaCl2_2$ injection, lead to a decrease in POSTN expression. The study also showed that fibronectin protein expression was also reduced in response to POSTN downregulation.

Other studies have previously reported the successful use of AONs to target POSTN expression. Tomaru (2017) showed that targeting of POSTN using AONs by direct administration into the fibrotic lungs of mice leads to a downregulation of POSTN, ameliorating pulmonary fibrosis. The mice were injected with 20µg of AON and harvested 22 days after injection. Periostin levels in the lung tissue were shown to

decrease significantly compared to mice injected with saline. This reduction of POSTN was also linked to a decrease in fibrotic changes in the lung as subpleural fibrosis and destruction of lung parenchymal architecture was less prominent. Mael Ainin *et al.* (2014) also reported that targeting POSTN, using a cocktail of two AONs directed to the ATG signal, protected the kidney from fibrosis following L-NAME injection. AONS cocktail was injected intraperitoneally every 24 hours with a pre-injection 48 hours before administration of L-NAME.

Our study also showed that damaged TA injected with PMO recovered at a faster rate than the control TA, with less collagen and fibronectin deposition in the ECM and lower intracellular α-SMA expression . Similar reports have been previously described by Lorts *et al.* (2012a) where POSTN was deleted in *Sgcs*$^{-/-}$ mice it led to enhanced tissue regeneration and reduced levels of fibrosis. Having said this, another study by Chen *et al.* (2017) reported that ablation of POSTN inhibited post-infraction myocardial regeneration in neonatal mice. This highlights the complexity of POSTN function and expression at different time points and in different tissues. More investigation into POSTN expression patterns, isoforms and function is required in order to target POSTN in a completely specific and safe way.

Although $BaCl_2$ induces muscle necrosis that is repaired by infiltration of mononuclear cells such as neutrophils and macrophages and subsequent regeneration, it does not lead to chronic inflammation and fibrosis (Hardy *et al.*, 2016). Therefore, though $BaCl_2$ injection increases POSTN expression and allows assessing bioactivity of AONs it is not a suitable model for investigating the subsequent effect of POSTN down-regulation on fibrosis.

7.2 Evaluation and future directions

The role of POSTN in fibrosis is rapidly expanding in various fields especially in lung, kidney and heart fibrotic disease. Periostin's role in skeletal muscle fibrosis in dystrophic muscle are virtually unexplored, and this work offers the first study in designing antisense oligonucleotides targeting POSTN expression through exon exclusion and disruption of the open reading frame. With significant results being achieved in the restoration of dystrophin in DMD models (Liang *et al.*, 2004; Lu-Nguyen *et al.*, 2017) the fibrosis of muscle tissue is one of the biggest barriers in humans when it comes to tackling DMD and restoring dystrophin (More in chapter 1). Multi-combinatorial treatment of DMD addressing fibrosis and restoration of dystrophin seems like the only logical way forward. Knockdown of POSTN is showing significant results in lowering fibrosis levels in models such as the heart, kidney, lung and skeletal muscle (Mael-ainin *et al.*, 2014; Zhao *et al.*, 2014; Semba *et al.*, 2018b).

Having shown the success of the designed Pex3.28.2 PMO in downregulation of POSTN *in vitro* and *in vivo*, it is important to investigate the effects of PMO induced POSTN knockdown in skeletal muscle of dystrophic models such as the *mdx* mouse, or the more fibrotic DMD rat where fibrosis is more similar to that found in human DMD muscle (Larcher, Lafoux, Tesson, Remy *et al.*, 2014). Following investigations into the effect of Periostin knockdown on muscle fibrosis in such models, it would then be logical to assess the effect of a multi-combinatorial treatment in the DMD rat where dystrophin is restored while POSTN and MSTN are downregulated.

We have shown that exclusion of exon 3 of POSTN, disrupting the open reading frame, is an effective way of reducing POSTN expression, but it is also worth noting that

targeting exon 3 would be targeting all POSTN isoforms. More investigation is required on POSTN expression in muscle tissue and the role of different POSTN isoforms in muscle function in order to assure the safety of downregulating all isoforms. Investigating muscle repair and regeneration in more detail in the absence or reduction of POSTN using AONs may provide valuable insight into POSTN function in muscle and fibrosis. It would also be preferable to test more extreme knock down of POSTN. Short hairpin RNA(shRNA) has been shown to be successful in efficient and reversible knockdown of target genes (Seibler *et al.,* 2007). Using shRNA would allow a more complete study into the full extent of POSTN knockdown on dystrophic muscle tissue and the fibrotic pathway.

8. Bibliography

{Romero, Norma B and Braun, Serge and Benveniste, Olivier and Leturcq, France and Hogrel, Jean-Yves and Morris, Glenn E and Barois, Annie and Eymard, Bruno and Payan, C. and O. (2004) 'Phase I study of dystrophin plasmid-based gene therapy in Duchenne/Becker muscular dystrophy', *Human gene therapy*, 15(11), pp. 1065–1076.

Aartsma-Rus, A. *et al.* (2002) 'Targeted exon skipping as a potential gene correction therapy for Duchenne muscular dystrophy.', *Neuromuscular disorders : NMD*, 12 Suppl 1, pp. S71-7. Available at: http://www.ncbi.nlm.nih.gov/pubmed/12206800 (Accessed: 10 February 2019).

Aartsma-Rus, A. *et al.* (2009) 'Antisense-Mediated Exon Skipping for Duchenne Muscular Dystrophy', *In: HUMAN GENE THERAPY. (pp. 660 - 661). MARY ANN LIEBERT INC (2009)* . MARY ANN LIEBERT INC. Available at: http://discovery.ucl.ac.uk/1332615/ (Accessed: 10 February 2019).

Aartsma-Rus, A., van Vliet, L., Hirschi, M., Janson, A. A. M., *et al.* (2009) 'Guidelines for antisense oligonucleotide design and insight into splice-modulating mechanisms.', *Molecular therapy : the journal of the American Society of Gene Therapy*. American Society of Gene & Cell Therapy, 17(3), pp. 548–53. doi: 10.1038/mt.2008.205.

Aartsma-Rus, A., van Vliet, L., Hirschi, M., Janson, A. A., *et al.* (2009) 'Guidelines for Antisense Oligonucleotide Design and Insight Into Splice-modulating Mechanisms', *Molecular Therapy*, 17(3), pp. 548–553. doi: 10.1038/mt.2008.205.

Aartsma-Rus, A. and van Ommen, G.-J. B. (2007) 'Antisense-mediated exon skipping: a versatile tool with therapeutic and research applications.', *RNA (New York, N.Y.)*. Cold Spring Harbor Laboratory Press, 13(10), pp. 1609–24. doi: 10.1261/rna.653607.

Abdel-Hamid, H. and Clemens, P. R. (2012) 'Pharmacological therapies for muscular dystrophies', *Current Opinion in Neurology*, 25(5). Available at: http://journals.lww.com/co-

neurology/Fulltext/2012/10000/Pharmacological_therapies_for_muscular_dystrophies.14.aspx.

Acuña, M. J. *et al.* (2014) 'Restoration of muscle strength in dystrophic muscle by angiotensin-1-7 through inhibition of TGF-β signalling', *Human Molecular Genetics* , 23(5), pp. 1237–1249. doi: 10.1093/hmg/ddt514.

Akpulat, U. *et al.* (2018) 'Shorter Phosphorodiamidate Morpholino Splice-Switching Oligonucleotides May Increase Exon-Skipping Efficacy in DMD.', *Molecular therapy. Nucleic acids*. American Society of Gene & Cell Therapy, 13, pp. 534–542. doi: 10.1016/j.omtn.2018.10.002.

Allen, H. D. *et al.* (2013) 'A Randomized , Double - Blind Trial of Lisinopril and Losartan for the Treatment of Cardiomyopathy in Duchenne Muscular Dystrophy'. doi: 10.1371/currents.md.2cc69a1dae4be7dfe2bcb420024ea865.Authors.

Amantana, A. and Iversen, P. L. (2005) 'Pharmacokinetics and biodistribution of phosphorodiamidate morpholino antisense oligomers', *Current Opinion in Pharmacology*. Elsevier, 5(5), pp. 550–555. doi: 10.1016/J.COPH.2005.07.001.

Amirouche, A. *et al.* (2009) 'Down-regulation of Akt/mammalian target of rapamycin signaling pathway in response to myostatin overexpression in skeletal muscle.', *Endocrinology*, 150(1), pp. 286–94. doi: 10.1210/en.2008-0959.

Amthor, H. and Hoogaars, W. M. H. (2012) 'Interference with myostatin/ActRIIB signaling as a therapeutic strategy for Duchenne muscular dystrophy.', *Current gene therapy*. Netherlands, 12(3), pp. 245–259.

Andreetta, F. *et al.* (2006) 'Immunomodulation of TGF-beta1 in mdx mouse inhibits connective tissue proliferation in diaphragm but increases inflammatory response: Implications for antifibrotic therapy', *Journal of Neuroimmunology*, 175(1–2), pp. 77–86. doi: http://dx.doi.org/10.1016/j.jneuroim.2006.03.005.

Aoki, Y. *et al.* (2013) 'Highly efficient in vivo delivery of PMO into regenerating myotubes and rescue in laminin-α2 chain-null congenital muscular dystrophy mice', *Human Molecular Genetics*, 22(24), pp. 4914–4928. doi: 10.1093/hmg/ddt341.

Ardite, E. *et al.* (2012) 'PAI-1–regulated miR-21 defines a novel age-associated fibrogenic pathway in muscular dystrophy', *The Journal of Cell Biology*, 196(1), p. 163 LP-175. Available at: http://jcb.rupress.org/content/196/1/163.abstract.

Argilés, J. M. *et al.* (2012) 'Myostatin: more than just a regulator of muscle mass.', *Drug discovery today*, 17(13–14), pp. 702–9. doi: 10.1016/j.drudis.2012.02.001.

Arnold, L. *et al.* (2007) 'Inflammatory monocytes recruited after skeletal muscle injury switch into antiinflammatory macrophages to support myogenesis', *The Journal of Experimental Medicine*, 204(5), p. 1057 LP-1069. Available at: http://jem.rupress.org/content/204/5/1057.abstract.

Attie, K. M. *et al.* (2013) 'A single ascending-dose study of muscle regulator ACE-031 in healthy volunteers.', *Muscle & nerve*. United States, 47(3), pp. 416–423. doi: 10.1002/mus.23539.

Bai, Y. *et al.* (2010) 'Novel Isoforms of Periostin Expressed in the Human Thyroid', *Japanese Clinical Medicine*, 1, p. JCM.S5899. doi: 10.4137/JCM.S5899.

Bao, S., Ouyang, G. and Bai, X. (2004) 'Periostin potently promotes metastatic growth of colon cancer by augmenting cell survival via the Akt/PKB pathway', *Cancer Cell*, 5. doi: 10.1016/S1535-6108(04)00081-9.

Barabino, S. M. and Keller, W. (1999) 'Last but not least: regulated poly(A) tail formation.', *Cell*. UNITED STATES, 99(1), pp. 9–11.

Baril, P., Gangeswaran, R. and Mahon, P. C. (2007) 'Periostin promotes invasiveness and resistance of pancreatic cancer cells to hypoxia-induced cell death: role of the beta4 integrin and the PI3k pathway', *Oncogene*, 26. doi: 10.1038/sj.onc.1210009.

Barth, M. L., Fensom, A. and Harris, A. (1993) 'Prevalence of common mutations in the arylsulphatase A gene in metachromatic leukodystrophy patients diagnosed in Britain.', *Human genetics*. GERMANY, 91(1), pp. 73–77.

Bell, C. D. and Conen, P. E. (1968) 'Histopathological changes in Duchenne muscular dystrophy', *Journal of the Neurological Sciences*, 7(3), pp. 529–544. doi: http://dx.doi.org/10.1016/0022-510X(68)90058-0.

Bertoni, C. *et al.* (2006) 'Enhancement of plasmid-mediated gene therapy for muscular dystrophy by directed plasmid integration', *Proceedings of the National Academy of Sciences of the United States of America* , 103(2), pp. 419–424. doi: 10.1073/pnas.0504505102.

Bish, L. T. *et al.* (2011) 'Chronic Losartan Administration Reduces Mortality and Preserves Cardiac but Not Skeletal Muscle Function in Dystrophic Mice', *PLoS ONE*. Public Library of Science, 6(6), pp. 1–6. doi: 10.1371/journal.pone.0020856.

Bo Li, Z., Zhang, J. and Wagner, K. R. (2012) 'Inhibition of myostatin reverses muscle fibrosis through apoptosis.', *Journal of cell science*, 125(Pt 17), pp. 3957–65. doi: 10.1242/jcs.090365.

Bogdanovich, S. *et al.* (2002) 'Functional improvement of dystrophic muscle by myostatin blockade', 420(November), pp. 418–421. doi: 10.1038/nature01242.1.

Bolster, D. R., Jefferson, L. S. and Kimball, S. R. (2004) 'Regulation of protein synthesis associated with skeletal muscle hypertrophy by insulin-, amino acid- and exercise-induced signalling.', *The Proceedings of the Nutrition Society*. England, 63(2), pp. 351–356. doi: 10.1079/PNS2004355.

Bonnet, N. *et al.* (2009) 'The Matricellular Protein Periostin Is Required for Sost Inhibition and the Anabolic Response to Mechanical Loading and Physical Activity', *The Journal of Biological Chemistry*. 9650 Rockville Pike, Bethesda, MD 20814, U.S.A.: American Society for Biochemistry and Molecular Biology, 284(51), pp. 35939–35950. doi: 10.1074/jbc.M109.060335.

Bornstein, P. *et al.* (1995) 'Metaxin, a gene contiguous to both thrombospondin 3 and glucocerebrosidase, is required for embryonic development in the mouse: implications for Gaucher disease', *Proceedings of the National Academy of Sciences* , 92(10), pp. 4547–4551. Available at: http://www.pnas.org/content/92/10/4547.abstract.

Bowen, T., Jenkins, R. H. and Fraser, D. J. (2013) 'MicroRNAs, transforming growth factor beta-1, and tissue fibrosis', *The Journal of Pathology*. John Wiley & Sons, Ltd, 229(2), pp. 274–285. doi: 10.1002/path.4119.

Bridges, L. R. (1986) 'The association of cardiac muscle necrosis and inflammation with

the degenerative and persistent myopathy of {MDX} mice', *Journal of the Neurological Sciences*, 72(2–3), pp. 147–157. doi: http://dx.doi.org/10.1016/0022-510X(86)90003-1.

Bulfield, G. *et al.* (1984) 'X chromosome-linked muscular dystrophy (mdx) in the mouse', *Proceedings of the National Academy of Sciences* , 81(4), pp. 1189–1192. Available at: http://www.pnas.org/content/81/4/1189.abstract.

Busquets, S. *et al.* (2012) 'Myostatin blockage using actRIIB antagonism in mice bearing the Lewis lung carcinoma results in the improvement of muscle wasting and physical performance', *Journal of Cachexia, Sarcopenia and Muscle*. Berlin/Heidelberg: Springer-Verlag, 3(1), pp. 37–43. doi: 10.1007/s13539-011-0049-z.

Butcher, J. T. *et al.* (2007) 'Periostin promotes atrioventricular mesenchyme matrix invasion and remodeling mediated by integrin signaling through Rho/PI 3-kinase', *Dev Biol*, 302. doi: 10.1016/j.ydbio.2006.09.048.

Caldwell, C. J., Mattey, D. L. and Weller, R. O. (1990) 'Role of the basement membrane in the regeneration of skeletal muscle.', *Neuropathology and applied neurobiology*, 16(3), pp. 225–38. Available at: http://www.ncbi.nlm.nih.gov/pubmed/2402330 (Accessed: 29 October 2018).

Callebaut, I. *et al.* (2003) '{EMI} domains are widespread and reveal the probable orthologs of the Caenorhabditis elegans CED-1 protein', *Biochemical and Biophysical Research Communications*, 300(3), pp. 619–623. doi: http://dx.doi.org/10.1016/S0006-291X(02)02904-2.

Campbell, C. and Jacob, P. (2003) 'Deflazacort for the treatment of Duchenne Dystrophy: A systematic review', *BMC Neurology*, 3(1), pp. 1–10. doi: 10.1186/1471-2377-3-7.

Caputi, M., Kendzior, R. J. and Beemon, K. L. (2002) 'A nonsense mutation in the fibrillin-1 gene of a Marfan syndrome patient induces NMD and disrupts an exonic splicing enhancer', *Genes & Development*, 16(14), pp. 1754–1759. doi: 10.1101/gad.997502.

Cartegni, L. *et al.* (2003) 'ESEfinder: A web resource to identify exonic splicing enhancers.', *Nucleic acids research*, 31(13), pp. 3568–71. Available at: http://www.ncbi.nlm.nih.gov/pubmed/12824367 (Accessed: 10 February 2019).

Cartegni, L. and Krainer, A. R. (2002) 'Disruption of an SF2/ASF-dependent exonic splicing enhancer in SMN2 causes spinal muscular atrophy in the absence of SMN1', *Nature Genetics*, 30(4), pp. 377–384. doi: 10.1038/ng854.

Casar, J. C. (2004) 'Heparan sulfate proteoglycans are increased during skeletal muscle regeneration: requirement of syndecan-3 for successful fiber formation', *Journal of Cell Science*, 117(1), pp. 73–84. doi: 10.1242/jcs.00828.

Castelhano-Barbosa, E. C. *et al.* (2005) 'Temporal and spatial expression of the myostatin gene during chicken embryo development.', *Growth, development, and aging : GDA*. United States, 69(1), pp. 3–12.

Chamberlain, J. R. and Chamberlain, J. S. (2017) 'Progress toward Gene Therapy for Duchenne Muscular Dystrophy', *Molecular Therapy*, 25(5), pp. 1125–1131. doi: 10.1016/j.ymthe.2017.02.019.

Chan, J. H., Lim, S. and Wong, W. F. (2006) 'ANTISENSE OLIGONUCLEOTIDES: FROM DESIGN TO THERAPEUTIC APPLICATION', *Clinical and Experimental Pharmacology and Physiology*, 33(5–6), pp. 533–540. doi: 10.1111/j.1440-1681.2006.04403.x.

Chu, M. L. *et al.* (1988) 'Amino acid sequence of the triple-helical domain of human collagen type VI.', *The Journal of biological chemistry*, 263(35), pp. 18601–6. Available at: http://www.ncbi.nlm.nih.gov/pubmed/3198591 (Accessed: 5 November 2018).

Chu, V. *et al.* (2002) 'Electrocardiographic findings in mdx mice: A cardiac phenotype of Duchenne muscular dystrophy', *Muscle & Nerve*. Wiley Subscription Services, Inc., A Wiley Company, 26(4), pp. 513–519. doi: 10.1002/mus.10223.

Colot, H. V, Stutz, F. and Rosbash, M. (1996) 'The yeast splicing factor Mud13p is a commitment complex component and corresponds to CBP20, the small subunit of the nuclear cap-binding complex.', *Genes & development*. UNITED STATES, 10(13), pp. 1699–1708.

Covi, J. A., Kim, H.-W. and Mykles, D. L. (2008) 'Expression of alternatively spliced transcripts for a myostatin-like protein in the blackback land crab, Gecarcinus lateralis.', *Comparative biochemistry and physiology. Part A, Molecular & integrative physiology*. United States, 150(4), pp. 423–430. doi: 10.1016/j.cbpa.2008.04.608.

Crawford, J. *et al.* (2015) 'Periostin induces fibroblast proliferation and myofibroblast persistence in hypertrophic scarring', *Experimental Dermatology*, 24(2), pp. 120–126. doi: 10.1111/exd.12601.

Dai, Y. *et al.* (1995) 'Cellular and humoral immune responses to adenoviral vectors containing factor IX gene: tolerization of factor IX and vector antigens allows for long-term expression.', *Proceedings of the National Academy of Sciences of the United States of America*. UNITED STATES, 92(5), pp. 1401–1405.

Danckwardt, S., Hentze, M. W. and Kulozik, A. E. (2008) '3' end mRNA processing: molecular mechanisms and implications for health and disease.', *The EMBO journal*, 27(3), pp. 482–98. doi: 10.1038/sj.emboj.7601932.

DANIALOU, G. *et al.* (2001) 'Dystrophin-deficient cardiomyocytes are abnormally vulnerable to mechanical stress-induced contractile failure and injury', *The FASEB Journal* , 15(9), pp. 1655–1657. Available at: http://www.fasebj.org/content/15/9/1655.short.

Desguerre, I. *et al.* (2009) 'Endomysial Fibrosis in Duchenne Muscular Dystrophy: A Marker of Poor Outcome Associated With Macrophage Alternative Activation', *Journal of Neuropathology & Experimental Neurology*, 68(7), p. 762 LP-773. Available at: http://jnen.oxfordjournals.org/content/68/7/762.abstract.

Desmet, F.-O. *et al.* (2009) 'Human Splicing Finder: an online bioinformatics tool to predict splicing signals', *Nucleic Acids Research*, 37(9), pp. e67–e67. doi: 10.1093/nar/gkp215.

Dickson, G., Hill, V. and Graham, I. R. (2002) 'Screening for antisense modulation of dystrophin pre-mRNA splicing.', *Neuromuscular disorders : NMD*, 12 Suppl 1, pp. S67-70. Available at: http://www.ncbi.nlm.nih.gov/pubmed/12206799 (Accessed: 10 February 2019).

Ding, Y., Chan, C. Y. and Lawrence, C. E. (2004) 'Sfold web server for statistical folding and rational design of nucleic acids.', *Nucleic acids research*. Oxford University Press, 32(Web Server issue), pp. W135-41. doi: 10.1093/nar/gkh449.

Duance, V. C. *et al.* (1980) 'A role for collagen in the pathogenesis of muscular

dystrophy?', *Nature*, 284(5755), pp. 470–472. Available at: http://dx.doi.org/10.1038/284470a0.

Dunckley, M. G. *et al.* (1993) 'Direct retroviral-mediated transfer of a dystrophin minigene into mdx mouse muscle in vivo', *Human Molecular Genetics* , 2(6), pp. 717–723. doi: 10.1093/hmg/2.6.717.

Dunckley, M. G. *et al.* (1998) 'Modification of splicing in the dystrophin gene in cultured Mdx muscle cells by antisense oligoribonucleotides.', *Human molecular genetics*. ENGLAND, 7(7), pp. 1083–1090.

Eagle, M. *et al.* (2016) 'Survival in Duchenne muscular dystrophy: improvements in life expectancy since 1967 and the impact of home nocturnal ventilation', *Neuromuscular Disorders*. Elsevier, 12(10), pp. 926–929. doi: 10.1016/S0960-8966(02)00140-2.

Egholm, M. *et al.* (1993) 'PNA hybridizes to complementary oligonucleotides obeying the Watson-Crick hydrogen-bonding rules.', *Nature*. ENGLAND, 365(6446), pp. 566–568. doi: 10.1038/365566a0.

Elbaz, M. *et al.* (2012) 'Losartan, a therapeutic candidate in congenital muscular dystrophy: Studies in the dy2J/dy2J Mouse', *Annals of Neurology*. Wiley Subscription Services, Inc., A Wiley Company, 71(5), pp. 699–708. doi: 10.1002/ana.22694.

Elkina, Y. *et al.* (2011) 'The role of myostatin in muscle wasting: an overview.', *Journal of cachexia, sarcopenia and muscle*, 2(3), pp. 143–151. doi: 10.1007/s13539-011-0035-5.

Fabani, M. M. and Gait, M. J. (2008) 'miR-122 targeting with LNA/2'-O-methyl oligonucleotide mixmers, peptide nucleic acids (PNA), and PNA-peptide conjugates.', *RNA (New York, N.Y.)*. United States, 14(2), pp. 336–346. doi: 10.1261/rna.844108.

Fairbrother, W. G. *et al.* (2002) 'Predictive Identification of Exonic Splicing Enhancers in Human Genes', *Science*, 297(5583), pp. 1007–1013. doi: 10.1126/science.1073774.

Fairbrother, W. G. *et al.* (2004) 'RESCUE-ESE identifies candidate exonic splicing enhancers in vertebrate exons', *Nucleic Acids Research*, 32(Web Server), pp. W187–W190. doi: 10.1093/nar/gkh393.

Farini, A. *et al.* (2007) 'T and B lymphocyte depletion has a marked effect on the fibrosis

of dystrophic skeletal muscles in the scid/mdx mouse', *The Journal of Pathology*. John Wiley & Sons, Ltd., 213(2), pp. 229–238. doi: 10.1002/path.2213.

Feener, C. A., Koenig, M. and Kunkel, L. M. (1989) 'Alternative splicing of human dystrophin mRNA generates isoforms at the carboxy terminus', *Nature*, 338(6215), pp. 509–511. Available at: http://dx.doi.org/10.1038/338509a0.

Fukada, S. *et al.* (2013) 'Isolation, characterization, and molecular regulation of muscle stem cells', *Frontiers in Physiology*, 4. doi: 10.3389/fphys.2013.00317.

Gebski, B. L. *et al.* (2003) 'Morpholino antisense oligonucleotide induced dystrophin exon 23 skipping in mdx mouse muscle.', *Human molecular genetics*. England, 12(15), pp. 1801–1811.

George Carlson, C. *et al.* (2011) 'Soluble activin receptor type IIB increases forward pulling tension in the mdx mouse.', *Muscle & nerve*. United States, 43(5), pp. 694–699. doi: 10.1002/mus.21944.

Giacca, M. (2010) 'Introduction to Gene Therapy', in *Gene Therapy*. Milano: Springer Milan, pp. 1–7. doi: 10.1007/978-88-470-1643-9_1.

Gibson, J. N., Smith, K. and Rennie, M. J. (1988) 'Prevention of disuse muscle atrophy by means of electrical stimulation: maintenance of protein synthesis.', *Lancet (London, England)*. ENGLAND, 2(8614), pp. 767–770.

Gibson, U. E. M., Heid, C. A. and Williams, P. M. (no date) 'A Novel Method for Real Time Quantitative RT-PCR'. Available at: https://genome.cshlp.org/content/6/10/995.full.pdf (Accessed: 7 June 2018).

Gilbert, R. *et al.* (2003) 'Prolonged dystrophin expression and functional correction of mdx mouse muscle following gene transfer with a helper-dependent (gutted) adenovirus-encoding murine dystrophin', *Human Molecular Genetics* , 12(11), pp. 1287–1299. doi: 10.1093/hmg/ddg141.

Glass, D. J. (2005) 'Skeletal muscle hypertrophy and atrophy signaling pathways.', *The international journal of biochemistry & cell biology*. England, 37(10), pp. 1974–1984. doi: 10.1016/j.biocel.2005.04.018.

Golshirazi, G. *et al.* (2018) 'Antisense Oligonucleotide Targeting of 3'-UTR of mRNA for Expression Knockdown', in, pp. 91–124. doi: 10.1007/978-1-4939-8651-4_6.

Gonzalez-Cadavid, N. F. *et al.* (1998) 'Organization of the human myostatin gene and expression in healthy men and HIV-infected men with muscle wasting.', *Proceedings of the National Academy of Sciences of the United States of America*. UNITED STATES, 95(25), pp. 14938–14943.

Gordon, S. (2003) 'Alternative activation of macrophages', *Nat Rev Immunol*, 3(1), pp. 23–35. Available at: http://dx.doi.org/10.1038/nri978.

Graham, I. R. *et al.* (2004) 'Towards a therapeutic inhibition of dystrophin exon 23 splicing inmdx mouse muscle induced by antisense oligoribonucleotides (splicomers): target sequence optimisation using oligonucleotide arrays', *The Journal of Gene Medicine*, 6(10), pp. 1149–1158. doi: 10.1002/jgm.603.

Gregorevic, P. *et al.* (2004) 'Systemic delivery of genes to striated muscles using adeno-associated viral vectors', *Nat Med*, 10(8), pp. 828–834. Available at: http://dx.doi.org/10.1038/nm1085.

Gregorevic, P. *et al.* (2006) 'rAAV6-microdystrophin preserves muscle function and extends lifespan in severely dystrophic mice', *Nat Med*. Nature Publishing Group, 12(7), pp. 787–789. Available at: http://dx.doi.org/10.1038/nm1439.

Griggs, R. C. *et al.* (1993) 'Duchenne dystrophy: Randomized, controlled trial of prednisone (18 months) and azathioprine (12 months)', *Neurology*, 43. doi: 10.1212/WNL.43.3_Part_1.520.

Grobet, L. *et al.* (2003) 'Modulating skeletal muscle mass by postnatal, muscle-specific inactivation of the myostatin gene.', *Genesis (New York, N.Y. : 2000)*, 35(4), pp. 227–38. doi: 10.1002/gene.10188.

Haecker, Sarah Ehlen and Stedman, Hansell H and Balice-Gordon, Rita J and Smith, Daniel BJ and Greelish, James P and Mitchell, Marilyn A and Wells, Amber and Sweeney, H Lee and Wilson, J. M. (1996) 'In vivo expression of full-length human dystrophin from adenoviral vectors deleted of all viral genes', *Human gene therapy*, 7(15), pp. 1907–1914.

Han, H. Q. and Mitch, W. E. (2011) 'Targeting the Myostatin Signalng Pathway to Treat Muscle Wasting Disease', *National Institute of Health*, 5(4), pp. 334–341. doi: 10.1097/SPC.0b013e32834bddf9.Targeting.

Hardy, D. *et al.* (2016) 'Comparative Study of Injury Models for Studying Muscle Regeneration in Mice.', *PloS one*. Public Library of Science, 11(1), p. e0147198. doi: 10.1371/journal.pone.0147198.

Hill, J. J. *et al.* (2002) 'The myostatin propeptide and the follistatin-related gene are inhibitory binding proteins of myostatin in normal serum.', *The Journal of biological chemistry*, 277(43), pp. 40735–41. doi: 10.1074/jbc.M206379200.

Ho, S. *et al.* (1996) 'Potent antisense oligonucleotides to the human multidrug resistance-1 mRNA are rationally selected by mapping RNA-accessible sites with oligonucleotide libraries', *Nucleic Acids Research*. Oxford University Press, 24(10), pp. 1901–1907. doi: 10.1093/nar/24.10.1901.

Hoersch, S. and Andrade-Navarro, M. A. (2010) 'Periostin shows increased evolutionary plasticity in its alternatively spliced region', *BMC Evolutionary Biology*, 10(1), pp. 1–19. doi: 10.1186/1471-2148-10-30.

Horiguchi, M., Ota, M. and Rifkin, D. B. (2012) 'Matrix control of transforming growth factor-β function', *Journal of Biochemistry* , 152(4), pp. 321–329. doi: 10.1093/jb/mvs089.

Huang, K.-L. *et al.* (2011) 'Developmental expression and alternative splicing of the duck myostatin gene.', *Comparative biochemistry and physiology. Part D, Genomics & proteomics*. Netherlands, 6(3), pp. 238–243. doi: 10.1016/j.cbd.2011.04.002.

Hübner, C. *et al.* (2004) 'Myostatin Mutation Associated with Gross Muscle Hypertrophy in a Child', *The New England Journal of Medicine*, (350), pp. 2682–8.

Ito, T. *et al.* (2013) 'Imatinib attenuates severe mouse dystrophy and inhibits proliferation and fibrosis-marker expression in muscle mesenchymal progenitors', *Neuromuscular Disorders*, 23(4), pp. 349–356. doi: http://dx.doi.org/10.1016/j.nmd.2012.10.025.

Jeanplong, F. *et al.* (2013) 'Discovery of a mammalian splice variant of myostatin that stimulates myogenesis', *PLoS ONE*, 8(12), p. e81713. doi: 10.1371/journal.pone.0081713.

Joanisse, S. *et al.* (2016) 'Exercise conditioning in old mice improves skeletal muscle regeneration', *The FASEB Journal*, 30(9), pp. 3256–3268. doi: 10.1096/fj.201600143RR.

Junqueira, L. C., Bignolas, G. and Brentani, R. R. (1979) 'Picrosirius staining plus polarization microscopy, a specific method for collagen detection in tissue sections.', *The Histochemical journal*, 11(4), pp. 447–55. Available at: http://www.ncbi.nlm.nih.gov/pubmed/91593 (Accessed: 28 October 2018).

Kadi, F. and Thornell, L. E. (1999) 'Training affects myosin heavy chain phenotype in the trapezius muscle of women.', *Histochemistry and cell biology*. GERMANY, 112(1), pp. 73–78.

Kafri, T. *et al.* (1997) 'Sustained expression of genes delivered directly into liver and muscle by lentiviral vectors', *Nat Genet*, 17(3), pp. 314–317. Available at: http://dx.doi.org/10.1038/ng1197-314.

Kamola, P. J. *et al.* (2015) '*In silico* and *in vitro* evaluation of exonic and intronic off-target effects form a critical element of therapeutic ASO gapmer optimization', *Nucleic Acids Research*, 43(18), pp. 8638–8650. doi: 10.1093/nar/gkv857.

Kang, J. K. *et al.* (2011a) 'Antisense-induced myostatin exon skipping leads to muscle hypertrophy in mice following octa-guanidine morpholino oligomer treatment.', *Molecular therapy : the journal of the American Society of Gene Therapy*. Nature Publishing Group, 19(1), pp. 159–64. doi: 10.1038/mt.2010.212.

Kang, J. K. *et al.* (2011b) 'Antisense-induced myostatin exon skipping leads to muscle hypertrophy in mice following octa-guanidine morpholino oligomer treatment.', *Molecular therapy : the journal of the American Society of Gene Therapy*. American Society of Gene & Cell Therapy, 19(1), pp. 159–64. doi: 10.1038/mt.2010.212.

Katsuragi, N. *et al.* (2004) 'Periostin as a Novel Factor Responsible for Ventricular Dilation', *Circulation*, 110, pp. 1806–1813. doi: 10.1161/01.CIR.0000142607.33398.54.

Kharraz, Y. *et al.* (2014) 'Understanding the process of fibrosis in duchenne muscular dystrophy', *BioMed Research International*, 2014. doi: 10.1155/2014/965631.

Kii, I. *et al.* (2010) 'Incorporation of tenascin-C into the extracellular matrix by periostin underlies an extracellular meshwork architecture', *Journal of Biological Chemistry*, 285(3), pp. 2028–2039. doi: 10.1074/jbc.M109.051961.

Kii, I., Nishiyama, T. and Kudo, A. (2016) 'Periostin promotes secretion of fibronectin from the endoplasmic reticulum', *Biochemical and Biophysical Research Communications*, 470(4), pp. 888–893. doi: 10.1016/j.bbrc.2016.01.139.

Kim, J. E., Kim, S. J. and Lee, B. H. (2000) 'Identification of motifs for cell adhesion within the repeated domains of transforming growth factor-beta-induced gene, betaig-h3', *J Biol Chem*, 275. doi: 10.1074/jbc.M002752200.

Kimura, E. *et al.* (2009) 'Dystrophin Delivery to Muscles of mdx Mice Using Lentiviral Vectors Leads to Myogenic Progenitor Targeting and Stable Gene Expression', *Mol Ther*. The American Society of Gene & Cell Therapy, 18(1), pp. 206–213. Available at: http://dx.doi.org/10.1038/mt.2009.253.

Kinali, M. *et al.* (2009a) 'Local restoration of dystrophin expression with the morpholino oligomer AVI-4658 in Duchenne muscular dystrophy: a single-blind, placebo-controlled, dose-escalation, proof-of-concept study.', *The Lancet. Neurology*. England, 8(10), pp. 918–928. doi: 10.1016/S1474-4422(09)70211-X.

Kinali, M. *et al.* (2009b) 'Local restoration of dystrophin expression with the morpholino oligomer AVI-4658 in Duchenne muscular dystrophy: a single-blind, placebo-controlled, dose-escalation, proof-of-concept study.', *The Lancet. Neurology*. England, 8(10), pp. 918–928. doi: 10.1016/S1474-4422(09)70211-X.

Kissel, J. T. *et al.* (1991) 'Mononuclear cell analysis of muscle biopsies in prednisone-treated and untreated Duchenne muscular dystrophy', *Neurology* , 41(5), pp. 667–672. doi: 10.1212/WNL.41.5.667.

Kjær, M. *et al.* (2009) 'From mechanical loading to collagen synthesis, structural changes and function in human tendon', *Scandinavian Journal of Medicine & Science in Sports*. Blackwell Publishing Ltd, 19(4), pp. 500–510. doi: 10.1111/j.1600-0838.2009.00986.x.

Klingler, W. *et al.* (2012) 'The role of fibrosis in Duchenne muscular dystrophy', *Acta Myologica*, pp. 184–195.

Knupp, C. and Squire, J. M. (2001) 'A new twist in the collagen story--the type VI segmented supercoil', *The EMBO Journal*, 20(3), pp. 372–376. doi: 10.1093/emboj/20.3.372.

Koenig, M. *et al.* (1989) 'The molecular basis for Duchenne versus Becker muscular dystrophy: Correlation of severity with type of deletion', *American Journal of Human Genetics*, 45(4), pp. 498–506. Available at: http://www.ncbi.nlm.nih.gov/pmc/articles/PMC1683519/.

Konieczny, P., Swiderski, K. and Chamberlain, J. S. (2013) 'Gene and cell-mediated therapies for muscular dystrophy', *Muscle & Nerve*, 47(5), pp. 649–663. doi: 10.1002/mus.23738.

Kudo, A. (2011) 'Periostin in fibrillogenesis for tissue regeneration: periostin actions inside and outside the cell', *Cellular and Molecular Life Sciences*, 68(19), pp. 3201–3207. doi: 10.1007/s00018-011-0784-5.

Kuhn, U. and Wahle, E. (2004) 'Structure and function of poly(A) binding proteins.', *Biochimica et biophysica acta*. Netherlands, 1678(2–3), pp. 67–84. doi: 10.1016/j.bbaexp.2004.03.008.

Lai, Y. *et al.* (2005) 'Efficient in vivo gene expression by trans-splicing adeno-associated viral vectors', *Nat Biotech*. Nature Publishing Group, 23(11), pp. 1435–1439. Available at: http://dx.doi.org/10.1038/nbt1153.

Larcher, T., Lafoux, A., Tesson, L., Remy, S., *et al.* (2014) 'Characterization of dystrophin deficient rats: a new model for Duchenne muscular dystrophy.', *PloS one*. United States, 9(10), p. e110371. doi: 10.1371/journal.pone.0110371.

Larcher, T., Lafoux, A., Tesson, L., Remy, S. V., *et al.* (2014) 'Characterization of dystrophin deficient rats: A new model for duchenne muscular dystrophy', *PLoS ONE*, 9(10). doi: 10.1371/journal.pone.0110371.

Lee, S.-J. (2004) 'Regulation of muscle mass by myostatin.', *Annual review of cell and*

developmental biology, 20, pp. 61–86. doi: 10.1146/annurev.cellbio.20.012103.135836.

Li, G. *et al.* (2006) 'Phosphatidylinositol-3-kinase signaling mediates vascular smooth muscle cell expression of periostin in vivo and in vitro.', *Atherosclerosis*. NIH Public Access, 188(2), pp. 292–300. doi: 10.1016/j.atherosclerosis.2005.11.002.

Liang, K. W. *et al.* (2004) 'Restoration of dystrophin expression in mdx mice by intravascular injection of naked DNA containing full-length dystrophin cDNA', *Gene Ther*, 11(11), pp. 901–908. Available at: http://dx.doi.org/10.1038/sj.gt.3302239.

Litvin, J., Selim, A. and Montgomery, M. O. (2004) 'Expression and function of periostin-isoforms in bone', *J Cell Biochem*, 92. doi: 10.1002/jcb.20115.

Liu, H. X. *et al.* (2000) 'Exonic splicing enhancer motif recognized by human SC35 under splicing conditions.', *Molecular and cellular biology*, 20(3), pp. 1063–71. Available at: http://www.ncbi.nlm.nih.gov/pubmed/10629063 (Accessed: 10 February 2019).

Liu, H. X., Zhang, M. and Krainer, A. R. (1998) 'Identification of functional exonic splicing enhancer motifs recognized by individual SR proteins.', *Genes & development*, 12(13), pp. 1998–2012. Available at: http://www.ncbi.nlm.nih.gov/pubmed/9649504 (Accessed: 10 February 2019).

Liu, X. *et al.* (2005) 'Spliceosome-Mediated RNA Trans -Splicing with Recombinant Adeno-Associated Virus Partially Restores Cystic Fibrosis Transmembrane Conductance Regulator Function to Polarized Human Cystic Fibrosis Airway Epithelial Cells', *Human Gene Therapy*, 16(9), pp. 1116–1123. doi: 10.1089/hum.2005.16.1116.

Lorts, A. *et al.* (2012) 'Deletion of periostin reduces muscular dystrophy and fibrosis in mice by modulating the transforming growth factor-β pathway', *Proceedings of the National Academy of Sciences* , 109(27), pp. 10978–10983. doi: 10.1073/pnas.1204708109.

Love, D. R. *et al.* (1989) 'An autosomal transcript in skeletal muscle with homology to dystrophin', *Nature*, 339(6219), pp. 55–58. Available at: http://dx.doi.org/10.1038/339055a0.

Lu-Nguyen, N. *et al.* (2017) 'Systemic Antisense Therapeutics for Dystrophin and

Myostatin Exon Splice Modulation Improve Muscle Pathology of Adult mdx Mice.', *Molecular therapy. Nucleic acids*. American Society of Gene & Cell Therapy, 6, pp. 15–28. doi: 10.1016/j.omtn.2016.11.009.

Lu-Nguyen, N. B. *et al.* (2015) 'Combination Antisense Treatment for Destructive Exon Skipping of Myostatin and Open Reading Frame Rescue of Dystrophin in Neonatal mdx Mice', *Molecular Therapy*, 23(8), pp. 1341–1348. doi: 10.1038/mt.2015.88.

Lu, A. *et al.* (2014) 'Rapid depletion of muscle progenitor cells in dystrophic mdx/utrophin-/- mice.', *Human molecular genetics*. Oxford University Press, 23(18), pp. 4786–800. doi: 10.1093/hmg/ddu194.

Maccatrozzo, L. *et al.* (2001) 'A novel second myostatin gene is present in teleost fish.', *FEBS letters*. Netherlands, 509(1), pp. 36–40.

Mael-ainin, M. *et al.* (2014) 'Inhibition of Periostin Expression Protects against the Development of Renal In fl ammation and Fibrosis', pp. 1–13. doi: 10.1681/ASN.2013060664.

Malerba, A., Kang, J. K., McClorey, G., Saleh, A. F., Popplewell, L., Gait, M. J., Wood, M. J., *et al.* (2012) 'Dual Myostatin and Dystrophin Exon Skipping by Morpholino Nucleic Acid Oligomers Conjugated to a Cell-penetrating Peptide Is a Promising Therapeutic Strategy for the Treatment of Duchenne Muscular Dystrophy.', *Molecular therapy. Nucleic acids*, 1(October), p. e62. doi: 10.1038/mtna.2012.54.

Malerba, A., Kang, J. K., McClorey, G., Saleh, A. F., Popplewell, L., Gait, M. J., Wood, M. J., *et al.* (2012) 'Dual Myostatin and Dystrophin Exon Skipping by Morpholino Nucleic Acid Oligomers Conjugated to a Cell-penetrating Peptide Is a Promising Therapeutic Strategy for the Treatment of Duchenne Muscular Dystrophy', *Molecular Therapy - Nucleic Acids*, 1, p. e62. doi: 10.1038/mtna.2012.54.

Maniatis, T. *et al.* (1976) 'Amplification and characterization of a beta-globin gene synthesized in vitro.', *Cell*. ENGLAND, 8(2), pp. 163–182.

Mann, C. J. *et al.* (2002) 'Improved antisense oligonucleotide induced exon skipping in themdx mouse model of muscular dystrophy', *The Journal of Gene Medicine*, 4(6), pp. 644–654. doi: 10.1002/jgm.295.

March, J. *et al.* (2018) 'Targeting TGFβ Signaling to Address Fibrosis Using Antisense Oligonucleotides', *Biomedicines*. Multidisciplinary Digital Publishing Institute, 6(3), p. 74. doi: 10.3390/biomedicines6030074.

Marsollier, A.-C. *et al.* (2016) 'Antisense targeting of 3' end elements involved in *DUX4* mRNA processing is an efficient therapeutic strategy for facioscapulohumeral dystrophy: a new gene-silencing approach', *Human Molecular Genetics*, 25(8), pp. 1468–1478. doi: 10.1093/hmg/ddw015.

Maruhashi, T. *et al.* (2010) 'Interaction between Periostin and BMP-1 Promotes Proteolytic Activation of Lysyl Oxidase * □', 285(17), pp. 13294–13303. doi: 10.1074/jbc.M109.088864.

Mathews, D. H. and Turner, D. H. (2006) 'Prediction of RNA secondary structure by free energy minimization', *Current Opinion in Structural Biology*, 16(3), pp. 270–278. doi: 10.1016/j.sbi.2006.05.010.

Matsumura, K., Campbell, K. P. and Nonaka, I. (1993) 'Abnormal expression of dystrophin-associated proteins in Fukuyama-type congenital muscular dystrophy', *The Lancet*, 341(8844), pp. 521–522. doi: http://dx.doi.org/10.1016/0140-6736(93)90279-P.

Mauro, a. (1961) 'Satellite Cell of Skeletal Muscle Fibers', *Journal of Biophysics and Biochemistry Cytology*, 9(2), pp. 493–495. doi: 10.1083/jcb.9.2.493.

McArdle, A., Edwards, R. H. T. and Jackson, M. J. (2016) 'How does dystrophin deficiency lead to muscle degeneration? — Evidence from the MDX mouse', *Neuromuscular Disorders*. Elsevier, 5(6), pp. 445–456. doi: 10.1016/0960-8966(95)00001-4.

McDonald, C. M. *et al.* (1995) 'PROFILES OF NEUROMUSCULAR DISEASES: Duchenne Muscular Dystrophy.', *American Journal of Physical Medicine & Rehabilitation*, 74(5). Available at: http://journals.lww.com/ajpmr/Fulltext/1995/09001/PROFILES_OF_NEUROMUSCULAR_DISEASES__Duchenne.3.aspx.

McLoon, L. K. (2008) 'Focusing on fibrosis: halofuginone-induced functional improvement in the *mdx* mouse model of Duchenne muscular dystrophy', *American*

Journal of Physiology-Heart and Circulatory Physiology, 294(4), pp. H1505–H1507. doi: 10.1152/ajpheart.00176.2008.

McPherron, A. C., Lawler, A. M. and Lee, S.-J. (1997) 'Regulation of skeletal muscle mass in mice by a new TGF-p superfamily member', *Nature*, 387(6628), pp. 83–90. Available at: http://dx.doi.org/10.1038/387083a0.

McPherron, A. C. and Lee, S.-J. (2002) 'Suppression of body fat accumulation in myostatin-deficient mice.', *The Journal of clinical investigation*. United States, 109(5), pp. 595–601. doi: 10.1172/JCI13562.

McPherron, A. C. and Lee, S. (1997) 'Double muscling in cattle due to mutations in the myostatin gene', *Proc. Natl. Acad. Scie. USA*, 94(November), pp. 12457–12461.

Ménissier, F. (1982) 'Present State of Knowledge About the Genetic Determination of Muscular Hypertrophy or the Double Muscled Trait in Cattle', in King, J. W. B. and Ménissier, F. (eds) *Muscle Hypertrophy of Genetic Origin and its use to Improve Beef Production SE - 34*. Springer Netherlands (Current Topics in Veterinary Medicine and Animal Science), pp. 387–428. doi: 10.1007/978-94-009-7550-7_34.

Merle, B. and Garnero, P. (2012) 'The multiple facets of periostin in bone metabolism', *Osteoporosis International*, 23(4), pp. 1199–1212. doi: 10.1007/s00198-011-1892-7.

Merlini, L. *et al.* (2003) 'Early prednisone treatment in Duchenne muscular dystrophy', *Muscle & Nerve*. Wiley Subscription Services, Inc., A Wiley Company, 27(2), pp. 222–227. doi: 10.1002/mus.10319.

Michelle H. Nelson *et al.* (2005) 'Arginine-Rich Peptide Conjugation to Morpholino Oligomers: Effects on Antisense Activity and Specificity'. American Chemical Society . doi: 10.1021/BC0501045.

Molnar, M. J. *et al.* (2004) 'Factors Influencing the Efficacy, Longevity, and Safety of Electroporation-Assisted Plasmid-Based Gene Transfer into Mouse Muscles', *Mol Ther*, 10(3), pp. 447–455. Available at: http://dx.doi.org/10.1016/j.ymthe.2004.06.642.

Morales, M. G. *et al.* (2013) 'Reducing CTGF/CCN2 slows down mdx muscle dystrophy and improves cell therapy', *Human Molecular Genetics* , 22(24), pp. 4938–4951. doi:

10.1093/hmg/ddt352.

Morine, K. J. *et al.* (2010) 'Systemic Myostatin Inhibition via Liver-Targeted Gene Transfer in Normal and Dystrophic Mice', *PLoS ONE*. Public Library of Science, 5(2), p. e9176. Available at: http://dx.doi.org/10.1371/journal.pone.0009176.

Morita, H. and Komuro, I. (2016) 'Periostin Isoforms and Cardiac Remodeling After Myocardial Infarction', *Hypertension*. Lippincott Williams & WilkinsHagerstown, MD, 67(3), pp. 504–505. doi: 10.1161/HYPERTENSIONAHA.115.06449.

Morra, L. *et al.* (2012) 'Characterization of periostin isoform pattern in non-small cell lung cancer', *Lung Cancer*, 76(2), pp. 183–190. doi: 10.1016/j.lungcan.2011.10.013.

Morra, L. and Moch, H. (2011) 'Periostin expression and epithelial-mesenchymal transition in cancer: a review and an update', *Virchows Archiv*, 459(5), pp. 465–475. doi: 10.1007/s00428-011-1151-5.

Morral, N. *et al.* (1999) 'Administration of helper-dependent adenoviral vectors and sequential delivery of different vector serotype for long-term liver-directed gene transfer in baboons', *Proceedings of the National Academy of Sciences* , 96(22), pp. 12816–12821. doi: 10.1073/pnas.96.22.12816.

Morrison, J. *et al.* (no date) 'T-Cell-Dependent Fibrosis in the mdx Dystrophic Mouse', *Lab Invest*, 80(6), pp. 881–891. Available at: http://dx.doi.org/10.1038/labinvest.3780092.

Murphy, K. T. *et al.* (2011) 'Antibody-directed myostatin inhibition enhances muscle mass and function in tumor-bearing mice.', *American journal of physiology. Regulatory, integrative and comparative physiology*, 301(3), pp. R716-26. doi: 10.1152/ajpregu.00121.2011.

Naldini, L. *et al.* (1996) 'In vivo gene delivery and stable transduction of nondividing cells by a lentiviral vector.', *Science (New York, N.Y.)*, 272(5259), pp. 263–7. doi: 10.1126/science.272.5259.263.

Niebroj-dobosz, I. *et al.* (2001) 'Does Normal Nitric Oxide Synthase Prevent Pathologic Muscle Changes in Dystrophin Deficiency ?', *BAM-PADOVA*, 11(2), pp. 105–110.

Nishiyama, T. *et al.* (2011) 'Delayed Re-Epithelialization in Periostin-Deficient Mice during Cutaneous Wound Healing', *PLoS ONE*. Public Library of Science, 6(4), pp. 1–14. doi: 10.1371/journal.pone.0018410.

Nolan, T., Hands, R. E. and Bustin, S. A. (2006) 'Quantification of mRNA using real-time RT-PCR', *Nature Protocols*, 1(3), pp. 1559–1582. doi: 10.1038/nprot.2006.236.

Norris, R. A., Damon, B. and Mironov, V. (2007) 'Periostin regulates collagen fibrillogenesis and the biomechanical properties of connective tissues', *J Cell Biochem*, 101. doi: 10.1002/jcb.21224.

O'Brien, K. F. and Kunkel, L. M. (2001) 'Dystrophin and muscular dystrophy: past, present, and future.', *Molecular genetics and metabolism*. United States, 74(1–2), pp. 75–88. doi: 10.1006/mgme.2001.3220.

Oka, T., Xu, J. and Kaiser, R. A. (2007) 'Genetic manipulation of periostin expression reveals a role in cardiac hypertrophy and ventricular remodeling', *Circ Res*, 101. doi: 10.1161/CIRCRESAHA.107.149047.

Ontsuka, K. *et al.* (2012) 'Periostin, a matricellular protein, accelerates cutaneous wound repair by activating dermal fibroblasts', *Experimental Dermatology*. Blackwell Publishing Ltd, 21(5), pp. 331–336. doi: 10.1111/j.1600-0625.2012.01454.x.

Özdemir, C. *et al.* (2014) 'Periostin is temporally expressed as an extracellular matrix component in skeletal muscle regeneration and differentiation', *Gene*. Elsevier, 553(2), pp. 130–139. doi: 10.1016/J.GENE.2014.10.014.

PARTRIDGE, T. (1991) 'Animal models of muscular dystrophy – what can they teach us?', *Neuropathology and Applied Neurobiology*. Blackwell Publishing Ltd, 17(5), pp. 353–363. doi: 10.1111/j.1365-2990.1991.tb00735.x.

Passaquin, A. C. *et al.* (1993) 'Prednisolone enhances myogenesis and dystrophin-related protein in skeletal muscle cell cultures from mdx mouse', *Journal of Neuroscience Research*. Wiley Subscription Services, Inc., A Wiley Company, 35(4), pp. 363–372. doi: 10.1002/jnr.490350403.

Pastoret, C. and Sebille, A. (1995) 'mdx mice show progressive weakness and muscle

deterioration with age', *Journal of the Neurological Sciences*, 129(2), pp. 97–105. doi: http://dx.doi.org/10.1016/0022-510X(94)00276-T.

Patel, K. and Amthor, H. (2005) 'The function of Myostatin and strategies of Myostatin blockade-new hope for therapies aimed at promoting growth of skeletal muscle.', *Neuromuscular disorders : NMD*, 15(2), pp. 117–26. doi: 10.1016/j.nmd.2004.10.018.

Pereverzev, A. P. *et al.* (no date) 'Method for quantitative analysis of nonsense-mediated mRNA decay at the single cell level'. doi: 10.1038/srep07729.

Pistilli, E. E. *et al.* (2011) 'Targeting the activin type IIB receptor to improve muscle mass and function in the mdx mouse model of Duchenne muscular dystrophy.', *The American journal of pathology*. Elsevier Inc., 178(3), pp. 1287–97. doi: 10.1016/j.ajpath.2010.11.071.

Popplewell, L. J. *et al.* (2009) 'Design of phosphorodiamidate morpholino oligomers (PMOs) for the induction of exon skipping of the human DMD gene.', *Molecular therapy : the journal of the American Society of Gene Therapy*. American Society of Gene & Cell Therapy, 17(3), pp. 554–61. doi: 10.1038/mt.2008.287.

Porte, S. D. La, Morin, S. and Koenig, J. (1999) 'Characteristics of Skeletal Muscle in Mdx Mutant Mice', in Jeon, K. W. (ed.). Academic Press (International Review of Cytology), pp. 99–148. doi: http://dx.doi.org/10.1016/S0074-7696(08)60158-8.

Pramono, Z. A. D. *et al.* (2012) 'A prospective study in the rational design of efficient antisense oligonucleotides for exon skipping in the DMD gene.', *Human gene therapy*. Mary Ann Liebert, Inc., 23(7), pp. 781–90. doi: 10.1089/hum.2011.205.

Proudfoot, N. J., Furger, A. and Dye, M. J. (2002b) 'Integrating mRNA processing with transcription.', *Cell*. United States, 108(4), pp. 501–512.

Proudfoot, N. J., Furger, A. and Dye, M. J. (2002a) 'Integrating mRNA processing with transcription.', *Cell*. United States, 108(4), pp. 501–512.

Puchtler, H., Waldrop, F. S. and Valentine, L. S. (1973) 'Polarization microscopic studies of connective tissue stained with picro-sirius red FBA.', *Beitrage zur Pathologie*, 150(2), pp. 174–87. Available at: http://www.ncbi.nlm.nih.gov/pubmed/4129194 (Accessed: 28

October 2018).

Qu, X. *et al.* (2011) 'The ribosome uses two active mechanisms to unwind messenger RNA during translation', *Nature*. Nature Publishing Group, 475(7354), pp. 118–121. doi: 10.1038/nature10126.

Ragot, T. *et al.* (1993) 'Efficient adenovirus-mediated transfer of a human minidystrophin gene to skeletal muscle of mdx mice', *Nature*, 361(6413), pp. 647–650. Available at: http://dx.doi.org/10.1038/361647a0.

Raz, V. *et al.* (2014) 'A Novel Feed-Forward Loop between ARIH2 E3-Ligase and PABPN1 Regulates Aging-Associated Muscle Degeneration', *The American Journal of Pathology*, 184(4), pp. 1119–1131. doi: 10.1016/j.ajpath.2013.12.011.

Ricard-Blum, S. and Ruggiero, F. (2005) 'The collagen superfamily: from the extracellular matrix to the cell membrane', *Pathologie Biologie*. Elsevier Masson, 53(7), pp. 430–442. doi: 10.1016/J.PATBIO.2004.12.024.

Rios, H., Koushik, S. V and Wang, H. (2005) 'periostin null mice exhibit dwarfism, incisor enamel defects, and an early-onset periodontal disease-like phenotype', *Mol Cell Biol*, 25. doi: 10.1128/MCB.25.24.11131-11144.2005.

Rodgers, B. D. and Garikipati, D. K. (2008) 'Clinical, Agricultural, and Evolutionary Biology of Myostatin: A Comparative Review', *Endocrine Reviews*. The Endocrine Society, 29(5), pp. 513–534. doi: 10.1210/er.2008-0003.

van Roon-Mom, W. M. C. and Aartsma-Rus, A. (2012) 'Overview on applications of antisense-mediated exon skipping.', *Methods in molecular biology (Clifton, N.J.)*. United States, 867, pp. 79–96. doi: 10.1007/978-1-61779-767-5_6.

Ryan, K., Calvo, O. and Manley, J. L. (2004) 'Evidence that polyadenylation factor CPSF-73 is the mRNA 3' processing endonuclease.', *RNA (New York, N.Y.)*. United States, 10(4), pp. 565–573.

RYU, J. K., DAVALOS, D. and AKASSOGLOU, K. (2009) 'Fibrinogen signal transduction in the nervous system', *Journal of Thrombosis and Haemostasis*. Blackwell Publishing Ltd, 7, pp. 151–154. doi: 10.1111/j.1538-7836.2009.03438.x.

Sakamoto, M. *et al.* (2002) 'Micro-dystrophin cDNA ameliorates dystrophic phenotypes when introduced into mdx mice as a transgene', *Biochemical and Biophysical Research Communications*, 293(4), pp. 1265–1272. doi: http://dx.doi.org/10.1016/S0006-291X(02)00362-5.

Samarakoon, R. *et al.* (2013) 'Induction of renal fibrotic genes by TGF-β1 requires {EGFR} activation, p53 and reactive oxygen species', *Cellular Signalling*, 25(11), pp. 2198–2209. doi: http://dx.doi.org/10.1016/j.cellsig.2013.07.007.

Sandri, M. *et al.* (2004) 'Foxo transcription factors induce the atrophy-related ubiquitin ligase atrogin-1 and cause skeletal muscle atrophy.', *Cell*. United States, 117(3), pp. 399–412.

Sapp, J. L., Bobet, J. and Howlett, S. E. (1996) 'Contractile properties of myocardium are altered in dystrophin-deficient mdx mice', *Journal of the Neurological Sciences*, 142(1–2), pp. 17–24. doi: http://dx.doi.org/10.1016/0022-510X(96)00167-0.

Sazani, P. *et al.* (2001) 'Nuclear antisense effects of neutral, anionic and cationic oligonucleotide analogs.', *Nucleic acids research*. Oxford University Press, 29(19), pp. 3965–74. Available at: http://www.ncbi.nlm.nih.gov/pubmed/11574678 (Accessed: 6 February 2019).

di Schiaffino, S., Gorza, L. and Parry, D. (1993) 'Age-related failure of muscle regeneration in the dystrophic DY2J/DY2J mouse', *Rendiconti Lincei*. Springer-Verlag, 4(3), pp. 269–277. doi: 10.1007/BF03001579.

Schiedner, G. *et al.* (1998) 'Genomic DNA transfer with a high-capacity adenovirus vector results in improved in vivo gene expression and decreased toxicity', *Nat Genet*, 18(2), pp. 180–183. Available at: http://dx.doi.org/10.1038/ng0298-180.

Schmajuk, G., Sierakowska, H. and Kole, R. (1999) 'Antisense oligonucleotides with different backbones. Modification of splicing pathways and efficacy of uptake.', *The Journal of biological chemistry*. UNITED STATES, 274(31), pp. 21783–21789.

Schoch, K. M. and Miller, T. M. (2017) 'Antisense Oligonucleotides: Translation from Mouse Models to Human Neurodegenerative Diseases', *Neuron*, 94(6), pp. 1056–1070. doi: 10.1016/j.neuron.2017.04.010.

Schultz, B. R. and Chamberlain, J. S. (2008) 'Recombinant Adeno-associated Virus Transduction and Integration', *Mol Ther*. The American Society of Gene Therapy, 16(7), pp. 1189–1199. Available at: http://dx.doi.org/10.1038/mt.2008.103.

Schultz, E. (1996) 'Satellite Cell Proliferative Compartments in Growing Skeletal Muscles', *Developmental Biology*, 94(0097), pp. 84–94.

Seibler, J. *et al.* (2007) 'Reversible gene knockdown in mice using a tight, inducible shRNA expression system', *Nucleic Acids Research*. Narnia, 35(7), p. e54. doi: 10.1093/nar/gkm122.

Semba, T. *et al.* (2018a) 'Periostin antisense oligonucleotide suppresses bleomycin-induced formation of a lung premetastatic niche for melanoma', *Cancer Science*. Wiley/Blackwell (10.1111). doi: 10.1111/cas.13554.

Semba, T. *et al.* (2018b) 'Periostin antisense oligonucleotide suppresses bleomycin-induced formation of a lung premetastatic niche for melanoma', *Cancer Science*, 109(5), pp. 1447–1454. doi: 10.1111/cas.13554.

Sherratt, T. G. *et al.* (1993) 'Exon skipping and translation in patients with frameshift deletions in the dystrophin gene.', *American journal of human genetics*, 53(5), pp. 1007–15. Available at: http://www.ncbi.nlm.nih.gov/pubmed/8213828 (Accessed: 10 February 2019).

Shi-Wen, X. *et al.* (2009) 'Requirement of transforming growth factor β–activated kinase 1 for transforming growth factor β–induced α-smooth muscle actin expression and extracellular matrix contraction in fibroblasts', *Arthritis & Rheumatism*. Wiley Subscription Services, Inc., A Wiley Company, 60(1), pp. 234–241. doi: 10.1002/art.24223.

Shi, Y. and Massague, J. (2003) 'Mechanisms of TGF-beta signaling from cell membrane to the nucleus.', *Cell*. United States, 113(6), pp. 685–700.

Shimazaki, M. *et al.* (2008) 'Periostin is essential for cardiac healingafter acute myocardial infarction', *The Journal of Experimental Medicine*, 205(2), p. 295 LP-303. Available at: http://jem.rupress.org/content/205/2/295.abstract.

Shimazaki, M., Nakamura, K. and Kii, I. (2008) 'Periostin is essential for cardiac healing after acute myocardial infarction', *J Exp Med*, 205. doi: 10.1084/jem.20071297.

Sicinski, P. *et al.* (1989) 'The molecular basis of muscular dystrophy in the mdx mouse: A point mutation', *Science*, 244(4912), pp. 1578–1580. doi: 10.1126/science.2662404.

da Silva Bizario, J. C. *et al.* (2009) 'Imatinib mesylate ameliorates the dystrophic phenotype in exercised mdx mice', *Journal of Neuroimmunology*, 212(1–2), pp. 93–101. doi: http://dx.doi.org/10.1016/j.jneuroim.2009.05.006.

Siva, K., Covello, G. and Denti, M. a (2014) 'Exon-skipping antisense oligonucleotides to correct missplicing in neurogenetic diseases.', *Nucleic acid therapeutics*, 24(1), pp. 69–86. doi: 10.1089/nat.2013.0461.

Small, J. V (1995) 'Structure-function relationships in smooth muscle: the missing links.', *BioEssays : news and reviews in molecular, cellular and developmental biology*. ENGLAND, 17(9), pp. 785–792. doi: 10.1002/bies.950170908.

Smith, P. J. *et al.* (2002) *An Exonic Splicing Enhancer in Human IGF-I Pre-mRNA Mediates Recognition of Alternative Exon 5 by the Serine-Arginine Protein Splicing Factor-2/ Alternative Splicing Factor*. Available at: https://core.ac.uk/download/pdf/33025404.pdf (Accessed: 10 February 2019).

Smith, R. C. and Lin, B. K. (2013a) 'Myostatin inhibitors as therapies for muscle wasting associated with cancer and other disorders.', *Current opinion in supportive and palliative care*. United States, 7(4), pp. 352–360. doi: 10.1097/SPC.0000000000000013.

Smith, R. C. and Lin, B. K. (2013b) 'Myostatin inhibitors as therapies for muscle wasting associated with cancer and other disorders.', *Current opinion in supportive and palliative care*. United States, 7(4), pp. 352–360. doi: 10.1097/SPC.0000000000000013.

Snider, P., Hinton, R. B. and Moreno-Rodriguez, R. A. (2008) 'Periostin is required for maturation and extracellular matrix stabilization of noncardiomyocyte lineages of the heart', *Circ Res*, 102. doi: 10.1161/CIRCRESAHA.107.159517.

Specks, U. *et al.* (1995) 'Increased expression of type VI collagen in lung fibrosis.', *American Journal of Respiratory and Critical Care Medicine*, 151(6), pp. 1956–1964. doi:

10.1164/ajrccm.151.6.7767545.

Spencer, M. J., Croall, D. E. and Tidball, J. G. (1995) 'Calpains are activated in necrotic fibers from mdx dystrophic mice', *Journal of Biological Chemistry*, pp. 10909–10914. doi: 10.1074/jbc.270.18.10909.

Sproat, B. S. *et al.* (1989) 'Highly efficient chemical synthesis of 2'-O-methyloligoribonucleotides and tetrabiotinylated derivatives; novel probes that are resistant to degradation by RNA or DNA specific nucleases.', *Nucleic acids research*. ENGLAND, 17(9), pp. 3373–3386.

Stedman, H. H. *et al.* (1991) 'The mdx mouse diaphragm reproduces the degenerative changes of Duchenne muscular dystrophy', *Nature*, 352(6335), p. 536—539. doi: 10.1038/352536a0.

Stojdl, D. F. and Bell, J. C. (1999) 'SR protein kinases: the splice of life.', *Biochemistry and cell biology = Biochimie et biologie cellulaire*, 77(4), pp. 293–8. Available at: http://www.ncbi.nlm.nih.gov/pubmed/10546892 (Accessed: 10 February 2019).

Summerton, J. E. (no date) *Endo-Porter: A Novel Reagent For Safe, Effective Delivery Of Substances Into Cells*. Available at: http://www.gene-tools.com/sites/default/files/Endo-Porter2005JES.pdf (Accessed: 14 August 2018).

Sun, G. *et al.* (2008) 'Connective tissue growth factor is overexpressed in muscles of human muscular dystrophy', *Journal of the Neurological Sciences*, 267(1–2), pp. 48–56. doi: http://dx.doi.org/10.1016/j.jns.2007.09.043.

Sun, S.-C., Peng, Y.-S. and He, J.-B. (2008) '[Changes of serum creatine kinase levels in children with Duchenne muscular dystrophy].', *Zhongguo dang dai er ke za zhi = Chinese journal of contemporary pediatrics*. China, 10(1), pp. 35–37.

Sundrud, M. S. *et al.* (2009) '<div xmlns="http://www.w3.org/1999/xhtml">Halofuginone Inhibits T_H17 Cell Differentiation by Activating the Amino Acid Starvation Response</div&gt';, *Science*, 324(5932), p. 1334 LP-1338. Available at: http://science.sciencemag.org/content/324/5932/1334.abstract.

SWEAT, F., PUCHTLER, H. and ROSENTHAL, S. I. (1964) 'SIRIUS RED F3BA AS A STAIN FOR CONNECTIVE TISSUE.', *Archives of pathology*, 78, pp. 69–72. Available at: http://www.ncbi.nlm.nih.gov/pubmed/14150734 (Accessed: 28 October 2018).

Szabo, G. *et al.* (1998) 'A deletion in the myostatin gene causes the compact (Cmpt) hypermuscular mutation in mice.', *Mammalian genome : official journal of the International Mammalian Genome Society*. UNITED STATES, 9(8), pp. 671–672.

Takayama, G., Arima, K. and Kanaji, T. (2006) 'Periostin: a novel component of subepithelial fibrosis of bronchial asthma downstream of IL-4 and IL-13 signals', *J Allergy Clin Immunol*, 118. doi: 10.1016/j.jaci.2006.02.046.

Takeshita, S. *et al.* (1993) 'Osteoblast-specific factor 2: cloning of a putative bone adhesion protein with homology with the insect protein fasciclin I', *Biochemical Journal*, 294(1), p. 271 LP-278. Available at: http://www.biochemj.org/content/294/1/271.abstract.

Tian, B. *et al.* (2005a) 'A large-scale analysis of mRNA polyadenylation of human and mouse genes.', *Nucleic acids research*, 33(1), pp. 201–12. doi: 10.1093/nar/gki158.

Tian, B. *et al.* (2005b) 'A large-scale analysis of mRNA polyadenylation of human and mouse genes.', *Nucleic acids research*, 33(1), pp. 201–12. doi: 10.1093/nar/gki158.

To, W. S. and Midwood, K. S. (2011) 'Plasma and cellular fibronectin: distinct and independent functions during tissue repair', *Fibrogenesis & Tissue Repair*. BioMed Central, 4(1), p. 21. doi: 10.1186/1755-1536-4-21.

Tobin, J. F. and Celeste, A. J. (2005) 'Myostatin, a negative regulator of muscle mass: implications for muscle degenerative diseases.', *Current opinion in pharmacology*, 5(3), pp. 328–32. doi: 10.1016/j.coph.2005.01.011.

Tomaru, A. *et al.* (2017) 'Oligonucleotide-targeting periostin ameliorates pulmonary fibrosis', *Gene Therapy*. Nature Publishing Group, 24(11), pp. 706–716. doi: 10.1038/gt.2017.80.

Trabold, O. *et al.* (2003) 'Lactate and oxygen constitute a fundamental regulatory mechanism in wound healing', *Wound Repair and Regeneration*. Blackwell Science Inc,

11(6), pp. 504–509. doi: 10.1046/j.1524-475X.2003.11621.x.

Trendelenburg, A. U. *et al.* (2009) 'Myostatin reduces Akt/TORC1/p70S6K signaling, inhibiting myoblast differentiation and myotube size.', *American journal of physiology. Cell physiology*, 296(6), pp. C1258-70. doi: 10.1152/ajpcell.00105.2009.

Valentine, B. A. *et al.* (1990) 'Canine X-linked muscular dystrophy: Morphologic lesions', *Journal of the Neurological Sciences*, 97(1), pp. 1–23. doi: http://dx.doi.org/10.1016/0022-510X(90)90095-5.

Veerasamy, M. *et al.* (2009) 'Differential regulation of E-cadherin and-smooth muscle actin by BMP 7 in human renal proximal tubule epithelial cells and its implication in renal fibrosis', *Am J Physiol Renal Physiol*, 297, pp. 1238–1248. doi: 10.1152/ajprenal.90539.2008.-Chronic.

Velloso, C. P. (2008) 'Regulation of muscle mass by growth hormone and', *British Journal of Pharmacology*, (October 2007), pp. 557–568.

Veltrop, M. *et al.* (2018) 'A dystrophic Duchenne mouse model for testing human antisense oligonucleotides', *PLOS ONE*. Edited by A. Asakura. Public Library of Science, 13(2), p. e0193289. doi: 10.1371/journal.pone.0193289.

Veltrop, M. and Aartsma-Rus, A. (2014) 'Antisense-mediated exon skipping: taking advantage of a trick from Mother Nature to treat rare genetic diseases.', *Experimental cell research*. Elsevier, 325(1), pp. 50–5. doi: 10.1016/j.yexcr.2014.01.026.

Verrotti, A. C. *et al.* (1996) 'Evolutionary conservation of sequence elements controlling cytoplasmic polyadenylylation.', *Proceedings of the National Academy of Sciences of the United States of America*. National Academy of Sciences, 93(17), pp. 9027–32. Available at: http://www.ncbi.nlm.nih.gov/pubmed/8799148 (Accessed: 6 March 2019).

Vickers, T. A. *et al.* (2001) 'Fully modified 2' MOE oligonucleotides redirect polyadenylation.', *Nucleic acids research*, 29(6), pp. 1293–9. Available at: http://www.ncbi.nlm.nih.gov/pubmed/11238995 (Accessed: 6 March 2019).

Vickers, T. A., Wyatt, J. R. and Freier, S. M. (2000) 'Effects of RNA secondary structure on cellular antisense activity', *Nucleic Acids Research*. Oxford University Press, 28(6), pp.

1340–1347. doi: 10.1093/nar/28.6.1340.

Viloria, K. and Hill, N. J. (2016) 'Embracing the complexity of matricellular proteins: the functional and clinical significance of splice variation', *Biomolecular Concepts*. De Gruyter, 7(2), pp. 117–132. doi: 10.1515/bmc-2016-0004.

Wada, T. *et al.* (2012) 'Antisense morpholino targeting just upstream from a poly(A) tail junction of maternal mRNA removes the tail and inhibits translation.', *Nucleic acids research*, 40(22), p. e173. doi: 10.1093/nar/gks765.

Wagner, K. R. (2002) 'Loss of Myostatin Attenuates Severity of Muscular Dystrophy in mdx Mice', *Annals of neurology*, 52, pp. 832–836.

Wagner, K. R. *et al.* (2008) 'A phase I/IItrial of MYO-029 in adult subjects with muscular dystrophy.', *Annals of neurology*. United States, 63(5), pp. 561–571. doi: 10.1002/ana.21338.

Wahab, N. A., Brinkman, H. and Mason, R. M. (2001) 'Uptake and intracellular transport of the connective tissue growth factor: a potential mode of action.', *The Biochemical journal*. Portland Press Ltd, 359(Pt 1), pp. 89–97. Available at: http://www.ncbi.nlm.nih.gov/pubmed/11563972 (Accessed: 9 March 2019).

Wang, B., Li, J. and Xiao, X. (2000) 'Adeno-associated virus vector carrying human minidystrophin genes effectively ameliorates muscular dystrophy in mdx mouse model', *Proceedings of the National Academy of Sciences* , 97(25), pp. 13714–13719. doi: 10.1073/pnas.240335297.

Ward, A. J. *et al.* (2014) 'Nonsense-mediated decay as a terminating mechanism for antisense oligonucleotides', *Nucleic Acids Research*, 42(9), pp. 5871–5879. doi: 10.1093/nar/gku184.

Wehling-Henricks, M., Lee, J. J. and Tidball, J. G. (2004) 'Prednisolone decreases cellular adhesion molecules required for inflammatory cell infiltration in dystrophin-deficient skeletal muscle', *Neuromuscular Disorders*, 14(8–9), pp. 483–490. doi: http://dx.doi.org/10.1016/j.nmd.2004.04.008.

Wehling, M., Spencer, M. J. and Tidball, J. G. (2001) 'A nitric oxide synthase transgene

ameliorates muscular dystrophy in mdx mice', *The Journal of Cell Biology*, 155(1), p. 123 LP-132. Available at: http://jcb.rupress.org/content/155/1/123.abstract.

Wilton, S. D. and Fletcher, S. (2005) 'Antisense oligonucleotides in the treatment of Duchenne muscular dystrophy: Where are we now?', *Neuromuscular Disorders*, 15(6), pp. 399–402. doi: 10.1016/j.nmd.2005.03.003.

Wolff, J. A. *et al.* (1990) 'Direct gene transfer into mouse muscle in vivo', *Science*, 247(4949), p. 1465 LP-1468. Available at: http://science.sciencemag.org/content/247/4949/1465.abstract.

Wynn, T. A. (2004) 'Fibrotic disease and the TH1/TH2 paradigm', *Nat Rev Immunol*, 4(8), pp. 583–594. Available at: http://dx.doi.org/10.1038/nri1412.

Wynn, T. A. (2007) 'Common and unique mechanisms regulate fibrosis in various fibroproliferative diseases', *The Journal of Clinical Investigation*. The American Society for Clinical Investigation, 117(3), pp. 524–529. doi: 10.1172/JCI31487.

Wynn, T. A. (2008) 'Cellular and molecular mechanisms of fibrosis', *The Journal of Pathology*. John Wiley & Sons, Ltd., 214(2), pp. 199–210. doi: 10.1002/path.2277.

YAFFE, D. and SAXEL, O. (1977) 'Serial passaging and differentiation of myogenic cells isolated from dystrophic mouse muscle', *Nature*. Nature Publishing Group, 270(5639), pp. 725–727. doi: 10.1038/270725a0.

Yang, W. *et al.* (2007) 'Myostatin induces cyclin D1 degradation to cause cell cycle arrest through a phosphatidylinositol 3-kinase/AKT/GSK-3 beta pathway and is antagonized by insulin-like growth factor 1.', *The Journal of biological chemistry*. United States, 282(6), pp. 3799–3808. doi: 10.1074/jbc.M610185200.

Zammit, P. S., Partridge, T. A. and Yablonka-Reuveni, Z. (2006) 'The skeletal muscle satellite cell: the stem cell that came in from the cold.', *The journal of histochemistry and cytochemistry : official journal of the Histochemistry Society*. United States, 54(11), pp. 1177–1191. doi: 10.1369/jhc.6R6995.2006.

Zeman, R. J. *et al.* (2000) 'Clenbuterol reduces degeneration of exercised or aged dystrophic (mdx) muscle', *Muscle & Nerve*. John Wiley & Sons, Inc., 23(4), pp. 521–528.

doi: 10.1002/(SICI)1097-4598(200004)23:4<521::AID-MUS10>3.0.CO;2-8.

Zhao, S. *et al.* (2014) 'Periostin expression is upregulated and associated with myocardial fibrosis in human failing hearts', *Journal of Cardiology*, 63(5), pp. 373–378. doi: http://dx.doi.org/10.1016/j.jjcc.2013.09.013.

Zhou, L. *et al.* (2006) 'Temporal and spatial mRNA expression patterns of TGF-β1, 2, 3 and TβRI, II, {III} in skeletal muscles of mdx mice', *Neuromuscular Disorders*, 16(1), pp. 32–38. doi: http://dx.doi.org/10.1016/j.nmd.2005.09.009.

Zhou, X. *et al.* (2010) 'Reversal of cancer cachexia and muscle wasting by ActRIIB antagonism leads to prolonged survival.', *Cell*. Elsevier Ltd, 142(4), pp. 531–43. doi: 10.1016/j.cell.2010.07.011.

Zimmers, T. A. *et al.* (2001) 'Induction of Cachexia in Mice by Systemically Administered Myostatin', 873(2000), pp. 2000–2003.